DE MONTFORT
UNIVERSITY

A MATHEMATICAL MODEL FOR LIQUID FUEL SPRAY COMBUSTION

Hobinanuwan Tikiri Banda Rajakaruna

A thesis submitted in partial fulfilment of the requirements of De Montfort university for the degree of Doctor of Philosophy (July 1997)

De Montfort University
Department of Mech. and Manf. Eng.
Leicester UK
LE1 9BH

ABSTRACT

A model capable of describing the evaporation, mixing and burning characteristics of a confined two-phase flow has been formulated. The flow considered results from the development and growth of a liquid fuel spray injected into a co-flowing air stream at high pressure and temperature. The work carried out during the formulation of the model can be divided into four main sections, these are: 1.) droplet studies to analyse the dispersed-phase evaporation, covering transient integral type models, liquid heating and unsteady gas-phase formulations. 2.) a two-dimensional steady-state Navier Stokes solver for predicting the mixing characteristics of confined gaseous flows. 3.) A locally homogeneous flow (LHF) type two-phase program to model the evaporation and mixing of a liquid fuel spray in a coaxial air stream, and finally, 4.) a 'mix-is-burnt' type combustion model based on the minimisation of the Gibbs free energy.

The droplet studies show that the evaporation process is unsteady throughout the life-time of the droplet and that the life-time predicted by the unsteady gas-phase formulation is much longer than that predicted by a quasi-steady analysis. It is concluded that the liquid heating is only significant in the heating up period. The importance of using variable properties in the fuel-vapour-air film surrounding the droplet is demonstrated together with the effect of system pressure on the droplet life-time. It is shown that increasing the system pressure causes a corresponding increase in the droplet life-time.

Predicted results from the two-phase model are compared with existing experimental results, showing reasonable agreement with the experimental data, particularly in the axial direction. It is also shown that the model is able to predict the experimentally observed recirculation regions. The applicability of the model over a wide range of pressure, temperature and input equivalence ratios is investigated in a parametric study. Possible applications of the model to practical combustion systems, with some modifications are analysed and suggested. Finally the model is compared to other LHF type models. It is shown that it has the advantage over most existing LHF type formulations in that it accounts for the dispersed phase evaporation via a simultaneous solution of a droplet module with the gas-phase equations.

ACKNOWLEDGEMENTS

First I would like to express my gratitude to De Montfort University and Prof. J. Knight for initiating this project and supporting me during the past three years. Above all, it is the continuing interest and support of my supervisor Dr. M. A. A. Nazha and his contributions in all aspects which has been a great source of inspiration and made the work worthwhile. I shall always be grateful for his undying enthusiasm during many difficult periods of thought. I am grateful to Dr. W. Malalasekera of Loughborough University of Technology for allowing me to use his CFD codes and his continuos support all throughout the project.

My most sincere thanks go to my good friend Andy Rylott for introducing me to SUN operating system and teaching me SUN system administration, which has enabled me to make best use of the Sun Network as a tool for this project. Also my gratitude goes to my friend Narendra Karia for his support and ideas, to Rev. Rathanajothi and Rev. Ananda of the Leicester Buddhist Association for their inspiring discussions.

Finally I would like to express my appreciation to all friends and colleagues at the school of engineering of De Montfort University for making it an interesting place to work.

CONTENTS

CHAPTER-3

THEORETICAL AND COMPUTATIONAL FORMULATION OF DROPLET EVAPORATION MODELS

CHAPTER-4

MATHEMATICAL FORMULATION AND PROGRAMMING TECHNIQUES OF THE SINGLE-PHASE AND THE TWO-PHASE MIXING MODELS

CHAPTER-5

COMBUSTION MODULE

CHAPTER-6

RESULTS AND DISCUSSION

CHAPTER-7

CONCLUSIONS AND RECOMMENDATIONS

Appendix-A

PROPERTY CALCULATIONS

Appendix-B

Graphs: (droplet results)

Appendix-C

Graphs:(spray results)

CHAPTER-1

INTRODUCTION

The burning of liquid fuel introduced into the combustion zone in the form of an atomised spray provides the basis of a wide range of practical combustion systems. The processes taking place during the combustion of these sprays are varied and complex and render complete analysis very difficult. As a consequence, current predictive models, irrespective of the complexity of the numerical technique used, remain no more than first steps providing preliminary insight into the physical and chemical processes involved in spray combustion. Yet the ability to understand and model these processes is essential if the task of designing rocket engines, gas turbines, industrial furnaces and diesel engines is to be made easier and more cost effective, and if the subsequent operation of these systems is to be made safer, cleaner and more efficient.

The wide-spread application of spray combustion motivated many workers to strive continuously towards improving their understanding of the processes involved, and their ability to simulate and model these processes. The literature is rich with experimental works and theoretical treatments addressing one aspect or another of the combustion of liquid fuel sprays. Early attempts were by necessity crude and oversimplified. As experimental technique improved and new sophisticated diagnostic equipment became available more reliable experimental data contributed towards an improved understanding of the phenomenon. This coupled with the recent advances in computing power enabled more sophisticated models to be explored. Despite these advances,

predictive models remain in their infancy, irrespective of the complexity of the numerical technique used. This is due to many factors; prominent amongst these are: the complexity and multiplicity of the processes involved; the wide-ranging operating conditions encountered in the applications of spray combustion; insufficient data regarding the physical properties of combustion gases and finally, the lack of a full understanding of many aspects of the subject. This last point results from the preceding ones; the multiplicity of the processes and the widely varying conditions make the provision of experimental data, isolating the influence of a particular parameter on a specific process, difficult and expensive. Furthermore, theoretical treatments must address the processes separately and must explore the effects of the various conditions on each process. Finally the models describing all the physical and chemical processes must be brought together in a single comprehensive model describing the overall process from injector to exhaust.

The modelling process of a reacting two phase flow is a very complex subject involving fluid mechanics, thermodynamics, physical chemistry, chemical kinetics, numerical methods and computer programming techniques. The areas of interest could be categorised as follows; droplet evaporation and combustion modelling, bulk gas flow and particle (droplet) interaction modelling and the modelling of combustion and chemical kinetics. It is not feasible to carry out research in all these areas within a short period, therefore in this research project only droplet evaporation modelling and the development and mixing of a liquid fuel spray in a coaxial air stream are analysed in detail.

1.1 Objective :

The objective of the research program is to develop a mathematical model capable of predicting the evaporation, mixing and burning characteristics of a confined liquid fuel spray in a high pressure, high temperature air stream, and to carry out parametric studies and compare the results and the model with existing experimental findings and mathematical models.

1.2 Definition of the problem :

When liquid fuel is injected into a combustion chamber, the resulting spray forms a jet entraining the surrounding gas. In the case under consideration the jet has the following unique characteristics. The jet consists of evaporating and burning liquid fuel droplets suspended in a hot gas environment. There is slip between the droplets and the bulk gas, leading to momentum, mass and energy transfer between the two phases. The growth of the jet is confined by the chamber walls, resulting in the establishment of a recirculation region.

1.3 The model :

The developed model is of the LHF (Locally Homogeneous Flow) type, two dimensional (2-D), steady state and finite volume formulation. The work carried out during the formulation of the model can be divided into four main sections :-

droplet evaporation

To analyse the characteristics of liquid fuel droplet evaporation three droplet evaporation models were formulated.

- A fully integral quasi-steady gas-phase model where a solution procedure based on the 4th order Runge-Kutta method.
- A model with a quasi-steady gas phase and spatially and temporally varying liquid phase (liquid heating model). Where the solution procedure is based on a fully implicit finite difference method with predictor-corrector type optimisation.
- A model with an unsteady gas phase and a quasi-steady liquid phase (unsteady gas phase model), again the solution procedure based on the above mentioned finite difference method.

gaseous jet

A two-dimensional steady state Navier Stokes solver capable of predicting the mixing of two co-flowing gaseous species injected into a cylindrical combustion chamber. The method of solution is by finite volume technique. The program uses the k-ε turbulence model and variable, thermodynamic and chemical properties.

spray

A locally homogeneous flow type two-phase program, to model the evaporation and mixing of a liquid fuel spray in a coaxial air stream. This program unifies a previously discussed droplet model with the single-phase mixing program.

combustion

A 'mix-is-burnt' type combustion model based on the minimisation of the Gibbs free energy function was also formulated. The sole purpose of this module is to validate the findings of the two-phase program, since experimental data is only available for post combustion products.

1.4 Layout of the report :

A detailed literature survey of mathematical modelling of droplet evaporation, single-phase flows, turbulence models and two-phase spray modelling is given in *chapter-2*. A mathematical description of the three droplet evaporation models developed and the corresponding computer programs are then introduced in *chapter-3*. This is followed by *chapter-4* which covers the techniques of compressible flow modelling, and include details of the two computer programs for modelling of single-phase and two-phase flows. The combustion model with the programming detail is described in *chapter-5*. Results of both the droplet models and the spray model are presented and discussed in *chapter-6*. Finally conclusions and recommendations are given in *chapters-7*, followed by the *Appendices*; where property routines (*Appendix-A*) , the relevant figures (*Appendices B and C*), references (*Appendix-D*), nomenclature and abbreviations (*Appendices E and F*) are provided.

CHAPTER-2

LITERATURE REVIEW :
droplets, sprays and turbulence

2.1 Introduction :

The chapter presents a literature review describing the history, development and state of the art of droplet evaporation modelling, gaseous flow and two phase spray simulation. The structure of the chapter is as follows. Section one is a discussion of the developments in the field of droplet modelling. Starting from the earliest steady state models to the current unsteady formulations. The scope of the droplet modelling review is confined to single droplet evaporation and combustion studies. Section two explains the computational modelling of single phase gaseous jets, turbulence models, two-phase (liquid-gas) flows followed by a brief description of combustion modelling techniques.

2.2 History and Development of Droplet Evaporation Models :

Liquid fuels are usually introduced into combustion chambers as droplet sprays. Once inside the combustion chamber, they start to evaporate due to the temperature and concentration gradients existing between the droplets and the surrounding gaseous environment, leading to heat and mass transfer between the two phases. These heat and mass transfer processes are markedly affected by the droplet size distribution and their respective velocities relative to the air. After an appropriate time each droplet attains an

equilibrium temperature equal to the wet bulb temperature corresponding to the conditions present at the moment. Inside the combustion chamber the droplets will rapidly loose their initial relative velocity due to aerodynamic drag forces. The larger droplets, due to their high initial momentum travel further down stream than the smaller ones, which evaporate completely at a shorter distance. A cloud of fuel vapour and air is thus rapidly formed and moves along with the main stream of air. The mass of vapour given away by the remaining droplets is also added to this vapour cloud. Somewhere in the combustion chamber a combustible mixture of air and fuel vapour is formed. Once the temperature of the mixture reaches the ignition temperature combustion takes place leading to a sudden rise in the surrounding temperature. Therefore understanding the evaporation and combustion dynamics of fuel droplets play a significant part in the design and development of gas turbines, industrial furnaces, diesel engines and rocket engines etc. [1].

Although droplet models are not used on their own, the knowledge obtained from these models are incorporated into spray combustion models (The droplet evaporation model runs in parallel with the main gas phase solver with data passing between the two modules). It is reasonable to assume that the individual droplet evaporation and burning characteristics may significantly influence the bulk spray characteristics, which in turn determines the combustion performance of the system under consideration.

Ideally in single droplet studies the ultimate droplet model should be able to account for the variations in all chemical and thermodynamic properties due to diffusive and

convective transport of energy and mass within the air-vapour film surrounding the droplet and within the liquid core. The droplet could be made up of many fuel species, therefore the model should be able to track the diffusion of each fuel component relative to the other and adjust the evaporation based on the surface area occupied by each species. It should also be able to predict the boundary layer effects near the surface and to account for the departure from spherical symmetry, which is significant in multi-component droplets made up of fuel species that could give rise to internal boiling.

Although non of the models described in this review can simulate all the conditions given above (specially the simulation of multi-component droplets), the more recently developed unsteady models, based on the solution of the Navier-Stokes equation set can predict a great deal about the temperature contours within the droplet, and outside, in the surrounding air-vapour film and the formation of boundary layers at the droplet surface. Solution of the Navier Stokes equation set of continuity, momentum in radial and tangential directions, species mass conservation and the energy equation with an appropriate equation of state is the most fundamental approach to the problem at hand. It is not possible to obtain analytical solutions to the Navier Stokes equation set, the solution is based on numerical methods such as finite volume method (FVM) or finite difference method (FDM). Before writing the equations in FVM or FDM the physical equations have to be transformed into a new co-ordinate system governed by the grid system used in the FVM or FDM method. This system is capable of taking account of the receding boundary at the liquid gas inter-phase. When the equations are formulated, to solve them high speed computers with large storage capacities are required. Until

recently the numerical methods and high speed computers were not available to carry out these detailed calculations. Therefore various assumptions were carried out to simplify the modelling process.

A significant amount of experimental and theoretical work has been done in this field during the past few decades. The early work on droplet combustion was laid by Godsave [2], Goldsmith and Penner [3], Spalding [4-6], Agafanova [7], Williams [8-9] and others. These early models were pure component droplets evaporating or burning in a stagnant oxidising environment. In the past few years significant changes have been incorporated into these basic models. Such as transient heating, effect of variable transport properties, internal circulation effects of moving droplets, species mass diffusion in the liquid phase for multi-component droplets and fuel vapour accumulation effects in the air vapour film of burning droplets, etc. In the following pages these advances will be described in a detailed manner.

2.2.1 Theoretical Aspects Of Droplet Evaporation And Combustion :

Progress in developing droplet evaporation and combustion models can be broadly summarised in the diagram below. Starting with the simple steady state model this research area has developed into a very complex field, where state of the art numerical procedures and high speed computers are now dominating the analysis.

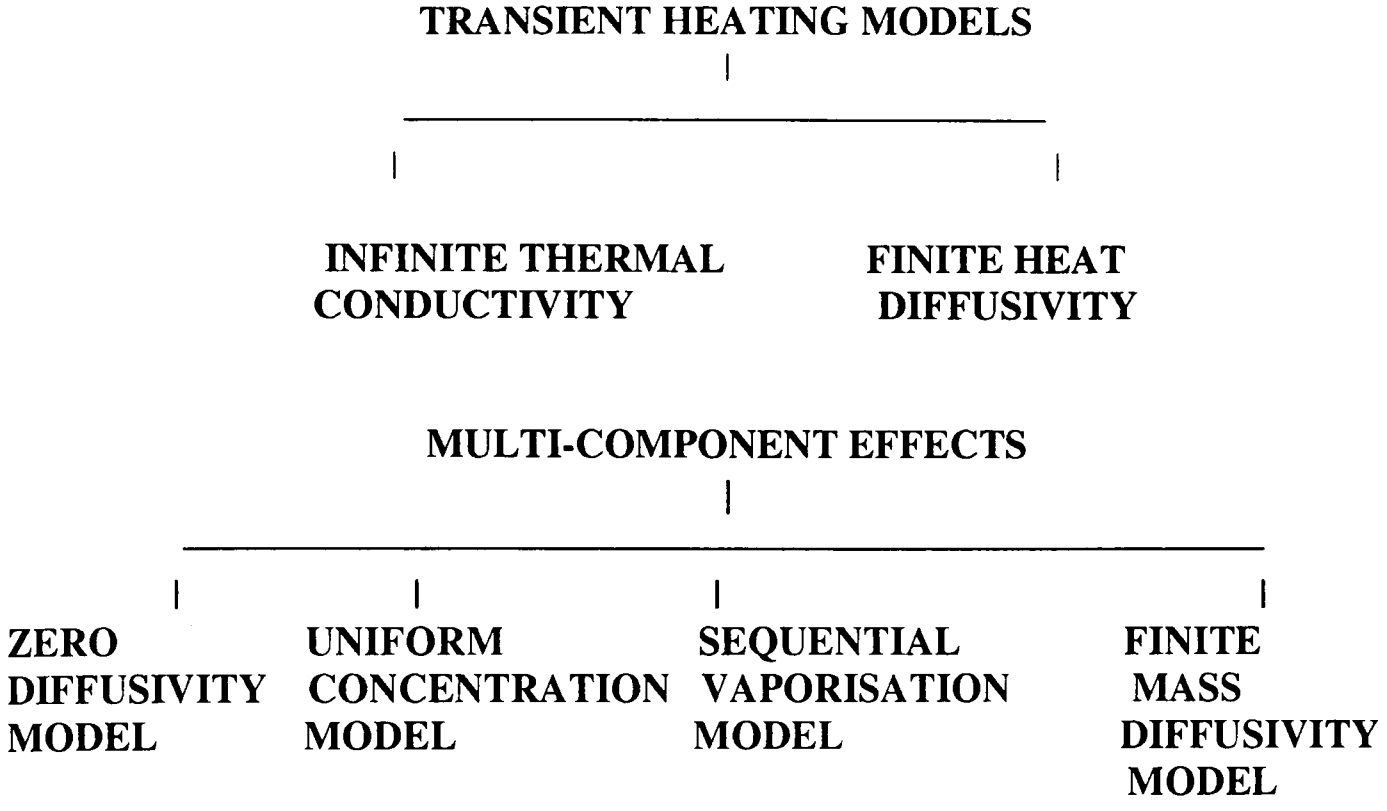

fig. 2.1 sequential development of droplet models

2.2.2 The Steady State Model :

The steady state model is the simplest droplet evaporation / combustion model. Transient heating is neglected in this model and the droplet temperature is assumed constant with time.

2.2.2.1 assumptions built into this model :

1. The droplet is spherically symmetric
2. The droplet consists of a single component
3. The temperature inside the droplet is spatially and temporally constant at its wet bulb temperature. This implies that the heating up period is neglected, and that all heat entering the gas-liquid interface is taken up for vaporising the droplet.
4. Equilibrium exists at the droplet surface (Typically a Clausius Clapeyron type relationship is employed to satisfy this condition.)
5. Spatially and temporally constant gas phase transport properties. Gas specific heats and thermal conductivity are constants and the Lewis number is unity. (These cause considerable uncertainty in the estimation of the gasification rate.)
6. Mass transfer is due to diffusion only
7. Constant pressure process
8. Flame sheet combustion. (Chemical reaction rates are much faster than gas phase diffusion rates such that the flame is of infinitesimal thickness and can be treated simply as a sink for the reactants and a source of chemical heat release and products.)
9. No radiation effects

Since the liquid is single species and at a constant uniform temperature the liquid phase heat and mass transfer is completely neglected in this model, therefore this model is essentially a steady state gas phase model. This model predicts a linear relationship between the droplet diameter squared and time.

2.2.2.2 results predicted by steady state models :

The steady state model predicts a linear relationship between the square of the droplet diameter and time. Therefore this model is also known as the d^2 law.

$$d^2 = d_0^2 + kt \qquad (2.1)$$

Where k is the burning rate coefficient and is given by

$$k = \frac{8\rho_g \delta_g}{\rho_L} \ln(1+B) \qquad (2.2)$$

Where B is the Transfer number, and is normally defined as :

$$B = \frac{C_{Pg}(T_\infty - T_S) + (Y_{0\infty}/\sigma)Q}{H} \qquad (2.3)$$

For a steady state formulation H, the effective heat of gasification (Droplet heating + Enthalpy of evaporation) is equal to the enthalpy of evaporation due to the constant droplet temperature assumption. Therefore B has to be redefined for the steady state model as :

$$B = \frac{C_{pg}(T_\infty - T_s) + (Y_{0\infty}/\sigma)Q}{L}$$

The other important relevant factors are [10]

The mass gasification rate :

$$\dot{m} = 4\pi \rho_g D_g r_s \ln(1+B) \qquad (2.4)$$

The flame front stand off ratio ($r_{fs} = r_f / r_s$) :

$$r_{fs} = \frac{\ln(1+B)}{\ln(1+Y_{o\infty}/\sigma)} \qquad (2.5)$$

The flame temperature :

$$C_{pg}(T_f - T_s) = \frac{C_{pg}(T_\infty - T_s) + (Y_{o\infty}/\sigma)Q}{(1+Y_{o\infty}/\sigma)} \qquad (2.6)$$

In the derivation of the above quantities the gas phase Lewis number has been assumed to be one. This implies that the heat transfer rate and the mass transfer rate within the gas phase are equal.

$$Le_g = \lambda_g / (C_{pg}\rho_g D_g) = 1 \qquad (2.7)$$

The above equations are applicable to both burning and evaporating droplets. For an evaporating droplet the flame is considered to be at infinity ($r_{fs} = \infty$), $T_f = T\infty$ And $Y_{of} = Y_{O\infty} = 0$and $Y_{Ff} = Y_{F\infty} = 0$. For a burning droplet $Y_{Ff} = 0$ and $Y_{of} = 0$. It is important

to note that for the steady state formulation T_S, T_f, $\dot{m}$ and r_{fs} are all constants for a given system.

2.2.2.3 inadequacies of the d^2 law model :

Experimental investigations into burning droplets have revealed the following inadequacies of the d^2 law [10].

1. In the heating up period the droplet diameter increases due to thermal expansion. This has been neglected in this model.
2. The flame front stand-off ratio is not constant but varies with time. This is due to the fuel vapour accumulation effects in the air/vapour film.
3. The experimental flame front stand-off ratio is much smaller than the theoretically predicted value. This is due to the use of constant transport properties and the assumption of unity Lewis number.

2.2.3 Variable Transport And Thermal Properties :

The d^2 law is based on the assumption of Cp_g, λ_g, ρ_g, D_g being constants and on Lewis number equal to one. Realistically the transport properties are functions of temperature, pressure and species mole fraction. Therefore the assumption of constant transport properties is in error. The first attempt at rectifying this was to modify the steady state model by including some sort of variability in the transport coefficients. Wise *et al* [11]

allowed heat capacity and thermal conductivity to assume different values in the inner and outer regions of the flame, for a burning droplet. Goldsmith and Penner [3] assumed heat capacity and thermal conductivity as linear functions of temperature in the inner region. Kassoy and Williams[12] developed a model in which the thermal conductivity and the product of the density and diffusion coefficient are both proportional to temperature raised to a power (which is less than one). Where the coefficients in the power law dependence, having different values in the two diffusion regions.

In all of the above models the properties were considered as functions of temperature only, the concentration dependency was not considered. A model was formulated by Law and Law [13] to take account of both concentration and temperature dependencies of λ, ρ and *Cp*, in the two diffusion zones (i.e. inside and outside the flame), but the droplet surface temperature and latent heat of gasification were taken as constants. The model gave better results compared to constant property models in predicting the flame-front stand-off ratio. The constant property models usually over predicts the flame front stand-off ratio by a factor of 2 to 3 times higher than the experimentally obtained value, but the value predicted by this model differs from the experimental ones by a few percentage points only. Using this model as a reference Law *et al* [13] carried out a parametric study to see the effect of various averaging techniques (arithmetic mean, geometric mean, etc.) of film temperature used in property calculations. They concluded that the calculation of properties, for the two diffusion regions using two average temperatures, based on the arithmetic mean gives better results compared to other averaging techniques (geometric mean, etc.).

When transient heating (section 2.2.4) is introduced into the modelling process the necessity of using variable properties becomes more significant due to the temperature range that the droplet passes through before attaining a steady wet bulb temperature. Transient heating models with variable properties have been formulated by Nazha [14], Law [15] and Hubbard *et al* [16].

2.2.4 The Transient Heating Models:

A major drawback of the steady state model is the assumption of constant droplet temperature, leading to the neglect of the droplet heating up period. The next advancement of the droplet models was the inclusion of the liquid heating in the governing energy equation. The gas phase now changes from being completely steady to quasi-steady. The quasi steadiness can be explained as follows :

Due to the significant density difference between the gas and the liquid phases, the liquid properties at the droplet surface change at rates much slower than those of the gas phase transport processes. Therefore over the characteristic time for gas phase diffusion the liquid droplet boundary location and conditions such as concentration and temperature can be treated as constant. Since the environment conditions are always considered constant, the conditions at the boundary $r = r_{\infty}$ are also constant. This implies that the gas phase which is inside these boundaries can be considered as steady over the gas phase diffusion characteristic time.

2.2.4.1 infinite thermal conductivity model :

The first approach to this problem was by El Wakil *et al* [17] They modelled the temperature field in the droplet as a temporally varying but spatially uniform variable.

The general form of the heat transfer equation in a spatially uniform liquid heating model has the following form :

$$q_g = \dot{m} L + mC_p \frac{dT_s}{dt} \qquad (2.8)$$

Which could be rewritten more explicitly as :

$$mC_p \frac{dT_s}{dt} = h4\pi r_s^2 (T_\infty - T_s) - \dot{m} L \qquad (2.9)$$

The above equation is solved with the mass gasification equation given below :

$$\dot{m} = 4\pi \rho_g D_g r_s \ln(1 + B) \qquad (2.10)$$

Equation (2.8) implicitly assumes that the liquid thermal conductivity is infinite. Some authors refer to this model as the rapid mixing model. (Sirignano and Prakesh [18-19], Law [10]).

2.2.4.2 finite heat diffusivity model :

In reality the rate of heat diffusion inside the droplet is finite, depending on the thermal conductivity of the liquid, therefore it is more realistic to consider the liquid phase temperature as spatially and temporally varying. This is the basis of the Finite heat diffusivity model. In this model the gas phase is still quasi-steady but the liquid phase is unsteady.

The gas phase heat transfer equations are modified as follows :

$$q_g = \dot{m} L + q_L \qquad (2.11)$$

where

$$q_L = 4\pi\lambda_L r_S^2 \left(\frac{\partial T}{\partial r}\right)_{L,s} \qquad (2.12)$$

equation (2.11) is solved with the partial differential equation for heat diffusion in the liquid phase to obtain a more accurate picture of the transient heating effect.

$$\frac{\partial T_l}{\partial t} = \alpha_l\left(\frac{\partial^2 T}{\partial r^2} + \frac{2}{r}\frac{\partial T_l}{\partial r}\right) \qquad (2.13)$$

Where α is defined as $k/(\rho C_P)$ and the equation (2.13) is subject to the boundary conditions below,

$$T(r)_{t=0} = T_0(r)$$
$$(\frac{\partial T}{\partial r})_{r=0} = 0 \qquad (2.14)$$

In the above model the heat transfer process in the liquid phase is only governed by diffusion. Therefore it is known as the diffusion limit model. Sirignano [20] suggests the diffusion limit model is ideally suited to study spherically symmetric (non convective) droplet evaporation problems.

These two transient heating models considered above represent the two extreme limits of the liquid phase heat transport process. Equation (2.13) allows diffusion only therefore it is the slowest limit. Equation (2.8) implies that there is an infinitely fast transport process therefore it is the fastest limit. In a more realistic situation, internal circulation within the droplet occurs, due to convective forces. Therefore the true nature of the heat transfer process lies some where between these two limits. Although the diffusion limit model predicts a low heat transfer rate due to its complete neglect of convective heat transfer effects, the author argues that this model could be used for a highly viscous fuel were the internal circulation effects can be neglected.

2.2.4.3 effect of droplet heating on overall evaporation and burning of the droplet :

Law[10] has drawn out the following conclusions regarding the droplet heating of a single component fuel in a constant environment :

1. Droplet heating proceeds fairly rapidly during the droplet life time
2. Droplet heating slightly prolongs the total burning time of the droplet
3. The period of heating subsequent to ignition is expected to be not too sensitive to the fuel volatility
4. The bulk gas-phase combustion characteristics (instantaneous burning rate etc.) are insensitive to the detailed heat transfer processes within the droplet.
5. At high pressure near the critical point droplet heating effects occupy a significant portion of the droplet life time.

2.2.5 Fuel Vapour Accumulation Effects Of Burning Droplets :

In most droplet combustion models the mass gasification at the droplet surface is taken as,

gasification rate at the droplet surface = mass consumption at the flame.

This means all the gasified fuel will be consumed at the flame. However, research carried out by Law, Chung and Sirinivasan [21], using a model consisting of a spatially uniform but time varying liquid phase and a quasi-steady gas phase, showed that the accumulation of fuel vapour causes significant changes in the burning characteristics of the droplet. Therefore to accommodate accumulation of fuel vapour, the mass balance at the droplet surface has to be modified as follows :

Gasification rate at the droplet surface

=

consumption rate at the flame

+/-

Accumulation/depletion rate at the inner region to the flame

Law et al [21] summarised some interesting facts about this process :

1. After ignition of the droplet the fuel consumption rate is less than the mass gasification rate. However in the latter part of the droplet life the fuel consumption rate is greater than the gasification rate. This implies that the initially accumulated fuel is now being depleted. The d^2 law requirement of *gasification is equal to consumption* is achieved only at one instant in the droplet life time.
2. Even after complete droplet gasification some fuel vapour is still left behind when the environment is oxygen lean, Although complete consumption can occur when the environment is oxygen rich.
3. Droplet heating dominates the droplet size history and fuel vapour accumulation effect dominates the flame size history.

2.2.6 Multi-Component Droplets :

The processes of evaporation and internal mass diffusion of multi-component droplets are important since most commercial liquid fuels are a combination of several hydro-carbons with wide ranging boiling points. Also synthetic fuels derived from coal, tarsand

and oil shale have complex compositions. Hybrid fuels such as water /oil emulsions, coal / oil mixtures and alcohol / oil mixtures have different physical and chemical properties that could affect the combustion and evaporation characteristics. This necessitates the use of droplet models which can take account of multi-component effects.

2.2.6.1 mass diffusivity in multi-component droplets :

In the vaporisation process of a multi-component droplet, early in the droplet life-time the more volatile substances in the fuel at the droplet surface will vaporise, leaving the less volatile material at the surface. Due to the concentration gradient at the surface and in the interior of the droplet the less volatile components will then diffuse towards the interior. This diffusion is balanced by the counter diffusion of the more volatile fuel components towards the surface. The result is that different components have different vaporisation rates at the droplet surface.

The following models have been formulated to represent the mass diffusion process in multi-component droplets.

2.2.6.2 the zero diffusivity model :

In this model it is assumed that the droplet maintains it's initial composition throughout it's life-time i.e. The concentration of each component is spatially and temporally uniform. Therefore to keep the species concentrations at their initial values throughout the droplet life-time, the evaporation rate of each species at the surface is assumed to be

proportional to the species initial concentration; e.g., for a droplet of 40% by mass Octane and 60% by mass Decane the total evaporated mass after a given time will consist of 40% by mass Octane and 60% by mass Decane. This model implies that the diffusion inside the droplet is zero or frozen.

2.2.6.3 uniform concentration (infinite mass diffusivity model) :

In this model it is assumed the concentration is spatially uniform but time dependent. The evaporation rate of each species is governed by its saturation vapour pressure at the droplet surface. There is no concentration dependency of the evaporation rate. At the end of each evaporation time step liquid properties are recalculated based on the remaining species mass fractions. This model implies that there is an infinitely fast diffusion process inside the droplet. Sirignano has pointed out [20] that this limit is only applicable to low temperature situations, where the droplet life-time is so long, that the diffusion can be considered to be fast enough for the concentrations to become uniform.

2.2.6.4 sequential vaporisation model :

The sequential vaporisation model is a limiting condition of the uniform concentration model. If the volatilities of the species differ widely the most volatile component will evaporate first completely leaving the rest of the components inside the droplet. Then the next most volatile component will evaporate, this process will continue until the least volatile component evaporates.

The model implies that when a particular component is evaporating from the surface the rest of that component will diffuse from the interior towards the surface. The other components at the surface will diffuse to the interior at the same time. Thus the surface will always constitute of the lightest component remaining in the droplet at a given time.

2.2.6.5 finite mass diffusivity model :

In the above described multi-component models the mass diffusion process is either happening at an infinitely fast rate or at an infinitely slow rate. A more reasonable model could be formulated if the diffusion rate is considered to be finite. This is the basis of the finite mass diffusivity model.

The mass fraction $\mathbf{Y_{l,i}}$ of the i th species in a spherically symmetrical droplet obeys the diffusion equation given below.

$$\frac{\partial Y_{\mathrm{L.i}}}{\partial \mathrm{t}} = D_{\mathrm{L}}\left(\frac{\partial Y_{\mathrm{L.i}}}{\partial r^2} + \frac{2}{r}\frac{\partial Y_{\mathrm{L.i}}}{\partial \mathrm{r}}\right) \qquad (2.15)$$

$$t \geq 0,\ 0 \leq r \leq \mathrm{R(t)}$$

This is identical to the heat transfer equation (2.13) expect that the mass diffusion coefficient D_{L} is much smaller than the heat diffusion α_{L} . The above equation models the liquid phase mass diffusion as temporally and spatially varying quantity. By

transforming the above equation into a fixed boundary problem Landis and Mills [22] solved the two partial differential equations for heat and mass diffusivity for a bi-component droplet. Later on Law and Sirignano [23] and Law *et al* [24] also approached the liquid phase mass diffusion problem with a finite mass diffusivity model.

Landis and Mills concluded that infinite mass diffusion models are highly inaccurate in predicting the vaporisation rates of individual components. In their model they used fixed values for both D_L and α_L; further research should be done to take account of the spatial and temporal dependency of these two quantities.

2.2.6.6 the nature of the micro-explosions phenomenon and it's significance :

Landis and Mills model is a good example of theory predicting experimentally observed phenomena. Their calculations indicated the occurrence of disruptive boiling (micro-explosion) inside multi-component droplets. This had been observed in experimental studies of burning multi-component droplets [25, 26].

Landis and Mills suggested that the phenomenon is due to local temperature in some regions of the droplet exceeding the local boiling point and so causing internal boiling. The initiation of internal boiling is aided by the presence of suitable heterogeneous nucleation sites. Since conventional liquid fuel blends do not normally contain heterogeneous nucleation sites Law [27] demonstrated that internal boiling can be initiated only when the internal states have reached the limit of super heat.

Experimental research in this area was primarily done by Law and co-workers [28. 29] in the United States and Crookes and Nazha [30] in the United Kingdom. Nazha [14] and Nazha and Crookes [31] have experimentally verified some interesting facts about emulsions. They showed emulsified fuels tend to reduce the amount of NO and soot formation in diffusion flames and combustion products in general. Therefore the effects of disruptive boiling or micro-explosions may have many practical implications. Also micro-explosions could be used as a possible mechanism in preventing the formation of large coal particle agglomerates in coal slurry fuels.

2.2.6.7 treating a multi-component fuel as a single component fuel :

Multi-component fuels such as diesel are made up of many different hydrocarbon species. considering the diffusion of each species on its own leads to the model becoming complicated and requiring a substantial portion of computer CPU time. For these types of fuel it is possible to use a single saturation pressure function [14] obtained from experimental data [32], instead of considering each component on its own. The author suggests that this type of analysis is useful when sufficient information about the fuel composition is not available.

2.2.7 Convective Effects :

When fuel is injected into a combustion chamber the resulting droplets have relative velocities with respect to the surrounding gas. This means convective heat and mass transfer effects may have an influence in spray combustion. Until recently the approach

was to model these effects using simplified experimental correlation laws developed for heat transfer of spheres. A popular correlation of this type is that due to Ranz and Marshall [33-34].

$$Nu = 2 + 0.6\, Re^{0.5}\, Pr^{0.5} \qquad (2.16)$$

$$Sh = 2 + 0.6\, Re^{0.5}\, Sc^{0.5} \qquad (2.17)$$

The above correlation could be interpreted as a correction for the convective effects on heat and mass transfer rates calculated in the absence of convection.

2.2.7.1 internal circulation effects :

The magnitude of the relative velocity between the droplet and the surrounding gas causes slip between the two phases. This leads to formation of a laminar boundary layer at the surface of the droplet in the gas moving past the droplet [20]. The shear forces created by this effect causes internal circulation of liquid inside the droplet. This, in turn, leads to the formation of another boundary layer; at the inner surface of the droplet, an internal wake along the symmetry axis, and a toroidal nearly invisid vortical core. The roughest approximation to this liquid motion is given by Hill's spherical vortex [35].

The result of this internal circulation is a significant decrease in the liquid phase heat and mass transfer characteristic times. However this does not justify the rapid mixing limit (sec 2.2.4.1) were the characteristic heat and mass transfer rates are taken as infinitely fast.

2.2.7.2 vortex model:

Models which take account of the above described liquid phase internal circulation effects have been primarily developed by Sirignano *et al* [18,19,25,36,37-39]. these models are known as **vortex models.**

The first convective droplet evaporation model was developed by Prakesh and Sirignano [18, 19, 40]. Their approach was to solve the boundary layer around the gas liquid interface with quasi steady two dimensional partial differential equations with integral and numerical methods. In this model the gas phase and the gas boundary layer are taken as quasi steady with constant property assumptions. The liquid viscosity is assumed to be a temporally varying function of temperature, also the enthalpy of evaporation is taken as time and temperature dependent. The temperature within the droplet is considered as uniform along a stream-line, but allowed to vary normal to the streamline. This effectively makes the liquid phase heat transfer process one dimensional when a stream-wise co-ordinate system is used. The authors concluded that, unsteadiness prevails during most of the droplet life time; internal circulation shortens the heat diffusion time by an order of magnitude but not to the point where droplet internal temperature can be considered as spatially uniform; the difference between the surface temperature and the temperature inside the droplet is higher for heavier and less volatile fuels. Extensions of this boundary matching formulations to multi-component fuels were carried out by Lara-Urbanejo and Sirignano [36].

The two dimensional analysis of the gas phase boundary layer was simplified by Tong and Sirignano [37, 38, 39] assuming a Blasius profile for the gas phase boundary layer governed by the following third order differential equation.

$$\frac{d^3 f}{d\eta^3} + f\frac{d^2 f}{d\eta^2} = 0 \qquad (2.18)$$

The liquid phase equations of the above model for the heat diffusion and mass diffusion are as follows:

$$\frac{\partial T}{\partial r} = \phi\frac{\partial^2 T}{\partial \phi^2} + (1 + C\phi)\frac{\partial T}{\partial \phi} \qquad (2.19)$$

$$\frac{\partial Y_{il}}{\partial \tau} = \frac{\phi}{Le}\frac{\partial^2 Y_{il}}{\partial \phi} + (\frac{1}{Le} + C\phi)\frac{\partial Y_{il}}{\partial \phi} \qquad (2.20)$$

Where ϕ is the normalised stream function and C is a function of the non-dimentionalised time.

This simplified model was compared by Sirignano *et al* with the more complex model of Prakesh and Sirignano and they have stated that it agrees well with the complex model results. Because of the one dimensional formulation, this model uses less computer time compared to the earlier model of Prakesh and Sirignano [18, 19]. This makes it more feasible to be used in an overall spray combustion program [41, 42]. Based on the results of the above model Sirignano and Tong concluded that the Ranz Marshall correlation

[33-34] over predicts the vaporisation rate, therefore the use of the correlation is not suitable for transient evaporation situations.

The most important finding resulting from this model is that the internal circulation effects cannot justify the assumption of infinite heat and mass transfer in liquid phase assumed in rapid mixing models.

2.2.8 Effective Conductivity Model :

The idea behind the effective conductivity model is to embed the liquid heating and mass diffusion effects due to internal circulation into the spherically symmetrical mass and heat diffusion equations (eq. 2.13-2.15). This is done by modifying the thermal conductivity and mass diffusivity terms in these equations [43]. Where the effective conductivity is defined as a constant times the thermal conductivity of the liquid; $K_{Fe}=\chi K$ $(1\leq\chi\geq 2.72)$.

Based upon the results of Johns and Beckman [44], Abramzon and Sirignano [43] proposed the following approximate correlation for the χ term of the above equation.

$$\chi = 1.86+0.86 \tanh[2.45 \log_{10}(Pe_L/ 30)] \qquad (2.21)$$

Where the liquid Peclet number is given as $Pe_L=2u_sR/\alpha_L$. Abramzon and Sirignano [43] assumed the gas phase heat and mass transfer processes to be quasi-steady and the thermophysical properties in the gas to be constants, provided they are evaluated at some reference (temperature and fuel concentration) condition.

$$\bar{T} = T_s + A_r(T_\infty - T_s)$$
$$\bar{Y}_F = Y_{Fs} + A_r(Y_{F\infty} - Y_{Fs}) \qquad (2.22)$$

Where A_r is an averaging parameter which is taken as 1/3 based on the results of Yuen and Chen [45].

They also modified the Nu and Sh numbers to account for the discrepancies in the ln(1+B) term in the mass transfer equation (2.10) (based on Spalding transfer number). The ln(1+B) term in the droplet mass gasification equation is based on zero Reynolds number conditions, Sirignano *et al* have shown this number does not approach the correct asymptotic behaviour for large Reynolds numbers

$$Nu^* = \frac{2r_s}{(T_s - T_\infty)}\left(\frac{dT}{dr}\right)_s \qquad (2.23)$$

$$Sh^{*} = \frac{2r_s}{(Y_{Fs} - Y_{F\infty})}\left(\frac{dY_F}{dr}\right)_s \qquad (2.24)$$

Extension of this method to model the mass diffusivity in multi-component droplets were carried out by Continillo and Sirignano [46] where an equation similar to equation (2.21) was used to model the convective mass diffusivity effects.

Delplanque *et al* [47] used the effective conductivity assumption in a mathematical model developed to evaluate the effects of dopants on liquid waste incineration. They tested the model using 200μm droplet having the properties of Hexane and a relative velocity of 0.25m/s higher than the gas phase. They have found that the droplet surface temperature predicted by the effective conductivity model is lower in the initial stage of droplet evaporation than the surface temperature predicted by a model without internal circulation (conduction limit). A lower temperature at the surface causes more heat to be conducted from the gas into the liquid. This eventually results in a high liquid temperature during the latter part of the droplet life time, leading to a higher rate of vaporisation than that of the conduction limit model. Therefore this study suggests that the use of models that do not take account of liquid heating effects would underestimate the rate of vaporisation in convective situations.

The main advantage of this model is its simplicity in representing the convective effects, leading to less CPU time taken for the calculations. Therefore this model could be incorporated in a spay program without demanding too much computing resources.

However it is important to note that, as far as the author is aware, this model has not been compared with the more detailed models of Sirignano *et al,* which deal with convective effects in a more detailed manner.

2.2.9 Navier Stokes Models :

The droplet models described so far could be classified as simplified models. These models are not valid over the whole life-time of the droplet and for certain Reynolds number ranges. The finite (mass and heat) diffusivity model is only valid if the effects of convection on heat and mass transfer processes are neglected. The vortex models developed by Prakesh and Sirignano [18, 19], Lara and Sirignano [36], Tong and Sirignano [37-39], are strictly correct only at high Reynolds numbers due to boundary layer approximations. Therefore the exact solutions of the complete Navier Stokes equations with minimum assumptions has become highly attractive. Navier Stokes equation models have been developed by Yuen and Renksizbulut [48], Heywood [49] Dwyer and Sanders [50-57], Chiang, Raju and Sirignano [58], Patnaik [54,59], Dash and Som [60]. Some of these models are discussed below.

2.2.9.1 Dwyer and Sanders analysis :

Dwyer and Sanders have developed an unsteady model introducing vaporisation and combustion at various stages of the model development. Firstly, they carried out a comparative study on non vaporising and vaporising droplets at high Peclet and Reynolds numbers with constant gas and liquid phase properties [52, 53]. The idea behind this

formulation was to isolate the affects of surface mass transfer, and to obtain information about the unsteady effects of this mass transfer process.

The numerical solutions were obtained using finite difference methods. The finite difference equations were solved by transforming them into generalised non orthogonal co-ordinates and using adaptive grid techniques [50,51]. Dwyer and Sanders concluded following from their work :

1. The isothermal and stream-line patterns inside the droplet and outside in the gas phase indicate that droplet heating is highly unsteady even for a constant diameter constant property models, [52]. They attributed this unsteadiness mainly to the dependency of liquid phase transport properties on temperature. The results described in their paper were obtained for a constant Peclet number of 1000 inside the droplet. Since the Peclet number is defined as the product of the Reynolds number and the liquid phase Prandtl number, they lowered the Reynolds number by a factor of 10 and increased the Prandtl number by the same factor to demonstrate the differences in solutions with a constant Peclet number but with different Reynolds and Prandtl numbers. This created a significant change in the distribution of the isothermal patterns both inside and outside the droplet giving a completely different picture of the heat distribution. Apart form the above, the reduction in droplet size due to evaporation also contributes to this unsteadiness.
2. The results are also very sensitive to pressure which has a large consequence on gas phase Reynolds number while not influencing the liquid conditions. Therefore any

solution which has time varying pressure will be very difficult to characterise by the quasi steady analysis.

3. The heat and mass transfer processes inside the droplet are initially dominated by convection and then become diffusion and conduction dominated during the latter part of the droplet life time. Therefore the use of the earlier models is limited to certain stages of the droplet life-time, i.e. the one dimensional diffusion model seems to be applicable to latter stages of the droplet life [53].

As explained by Patnaik *et al* [54], the use of constant density in the gas phase in the above Dwyer and Sander evaporation model [53] makes it's application to high temperature and high concentration gradients situations unsuitable. When a droplet is evaporating, there is a thin gas boundary layer surrounding it. In this thin boundary layer steep concentration and temperature gradients occur, leading to density gradients. Therefore to make the model more realistic these density gradients have to be taken into account. Patnaik [54] modified the model so that variable density could be included in the calculations making it applicable to large density gradients. To calculate gas density Patnaik used the equation of state for an ideal gas.

Patnaik[59] noted a significant discrepancy between his results and those of Dwyer and Sanders. His model gives a droplet life-time which is higher than that predicted by Dwyer and Sanders model. Patnaik attributed this to underestimation of gas density at the droplet surface in the Dwyer and Sanders model.

Patnaik *et al* [54] came to the following conclusions. 1.) The heat and mass transfer processes are first convection dominated, then after a period of both convection and diffusion playing an important role, diffusion dominates. 2.) For a given fuel type and initial temperature, the droplet transfer number is a function of the Reynolds number, indicating that the Reynolds number could be taken as a similarity parameter in droplet evaporation studies. The first conclusion confirms the earlier findings of Dwyer and Sanders [53].

The next stage of the Dwyer and Sanders study was to introduce chemical kinetics, ignition and combustion to the model [55, 56]. To focus attention on chemical kinetics and flame structure they carried out a numerical study simulating a 100μm n-Decane droplet at constant temperature close to its boiling point (with a free stream Re number between 2 and 100). This study showed that for small droplets (100μm or less) the time scale for heat diffusion is sufficiently small to cause the flame surrounding the droplet to be diffuse and thick relative to the droplet size [55]. Another important observation made by them was the fuel vapour accumulation between the droplet surface and the reaction zone (flame) at low Reynolds numbers. These observation of thick reaction zone and fuel vapour accumulation make the assumptions of steady state gas phase and flame sheet combustion in the simplified models questionable, specially for low Re number situations and for small droplets.

Using the same physical and thermodynamics parameters as in the above model they carried out another study (0<Re>10) in which more emphasis was given to the ignition

process[56]. This showed that ignition was the most unsteady process in a burning droplet. From this study they concluded that the ignition process occurs on a shorter time scale than any other process and it has more influence on the droplet life history than any other condition.

The most significant finding of this work can be summarised as follows:

1. The most important process in the early lifetime of a hydrocarbon droplet is the heating up period which determines the surface mass transfer characteristics and the strongly coupled drag and heat transfer between the gas and the liquid phases.
2. Time dependent solutions have shown that the liquid phase processes have a significant influence on the ignition process.
3. Although the flame sheet combustion is not strictly correct for small droplets, the d^2 law has been reproduced by this result.

Dwyer[57] has stated that the qualitative values of the model is limited since many characteristics of the flow are sensitive to the transport coefficients and chemical rate terms, which are not properly defined in this model. This shows the importance of using variable properties in droplet models.

2.2.9.2 Yuen and Renksizbulut analysis:

Yuen and Renksizbulut carried out finite difference solutions for high temperature air flowing past water droplets, methanol droplets and solid spheres, and for super heated

steam flowing past water droplets, in the Reynolds number range of 10 to 100 [48]. In their analysis it was assumed that, based on previous numerical work of Hubbard, Denny and Mills [16], the gas phase transport processes are quasi steady. The liquid phase motion and the heating up process were also neglected; this made the model of the steady state type. Based on their numerical [48] and experimental [61] results they came up with correlations for total drag and for Nusselt number. Comparing these correlations with the numerically obtained values of Dwyer and Sanders[54-56] and of Dwyer [57], they showed that these correlations for drag and Nusselt number are only valid for certain stages of the droplet life time.

2.2.9.3 Heywood's analysis:

Heywood carried out a variable-property time-dependent analysis (in both gas and liquid phase) of cold Heptane droplets evaporating in air at 800K and 1 atm [49]. The model is a finite volume formulation with liquid phase internal motion and heating included. Heywood presented correlations for total drag and for Nusselt number based on this numerical results. He stated that the deceleration of the droplet under the influence of its own drag is an important transient effect. According to Dwyer [57] Heywood's model gives good results after the droplet heat up period.

2.2.9.4 Chiang and Sirignano's analysis :

Chiang and Sirignano model consists of introducing a cold fuel droplet into a hot gas stream. The effects of variable transport properties, transient heating, liquid internal circulation, deceleration of flow due to drag, droplet boundary layer blowing and moving

interfaces are included in this model [58]. The equations were transformed using implicit finite difference schemes. Their results confirmed those of Dwyer and Sanders. which showed that transient droplet heating and reduction in droplet Reynolds number are major sources of droplet unsteady behaviour and persist during most part of the droplet life-time. They also showed that the nature of the heat transfer process inside the droplet becomes convection dominated and then diffusion dominated. Chiang and Sirignano concluded that, variable property effects cannot be neglected otherwise the global results may be seriously over estimated.

2.2.10 Chemical Kinetics :

In most combustion models it is assumed that the chemical kinetics are infinitely fast. This means, chemical reaction rate is not a controlling factor in the rate of droplet disappearance. Therefore the rate of chemical reactions were neglected in most early models.

The chemical reaction rates were first introduced by adopting an overall reaction equation. In this method the oxidation of fuel is described by the single reaction equation:

$$\text{Fuel} + x_i O_2 \rightarrow x_2\, CO_2 + x_3 H_2O \qquad (2.25)$$

Where parameters x_i are determined by the fuel type. The above equation is a simple way of approximating the many reactions that actually occur in a real combustion

situation. Therefore the rate expression for this single step reaction equation is an overall rate expression, which is usually expressed as :

$$K_{OV} = AT^{n} \exp(-ER/T)[\text{Fuel}]^{a}[\text{Oxidiser}]^{b} \qquad (2.26)$$

where 'R' is the universal gas constant and the parameters, *A*, *E*, n, *a*, *b* are constants.

Although single step equation models predict the flame characteristics reliably at adiabatic flame temperatures of typical hydro-carbon fuels, significant amounts of CO and H_2 also exist in equilibrium with CO_2 and H_2O. This equilibrium lowers the heat of reaction and the adiabatic flame temperature below the values predicted by the single step equation. To account, at least, for part of this effect of incomplete conversion of fuel, the global equation could be modified by a two step equation where the second equation is for CO-CO_2 equilibrium [62].

The above method could be further refined by including an equation for the H_2-H_2O equilibrium. As far as the author knows only single step and two step reaction equations are used in droplet combustion models due to the penalty they cost in computer time. When a droplet is burning, apart from CO_2, H_2O, CO and H_2, various other compounds are formed. Taking account of all these quantities is an impossible task due to the immense amount of computer time it takes to perform the calculations. Therefore the use

of simplified reaction mechanisms have become the norm when it comes to droplet combustion modelling.

2.2.11 Experimental Techniques Used In Droplet Studies :

The section below describes briefly the experimental research carried out in droplet evaporation and burning studies. It is not a detailed review of experimental work. It is included to demonstrate that theoretical findings such as the burning rate coefficient can be verified experimentally and to highlight the complexities associated with experimental studies.

Three techniques have been used to investigate the droplet burning and evaporation characteristics. These are :

1. The suspended (or captive) drop method
2. The supporting drop method
3. The free drop method

2.2.11.1 the suspended (captive) drop method :

In the suspended drop technique a single drop (or an array of droplets) is suspended from a silica fibre. The drop is then ignited and the combustion is recorded photographically [3, 63, 64]. With this method it is possible to obtain the burning rate coefficient k from the d^2 law using the equation given below.

$$k = \frac{2\,\dot{m}}{\pi\ \rho_L\ r_s} \qquad (2.27)$$

A substantial amount of work using this technique on burning rate coefficients have been reported on single droplet combustion, work has upto 1968 been reviewed by Wise and Agoston [65] and Williams [66]. Experimental results regarding burning rate coefficients of arrays of suspended droplets indicate that the d^2 law holds for such arrays but the burning rate coefficient vary according to the droplet position and type of array. For two and five drop arrays [67] the burning rate coefficient first increases then decreases as the inter droplet distance decreases. This is due to the opposing effects of enhanced heat transfer and natural convection against the decrease in Oxygen availability. In large arrays [67, 68] of 5 to 9 droplets, the burning rate coefficient is higher for the central droplet.

the above method has the following drawbacks :

1. Because of the thickness of the suspension fibre it is difficult to suspend a droplet much smaller than 1 mm in diameter (much larger than typical droplet size within sprays).

2. Due to viscous effects, the droplet shape distorts when it is suspended by a fibre. This distortion is very severe towards the end of the droplet life time, when the droplet size becomes comparable with the suspension fibre. To correct for this effect an "equivalent diameter" is usually used [66].

3. Heat is transferred from the droplet to the suspended fibre, the amount of heat conducted represents a heat loss. Okijama and Kumagai [69] have shown this causes a slight reduction in burning rate.

4. This technique is limited to fuels which are relatively non volatile. Significant portion of a droplet of volatile fuel could vaporise by the time it is being suspended and charging the chamber with the proper environment. This is specially significant for multi-component droplets. The different volatility rates of each individual species causes the composition of the droplet to be altered by the time the experiment is set-up.

Work carried out by Law *et al* [29] and Miyasaka and Law [70] have shown that distortion and heat loss effects can be neglected if the fibre diameter is less than 100μm.

2.2.11.2 supporting sphere technique :

This technique is used to study the steady-state combustion effects using a simulated droplet burning environment. The method was first used by Khudyakov [71] and Spalding [4] In this method fuel is supplied to a supporting inert porous sphere at a rate equal to the rate of combustion. This method is widely used to analyse the flame structure [72], shape and other flame characteristics. Detailed studies of flame temperature [73, 74], flame composition profiles [69, 29, 70] and position of the contact surface [75, 76] could be found in the above references.

The main drawbacks are: exceedingly large size of the supporting sphere and unobservability of the transient phenomena which are present during droplet combustion.

2.2.11.3 free drop technique :

Free drop technique is used to obtain information on moving droplets. This technique is more realistic since it is closer to a spray combustion situation. In this technique a single droplet or a low density cloud of droplets is produced by a suitable drop generator such as ultra sonic atomiser [77], spinning disc atomiser [78, 79], a simple orifice [80] or a vibrating capillary [81]. Theses droplets are of controlled size. They are allowed to fall under the gravitational force or are projected into a hot environment. In the latter case self ignition occurs or is caused by a pilot flame. The droplet is photographed throughout this process by stroboscopic methods.

The main advantages of this method are: small droplets can be used, non-interference from supporting fibre and the capability of using volatile fuels. However the experiment methodology is more complex. Furthermore since drops are not stationary the obtaining of photographic record is very involved.

2.2.11.4 the effect of gravity on experimental results :

All combustion experiments conducted under gravity are complicated by buoyancy. By its nature combustion causes an increase in temperature in the gaseous mixture surrounding the droplet. This increase in temperature leads to a significant density

difference between the air-vapour film in the vicinity of the droplet and the ambient surrounding gas, which in the presence of gravity causes buoyant motions. The effects of buoyancy are manifested in two ways; the burning rate is increased because of the enhanced transport rate, and the flame shape is distorted from spherical symmetry. This distortion could be very severe in some cases making it meaningless to talk of a flame diameter. The distortion is proportional to the droplet size, hence the effects are transient in nature.

To minimise the effects of buoyancy the following two techniques have been employed [69, 70].

1.) The use of freely falling chamber, where initially the droplet is suspended inside the chamber. Before the free fall starts the suspension fibre is impulsively pulled upwards. This frees the droplet from the suspension fibre. The combustion chamber is timed to fall freely at a predetermined time after the droplet has reached the highest point of its trajectory. Theoretically this makes the droplet stationary inside the chamber resulting in a gravity free droplet. The method was first used by Kumagai *et al* [69, 82]. (In Kumagis' experiments the droplet had a very low constant velocity of few centimetres per second, relative to the combustion chamber.)

2.) The second technique is more simple. The experiment is conducted under low pressure (down to about 0.1 of atmospheric pressure) [29, 70]. The underlying principle behind this method as argued by Law *et al* [70] is that since the spherically

symmetric droplet combustion is diffusion controlled and therefore pressure independent, reducing the chamber pressure diminishes buoyancy without affecting the combustion kinetics up to a certain lower limit of system pressure.

Although the theoretical modelling has gained significant progress over the years the experimental side has not developed in that manner. This is mainly due to the complexity of the experiments and the cost associated with the setting up of combustion rigs and high speed photographic equipment.

2.2.12 Further Research Areas :

The author's conclusion is that further research in the following areas need to be carried out to improve the present state of knowledge in this field.

1. The use of better correlation laws to calculate the thermodynamic and transport coefficients in the gas phase. It has been pointed out buy many researcher (Dwyer [57], Sirignano [83], Law [10]) that property variations have a significant effect on the droplet evaporation and burning characteristics. At the present time the CHEMKIN [84, 85] package developed by the Sandia National Laboratories is one of the best general purpose chemical data base packages available for property calculations. This type of databases could be used directly as a subroutine in droplet programs to obtain chemical data. Because of computer CPU time considerations these packages are seldomly used in the droplet models at the moment.

2. More research need to be done in the area of chemical kinetics of burning droplets; because it appears that the currently used chemical kinetic rate expressions are inadequate. The widely used single step and two step types reaction rate equations can be further refined by a three step equation where the third step is for H_2-H_2O equilibrium) [62].

3. Further research could be done in the area of combustion at elevated pressures close to the critical state. As the droplet approach the critical state its ability to hold the spherical shape becomes greatly diminished and under super critical conditions the droplet no longer exists, it becomes a puff of gas. There are only a few research papers published in this area [86-88], so it seems that this is a very interesting area for future research.

4. Evaporation and combustion of multi-component fuels need to be looked at in more detail, particularly the burning characteristics of emulsified fuels. Occurrence of micro-explosions in multi-component fuels has a great implication in the design of fuel injectors. The fine atomisation of fuel droplets which is the primary concern in the design of these devices need not be of critical importance if the physics behind liquid phase mass and heat transfer processes of these fuels are properly understood. In fact it is advantageous to have large droplets with sufficient inertia to penetrate into the combustion chamber in order to achieve an optimal distribution. Upon penetration rapid gasification and burning can be achieved due to micro-explosions.

2.2.13 Conclusion :

Although the steady state model has been out performed by all the other models it can be seen that the d^2 law which was derived from this model is qualitatively valid. Therefore this model could be used as a basis against which the performance of the more advanced models could be evaluated.

The author argues that, when a droplet model is used for a spray combustion program, it should be the quasi-steady type at least, with variable properties in the gas phase and it should take account of the heating up period. Also variable properties have a significant effect on overall evaporation rate and the flame front stand-off ratio.

Due to the development of high speed computers and the advancements made in the field of computational fluid dynamics, the modelling of droplets using full Navier Stokes equations has become attractive recently. The author thinks that the future of the droplet modelling lies in this area, where the most fundamental forms of the equations are used and solved numerically. Although these models have shown us hitherto unknown details about droplet dynamics, at present however, incorporating these models in a spray combustion program is questionable due to the excessive time it takes the program to run.

2.3 Review on Computational Fluid Dynamics Modelling of Sprays and Turbulent Combustion :

Attempts at modelling spray combustion (two-phase flow) have always been based on the experience gained in modelling single-phase turbulent flows. These have advanced appreciably in recent years, where the state of the art is that the flow field is described by a joint probability function of the velocity components and the composition variables (enthalpy and mass fractions). Development in two-phase flows has lagged behind that of single phase flows due to the added complexity of particle phase interactions, and due to the lack of experimental data, particularly in the dense region (near the injector). As a consequence most two phase models remain over-simplified and deterministic in nature.

It is intended in this section to review the numerical techniques of multi-dimensional flow modelling and the state of the art of both single and two phase flow simulation methods. Since most two phase models are extensions of corresponding single phase models, these will be reviewed initially.

2.3.1 Modelling Of Gaseous Flows :

The method of modelling flows mathematically has been established for some time. The earlier models were either zero dimensional or one dimensional ones. The zero dimensional models are considered thermodynamic models that do not address fluid mechanics. Such models give the final state based on the initial state only. One

dimensional models, on the other hand, can predict variations of properties in a one dimension. Both these types cannot provide qualitative information about the whole flow field. This information can only be obtained from multi-dimensional models, which are based on the solution of the Navier-Stokes equation set.

In a single-phase model the Navier-Stokes equations governing the transport of energy, overall mass, momentum, individual species mass (if more than one species is involved) are solved to obtain flow field information, such as temperature, velocity, species concentration distributions etc. Since the mixing process in many situations is inherently turbulent the model must account for turbulence to provide a realistic picture of the flow filed. In single-phase flow modelling, accounting for turbulence has become a major area of research. The methodology of turbulence modelling is quite complex, therefore it will be reviewed, together with the history of its development in the subsequent paragraphs. Apart from the above, the equations relating the change of thermodynamic and chemical properties of the gases involved (such as density, viscosity etc.) need to be included in the model. All of the above equations are solved iterativly until final converged solutions of temperature, mass fractions distribution etc. are obtained.

2.3.2 Historical Development and Mathematical Concepts in Turbulence Modelling:

At present turbulence flows are modelled using time averaged methods. Two types of decomposition methods are available for variable density flows. The first is the un-weighted decomposition represented by Reynolds averaging:

$$\phi = \bar{\phi} + \phi' \tag{2.28}$$

$$\bar{\phi} = \frac{1}{\Delta t}\int_{t}^{t+\Delta t} \phi(\tau)d\tau \tag{2.29}$$

The second is the density-weighted decomposition represented by Favre averaging :

$$\phi = \tilde{\phi} + \phi'' \tag{2.30}$$

$$\tilde{\phi} = \frac{1}{\rho}\frac{1}{\Delta t}\int_{t}^{t+\Delta t} \rho(\tau)\phi(\tau)d\tau \tag{2.31}$$

Experimentally measured quantities of flow variables are often presented as un-weighted temporally averaged values. This leads to Favre average quantities are being not readily comparable with measurements. Therefore Reynolds averaging is extensively used in most of the turbulence models.

The time averaged form of the turbulent generic flow equation is as follows [89, 90].

$$\frac{\partial(\rho\varphi)}{\partial t}+\frac{\partial(\rho v_j\varphi)}{\partial x_j}=\frac{\partial\left(\frac{\mu}{\sigma_\phi}\frac{\partial\varphi}{\partial x_j}\right)}{\partial x_j}-\frac{\partial(\rho\overline{v_j'\varphi'})}{\partial x_j}+S_\varphi \qquad (2.32)$$

Where φ is the generalised dependent variable and S_φ is the source term. The superscript ' denotes the fluctuating components of the generalised variable (φ) and the velocity component (v_j). For isotropic[1] turbulent flows, the turbulent quantities can be related to the mean flow properties by using the concept of isotropic scalar turbulent viscosity or eddy viscosity (μ_T) [89, 90]. This leads to the following relationships [90].

$$-\rho\,\overline{v_i'v_j'}=\mu_T\left(\frac{\partial v_i}{\partial x_i}+\frac{\partial v_i}{\partial x_j}\right) \qquad (2.33)$$

$$-\rho\overline{v_j'\varphi'}=\frac{\mu_T}{\sigma_\varphi}\left(\frac{\partial\varphi}{\partial x_j}\right) \qquad (2.34)$$

Substituting equations (2.33) and (2.34) in equation (2.32), gives

$$\frac{\partial(\rho\varphi)}{\partial t}+\frac{\partial(\rho v_j\varphi)}{\partial x_j}=\frac{\partial\left(\Gamma_\varphi\frac{\partial\varphi}{\partial x_j}\right)}{\partial x_j}+S\varphi \qquad (2.35)$$

[1] fluids whose properties do not depend on direction.

Where Γ_φ denotes the generalised transport coefficient given by $\Gamma_\phi = \mu_e/\sigma_\varphi$ and μ_e is the effective turbulent viscosity ($\mu_e = \mu_T + \mu_{laminar}$). In most engineering flows the values used for σ_φ are between 0.9 and 1.

The time averaged equation set (2.32) is not a closed system due to the unknown second order correlation term $-\rho\overline{v_j'\varphi'}$. This term represents the transport of mass, momentum and energy due to turbulent fluctuations. The idea behind turbulence modelling is to simulate this term directly or to simulate it using the concept of turbulent viscosity, μ_T. Over the years various turbulent models have been formulated. A good turbulence model has to be universal and not too complex to develop or use. Universality implies that a single set of empirical constants or functions inserted into the equations provides a close simulation of a variety of types of flow. Complexity could be measured by the number of differential equations that are in the model and the number of empirical constants and functions which are required as subsidiary steps in the solving of the differential equations. An increase in the first condition complicates the task of using the model, increasing the second condition complicates the formulation and solution procedure of the equation set. The following section briefly describes the development of the turbulent modelling techniques which have been used over the past few decades.

2.3.2.1 zero equation model (mixing length model) :

zero equation model is an algebraic model developed by Prandtl in 1925 [91]. The model directly simulates turbulent viscosity term by an algebraic expression of mean flow properties. The turbulent viscosity in this model is given as follows:

$$\mu_T = \rho l_m^2 \left| \frac{\partial v_j}{\partial x_i} + \frac{\partial v_i}{\partial x_j} \right| \qquad (2.36)$$

The term l_m is known as the mixing length which is determined by experiment or by intuition.

For free shear flows, taking μ_T only as a function of the radial co-ordinate, $\mu_T = \rho l_m^2 \left| \frac{\partial u}{\partial r} \right|$, the mixing lengths have been found out as follows [90] :

Plane jet in stagnant surroundings : l_m=0.09δ [δ = width of 1/2 jet]

Fan jet in stagnant surrounding : l_m=0.125δ [δ = width of 1/2 jet]

Advantages of the Mixing Length model

- the model is simple since no additional differential equations need to be solved

- provided good choices are made for the mixing length, realistic predictions can be made of the velocity, shear stress distributions and the general behaviour of boundary layer flows

Disadvantages of the model :

- the model cannot be used for recirculating flows
- when the velocity gradient is zero the turbulent part of the effective viscosity, effective thermal conductivity and effective Prandtl and Shemidt numbers become zero
- the model takes no account of the effects of convection and diffusion processes on turbulence

2.3.2.2 the one equation model :

The main defect of the mixing length model is the 'localness' of turbulence. In a more realistic situation the effects of convection and diffusion of the flow variables upstream or down stream of the location considered should affect the local turbulence. This necessitated the development of models describing the turbulence through differential transport equations.

A method of predicting the turbulent viscosity by use of partial differential equations was first proposed by Kolmogorov[92] and Prandtl [93]. From these two models, Prandtls' model was a one equation model. Where turbulent viscosity was given as follows:

$$\mu_T = \text{Constant}\rho k^{0.5} l \qquad (2.37)$$

Where k is the turbulent kinetic energy and l is turbulence length scale.

The turbulent kinetic energy term is modelled using a partial differential equation obeying the conservation laws. The most general form of the k equation as given in [89] is shown below, but the turbulent length scale is still a mean property of the flow which must be prescribed as a function to the model. Since this model is based on the partial differential kinetic energy equation, it is also know as the energy equation model

$$\frac{\partial(\rho t)}{\partial t} + \frac{\partial(\rho v_j k)}{\partial x_j} = \frac{\partial(\frac{\mu_e}{\sigma_k}\frac{\partial k}{\partial x_j})}{\partial x_j} + G_j + G_b - C_D\,\rho k^{3/2}/l \qquad (2.38)$$

$$G_j = \mu_T(\frac{\partial v_i}{\partial x_j} + \frac{\partial v_j}{\partial x_i})\frac{\partial v_i}{\partial x_j} \quad , \quad G_b = \beta g_k \frac{\mu_T}{\sigma_T}\frac{\partial T}{\partial x_j}$$

where :

G_b buoyancy production term

G_k mean production term

β thermal expancivity

g is the body force term

C_D drag coefficient

σ_k effective Prandtl number for turbulent kinetic energy (taken as a constant)

σ_T known constant

advantages of the model :

The major advantage of the model is that the turbulent part of the effective transport coefficient ($\Gamma_{\phi,T}$) is no longer zero when the velocity gradient term becomes zero. This leads to the prediction of better temperature profiles in pipe flow problems [90].

disadvantages of the model :

Since sufficiently precise algebraic prescription of l can rarely be made, the use of one equation models did not offer much accuracy compared to the mixing length model.

2.3.2.3 the two equation model :

In two equation models the length scale is also described by a differential transport equation. Various two equation models have been developed such as, *k-kl* model of Rodi and Spalding [94], *k-W* model of Spalding [95-96] and the *k*-ε model first developed by Harlow and Nakayama [97] and later appeared in the work of Launder *et al* [98-99]. From these the *k*-ε model has become the most widely used two equation model.

The general form of the ε equation is as follows :

$$\frac{\partial(\rho\varepsilon)}{\partial t}+\frac{\partial(\rho v_i \varepsilon)}{\partial x_j}=\frac{\partial(\frac{\mu_e}{\sigma_e}\frac{\partial\varepsilon}{\partial x_j})}{\partial x_j}+\frac{\varepsilon}{k}(c_1 G_j - c_2\rho\varepsilon) \qquad (2.39)$$

where : c_1, c_2, σ_e are constants (for plane jets the constants can be found in reference [100]), and the term G_j is the same as the one in equation (2.38).

Advantages of the model :

The *k*-ε model is the simplest model which gives meaningful results for recirculating flows such as flows inside confined environments, (combustion chambers furnaces, etc.).

Disadvantages of the model :

more expensive to implement than the previously described models

poor performance in rotating flows

2.3.2.4 higher order models :

Most turbulent flows are non-isotropic turbulent flows. Therefore the Boussinesq expression representing the turbulent fluctuation terms have to be abandoned if more realistic simulation of turbulence is required. One way of doing this is to directly solve the Reynolds stress equation by use of the second order moment of closure [101] (i.e. This is to simulate the unknown third order terms in the equations with second order correlations.). This led to the development of the Reynolds stress transport model [101]. The main advantage of the Reynolds stress transport model is its ability to predict strongly swirling and buoyant flow situations in combustors and furnaces. The main drawback of the model is the number of simultaneous differential equations that have to

be solved compared to the k-ε model. In a three dimensional flow problem, for the turbulence model alone 11 equations have to be solved compared to the 2 equations in the k-ε model. Secondly it is difficult to determine the large number of empirical constants that are contained in the equations, 14 constants compared to the 3 constants in the k-ε model.

2.3.2.5 direct numerical simulation:

The most fundamental approach to turbulence modelling is to use Direct Numerical Simulation (DNS). In this method Navier-Stokes equations are solved in grid size of Kolmogorov scales. This makes the control volume comparable with the smallest eddy size, and the time scale comparable with the life time of the smallest eddies, thus removing the need to use turbulence models. Although the method is simple, it needs extremely large computer capacity and very high speed processors to solve the equation set even for a simple flow situation. Even the currently developed super computers are not viable enough for this type of modelling. Therefore this method is not practical at the present time for engineering flow calculations.

2.3.2.6 near wall turbulence modelling :

The high Re number[1] form of the k-ε model is inadequate close to walls where the local Re number is low. Therefore various methods have been formulated to obtain turbulent

[1] flow is fully turbulent

properties close to solid boundaries. In the past decade the k-ε equations have been extended by various researchers for low Re number situations [102]. The most simple method to model near wall turbulence effects is via the wall function approach. This method is used extensively in the TEACH family of codes [103] and in commercial programs (such as FLUENT etc.).

2.3.2.6.1 wall function approach :

Close to a wall it can be assumed that the flow is of 1-D couette type. The fluid layer is assumed to be one of constant shear $\tau=\tau_W$ and constant heat flux $q'' = q''_w$. As stated by Hinze [104] The wall region is made up of 3 zones, these are; 1.) the viscous sub layer where molecular viscous effects are predominant, 2.) buffer layer where both molecular viscous effects and turbulent effects have the same proportions, and 3.) inertial sub layer where the flow is completely turbulent but shear stress can be taken as a constant equal to the wall shear stress. This simplifies the momentum equation for the near wall region to the form given bellow.

$$\tau = (\mu + \mu_T)\frac{du}{dy} \qquad (2.40)$$

which is represented in non-dimensional form as follows :

$$\frac{\tau}{\tau_w} = (1 + \frac{\mu_T}{\mu})\frac{du^+}{dy^+} \qquad (2.41)$$

where : $u^+ = \frac{u}{u_\tau}$; $u_\tau = \sqrt{\frac{\tau_w}{\rho}}$; $y^+ = \frac{u_\tau\, y\rho}{\mu}$

Neglecting the buffer layer and defining a point y^+=11.63 where the linear velocity profile in the viscous sub-layer (equation-2.42) meets the logarithmic velocity profile in the inertial sub-layer (equation-2.43) turbulent viscosity for the near wall region can be calculated [103].

$0 < y^+ \leq 11.63$:

$\mu_T/\mu << 1$

hence $u^+=y^+$ (2.42)

$11.63 < y^+ < 400$:

$\mu_T/\mu >> 1$

taking $\upsilon_t = Kyu_\tau$ the non-dimensional velocity term can be written as :

$u^+=(1/k)\ln(Ey^+)$ (2.43)

where :

K = 0.4187 Von Karmen constant

E=9.793 roughness parameter (smooth wall)

μ_T= turbulent viscosity

u_τ = friction velocity

$\tau_{W=}$ wall shear stress

Similar approach is adopted for near wall heat transport [103]. The corresponding equation has the following forms .

$$\dot{q}'' = (\Gamma + \Gamma_T) C_p \frac{dT}{dy} \qquad (2.44)$$

non-dimensional form :

$$\frac{\dot{q}''}{\dot{q}_w''} = \left(\frac{\Gamma}{\mu} + \frac{\Gamma_T}{\mu_T}\right) \frac{dT^+}{dy^+} \qquad (2.45)$$

for $y^+ \leq 11.63$

$\Gamma >> \Gamma_T$ hence $T^+ = \sigma_\phi y^+$ (2.46)

for $y^+ > 11.63$

$$\Gamma << \Gamma_T \text{ and } \frac{\Gamma_T}{\rho} = \frac{\upsilon_T}{\sigma_{\phi.T}} \approx \frac{k\, y\, u_\tau}{\sigma_{\phi.T}} \qquad (2.47)$$

$$\text{hence } T^+ = \frac{\sigma_{\phi.T}}{k} \ln y^+ + C_T \qquad (2.48)$$

$$T^+ = \sigma_{\phi T}[u^+ + P(\frac{\sigma_\phi}{\sigma_{\phi.T}})]$$

$$P(\frac{\sigma_\phi}{\sigma_{\phi.T}}) = 9.24[(\frac{\sigma_\phi}{\sigma_{\phi T}})^{3/4} + 1] \qquad (2.49)$$

The constant of integration C_T is expressed as a p function, the form which is extensively used is due to experimental studies of Jayathilaka [105]. The turbulent kinetic energy, dissipation rate and other relevant quantities, as given in reference [103] are as follows.

turbulent kinetic energy :

$$k = \frac{\tau_w}{\rho C_\mu^{1/2}} \qquad (2.50)$$

turbulent dissipation rate :

$$\varepsilon = \frac{C_\mu^{3/4} k^{3/2}}{Ky} \qquad (2.51)$$

Shear stress in the inertial sub-layer :

$$\tau_w = \frac{\rho C_\mu^{1/4} k^{1/2} K u}{\ln(Ey^+)} \qquad (2.52)$$

non-dimensional distance :

$$y^+ = \frac{y}{\nu}\sqrt{\frac{\tau_w}{\rho}} = \frac{y\rho C_\mu^{1/4} k^{1/2}}{\mu} \qquad (2.53)$$

2.3.3 Applications Of Single Phase Flow Models With The *k*-ε Turbulence Model :

From the turbulence models discussed, the *k*-ε model of turbulence is the most widely used one. This is due to the relative ease of incorporating it within the rest of the flow simulation equations, the requirement of less empirical constants compared to the higher order closure models and most importantly, it being the most validated turbulence model. Also the *k*-ε model performs well for confined flows in cylindrical geometry [106], which makes it attractive in single phase and two-phase combustion studies.

Single-phase flow models have been applied successfully to many industrial situations. The application of CFD to the prediction of flow and heat transfer in the secondary heat exchanger of a condensing boiler is considered by Malalasekera *et al* [107] giving good general agreement with the experimentally measured flow patterns and temperature measurements. Patankar *et al* [108] modelled chimney plumes flow under V/STOL aircraft and obtained reasonable agreement with the experimental values of velocity [109]. It can be pointed out that in most cases the accuracy of the numerically predicted results could be increased if accurate boundary condition values and empirical constant values are used in the *k*-ε equations.

2.3.4 Two Phase Spray Modelling

The two phase spray models developed so far can be broadly categorised into two groups. Locally Homogeneous Flow (LHF) models and Separated Flow models (SF).

2.3.4.1 locally homogeneous flow models :

The basic premise of LHF models is that the rates of transport between phases are fast in comparison to the rate of development of the flow field as a whole. This approximation requires all the phases (gas and liquid) to be in dynamic and thermodynamic equilibria. (i.e. at each point in the flow both phases have the same velocity and temperature and are in phase equilibrium). Therefore the use of a LHF model implies that the process is mixing controlled. The dispersed phase must have infinitely small particle sizes for this model to be quantitatively correct.

With these assumptions, properties at each point in the flow correspond to a thermodynamic equilibrium state attained when injector fluid and ambient fluid, at their initial state, are adiabatically mixed together at the ambient pressure of the spray. The equation of state provides the relationship between f, the mixture fraction (defined in this situation as, fraction of mass at a given point which originated from the injector), and the composition, temperature and density of the mixture. The only feature that distinguishes a two phase flow from a single phase flow when LHF methods are used is the presence of liquid at a high mixture fractions in the control volume. The droplet calculations are not directly included in the model. The liquid evaporation is accounted for via a saturation vapour pressure function of the form given below [110]:

$$\log_{10} P_{fg} = a - \frac{b}{T} \quad (2.54)$$

Where P_{fg} is the partial pressure of the fuel vapour in the control volume and a and b are known constants for a specific fuel. Since molar fractions of the gas phase are proportional to the partial pressures, the mass fractions of the evaporated and the liquid parts of the fuel can be obtained by the following relationships.

$$Y_{Fg} = Y_A \, P_{Fg} \frac{M_F}{P_A M_A} \qquad (2.55)$$

$$Y_{Ff} = Y_F - Y_{Fg} \qquad (2.56)$$

where Y_{Fg} and Y_{Ff} are the mass fractions of the liquid and vapour parts of the fuel present in a control volume (P_A, Y_A, M_A are the partial pressure, mass fraction and the molar mass of the air; Y_F, M_F, are the molar mass of the fuel and the mass fraction of fuel in a gas phase control volume).

2.3.4.1.1 ***evaluation of LHF models*:**

droplet life history calculations provide a systematic method for the evaluation of LHF models [110, 111]. The evaporation and burning characteristics of moving droplets in a gas flow field can be used to establish the differences between the droplets and the gaseous flow, with regard to velocities and temperatures. This gives a direct indication of the validity of the LHF model, and of the maximum droplet size in the spray where the LHF model can be expected to provide accurate results. It is generally found that drops having initial diameters of less than 10μm are required to satisfy the LHF approximation [110,111,112] This is due to the effects of finite interface transport rates becoming significant with larger diameter droplets.

2.3.4.1.2 *advantages and disadvantages of LHF models :*

The major advantage of LHF models for spray analysis is that they require minimum information concerning injector characteristics. This is due to initial droplet sizes and velocity distributions playing no role in the computations of the LHF calculations. The performance of SF models become very poor in the absence of accurate initial conditions at the injector exit. On the other hand, LHF models require far fewer empirical constants than SF models which reduces the 'fine tuning' associated with SF models. They could be used as a base line check for more complex models. Since the transport equations used in the model are of single flow type, existing single phase programs can be converted into LHF models with major savings in computer time and cost.

The main drawbacks of the model are; 1.) very little information can be obtained about the dispersed phase. 2.) due to the neglect of the inter-phase transport processes, the model tends to overestimate the rate of development of the spray [110, 112].

2.3.4.2 separated flow models :

In this type of modelling the transfer of mass, momentum and energy between the two phases are considered. Separated flow models can be subdivided into Deterministic Separated flow models (DSF) and Stochastic Separated Flow models (SSF) [113]. There are three major classes of DSF models in use today. They are Particle Source In Cell

(PSIC) also known as Discrete Droplet Model (DDM), Continuous Droplet Model (CDM) and The Continuum Formulation Model (CFM) [112].

It is generally assumed that the spray is dilute in these models. Therefore the volume fraction of the liquid phase is considered to be negligibly small in most models. It is implied that although particles interact with the gas phase they do not interact with each other. Drop-drop effects such as collisions, coalescence and secondary break up effects are therefore neglected. Transport expressions for single drops evaporating in an infinite medium are used to calculate the transfer of mass, energy etc. between the two phases.

2.3.4.2.1 *discrete droplet model (DDM) or particle source in cell (PSIC)*

All DDM models employ a Eulerian formulation for gas motion and a Lagrangian formulation for the particle motion. This involves dividing the flow field, at the injector exit or at some other location down stream of the injector (where drop properties are assumed to be known) into a finite number of droplet groups. Each group is assigned an initial diameter, velocity, direction, temperature, position and concentration. The history of each group is then computed until complete evaporation occur or they pass out of the boundaries of the flow field.

the method of solution :

In order to apply the PSI-Cell method [114,115,116], it is first necessary to subdivide the flow field into a series of cells. Each cell is a control volume for the gaseous phase. As the droplets traverse these cells in the flow field they may be subjected to :

1. evaporation or condensation resulting in a source (or sink) of gaseous mass to the fluid in the cell.

2. acceleration or deceleration resulting in a momentum addition or subtraction in cell's fluid in the direction of the droplet motion.

3. heat transfer between the gas and the droplet results in a source (or sink) of thermal energy to the fluid in the cell.

The overall solution procedure for a PSIC model is shown in the following figure.

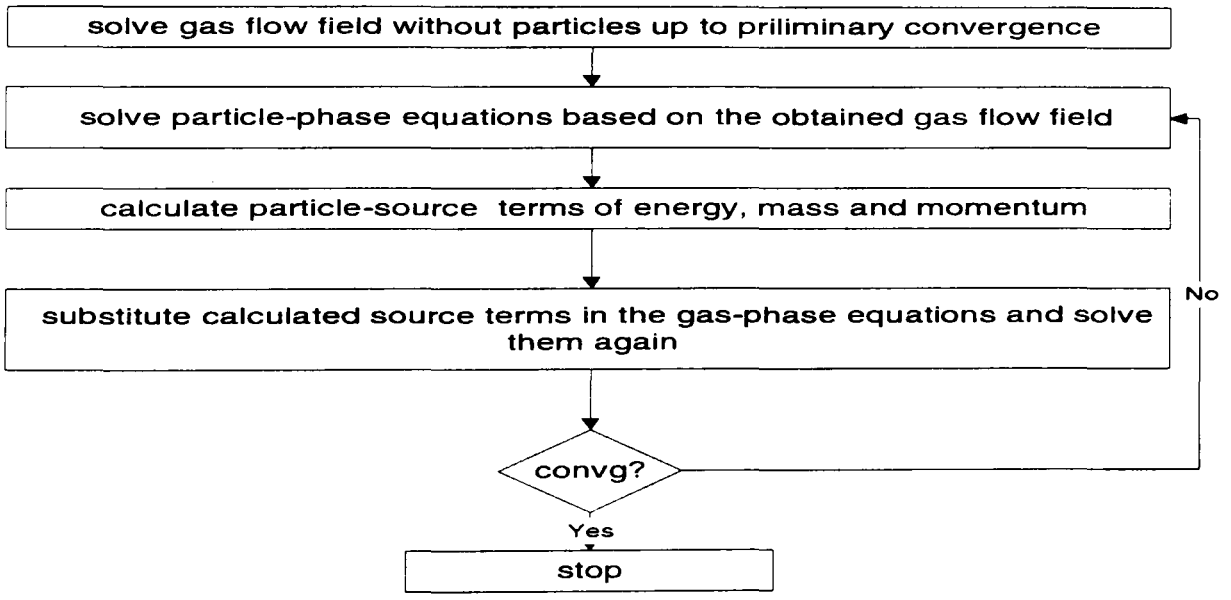

fig. 2.2 flow chart for the PSI-Cell method

The gas phase is normally solved by the use of the TEACH [103] code. Extra source terms are added to the code in order to accommodate the mass, momentum and energy transfer from the droplet phase [117].

The droplet trajectories, size and temperature history are obtained by integrating the equations of motion for the droplets in the gas flow field and utilising ordinary differential equations (ODEs) governing the droplet mass and heat transfer rates [114]. Recording the mass, momentum and energy of the droplets on crossing cell boundaries provides the droplet source terms for the gas flow equations.

2.3.4.2.2 *continuous droplet model (CDM)*

The basic features of the gas phase solution of this method is similar to the DDM approach [8,118] where extra source terms are added to the gas phase finite volume equations to incorporate the effects of the droplet phase. The two methods differ in that in the CDM method the drop properties are represented by a statistical distribution function defined at all positions of the flow field. Conservation principles yield a transport equation for the distribution function which is solved along with the gas conservation equations. This is in contrast to the PSIC or DDM method, where a discrete number of droplet sizes representing a droplet group are tracked in a Lagrangian manner from the injector by solving the ODEs with time as the independent variable.

Since the method requires the spray equation to be solved with the governing gas phase equations for the whole flow field, it presents serious computer storage requirements.

This is due to the number of dimensions needed to specify the spray probability function. Therefore CDM approach is best suited when only few phenomena are considered. For example, for drops of pure liquid evaporating at wet bulb conditions the probability distribution function contains no less than eight independent variables $f(r_p, x_p, u_p, t)dr_p dx_p du_p$ (droplet radii in the range of dr_p about r_p located in the volume dx_p about x_p with the velocities u_p at time t). The problem is compounded if additional factors such as temperature and concentration variation are to be considered, leading to significant increase in computer time and storage requirement. Therefore this type of modelling is the least used method.

2.3.4.2.3 *continuum formulation model (CFM)*

In this method both droplets and gas are treated as they were inter-penetrating continua, both droplets and gas phase having separate partial differential equations (PDEs) governing the transport of energy, mass, momentum, etc. The basic assumptions of the model are summarised below. The main feature of this model is the modelling of particle turbulent fluctuations, which is used to account for particle diffusion that occur in real combustion situations [89, 119].

1. at each location of the flow field, particle phase and gas phase coexist and inter-penetrate into each other. At these control volume locations each of the two phases, has its separate temperature, velocity and volume fraction. However each particle size group has the same velocity and temperature.

2. each particle group has its own turbulent fluctuation resulting in particle turbulent transport of mass momentum and energy.

3. The change in particle mass, momentum, energy and turbulent fluctuations are determined by convection, diffusion and production of these quantities governed by the droplet phase PDEs and the interaction with the gas-phase equations.

The advantages of the model are its ability to account for various turbulent transport processes of particle phase. Also the gas and the particle phase can be treated by a unified numerical method

The main disadvantage of CFM models is the numerical diffusion of the droplet phase. To avoid numerical diffusion (which becomes very significant near the injector exit) the model needs very small computational grid for the dispersed phase calculations.

2.3.4.2.4 ***stochastic separated flow models*** **:**

In most DSF models (apart from CFM formulation) the effect of dispersed phase turbulent interactions are ignored. There are three main types of turbulent interactions; (1) turbulent transport of the dispersed phase itself; (2) modification of continuos phase turbulent properties by transport from the dispersed phase (turbulence modulation) (3) modification of the properties of inter-phase transport rates by turbulence fluctuations

[113]. In the SSF method these disperse phase turbulence interactions are modelled using random walk computations for the motion of the disperse phase.

As stated by Faeth [113] the main features of the SSF method are as follows. In the SSF analysis as the disperse phase elements move through the flow they are assumed to interact with a succession of turbulent eddies. This is simulated by a random walk computation. Properties within a particular eddy are assumed to be uniform, but the properties would change in a random manner from one eddy to the next. The properties in each eddy are obtained from the continuous phase analysis. The dispersed phase calculations are the same as the DSF approach except that instantaneous properties are used for the local environment of the dispersed phase elements rather than mean properties. Thus in principle the method can treat all aspects of dispersed phase turbulence interactions, subjected to the limitations of the gas phase (continuous phase) turbulence model.

2.3.5 Modelling Of Combustion :

The combustion process can be broadly categorised into two kinds; diffusion governed and premixed. In a premixed situation the fuel and oxidiser are supplied to the combustion chamber already mixed according to a pre-determined ratio. Rocket engines and spark ignition engines are good examples of premixed combustion systems.

A diffusion flame is defined as any flame in which the fuel and oxidiser are initially separate [8]. In diffusion governed combustion the fuel is normally injected into an air

stream and the combustion process proceeds simultaneously with the mixing process. Diesel engines, gas turbine combustors and industrial furnaces provides examples of this type of combustion.

Historically two principal modelling approaches have been used for the combustion processes. One approach is to assume combustion has no affect on the mixing, therefore the effect of combustion on turbulence can be neglected. Although this could lead to errors on the micro-scale level, the method could provide good qualitative information about the flow field. This type of combustion modelling has been referred to in the literature as 'mixed-is-burnt' type. The advantage of the above method is that it allows a higher number of species to be taken into account in the combustion model without the addition of extra partial differential equations [14]. On the other hand turbulence-combustion interaction methods attempts to improve the micro-mixing predictions by including a simplified combustion model (such as a single step fast reaction), which is incorporated within the main flow equations. Although this type of modelling can improve the mixing predictions, the data obtained from the post combustion maps are less informative about the global picture than the mixed-is-burnt type models. This is primarily due to the use of fewer number of species in this type of models. Nevertheless, it is possible to improve the predictions if individual conservation equations for each (important) species are modelled with the rest of the flow equations. It should be borne in mind that each species adds an extra differential equation to the equation set leading to a further increase in computer time.

A great deal of research has been done on combustion-turbulence interactions. In the following paragraphs the fluid dynamic aspects of the combustion-turbulence interaction modelling will be introduced using a simplified fast reaction model. This will be followed by the joint probability distribution method, which is although only used in single-phase flow modelling at present, has a great potential in two-phase reactive flow situations.

2.3.5.1 simplified probability density function (PDF) fast reaction model :

In this approach the chemistry is assumed to be fast enough to be described by a global single step reaction. It is also assumed that one reactant which is locally in excess causes all other reactants to be consumed stiochiometrically or both reactants are present in stiochiometic proportions. The mass exchange coefficients ($\Gamma_{fuel} = \Gamma_{oxidiser}$) are also considered to be equal. By defining a strictly conservative scalar variable known as the mixture fraction (mass fraction of the total fuel, i.e. burnt and unburnt fuel), the combustion flow can be calculated using a single partial differential equation.

$$\frac{\partial(\rho f)}{\partial t} + \frac{\partial(\rho u_j f)}{\partial x_j} = \frac{\partial}{\partial x_j}\left(\Gamma_f \frac{\partial f}{\partial x_j}\right) \qquad (2.57)$$

The equation can be solved subject to boundary conditions of known values of mixture fraction at inlet (the local value of the mixture fraction will be zero if the mixture at a point only contains oxidant and equals 1 if it contains fuel only.) and zero flux across boundaries. Given the resulting mixture fraction values the mass fractions after combustion can be obtained by the following equations.

$$f_{st} < f < 1 \quad m_{ox} = 0 \quad m_{fu} = \frac{f - f_{st}}{1 - f_{st}} \qquad (2.58)$$

$$0 < f < f_{st} \quad m_{fu} = 0 \quad m_{ox} = \frac{f_{st} - f}{f_{st}} \qquad (2.59)$$

$$f_{st} = \frac{1}{s+1} \qquad (2.60)$$

where :

m_{ox} = mass fraction of oxidiser in the cell

m_{fu} = mass fraction of fuel in the cell

s = mass of oxidiser needed for the stiochiometric combustion of 1kg of fuel

In turbulent combustion the fuel stream breaks up into eddies with inter-diffusion at the eddy boundaries, which lead to the fluctuation of the mixture fraction. Therefore all dependent variables of the mixture fraction will also fluctuate. If this fluctuations are not taken into account the predicted temperature map will be unrealistic [120,121]. The most convenient way of considering the fluctuations is by a statistical approach, based on the modelled equation of mixture fraction variance (g) and an assumption about the form of the probability density function (PDF) of the mixture fraction[121,122,123].

$$g = (\hat{f} - \bar{f})^2 \qquad (2.61)$$

$$\frac{\partial(\rho g)}{\partial t}+\frac{\partial(\rho u_j g)}{\partial x_j}=\frac{\partial}{\partial x_j}\left(\Gamma_f \frac{\partial g}{\partial x_j}\right)+C_{g1}\mu_t\left(\frac{\partial f}{\partial x_j}\right)^2-C_{g2}\bar{\rho}\frac{\varepsilon}{k}g \qquad (2.62)$$

Where :

C_{g1} and C_{g2} are modelled constants and μ_t is the turbulent viscosity.

Various probability density functions have been used. The best results were obtained using clipped Gaussian [124] and Beta function [125] PDFs. Jones and Whitelaw [126] made comparisons between models using the clipped gaussian and the beta function and reported that the results were very similar.

2.3.5.1.1 the calculation procedure of time-averaged properties using the PDF method :

- The mean values of *f* and *g* for each control volume cell are calculated from their respective partial differential equations. The values of *f* and *g* are used to generate the chosen PDF.
- A large number of $\Delta\hat{f}$ values are generated between 0 and 1.
- For each $\Delta\hat{f}$ value the species mass fractions are calculated using equations (2.58 - 2.59) now considering the *f*s in the equations as instantaneous values ($\hat{f}$).
- A set of $\hat{h}$ (instantaneous enthalpy) are calculated based on a linear relationship between the mean values of *h*, f (of the control volume) and the instantaneous $\hat{f}$ set.

- A single value is guessed for the instantaneous temperature $\hat{T}$ set which is then used to generate a $\hat{Cp(T)}$ set.

- An iteration is performed between $\hat{T}, \hat{h}, \hat{m}_j, \hat{Cp}$ until the instantaneous temperature set is constant.

- Based on the converged values of $\hat{T}$, instantaneous density values are calculated using the ideal gas equation.

- Finally the time averaged values of each scalar variable for each cell is obtained by the following general equation.

$$\bar{\phi} = \int_0^1 \phi(\hat{f}) p(\hat{f}) d\hat{f} \qquad (2.63)$$

- The calculation then proceeds to the next iteration level to solve all the time averaged partial differential equations again.

Smith and Smoot [127] compared a PDF combustion model of the above type (i. e. with a top hat probability distribution) with experimental results obtained from a laboratory type axisymertic combustor. The fuel was natural gas which was injected from a centred jet. Preheated air was supplied from an annulus surrounding the fuel tube. They observed that the overall mixture fraction values agreed reasonably with the values obtained from corresponding experimental data. They also noticed that the mixture fraction values were least accurate in the early regions of the combustor near the centre line. This was attributed to the sensitivity of the technique to the initial turbulence levels

of the primary (fuel) and the secondary (air) streams. The above finding reiterates the fact that specifying accurate turbulence parameters is very important in combustion calculations.

Jones and Whitelaw [106] compared the computational results from a program developed by Jones [128] (with a beta PDF distribution) having the above chamber configuration and methane as fuel with the experimental results of Owen [129] and observed the following :-

The end of the recirculation region is found to be downstream of the measured values, and the subsequent calculated velocity changes are slower than the measured values. They also noted deficiencies in the calculated mixture fraction values. This was attributed to the mixing of fuel and air proceeding at too slow a rate. Reducing the exchange coefficient to an unrealistic value of 0.2 (normally the value is 0.7-0.9) did not alleviate this behaviour. The reason for the above was thought to be insufficient prediction of radial turbulent diffusion. This leads to the conclusion that deficiencies in turbulent modelling need to be corrected if more realistic values are to be obtained.

In general due to the simplicity of the geometry and the relative ease of supplying initial condition parameters, applying the model to coaxial jets discharged into sudden expansion chambers give good agreement with experimental results.

2.3.5.2 joint probability distributions and the Monte Carlo method :

The conventional approach of describing the system via the mixture fraction and its variance is limited to two species (fuel and oxidant). A more complete description of the flow field could be achieved using a joint probability density function (pdf) of the three components of velocity and the composition variables (mass fractions and the enthalpy). This method was pioneered and extensively used in the combustion field by Pope and co-workers [130-134].

Pdf methods derive their advantage from the more complete description of the turbulent flow field [134]. Consider a flow involving three scalars such as fuel mass fraction, oxidant mass fraction and enthalpy, with a two equation model of turbulence (k-ε) at each point the turbulence flow field is represented by 8 quantities. The three mean velocities, the three mean scalars and the k and ε. In the pdf method, on the other hand the flow is described by the joint probability of the three velocities and the three scalars. At each point this is a function of six independent variables (turbulence is modelled using conventional gradient diffusion techniques). The equation governing the transport of the above joint probability density function is solved using monte-carlo methods [133, 134] due to the computational efficiency of this method compared to the standard numerical techniques (If the equations are solved numerically the computational time will increase by α^n where n is the number of variables on the other hand if the monte-carlo method is

used the time will be $n\alpha_i$). Clearly the six dimensional pdf contains more information than the standard equation set which models each variable separately.

Another important feature of the method is the ability to incorporate the complicated reaction terms without modelling approximations. This is in marked contrast to conventional turbulence models in which the mean reaction rate can be determined only in special circumstances - when the reaction rate is linear, or when it is very fast or very slow compared with the turbulence time scales [130, 134]. This allows this type of model to handle both diffusion and premixed combustion with minimum modifications.

Since Coherent Anti-stokes Raman Spectroscopy (CARS) combined with Laser Doppler Velocimetry (LDV) measurements has allowed velocity-scalar measurements in turbulent reactive flow fields [135], the above method could be greatly enhanced in the future if this information is used to validate the modelled data.

2.3.6 Conclusion :

A major disadvantage of the current models (SF type) is their limited or non-applicability to churn flow regions (churning flow occurs near the nozzle exit, where the volume fraction of the mixture occupied by the liquid can equal or exceed that of the gas volume fraction.) where the liquid cannot be considered to be dispersed in the continuos gas phase. The process by which a churn flow is generated from a liquid sheet is part of the atomisation problem which has not been well understood so far. Only few attempts have

been taken to model this initial drop break up [136], also drop-drop effects such as coalescence, secondary break up which have significant effects in dense regions of the sprays are only considered in few models [137]. If a more complete understanding of two-phase spray flows is to be obtained the above effects need to be included in a more detailed manner in future models.

It has been suggested by may researchers [113, 138] that as a alternative to developing complex modules to calculate near injector properties, to use a LHF approach for the near injector region. A study carried out by Wu et al [138] at elevated pressures suggests that LHF provides reasonable estimates of the lateral spreads of the spray. Measurements of velocities of pressure atomised sprays, using LDA, were also given as evidence that LHF ideas may be pertinent in the near injector region [138].

Based on the above it can be stated that although the LHF analysis is a simplification of the true nature of the spray physics it could still be used as a good design tool on its own or in-conjunction with more advance SF models. Also as a further improvement to the current LHF models, a droplet evaporation module could be included within the program as explained in chapter-4 of this thesis.

CHAPTER-3

THEORETICAL AND COMPUTATIONAL FORMULATION OF DROPLET EVAPORATION MODELS

3.1 Introduction :

The chapter describes the mathematics and programming techniques used in the formulation of the droplet evaporation models. Three transient heating models were formulated as part of this research project. Namely:-

1.) a quasi-steady gas phase with infinite conductivity in the liquid phase type model

2.) a quasi-steady gas phase with finite liquid conductivity type model (liquid heating model) ; and

3.) an unsteady gas phase with an infinite conductivity in the liquid phase type model

After a general discussion of the evaporation process, the mathematical features of each model are discussed. This is then followed by a section describing the computational treatment, where again after a discussion of the common programming features, individual details and flow charts are presented.

3.2 Theoretical Formulation :

3.2.1 The physical representation of the problem :

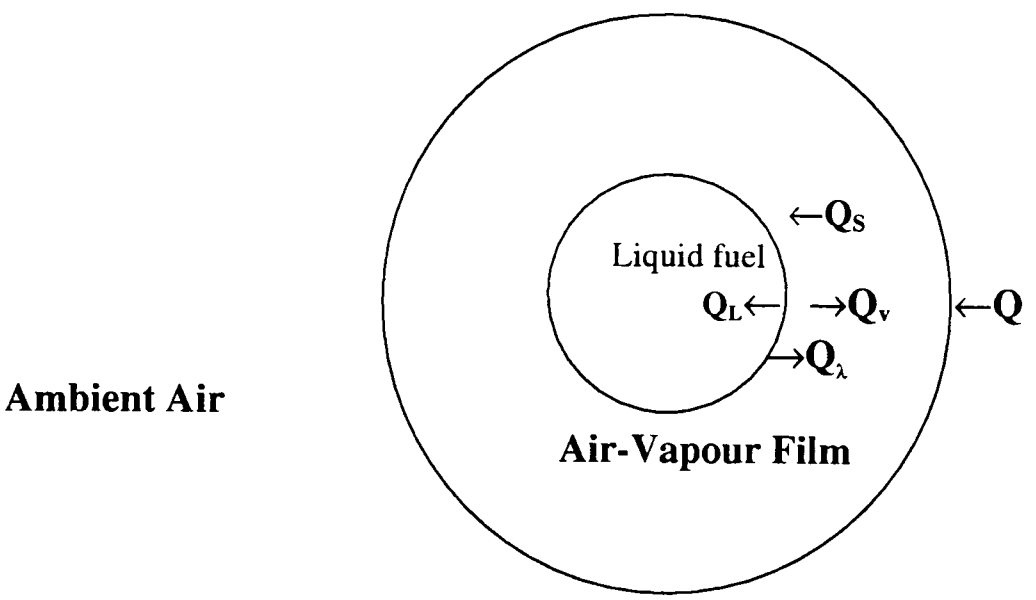

fig. 3.1 heat transfer to the droplet

Figure 3.1 shows the heat transfer process to a stationary droplet. Initially the droplet is at a low temperate. When it is introduced into a high temperature and high pressure environment such as a combustion chamber, heat transfer takes place from the surroundings to the droplet. This causes the droplet temperature to increase with time resulting in an increased rate of evaporation. The fuel vapour also diffuses away from the droplet surface, driven by a concentration gradient. The problem is one of combined heat and mass transfer. The total heat transfer(Q) from the surroundings to the droplet goes in three ways: (1) to heat up the liquid droplet (Q_L); (2) to vaporise the liquid ($Q\lambda$); and (3) to heat up the diffusing vapour to the surrounding film temperature (Q_v). Therefore, heat that finally arrives at the droplet surface (Q_S) is given by $Q_L + Q_\lambda$.

The following assumptions are common to all the models formulated in this research :

1. the droplet is spherically symmetrical (convective effects are neglected);
2. the air vapour film surrounding the droplet is at a constant pressure equal to the ambient air pressure;
3. the Mass transfer process is only diffusion driven and unidirectional;
4. the fuel droplet is at phase equilibrium with the gas phase at all times and the fuel vapour pressure at the droplet surface is at its saturation vapour pressure value.

3.2.2 The quasi-steady gas phase with infinite liquid conductivity model :

In this approach it is assumed that the droplet temperature is spatially uniform but temporally varying. The governing equations based on El Wakil *et al* formulation [17] for heat and mass transfer are as follows:

$$m_L C_{P_L} \frac{dT_d}{dt} = A_0 h_c (T_g - T_d) \frac{z}{e^z - 1} + L \frac{dm}{dt} \qquad (3.1)$$

$$\frac{dm}{dt} = -A_0 K_c P_{fl} \alpha \qquad (3.2)$$

where :

$$\alpha = \frac{P_T}{P_{fl}} \ln\left(\frac{P_T}{P_T - P_{fl}}\right) \qquad (3.3)$$

$$z = -\frac{dm}{dt} C_{P_g} / h_c A_0 \qquad (3.4)$$

Equation 3.1 gives the instantaneous droplet temperature and equation 3.2 gives the droplet gasification rate. Therefore solving these two equations, the droplet mass, diameter and temperature can be obtained for each time step. Since these two equations are two coupled ordinary differential equations they have to be solved simultaneously. There are no analytical solutions to these equations, therefore they are solved using a fourth order Runge-Kutta (RK) technique. (Computer implementation of the Runge-Kutta procedure is given in section 3.3.3)

At each time step all the property variables in the two governing equations are calculated for a mean mixture of air and fuel vapour, based on an average film temperature. Whenever possible correlations developed for high pressure gas mixtures are used for the property calculations (Appendix-A).

3.2.3 The quasi-steady gas phase with finite liquid conductivity model :

In this model it is no longer assumed that the liquid temperature is spatially constant. The liquid temperature is now spatially and temporally varying. To satisfy these conditions the heat transfer equation has to be modified in the following manner.

$$\frac{\partial T}{\partial t} = \alpha\left(\frac{\partial^2 T}{\partial r^2} + \frac{2}{r}\frac{\partial T}{\partial r}\right) \qquad (3.5)$$

$$\alpha = \frac{k_L}{C_{P_L}\,\rho_L} \qquad (3.6)$$

$$4\pi r^2 k_L \left(\frac{dT}{dr}\right)_s = h_c 4\pi r^2 (T_\infty - T_s)\frac{z}{e^z - 1} + \frac{dm}{dt} L \qquad (3.7)$$

$$\left(\frac{\partial T}{\partial r}\right)_{r=0} = 0 \qquad (3.8)$$

The mass transfer equation is taken as the one given in section 3.2.2 Since the droplet is evaporating, the droplet radius is also a function of time. Therefore the problem under consideration is a moving boundary problem. To over come this a normalised co-ordinate system is used. Transformation of the one dimensional heat transfer equation into a normalised form is as follows:-

T = temperature

t = time

r = radial position within the droplet

R = position of the droplet surface

R_0= initial position of the droplet surface

$\alpha = \alpha(T)$ thermal diffusivity

$\dot{m}''$ = mass gasification flux (<0)

$$\frac{\partial T}{\partial t} = \alpha\left(\frac{\partial^2 T}{\partial r} + \frac{2}{r}\frac{\partial T}{\partial r}\right) \qquad (3.9)$$

$$\tau = \frac{t}{R_0^2} \quad \omega = \frac{r}{R(\tau)} \quad \varsigma = \frac{R}{R_0} \qquad (3.10)$$

$$\frac{\partial \tau}{\partial t} = \frac{1}{R_0^2} \qquad (3.11)$$

$$\frac{\partial R}{\partial t} = \frac{dR}{dt} = \frac{\partial R(\tau)}{\partial \tau}\frac{\partial \tau}{\partial t} = \frac{\partial R}{\partial \tau}\frac{1}{R_0^2} \tag{3.12}$$

$$R_0 \frac{d\varsigma}{d\tau} = \frac{dR}{d\tau} \tag{3.13}$$

$$\frac{dR}{dt} = \frac{1}{R_0}\frac{d\varsigma}{d\tau} \tag{3.14}$$

by definition the surface regression rate is governed by the mass gasification rate, therefore :

$$\frac{d(\rho \frac{4}{3}\pi R^3)}{dt} = \dot{m}'' 4\pi R^2 \tag{3.15}$$

$$\frac{dR}{dt} = \frac{\dot{m}''}{\rho}$$

$$\frac{d\varsigma}{d\tau} = \frac{R_0 \dot{m}''}{\rho} \tag{3.16}$$

$$\omega = \omega(R, r) \tag{3.17}$$

$$\frac{\partial \omega}{\partial R} = -\frac{r}{R^2} \tag{3.18}$$

$$\frac{\partial \omega}{\partial t} = \frac{\partial \omega}{\partial R}\frac{\partial R}{\partial t} + \frac{\partial \omega}{\partial r}\frac{\partial r}{\partial t} \tag{3.19}$$

r is not a function of t therefore :

$$\frac{\partial \omega}{\partial t} = \frac{r}{R^2}\frac{\partial R}{\partial t} \tag{3.20}$$

$$T(r,t) \Rightarrow T(\omega,\tau) \tag{3.21}$$

$$\frac{\partial T}{\partial t} = \frac{\partial T}{\partial \tau}\frac{\partial \tau}{\partial t} + \frac{\partial T}{\partial \omega}\frac{\partial \omega}{\partial t} \tag{3.22}$$

$$\frac{\partial T}{\partial t} = \frac{\partial T}{\partial \tau}\frac{1}{R_0^2} + \frac{\partial T}{\partial \omega}\left(-\frac{r}{R^2}\frac{1}{R_0}\frac{d\varsigma}{d\tau}\right) \tag{3.23}$$

$$\frac{\partial T}{\partial r} = \frac{\partial T}{\partial \omega}\frac{\partial \omega}{\partial r} + \frac{\partial T}{\partial \tau}\frac{\partial \tau}{\partial r} \tag{3.24}$$

since τ is independent of r :

$$\frac{\partial T}{\partial r} = \frac{1}{R}\frac{\partial T}{\partial \omega} \tag{3.25}$$

$$\frac{\partial^2 T}{\partial r^2} = \frac{\partial\left(\frac{1}{R(\tau)}\frac{\partial T}{\partial \omega}\right)}{\partial r} = \frac{\partial T}{\partial \omega}\frac{\partial}{\partial r}\left[\frac{1}{R(\tau)}\right] + \frac{1}{R(\tau)}\frac{\partial}{\partial r}\left[\frac{\partial T}{\partial \omega}\right] \tag{3.26}$$

Since R is not a function of r :

$$\frac{\partial^2 T}{\partial r^2} = \frac{1}{R(\tau)}\left[\left[\frac{\partial^2 T}{\partial \omega^2}\frac{\partial \omega}{\partial r}\right] + \left[\frac{\partial^2 T}{\partial \omega \partial \tau}\frac{\partial \tau}{\partial \omega}\frac{\partial \omega}{\partial r}\right]\right] \tag{3.27}$$

Since T is not a function of r :

$$\frac{\partial^2 T}{\partial r^2} = \frac{1}{R^2}\frac{\partial^2 T}{\partial \omega^2} \tag{3.28}$$

substituting equations (3.23, 3.25, 3.28) in equation (3.9) we have :

$$\frac{\partial T}{\partial \tau}\frac{1}{R_0^2} + \frac{\partial T}{\partial \omega}\left(-\frac{r}{R^2}\frac{1}{R_0}\frac{d\varsigma}{d\tau}\right) = \alpha\left[\frac{2}{r}\frac{1}{R}\frac{\partial T}{\partial \omega} + \frac{1}{R^2}\frac{\partial^2 T}{\partial \omega^2}\right] \tag{3.29}$$

$$\varsigma^2\frac{\partial T}{\partial \tau} = \alpha\left[\frac{\partial^2 T}{\partial \omega^2} + \left(\frac{2}{\omega} + \omega\varsigma\frac{d\varsigma}{d\tau}\right)\frac{\partial T}{\partial \omega}\right] \tag{3.30}$$

The equation takes a special form at r=0 (ω=0) dictated by the *l'Hospitals* rule.

$$\varsigma^2 \frac{\partial T}{\partial \tau} = \alpha[\frac{\partial^2 T}{\partial \omega^2} + (0 + \lim_{\omega \to 0} \frac{2}{\omega} \frac{\partial T}{\partial \omega})] = \alpha[\frac{\partial^2 T}{\partial \omega^2} + 2.*1*\frac{\partial^2 T}{\partial \omega^2}] = 3\alpha \frac{\partial^2 T}{\partial \omega^2}$$

(3.31)

Finite Difference form of the above equations is as follows :

where superscript *n* stands for the known value and *n+1* is the value being calculated

for $\omega > 0$

$$\varsigma^2 \frac{(T_i^{n+1} - T_i^n)}{\Delta\tau} = \alpha[\frac{T_{i+1}^{n+1} - 2T_i^{n+1} + T_{i-1}^{n+1}}{\Delta\omega^2}] + \alpha[\frac{2}{\omega_i} + \omega_i \varsigma \frac{d\varsigma}{d\tau}][\frac{T_{i+1}^{n+1} - T_{i-1}^{n+1}}{\Delta\omega}]$$

(3.32)

$$T_{i+1}^{n+1}\ [\frac{\alpha}{\Delta\omega^2} + \alpha(\frac{2}{\omega_i} + \omega_i \varsigma \frac{d\varsigma}{d\tau})\frac{1}{2\Delta\omega}] \quad + \quad T_i^{n+1}[(-\frac{2\alpha}{\Delta\omega^2}) - \frac{\varsigma^2}{\Delta\tau}]$$

$$+ \quad T_{i-1}^{n+1}[\frac{\alpha}{\Delta\omega^2} - \alpha(\frac{2}{\omega_i} + \omega_i \varsigma \frac{d\varsigma}{d\tau})\frac{1}{2\Delta\omega}] = \quad -\frac{\varsigma^2}{\Delta\tau} T_i^n$$

(3.33)

For $\omega = 0$

$$\varsigma^2 \frac{(T_i^{n+1} - T_i^n)}{\Delta\tau} = 3\alpha \frac{(T_{i+1}^{n+1} - 2T_i^{n+1} + T_{i-1}^{n+1})}{\Delta\omega^2} \qquad (3.34)$$

due to symmetry at the droplet centre $T_{i-1} = T_{i+1}$

$$T_{i+1}^{n+1}(2 * \frac{3\alpha}{\Delta\omega^2}) + T_i^{n+1}(-2 * \frac{3\alpha}{\Delta\omega^2} - \frac{\varsigma^2}{\Delta\tau}) = \frac{\varsigma^2}{\Delta\tau} T_i^n \qquad (3.35)$$

The boundary condition at the surface is further modified by including a correction for heat transfer due to mass transfer based on El Wakil [17]. Also to accommodate two components if necessary (as in a multi-component droplet), the *dm/dt* terms for each component are included separately in the boundary condition equation.

$$\left(\frac{\partial T}{\partial \omega}\right)_s = \frac{h_c R_0 \varsigma (T_\infty - T_s)}{k_L} C_f + \frac{1}{k_L 4\pi R_0 \varsigma}\left(\frac{dm_1}{dt} L_1 + \frac{dm_2}{dt} L_2\right) \tag{3.36}$$

where $C_f = \dfrac{z}{e^z - 1}$ (3.37)

$$T_{i+1}^{n+1} = T_{i-1}^{n+1} + 2\Delta\omega \left[\frac{h_c R_0 \varsigma (T_\infty - T_i^{n+1})}{k_L} C_f + \frac{1}{k_L 4\pi R_0 \varsigma}\left(\frac{dm_1}{dt} L_1 + \frac{dm_2}{dt} L_2\right)\right] \tag{3.38}$$

substituting T_{i+1} term in equation (3.33), the following equation is obtained

$$\left(T_{i-1}^{n+1} + 2\Delta\omega \left[\frac{h_c R_0 \varsigma (T_\infty - T_i^{n+1})}{k_L} C_f + \frac{1}{k 4\pi R_0 \varsigma}\left(\frac{dm_1}{dt} L_1 + \frac{dm_2}{dt} L_2\right)\right]\right)\left[\frac{\alpha}{\Delta\omega^2} + \alpha\left(\frac{2}{\omega_i} + \omega_i \varsigma \frac{d\varsigma}{d\tau}\right)\frac{1}{2\Delta\omega}\right]$$

$$+ T_i^{n+1}\left[\left(-\frac{2\alpha}{\Delta\omega^2}\right) - \frac{\varsigma^2}{\Delta\tau}\right]$$

$$+ T_{i-1}^{n+1}\left[\frac{\alpha}{\Delta\omega^2} - \alpha\left(\frac{2}{\omega_i} + \omega_i \varsigma \frac{d\varsigma}{d\tau}\right)\right]\frac{1}{2\Delta\omega} = -\frac{\varsigma^2}{\Delta\tau} T_i^n \tag{3.39}$$

Which can be rearranged as follows:

$$T_i^{n+1}\left(-2\Delta\omega\frac{h_c R_0\varsigma}{k_L}C_f\left[\frac{\alpha}{\Delta\omega^2}+\alpha\left(\frac{2}{\omega_i}+\omega_i\varsigma\frac{d\varsigma}{d\tau}\right)\frac{1}{2\Delta\omega}\right]+\left(-\frac{2\alpha}{\Delta\omega^2}\right)-\frac{\varsigma^2}{\Delta\tau}\right)$$

$$+$$

$$T_{i-1}^{n+1}\left(\left[\frac{\alpha}{\Delta\omega^2}+\alpha\left(\frac{2}{\omega_i}+\omega_i\varsigma\frac{d\varsigma}{d\tau}\right)\frac{1}{2\Delta\omega}\right]+\left[\frac{\alpha}{\Delta\omega^2}-\alpha\left(\frac{2}{\omega_i}+\omega_i\varsigma\frac{d\varsigma}{d\tau}\right)\frac{1}{2\Delta\omega}\right]\right)$$

$$=$$

$$2\Delta\omega\left[-\frac{1}{k_L 4\pi R_0\varsigma}\left(\frac{dm_1}{dt}L_1+\frac{dm_2}{dt}L_2\right)-\frac{h_c R_0\varsigma T_\infty}{k_L}C_f\right]\left[\frac{\alpha}{\Delta\omega^2}+\alpha\left(\frac{2}{\omega_i}+\omega_i\varsigma\frac{d\varsigma}{d\tau}\right)\frac{1}{2\Delta\omega}\right]$$

$$-\frac{\varsigma^2}{\Delta\tau}T_i''$$

(3.40)

All of these equations have the basic form given below, which can be conveniently represented by a tri-diagonal matrix for calculation purposes.

$$T_{i+1}^{n+1}A_j + T_i^{n+1}B_j + T_{i-1}^{n+1}C_j = D_j \qquad (3.41)$$

The normalised heat transfer equation is solved using a fully implicit finite difference method and the mass transfer equation is solved using a predictor-corrector optimisation procedure. The method of solution is explained in section 3.3.5.

3.2.4 Unsteady gas phase model :

In this model the gas phase temperature and the mass fraction are taken as spatially and temporally varying. This makes the gas phase unsteady. To concentrate on the gas phase, the liquid temperature is kept spatially uniform.

The model is formulated by starting from the general Navier-Stokes equation set and simplifying it for a one dimensional isobaric non-convective situation (assuming that mass transfer in the air-vapour film is only diffusion driven).

The formulation for the necessary equations are carried out as follows :

energy equation :

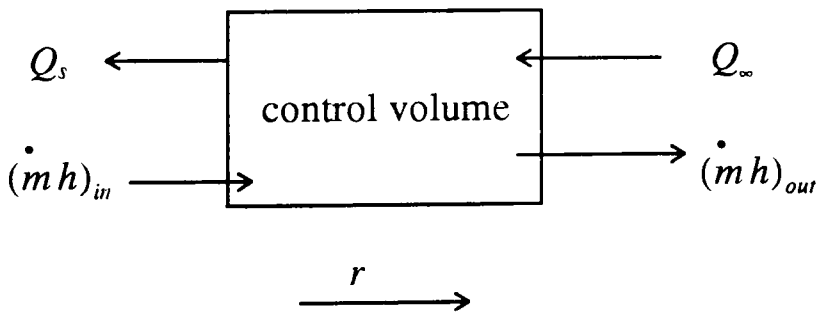

Q_s = heat energy out of the control volume [J/s]

Q_∞ = heat energy into the control volume [J/s]

h = enthalpy [J/(kg)]

$\dot{m}$ = mass transfer rate [kg/s]

C_{Pg} = isobaric heat capacity of fuel-vapour-air mixture [J/(kgK)]

C_{Pf} = isobaric heat capacity of fuel vapour [J/(kgK)]

(energy in) + (energy liberated) = (energy out) + (energy stored) (3.42)

If there is only evaporation,

0 = (energy out) - (energy in) + (energy stored) (3.43)

$$(Q_s - Q_\infty) + (\dot{m}_{out} h_{out} - \dot{m} h_{in}) + \frac{\partial(\rho 4\pi r^2 C_{P_g} T)}{\partial t}\delta r \tag{3.44}$$

$$0 = -\frac{\partial (4\pi r^2 k_g \frac{\partial T}{\partial r})}{\partial r}\delta r + \frac{\partial(4\pi r^2 \dot{m} h)}{\partial r}\delta r + \frac{\partial (4\pi r^2 C_{P_g} T \rho_g)}{\partial t}\delta r \tag{3.45}$$

rewriting the $\dot{m}$ as $\dot{m}_f$ (energy transfer due to diffusion of fuel vapour) and replacing the h as $C_{Pf}T$ in the second right hand side term of the above equation;

$$0 = -\frac{\partial (4\pi r^2 k_g \frac{\partial T}{\partial r})}{\partial r}\delta r + \frac{\partial(4\pi r^2 \dot{m}_f C_{P_f} T)}{\partial r}\delta r + \frac{\partial (4\pi r^2 C_{P_g} T \rho_g)}{\partial t}\delta r \tag{3.46}$$

$$\frac{\partial (r^2 k \frac{\partial T}{\partial r})}{\partial r} = \frac{\partial(r^2 \dot{m}_f C_{P_f} T)}{\partial r} + \frac{\partial (r^2 C_{P_g} T \rho_g)}{\partial t} \tag{3.47}$$

The above equation is subject to the boundary conditions given below :

at the droplet surface ($r = r_S$) :

$$4\pi r_s^2 k_{(T_s)} \left(\frac{\partial T}{\partial r}\right)_s = \dot{m}_{g_S} L_{(T_s)} + \frac{4\pi}{3} \rho_L \frac{\partial (C_{p_g} T r_s^3)}{\partial t} \qquad (3.50)$$

at $r = r_\infty$:

$$T = T_\infty \qquad (3.51)$$

Species mass conservation equation for the fuel vapour is written as :

$$\dot{m}_{in} + \dot{m}_{generated} - \dot{m}_{out} = \dot{m}_{stored} \qquad (3.52)$$

$$\dot{m}_{in} 4\pi r^2 + w_i 4\pi r^2 \delta r - (\dot{m}_{in} \pi r^2 + \frac{\partial m_{in} \pi r^2}{\partial r} \delta r) = \frac{\partial (\rho_i 4\pi r^2 \delta r)}{\partial t} \qquad (3.53)$$

Where

w_i is the generation term per a unit volume and a unit time

ρ_i is the density of the species of interest (fuel vapour)

$$-\frac{\partial \dot{m}_{in} r^2 \delta r}{\partial r} + w_i r^2 \delta r = \frac{\partial \rho_i r^2 \delta r}{\partial t} \qquad (3.54)$$

The mixture density could be replaced by :

$$\omega_i = \frac{\rho_i}{\rho} \tag{3.55}$$

since $\dot{m}$ is only diffusion driven, $\dot{m}$ of fuel vapour could be written as

$$\dot{m}_{in} = -\rho_g D_g \frac{\partial \omega_f}{\partial r} \tag{3.56}$$

substituting equation(3.24) and equation(3.25) in equation(3.23) and replacing ω with ω_f:

$$\frac{\partial \left(\omega_f \rho_g r^2\right)}{\partial t} = \frac{\partial r^2 \left(\rho_g D_g \frac{\partial \omega_f}{\partial r}\right)}{\partial r} + w_i r^2 \tag{3.57}$$

If we consider evaporation only there is no species creation or destruction. Therefore the final form of the fuel mass conservation equation is given by :

$$\frac{\partial \left(\omega_f \rho_g r^2\right)}{\partial t} = \frac{\partial r^2 \left(\rho_g D_g \frac{\partial \omega_f}{\partial r}\right)}{\partial r} \tag{3.58}$$

Which is solved with the boundary condition :

$r = r_\infty$:

$$\omega_f = 0 \tag{3.59}$$

At the droplet surface, the fuel mass fraction can be calculated using the partial pressure of the fuel, therefore this gives the boundary condition at the droplet surface. Equation 3.27 gives the fuel mass fraction at any point in the air vapour film.

To solve these two equations, an equation of state which describes the state of the gas mixture is needed. For this a modified Benedict Webb Rubin [139-140] type equation is used. Details about this equation is given in the property section (*Appendix-A*). The Finite difference forms of equations 3.49 and 3.58 are given below.

Finite difference code for temperature equation :

$$\frac{\partial \dot{m}_f C_{p_f} T r^2}{\partial r} + \frac{\partial C_{P_g} T \rho_g r^2}{\partial t} = \frac{\partial k_g r^2 (\frac{\partial T}{\partial r})}{\partial r}$$

$$\frac{\partial m_f C_{p_f} T r^2}{\partial r} + \frac{\partial C_{P_g} T \rho_g r^2}{\partial t} = k_g r^2 (\frac{\partial^2 T}{\partial r^2}) + 2k_g r (\frac{\partial T}{\partial r}) + r^2 (\frac{\partial T}{\partial r}) \frac{\partial k_g}{\partial r} \qquad (3.60)$$

$$\frac{\dot{m}_{f\,(i+1)}\, C_{pf(i+1)}\, T_{(i+1)}\, r_{(i+1)}^{2} - \dot{m}_{f(i-1)}\, C_{pf(i-1)}\, T_{(i-1)} r_{(i-1)}^{2}}{2\Delta r} \quad +$$

$$\frac{C_{pg_{(i)}}\, T_{(i)} \rho_{\,g(i)}\, r_{(i)} - C^{*}_{pg(i)}\, T^{*}_{(i)}\, \rho^{*}_{g(i)}\, r^{2*}_{(i)}}{\Delta\tau} \;=\; r_{(i)}^{2}\left[\frac{T_{(i+1)} - T_{(i-1)}}{2\Delta r}\right]\left[\frac{k_{g(i+1)} - k_{g(i-1)}}{2\Delta r}\right]$$

$$+2r_{(i)} k_{g(i)}\left[\frac{T_{(i+1)} - T_{(i-1)}}{2\Delta r}\right] \quad + \quad k_{g(i)}\, r_{(i)}^{2}\left[\frac{T_{(i+1)} - 2T_{(i)} + T_{(i-1)}}{(\Delta r)^{2}}\right] \tag{3.61}$$

The above equation can be rearranged as follows:

$$T_{(i+1)}\left[\frac{\dot{m}_{f(i+1)}\, C_{pf\,(i+1)} r_{(i+1)}^{2}}{2\Delta r} - \frac{k_{g(i)} r_{(i)}^{2}}{(\Delta r)^{2}} - \frac{2k_{g(i)} r_{(i)}}{2\Delta r} - \frac{r_{(i)}^{2}\, k_{g(i+1)}}{(2\Delta r)^{2}} + \frac{k_{g(i-1)} r_{(i)}^{2}}{(2\Delta r)^{2.}}\right] +$$

$$T_{(i-1)}\left[\frac{C_{pg_{(i)}} \rho_{g(i)} r_{(i)}^{2}}{\Delta t} + \frac{2\, k_{g(i)} r_{(i)}^{2}}{(\Delta r)^{2}}\right] +$$

$$T_{(i-1)}\left[-\frac{\dot{m}_{f\,(i-1)}\, C_{pf\,(i-1)} r_{(i-1)}^{2}}{2\Delta r} - \frac{k_{g(i)} r_{(i)}^{2}}{(\Delta r)^{2}} + \frac{2k_{g(i)} r_{(i)}}{2\Delta r} + \frac{r_{(i)}^{2}\, k_{g(i+1)}}{(2\Delta r)^{2}} - \frac{k_{g(i-1)} r_{(i)}^{2}}{(2\Delta r)^{2.}}\right] =$$

$$\frac{C^{*}{}_{pg_{(i)}} T^{*}{}_{(i)} r^{*2}_{(i)} \rho^{*}{}_{g(i)}}{\Delta t} \tag{3.62}$$

Which has the form given below :

$$A_j T_{(i+1)} + B_j T_{(i)} + C_j T_{(i-1)} = D_j \tag{3.63}$$

Finite difference form of the mass transfer equation for the film :

$$\frac{\partial\,(\omega_{f}\rho_{g}\,r^{2})}{\partial\,t} = \frac{\partial r^{2}(\rho_{g}D_{g}\,\frac{\partial\omega}{\partial r})}{\partial\,r}$$

differentiating the right hand side of the equation gives the following form :

$$\frac{\partial(\omega_{f}\rho_{g}\,r^{2})}{\partial t} = r^{2}\rho_{g}D_{g}\,\frac{\partial^{2}\omega_{f}}{\partial r^{2}} + \frac{\partial\omega_{f}}{\partial r}\rho_{g}\,D_{g}2r + \frac{\partial\omega_{f}}{\partial r}r^{2}\,\frac{\partial\rho_{g}\,D_{g}}{\partial r} \qquad (3.64)$$

$$\frac{\omega_{f(i)}\rho_{g(i)}\,r_{(i)}^{2} - \omega^{*}{}_{f(i)}\,\rho^{*}{}_{g(i)}r_{(i)}^{2*}}{\Delta\tau} = \frac{r_{(i)}^{2}\,\rho_{g(i)}\,D_{g(i)}}{(\Delta r)^{2}}[\omega_{f(i+1)} - 2\omega_{f(i)} + \omega_{f(i-1)}]$$

$$+ \qquad 2\rho_{g(i)}\,D_{g(i)}\,r_{(i)}\,\frac{\omega_{f(i+1)} - \omega_{f(i-1)}}{2\Delta r} \qquad +$$

$$(\frac{\rho_{g(i+1)}\,D_{g(i+1)} - \rho_{g(i-1)}\,D_{g(i-1)}}{2\Delta r})[\frac{\omega_{(i+1)} - \omega_{(i-1)}}{2\Delta r}]r_{(i)}^{2} \qquad (3.65)$$

The above equation can be rearranged with the heat transfer equation where the $\omega_f(i)$ values could be calculated by the tri-diagonal matrix elimination routine (TDMA).

$$A_{j}\omega_{f(i+1)} + B_{j}\omega_{f(i)} + C_{j}\omega_{f(i-1)} = D_{j} \qquad (3.66)$$

The computational implementation of the above model is describe in more detail in section 3.3.7

3.3 Computational Treatment :

The droplet Programs were written using FORTRAN77. Altogether there are 4 programs. Two transient heating models, one having improved pressure dependent property routines (identical in all other aspects), a program based on the liquid heating model and finally a program based on the unsteady gas phase formulation. All programs consist of a number of subroutines co-ordinated by a main routine.

3.3.1 Common Features Of The Computer Programs :

All variables are declared as double precision. This is done to minimise the numerical errors associated with the calculation of very small quantities and to minimise programming errors, by keeping all declarations consistent in the main program and the subroutines. Each property is calculated in a separate subroutine and the required values are passed to the main program. This enables a particular subroutine to be replaced by a new up to date one in the future, with minimum disruption to the overall program. Furthermore, most property routines are programmed in such a way that they can be easily modified by changing few variables in the routine and in the calling statement to take account of the new mixture. The property routines used in the programs are listed below.

PROPERTY	ROUTINE
Viscosity and Thermal conductivity of a gas mixture	VISCTHERM
Specific volume of the gas mixture	BWREOS
Ideal gas specific heat capacities of the gas mixture	CPCVIDL

heat capacity departure functions	HCDEP
Saturation vapour pressure of the fuel	PFL, PFLD, PFLO
Compressed liquid density of a *n*-component liquid	COSTLAD
Critical temperature and volume of a liquid mixture	CRITIC
Enthalpy of gasification (single component)	DELHVF
Binary diffusion coefficient of a 2 component gas mixture	DV
Liquid specific heat (single component)	CPL
Vapour specific heat (single component)	CPF
Liquid thermal conductivity	KL

table 3.1 property routines

3.3.2 Input Data :

Data to all programs are supplied through a data file. The supplied parameters are as follows :

ambient temperature /K	tb
droplet diameter /m	d
droplet initial surface temperature /K	tl
relative velocity of the droplet /m/s	u
ambient pressure (/N/m^2)	pt
density of the fuel at 15.6 °C (/kg/m^3)	dl156c
number of Carbon and Hydrogen atoms of the fuel for diffusion coefficient calculation	nc, nh (dimensionless)

boiling point of the fuel /K	
for single component model	tboil
for multi-component model	tboilo, tboild
critical temperature of (O_2, N_2, Fuel) /K	tc(n)
critical volume of (O_2, N_2, Fuel) /(cm3/mol)	vc(n)
acentric factor (dimensionless)	w(n)
molar mass /(g/mol)	molarm(n)

In the transient heating and the liquid heating models the time step (delt) is passed via the data file. In the unsteady gas phase model the time step and the radial step for the gas phase are given as run time inputs.

All the other variables which need to be changed when the program is run for different fuel species are explained in detail in each unit in the form of comment statements.

3.3.3 The Quasi-Steady Gas Phase With Infinite Liquid Conductivity Model :

In the transient heating models (sec. 3.2.2) two ordinary differential equations governing the rate of change of droplet temperature and the rate of mass gasification (equations 3.1 and 3.2) are solved by the fourth order Runge-Kutta method simultaneously for each time step. The FORTRAN implementation of this procedure is as follows.

The main program calls subroutine (RK) to optimise the values obtained for the mass gasification rate *dmdt* and the rate of change of the droplet temperature *dTdt*, (which are calculated in the main program) using the Runge-Kutta method at each time step. Subroutine RK has 4 entry points, where the intermediate values of the droplet temperature and mass are evaluated. These intermediate values are then passed to the main program, these are then used to calculate the thermodynamic and transport properties required for the calculation of the intermediate values of *dmdt* and *dTdt*, before being optimised by the RK routine. After the fourth pass through the RK routine the final values for mass and temperature are obtained and the calculation proceeds to the next time step.

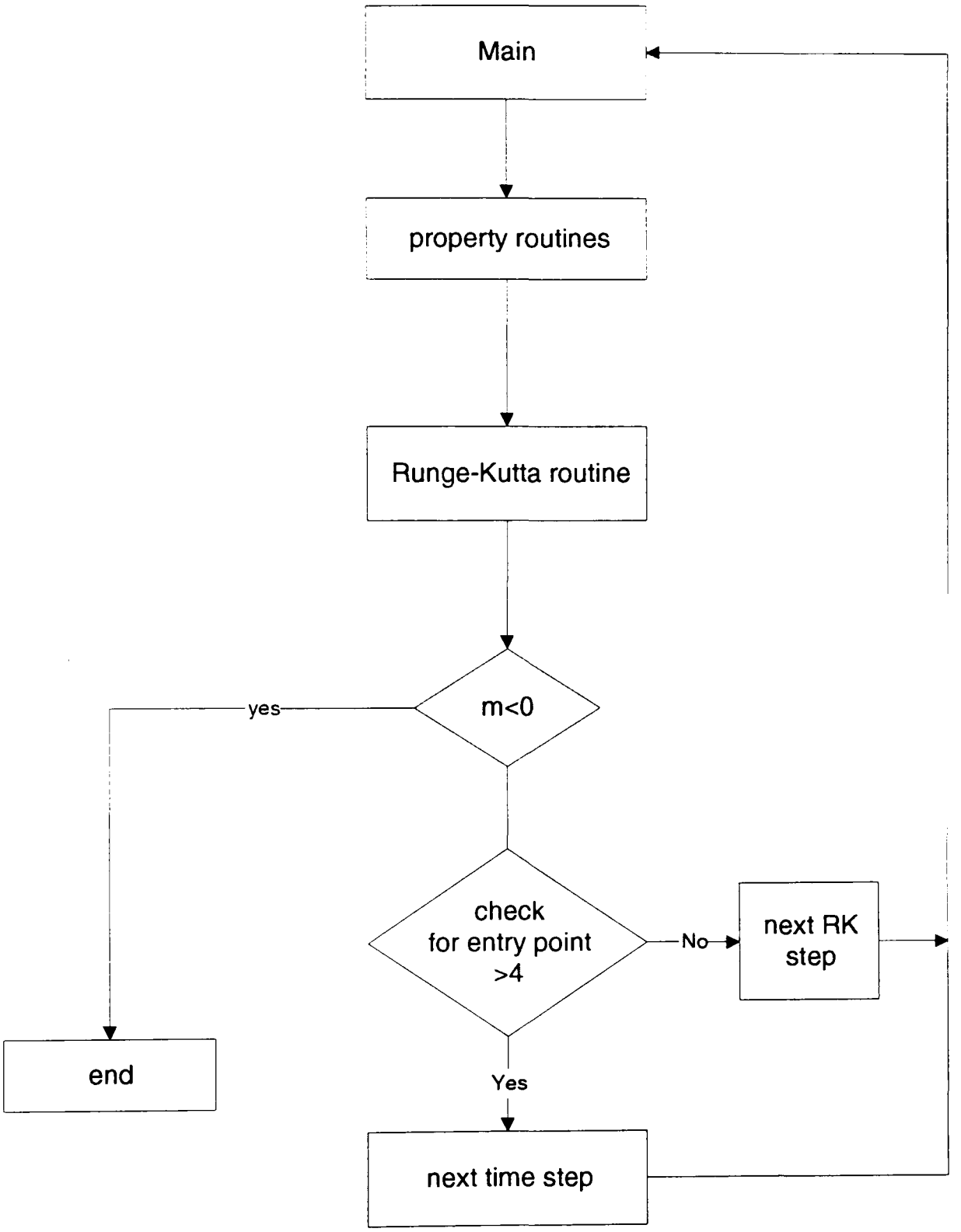

fig. 3.2 flow chart for the transient heating model

3.3.4 Error Control Associated With The RK Routine :

The calculated droplet temperature may exceed the boiling point of the fuel at the specified ambient pressure due to the approximations built into the model. Therefore the program includes a control to ensure against this happening. The control checks, and corrects as necessary, for this condition at each entry to the RK routine. Similarly the droplet mass could become negative inside the RK routine. Then the mass is set to zero and the program comes out of the iteration loop for final printing of variables.

3.3.5 The Quasi-Steady Gas Phase With Finite Liquid Conductivity Model :

In this model (sec 3.2.3) the heat transfer equation is solved using a fully implicit finite difference procedure. The advantage of using a fully implicit method is the overall reduction in computer CPU time taken to run the program. This is due to implicit methods being more stable for a relatively large time step compared to explicit methods. The finite difference form of the heat transfer equation and the associated boundary conditions are all in a single subroutine (LQDHEAT). This subroutine has access to a tri-diagonal matrix elimination routine (TDMA) which evaluates the tri-diagonal matrix formulated by the coefficients of the droplet internal and surface temperature values at each grid point. The routine can be easily modified to accommodate different number of grid points to check the grid dependency of the finite difference procedure.

To optimise the droplet mass calculated from the mass transfer equation (eq.-3.2) a predictor-corrector type optimisation method is used. The predictor-corrector code is

built into the main program. At the start of each time step a predictor calculation is carried out on the droplet mass. A flag is then set so the next optimisation is a corrector step optimisation. In this step the relative difference between the new value and the old value is calculated; if this is less than 0.01 another flag is set, which informs the program to proceed to the next time step. If the above condition is false the program calculates another predictor step in the same time level. The maximum number of iterations for the corrector step is limited to five. If convergence is not achieved after five corrector step iterations, the program moves to the next time step, (after displaying a warning message). The calculated value of mass after the fifth step is then taken as the final value of mass for that time step (This condition was never reached for the results given in this thesis).

After each pass through a predictor or a corrector section, the droplet surface and internal temperature is updated by calling the LQDHEAT routine. Therefore implicitly this method acts as a smoothing function on the solution of the heat transfer equation increasing the overall accuracy of the program.

3.3.6 Error Control Methods :

To make the LQDHEAT routine stable certain assumptions and numerical error control methods are built into the routine. These methods are explained below and further information is given in the program itself:-

- if the absolute difference between the newly calculated value of temperature and the previous one at any grid point is less than 0.001 the old value is retained until the difference is greater than 0.001;
- the maximum value of temperature at any grid point cannot exceed the boiling point of the fuel at the given ambient pressure;
- if necessary, intermediate results of temperature before corrections are applied could be displayed or written to a file by activating a write statement. This allows the user to adjust the 0.001 value to preserve the stability of the method.

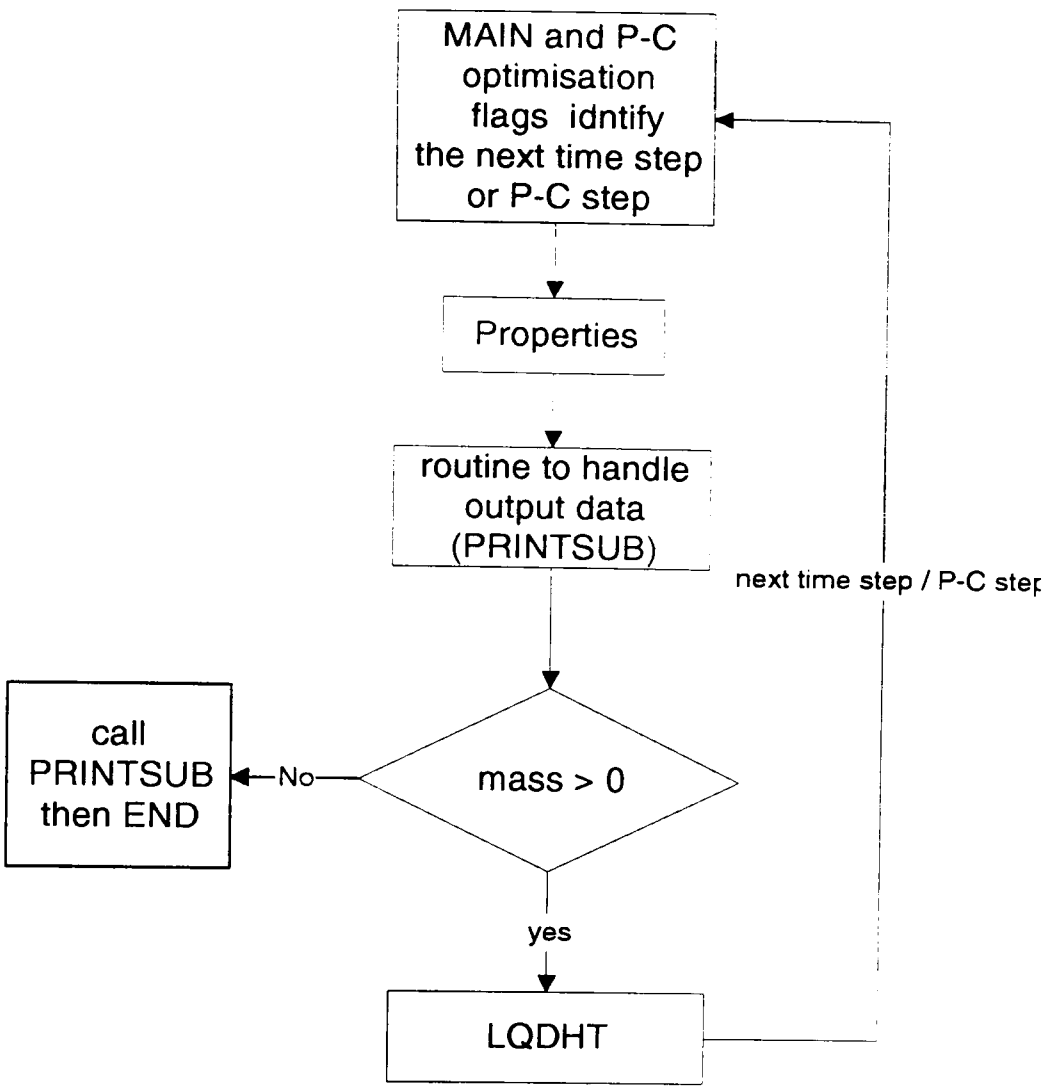

fig. 3.3 Flow chart for the Liquid heating model

3.3.7 The Unsteady Gas Phase Model :

As stated in section 3.2.4, the partial differential equations (PDEs) were solved using a fully implicit finite difference method. The two PDEs with their respective boundary conditions were programmed into two different subroutines (HEATNS, MASSNS). After the calculation of the relevant properties the main program calls these two routines. Initially it is assumed that the film temperature is equal to the ambient temperature for all grid points except the first one. This point represents the surface of

the droplet, therefore the temperature at this point is the initial droplet temperature. The same principle applies to the mass transfer equation where the initial fuel mass fraction is taken as zero for all grid points, minus the first point, where the fuel mass fraction is calculated based on the saturation vapour pressure of the fuel.

Once the new temperature and the fuel mass fraction are calculated, they are transferred to the main program to be compared with the previously calculated or known values. If they satisfy the specified convergence criteria calculations proceed to the next time step. Otherwise the two routines are called until convergence is achieved. The convergence criteria is checked at each grid point; this guaranties that the converged values of mass and temperature are the correct representation of the solutions for the two PDEs. Further information regarding HEATNS and MASSNS routines are given in the program itself.

Since the stability of the finite difference method depends on the grid spacing and on the time step; these two variables are passed to the program as run time inputs. This gives the user the option of selecting the appropriate step sizes for a given droplet diameter.

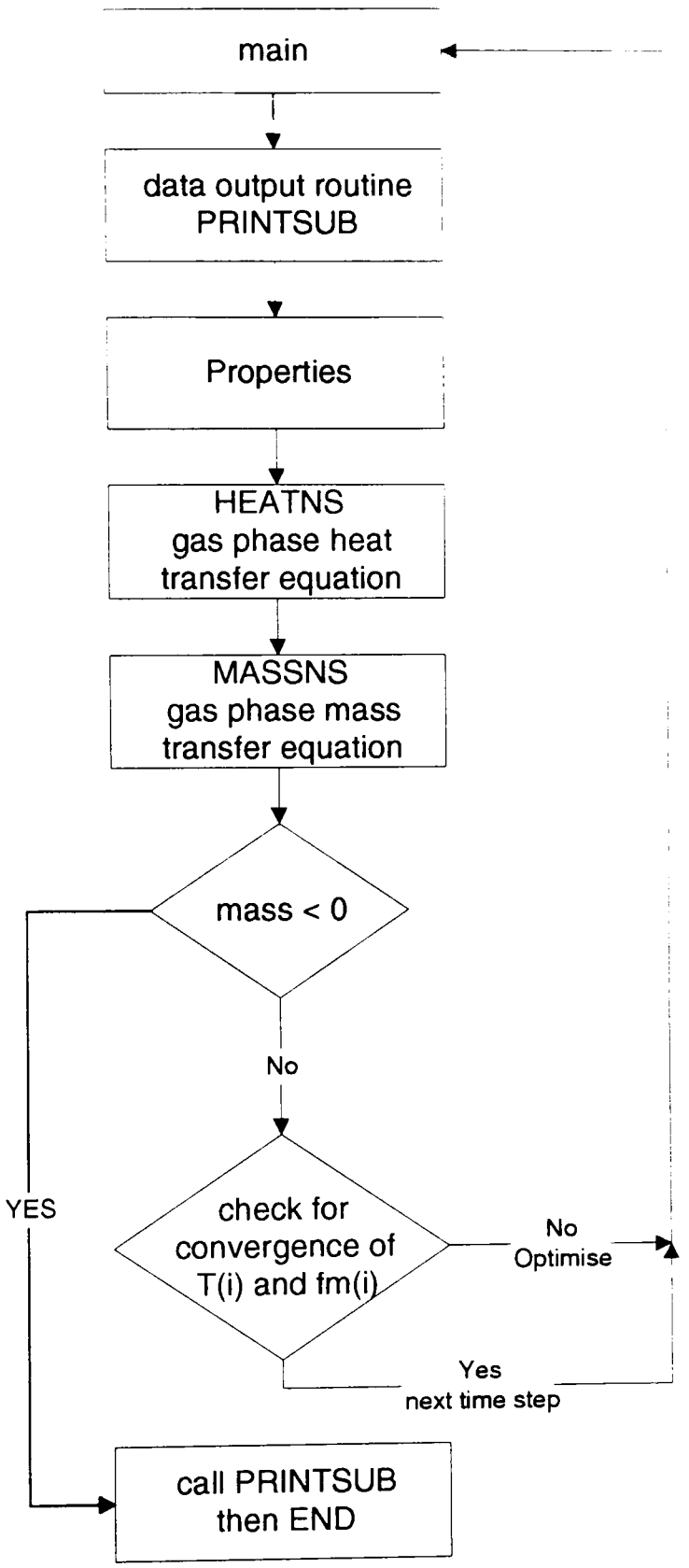

fig. 3.4 flow chart for the variable gas phase model

CHAPTER-4

MATHEMATICAL FORMULATION AND PROGRAMMING TECHNIQUES OF THE SINGLE-PHASE AND THE TWO-PHASE MIXING MODELS

4.1 Introduction :

The chapter begins with a section containing a general description of the finite volume method, the iterative procedure for the solution of the governing equations and the incorporation of boundary conditions. This is then followed by two sections describing the FORTRAN computer programs to simulate the mixing of two gaseous species and the mixing and evaporation of a two phase gas-liquid flow. The two programs have substantial amount of commonalty between them, therefore most of the common mathematical concepts are discussed in the first section (Compressible Flow Modelling). The repetition of common features is avoided in the description of the two-phase program.

4.2 Compressible flow modelling :

In compressible flow modelling, the physical and chemical processes involved can be described by fundamental equations governing overall mass balance, momentum transfer individual species mass fraction transfer and energy transfer. Since the flows encountered in the scope of this study are highly turbulent, to account for the effects of

turbulence on the mixing process a turbulence model needs to be solved with the above flow variables. The partial differential equations governing these processes are presented in steady state, two-dimensional axisymetric co-ordinate system [103, 141].

Continuity equation :

Conservation of total mass in both x and r directions is given by:

$$\frac{\partial(\rho r u)}{\partial x} + \frac{\partial(\rho r v)}{\partial r} = 0 \qquad (4.1)$$

Momentum equations:

According to Newton's second law the rate of change of momentum of a fluid particle equals the sum of forces acting on the particle.

Axial momentum equation :

Based on the above the axial momentum can be written as:- the rate of change of momentum of the fluid particle in the axial direction is equal to the viscous forces acting on the axial direction, plus the rate of increase of momentum due to any other source (such as pressure force, etc.).

$$\frac{1}{r}[\frac{\partial(r\rho uu)}{\partial x}+\frac{\partial(r\rho uv)}{\partial r}]=\frac{1}{r}[\frac{\partial}{\partial x}(r\mu_e\frac{\partial u}{\partial x})+\frac{\partial}{\partial r}(r\mu_e\frac{\partial u}{\partial r})]+S_u \qquad (4.2)$$

$$\mu_e=\mu_l+\mu_t$$

Where

$$S_u=-\frac{\partial P}{\partial x}+\frac{\partial}{\partial x}(\mu_e\frac{\partial u}{\partial x})+\frac{1}{r}\frac{\partial}{\partial r}(r\mu_e\frac{\partial v}{\partial x})+s_u \qquad (4.3)$$

Similarly, the radial momentum can be written as :

$$\frac{1}{r}[\frac{\partial(r\rho uv)}{\partial x}+\frac{\partial(r\rho vv)}{\partial r}]=\frac{1}{r}[\frac{\partial}{\partial x}(r\mu_e\frac{\partial v}{\partial x})+\frac{\partial}{\partial r}(r\mu_e\frac{\partial v}{\partial r})]+S_v \qquad (4.4)$$

$$S_v=-\frac{\partial P}{\partial r}+\frac{\partial}{\partial x}(\mu_e\frac{\partial u}{\partial r})+\frac{1}{r}\frac{\partial}{\partial}(r\mu_e\frac{\partial v}{\partial r})-\mu_e\frac{V}{r^2}+s_v$$

Energy equation :

Based on the first law of thermodynamics, the rate of increase of energy of a fluid particle is equal to the net rate of heat transfer to the particle plus the net rate of work done on the particle and the rate of energy increase due to any other source.

$$\frac{1}{r}[\frac{\partial(r\rho uT)}{\partial x}+\frac{\partial(r\rho vT)}{\partial r}]=\frac{1}{r}[\frac{\partial}{\partial x}(r\Gamma_h\frac{\partial T}{\partial x})+\frac{\partial}{\partial r}(r\Gamma_h\frac{\partial T}{\partial r})]+s_T \quad (4.5)$$

$$\Gamma_h=\frac{\mu_e}{\sigma_h}=\frac{\mu_e}{0.7}$$

Species mass fraction equation :

The transport of mass fraction by convection is equal to the transport of mass fraction by diffusion plus any source which generate or destroy the mass fraction.

$$\frac{1}{r}[\frac{\partial(r\rho uY_s)}{\partial x}+\frac{\partial(r\rho vY_s)}{\partial r}]=\frac{1}{r}[\frac{\partial}{\partial x}(r\Gamma_s\frac{\partial Y_s}{\partial x})+\frac{\partial}{\partial r}(r\Gamma_s\frac{\partial Y_s}{\partial r})]+s_y \quad (4.6)$$

$$\Gamma_s=\frac{\mu_e}{\sigma_s}=\frac{\mu_e}{0.7}$$

k-ε equations of turbulence modelling:

The transport of the turbulent kinetic energy (k) or the turbulent desipation rate (ε) by convection is equal to, the transport of k or ε by diffusion plus the rate of production of k or ε and minus the rate of destruction of k or ε..

Turbulent kinetic Energy :

$$\frac{1}{r}[\frac{\partial(r\rho uk)}{\partial x}+\frac{\partial(r\rho vk)}{\partial r}]=\frac{1}{r}[\frac{\partial}{\partial x}(r\Gamma_k\frac{\partial k}{\partial x})+\frac{\partial}{\partial r}(r\Gamma_k\frac{\partial k}{\partial r})]+S_k \quad (4.7)$$

$$\Gamma_k=\frac{\mu_e}{\sigma_k}$$

$$S_k=G-C_D\rho\varepsilon+s_k$$

$$G=\mu_e\{2[(\frac{\partial u}{\partial x})^2+(\frac{\partial v}{\partial r})^2+(\frac{v}{r})^2]+(\frac{\partial u}{\partial r}+\frac{\partial v}{\partial x})^2\}$$

Turbulent desipation rate :

$$\frac{1}{r}[\frac{\partial(r\rho u\varepsilon)}{\partial x}+\frac{\partial(r\rho v\varepsilon)}{\partial r}]=\frac{1}{r}[\frac{\partial}{\partial x}(r\Gamma_\varepsilon\frac{\partial\varepsilon}{\partial x})+\frac{\partial}{\partial r}(r\Gamma_\varepsilon\frac{\partial\varepsilon}{\partial r})]+S_\varepsilon \quad (4.8)$$

$$\Gamma_e=\frac{\mu_e}{\sigma_\varepsilon}$$

$$S_e=C_1\frac{\varepsilon}{k}G-C_2\frac{\rho}{k}\varepsilon^2+s_e$$

turbulent constants used in the above equations are as follows [103, 142]:

C_μ	C_D	C_1	C_2	σ_k	σ_ε
0.09	1.0	1.44	1.92	1.0	1.3

The use of the source term S_ϕ is two fold. Firstly, it allows the representation of all the above equations using a single generic form. If a particular equation has extra terms these can be incorporated later during the solution process via the source term (as in the *u*, *v*, *k* and ε in the above equation set). Secondly, the source term can be used to incorporate boundary conditions (s_ϕ term), other less significant transport mechanism, future additions (such as direct coupling of droplets mass, momentum energy transfer) etc. The use of the source term to incorporate boundary conditions to the discretised form of the above equations is explained in detail in section 4.2.10.

The above set of differential equations are solved with an equation of state and other thermodynamic and chemical property equations. The evaporation modelling program uses the BWR equation (Appendix-A) as the equation of state. The incorporated droplet model uses a modified form of the ideal gas equation as its equation of state. In this section only the equations regarding general single phase flows are presented. The formulation of the incorporated droplet model is explained in section 4.4

The above equations are solved using the finite volume discretisation method. To accommodate the non-linear nature of the underlying flow phenomena and the linkage between the pressure and velocity in a variable density fluid, the SIMPLE [141, 142,

143, 144] algorithm developed by Patankar and Spalding is used as the core of the solution procedure.

4.2.1 Finite Volume Equations And The Solution Procedure :

All differential equations (apart from the continuity equation) presented in the previous chapters are of the from :

$$\frac{\partial(\rho u_i \phi)}{\partial x_i} - \frac{\partial\left(\Gamma_i \frac{\partial \phi}{\partial x_i}\right)}{\partial x_i} = S\phi \qquad (4.9)$$

Where ϕ is the general flow variable and subscript i represents the x, y, z directions. To solve the partial differential equations they need to be numerically integrated over the domain. Integration is achieved via the finite volume technique.

In order to derive the finite difference equations, the calculation domain is divided into a number of nodes defined by the intersection of grid lines parallel to the two axis of the domain and finite difference cells surrounding the node points are considered. For a control volume V_p (a single cell), in the domain of the solution, the above equation can be integrated over the control volume to give :

$$\int_{CV} \frac{\partial}{\partial x_i}(\rho u_i \phi - \Gamma_\phi \frac{\partial \phi}{\partial x_i}) dV = \int_{CV} S_\phi dV \qquad (4.10)$$

If A is the boundary of the control volume then the second term in the above equation can be transformed into a surface integral using the Green's theorem as :

$$\int_A (\rho u_i \phi - \Gamma_\phi grad\phi) n ds = \int_{CV} S_\phi dV \qquad (4.11)$$

Where n is the unit vector normal to the boundary. The left hand side of the equation represents the flux of ϕ crossing the boundaries, and the right hand side the contribution from the sources of ϕ. Since the equations used in this thesis are of a 2D-formulation, the right hand side of the above equation could be represented by a surface integral. All equations here after are formulated using a 2D- co-ordinates system.

$$\int_A \rho u_i \phi - \Gamma_\phi grad\phi) n dA = \int_A S_\phi dA \qquad (4.12)$$

The finite difference representation of the above equation requires an understanding of the grid system. Therefore the finite difference form of each term of equation (4.12) is deferred until the grid system is discussed.

4.2.2 Grid System :

To ensure stability a staggered grid system is used [145, 146]. The scalar variables (temperature, turbulent parameters, etc.) are evaluated at the nodal points. The velocities (u and v) are defined at the faces of the scalar cell (mid points between the nodal points). Figure 4.1 shows this arrangement for a two dimensional cartesian co-ordinate system.

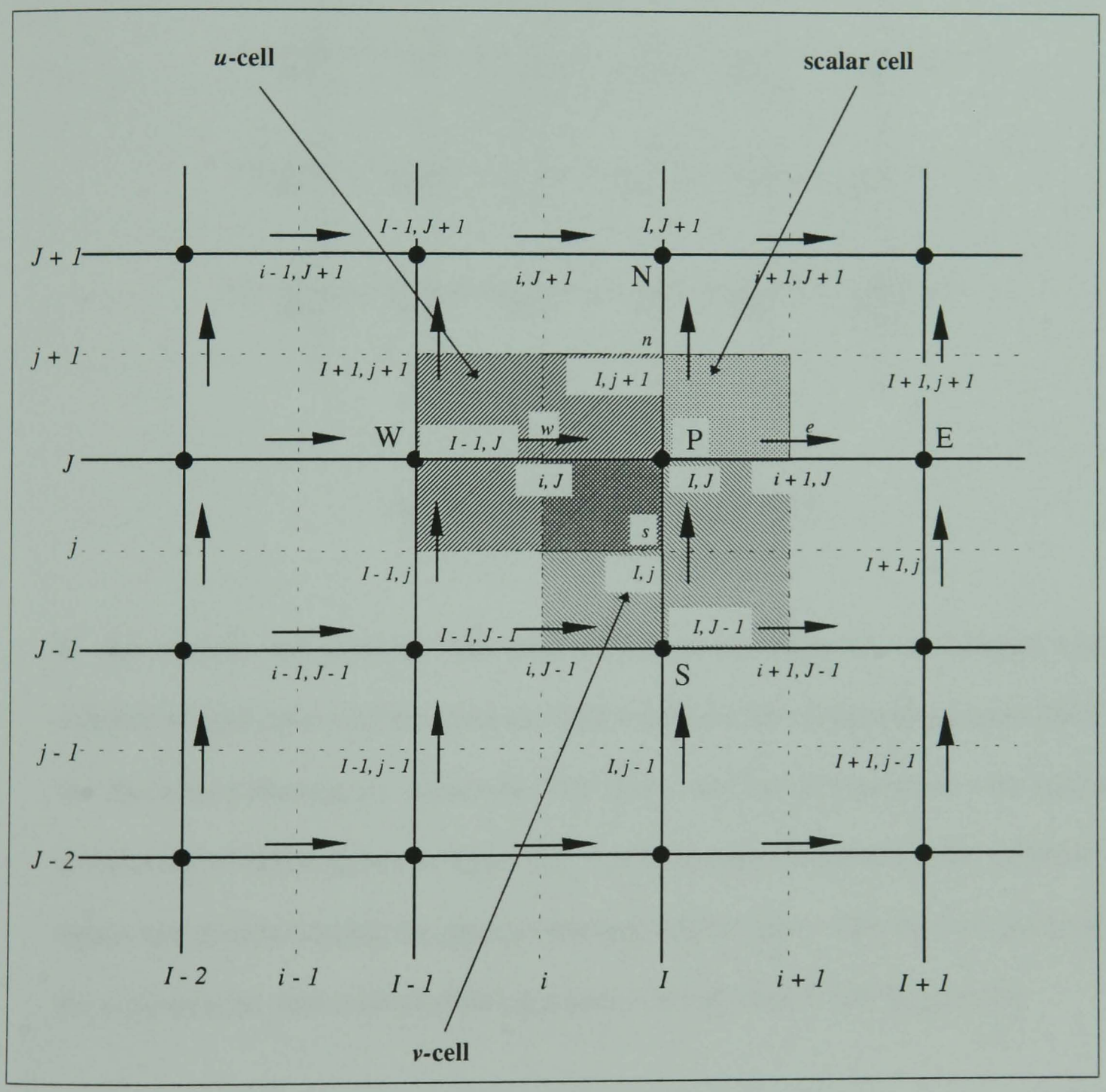

fig. 4.1 representation of the grid system
(arrows represents where velocities are calculated)

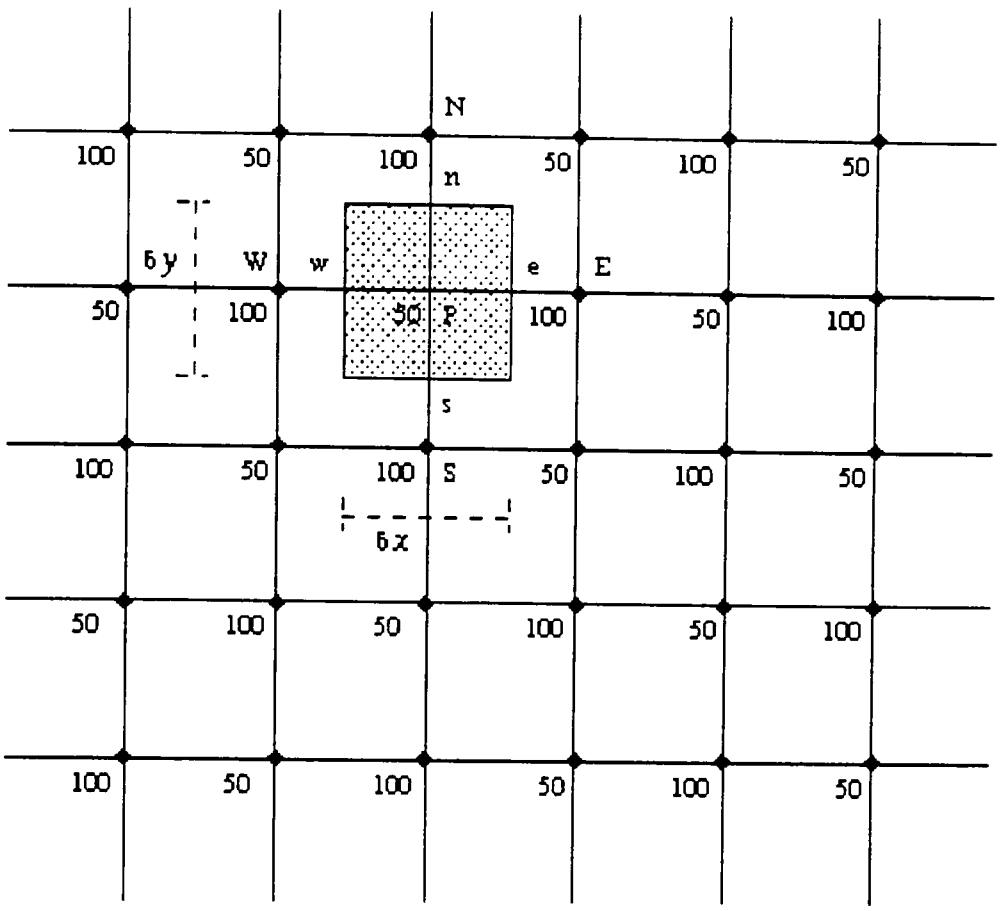

fig. 4.2 non-uniform pressure field

If the velocity and pressure were both defined at the nodes of an ordinary control volume, a highly non-uniform pressure field would act like a uniform pressure field for the discretised momentum equations. The above can be demonstrated with the two-dimensional situation shown in figure 4.2. Let us assume the pressure field shown in the figure was obtained during the iteration process at some stage. The pressure gradient for the u-momentum and v-momentum equations at nodal point P can be given by:

$$\frac{\partial P}{\partial x} = \frac{P_e - P_w}{\delta x} = \frac{\left(\frac{P_E + P_P}{2}\right) - \left(\frac{P_P - P_W}{2}\right)}{\delta x} = \frac{P_E - P_W}{2\delta x} \qquad (4.13)$$

$$\frac{\partial P}{\partial y} = \frac{P_N - P_S}{2\delta y} \qquad (4.14)$$

In the above expressions the pressure at node P does not appear in discretised form of the pressure gradients. Substituting the 'checker-board' pressure field in figure 4.2 in the above equations results in a pressure gradient of zero at the node P in both x and y directions, even though the pressure field exhibits spatial oscillations. Therefore the momentum equation sees this as a uniform pressure field which could lead to an unrealistic converged solution. In the staggered grid arrangement the pressure nodes coincide with the cell faces of the u and v control volumes. Based on figure 4.1 the new pressure gradients of the two momentum equations are given below.

$$\frac{\partial P}{\partial x} = \frac{P_P - P_W}{\delta x} \qquad (4.15)$$

$$\frac{\partial P}{\partial y} = \frac{P_P - P_S}{\delta y_v} \qquad (4.16)$$

It can be seen that substitution of appropriate values yields non-zero pressure gradient terms. Therefore the staggered grid of the velocity avoids the unrealistic behaviour of the discretised momentum equations.

A further advantage of the staggered grid is that it generates velocities at the exact locations where they are required for convection-diffusion calculations (i. e. mid point between two nodes). Hence no interpolation is required to calculate the velocities at the scalar cell faces.

4.2.3 Fluxes Across Cell Boundaries :

The net convective and diffusive flux for a cell can be represented as follows :

$$\int \rho u_i \phi - \Gamma_\phi grad\phi) ndA = \sum J_i \qquad (4.17)$$

where J_i are the fluxes across the boundaries.

$$\int_A (\rho u_i \phi - \Gamma_\phi grad\phi) ndA = J_e + J_w + J_n + J_s \qquad (4.18)$$

thus J_e for instance, is the flux crossing the east boundary.

$$J_e = \int_{A_e} (\rho u \phi - \Gamma_\phi \frac{\partial \phi}{\partial x})_e dA \qquad (4.19)$$

The flux J_e can be obtained by one-dimensional flow analysis [141], giving the following exact solution:

$$J_e = \rho_e u_e [f_e \phi_E + (1 - f_e)\phi_p] A_e \qquad (4.20)$$

where

$\rho_e = \frac{1}{2}.(\rho_E + \rho_P)$

A_e = area of the east face

$f_e = \exp(Pe_e) / (\exp(Pe_e) - 1)$

where Pe_w is the local Peclet number and is defined by :

$$Pe_e = \rho_e u_e (\frac{\delta x_{EP}}{\Gamma_{\phi.e}})$$

$$\Gamma_{\phi.e} = \frac{1}{2}(\Gamma_{\phi.E} + \Gamma_{\phi.P})$$

since exponentials are expensive to compute, a piece-wise linear fit is adopted to obtain a 'hybrid' formulation [147, 148] given by :

$$\frac{J_e}{\rho_e u_e A_e} = \begin{bmatrix} \frac{1}{2}[(1 + 2Pe_e^{-1})\phi_E + \frac{1}{2}[(1 - 2Pe_e^{-1})\phi_P] & for\ -2 < Pe_e < 2 \\ \phi_E & for\ Pe_e > 2 \\ \phi_P & for\ Pe_e < -2 \end{bmatrix} \qquad (4.21)$$

The above 'hybrid' scheme uses central differencing for low Peclet numbers and upwind differencing for high Peclet numbers. The use of upwind formulation for high Peclet numbers ensure better stability of the scheme than with central differencing [141].

4.2.4 Integration Of The Source Term:

The integrated source is expressed as a linear function of ϕ [141] given by :

$$\iint_A S_\phi \, dA = (b\phi_P + c)\Delta x \, \Delta y \qquad (4.22)$$

4.2.5 Assembly Of Finite Difference Equations :

Using expressions (4.12, 4.18) we obtain

$$J_e + J_w + J_s + J_n = (b\phi_P + c)\Delta x \Delta y \qquad (4.23)$$

The final form of the above equation after substitution for the *J* terms based on the hybrid difference scheme is given below. Detailed description of the method of derivation could be found in [142].

$$a_P\phi_P = a_W\phi_W + a_E\phi_E + a_N\phi_N + a_S\phi_S + (b\phi_P + c)\Delta x \Delta y \qquad (4.24)$$

where :

$$a_P = a_W + a_E + a_S + a_N + F_E - F_W + F_N - F_S \qquad (4.25)$$

a_W	$\max[F_W, (D_W + F_W/2), 0)]$
a_E	$\max[F_W, (D_W + F_W/2), 0)]$
a_S	$\max[F_W, (D_W + F_W/2), 0)]$
a_N	$\max[F_W, (D_W + F_W/2), 0)]$

table 4.1 coefficients of the general finite volume equation

F_E	$(\rho u)_E A_E$
F_W	$(\rho u)_W A_W$
F_S	$(\rho u)_S A_S$
F_N	$(\rho u)_N A_N$
D_E	$\frac{\Gamma_E}{\delta x_{EP}} A_E$
D_W	$\frac{\Gamma_W}{\delta x_{WP}} A_W$
D_S	$\frac{\Gamma_S}{\delta x_{SP}} A_S$
D_N	$\frac{\Gamma_N}{\delta x_{NP}} A_N$

table 4.2 convective and diffusive terms

4.2.6 Method Of Solution Of The Finite Difference Equations :

Although there is no direct equation to calculate the pressure, the pressure field is indirectly specified through the continuity equation i. e., when the correct pressure field is substituted in the momentum equation, the resulting velocity field should satisfy the continuity equation. The above solution technique is known as the SIMPLE (Semi Implicit Pressure Linked Equations) method [141-144]. A brief description of the method is given below.

The momentum equations are first solved for an assumed pressure field p^*, the continuity equation is used to calculate the pressure correction p' which is the difference between the correct pressure field p and the guessed value p^*. The calculated pressure corrections are then in turn used to correct the velocity field u^* and v^* obtained using the assumed pressure field p^*.

The relationship between the correct and the assumed values are as follows :

$$p = p^* + p' \qquad (4.26)$$

$$u = u^* + u' \qquad (4.27)$$

$$v = v^* + v' \qquad (4.28)$$

where u' and v' are corrections to the velocities u and v.

A guessed pressure field is initially used. Usually the previous step's pressure field is used, except in the first iteration where it may be taken as zero

Solving the discretised momentum equations using the guessed pressure field yield velocity components u^* and v^* as follows

discretised u-momentum equation :

$$a_{i,J}u_{i,J} = \sum a_{nb}u_{nb} - \left(P_{I,J} - P_{I-1,J}\right)A_{i,J} + b_{i,J} \qquad (4.29)$$

discretised v-momentum equation :

$$a_{I,j}v_{I,j} = \sum a_{nb}v_{nb} - \left(P_{I,J} - P_{I-1,J}\right)A_{i,j} + b_{I,j} \qquad (4.30)$$

after substitution of u^*, v^* and p^* the discretised equations have the following form

$$a_{i,J}u^*_{i,J} = \sum a_{nb}u^*_{nb} - \left(P^*_{I,J} - P^*_{I-1,J}\right)A_{i,J} + b_{i,J} \qquad (4.31)$$

$$a_{I,j}v^*_{I,j} = \sum a_{nb}v^*_{nb} - \left(P^*_{I,J} - P^*_{I-1,J}\right)A_{I,j} + b_{I,j} \qquad (4.32)$$

subtracting equations 4.31 and 4.32 from equations 4.29 and 4.30 respectively yields the equations for the correction terms.

$$a_{i,J}u'_{I,j} = \sum a_{nb}u'_{nb} - \left(P'_{I,J} - P'_{I-1,J}\right)A_{i,J} \qquad (4.33)$$

$$a_{I,j}v'_{i,J} = \sum a_{nb}v'_{nb} - \left(P'_{I,J} - P'_{I,J-1}\right)A_{i,J} \qquad (4.34)$$

At this point an approximation is introduced; the first terms in equations (4.33-4.34) are dropped. This is the main approximation of the SIMPLE algorithm. The velocity corrections can then be written as :

$$u'_{i,J} = d_{i,J}(P'_{I-1,J} - P'_{I,J}) \qquad (4.35)$$

$$v'_{I,j} = d_{I,j}(P'_{I-1,J} - P'_{I,J}) \qquad (4.36)$$

where $d_{i,J} = \frac{A_{i,J}}{a_{i,J}}$ and $d_{I,j} = \frac{A_{I,j}}{a_{I,j}}$

Therefore the corrected velocities are given as :

$$u_{i,J} = u^*_{i,J} + d_{i,J}(P'_{I-1,J} - P'_{I,J})$$
$$v_{I,j} = v^*_{I,j} + d_{I,j}(P'_{I,J-1} - P'_{I,J}) \qquad (4.37\text{-}4.38)$$

The above velocities are also constrained by the continuity equation.

$$[(\rho uA)_{i+1,J} - (\rho uA)_{i,J}] + [(\rho vA)_{I,j+1} - (\rho vA)_{I,j}] = 0 \qquad (4.39)$$

substituting the corrected velocities into the discretised continuity equation leads to the final discretised form of the continuity equation given below

$$a_{I,J}\dot{P}_{I,J} = a_{I+1,J}\dot{P}_{I+1} + a_{I-1,J}\dot{P}_{I-1,J} + a_{I,J+1}\dot{P}_{I,J+1} + a_{I,J}\dot{P}_{I,J-1} + \dot{b}_{I,J} \qquad (4.40)$$

where :

$$a_{I,J} = a_{I+1,J} + a_{I-1,J} + a_{I,J+1} + a_{I,J-1}$$

$a_{I+1,J}$	$a_{I-1,J}$	$a_{I,J+1}$	$a_{I,J-1}$	$b_{I,J}'$
$(\rho dA)_{i+1,J}$	$(\rho dA)_{i,J}$	$(\rho dA)_{I,,j+1}$	$(\rho dA)_{I,j}$	$(\rho u^* A)_{i,J}$ - $(\rho u^* A)_{i,+1,J}$ $+(\rho v^* A)_{I,j}$ - $(\rho v^* A)_{I,j+1}$

4.3 coefficients of the continuity equation

The above equation represent the continuity as an **equation of pressure correction P'.** The b' term represents the continuity imbalance arising from the use of incorrect velocity fields. The imbalance will tend to zero as the correct velocity fields are achieved by iteration.

By solving the pressure correction equation the pressure correction field P' at all points can be obtained. Once the pressure correction field is known, corrected pressure P can

be found from equation (4.26) and the velocities from equations (4.37) and (4.38). The $\sum a_{nb} u^*_{nb}$ *and* $\sum a_{nb} v^*_{nb}$ terms which were dropped in equations (4.33-4.34) do not affect the final solution because the pressure correction and velocity corrections will be zero in the final converged solution. The complete iterative solution procedure is given in the flow diagram of figure 4.3.

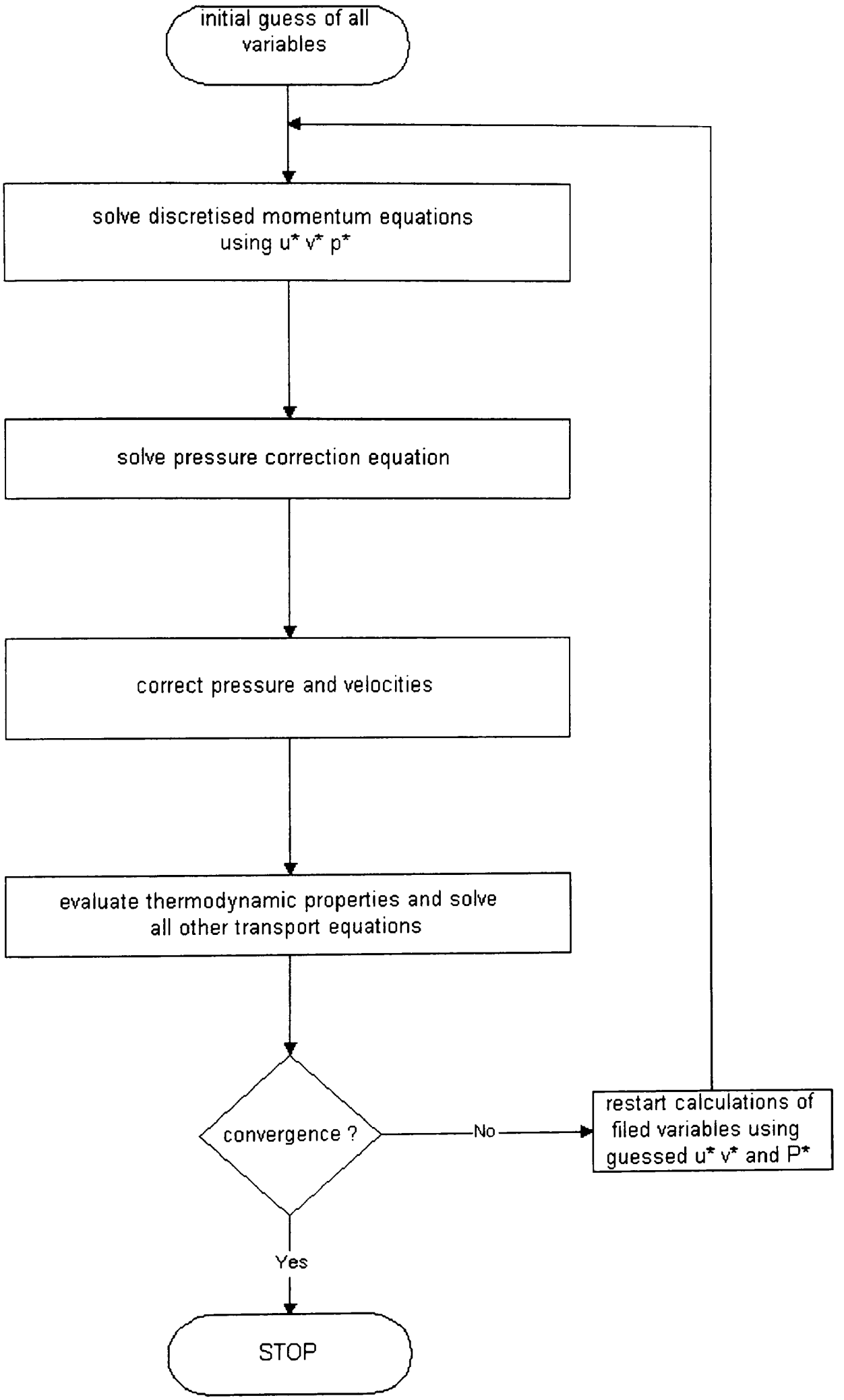

fig 4.3 flow chart for SIMPLE calculation procedure

4.2.7 Solution Of The Finite Difference Equation Set :

The solution in each plane is obtained through a line by line iteration procedure using the TDMA algorithm [141]. The operation is carried out in alternative directions along a set of lines in x and r plane.

In order to solve along the north-south lines the general finite difference equation is written as :

$$a_p\phi_p = a_N\phi_N + a_S\phi_S + [a_W\phi_W + a_E\phi_E + (b\phi_p + c)\Delta x\Delta y] \qquad (4.41)$$

The values of ϕ along the north-south line are obtained using TDMA and assuming that the quantity inside the bracket is temporarily known (i.e. using the old values). This is repeated for all north south lines. To solve along an east-west line the finite difference equation is written in the form given below and the same procedure is applied as above.

$$a_p\phi_p = a_N\phi_N + a_S\phi_S + [a_W\phi_W + a_E\phi_E + (b\phi_p + c)\Delta x\Delta y] \qquad (4.42)$$

4.2.8 Under Relaxation :

Instead of using the current value of a variable for the next iteration level, an under relaxed form of the variable is used to ensure computational stability. The under relaxation is programmed in such a way that it can be introduced independently to each variable of the finite difference equation set (u, v, T, P,μ,η, λ, k,ε).

$$\phi_P = \alpha \phi_P^{old} + (1-\alpha)\phi_P^{new} \qquad (4.43)$$

where superscripts *new* and *old* denote the current iteration and the old iteration values. α denotes the under relaxation factor.

4.2.9 Convergence Criteria :

The convergence criteria is based on the residual source term defined as :

$$R_\phi = a_P\phi_P - a_W\phi_W - a_E\phi_E - a_S\phi_S - a_N\phi_N - (b\phi_p + c)\Delta x\Delta y \qquad (4.44)$$

and convergence is satisfied when

$$\sum_{all\,nodes} |R_\phi| < R_{\phi,ref}$$

where $R_{\phi,ref}$ is a specified reference value for each variable

4.2.10 Incorporation Of Boundary Conditions :

4.2.10.1 inlet boundary conditions :

Distribution of all flow variables must be specified at the inlet boundaries. Numerical data of variables and the inlet X-plane data specification points are given in table 4.4.

Variable	specified value	grid location
u	u_{in}	$i=2$, $J=2$
v	0	$I=1$, $j=2$
p'	0	$I=1$, $J=2$
k	Iu_{in}^2	$I=1$, $J=2$
ε	$C_l\, k^{1.5}$	$I=1$, $J=2$
T	T_{in}	$I=1$, $J=2$
m_f	m_{fin}	$I=1$, $J=2$

table 4.4 inlet boundary conditions

where :

I is turbulent intensity and C_l is the turbulent length scale parameter taken in this study as a function of the diameter ratio of the inlet tubes.

4.2.10.2 wall boundary conditions :

When a wall is encountered the coefficients at the wall are suppressed by setting them to zero. (As an example, if there is a wall at the south boundary, the coefficients a_S closest to the south boundary are set to zero.) Then the boundary condition of the variable of interest is incorporated via the linearised source (sec 4.2.4) term.

Based on the value of y^+ the equations for shear stress, wall heat transfer etc. are selected for the laminar sub-layer and the inertial sub-layer. (refer to chapter 2.3.x for description of wall function approach).

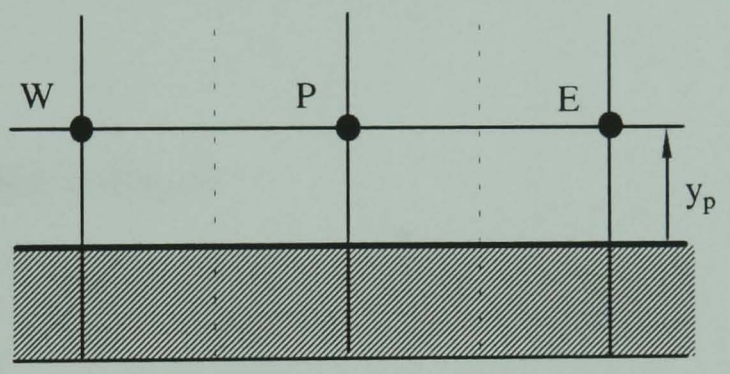

fig. 4.4 near wall cells

4.2.10.3 momentum equations tangential to the wall :

laminar region (y^+ <11.63) :

The shear force F_s can be written as :

$$F_s = -\tau_w A = -\mu_l \frac{u_P}{\Delta y_P} A \qquad (4.45)$$

where :

τ_w = wall shear stress

u_P = velocity at the grid node

μ_l = laminar viscosity

A = wall area of the control volume cell

Δy_P = distance to the node from the wall

When the above equation is represented as a linearised source term the equation has the following form :

$$\iint_A S_\phi \, dA = (b\phi + c)AREA = (bu_P)A$$

where :

$$b = -\mu_l \frac{1}{\Delta y_P} \qquad c = 0$$

turbulent region ($y^+ = 11.63$)

$$F_s = -\tau_w A = -(\rho C_\mu^{1/4} k_P^{1/2} \frac{u_P}{u^+})A \qquad (4.46)$$

where :

C_μ= friction coefficient

k= turbulent kinetic energy

u^+= non-dimensional velocity

ρ = local density

therefore the source term is :

$$\iint_A S_\phi dA = (b\phi + c)AREA = (bu_P)A$$

where:

$$b = (\rho C_\mu^{1/4} k_P^{1/2} \frac{1}{u^+}) \quad c = 0$$

4.2.10.4 momentum equation normal to a wall :

No special treatment is necessary, because the velocity normal to the wall is zero by definition.

4.2.10.5 energy equation :

laminar region :

Heat conduction from the wall at a fixed temperature T_w into a near wall cell is given by:

$$q_w = \lambda \frac{(T_w - T_P)}{\Delta y_P} = \frac{C_p \mu}{\sigma_l} \frac{(T_P - T_w)}{\Delta y_P} \qquad (4.47)$$

where :

q_w = heat transfer rate

λ = laminar thermal conductivity

C_p = specific heat capacity

T_w = wall temperature

T_P = node temperature

When the above boundary condition is linearised it has the following form.

$$\iint_A S_\phi \, dA = (b\phi + c)AREA = (bT_P + c)A$$

$$b = -\frac{\mu}{\sigma}\frac{C_P}{\Delta y_p} \qquad and \qquad c = \frac{\mu}{\sigma}\frac{C_P T_w}{\Delta y_p}$$

When the wall is adiabatic both b and c are zero.

the turbulent region :

wall heat transfer rate is defined as :

$$q_w = -\rho C_\mu^{1/4} k_P^{1/2} (T_P - T_w) / T^+ \qquad (4.48)$$

and the source term is linearised as above.

4.2.10.6 pressure correction equation :

No change is necessary.

4.2.10.7 *k* equation :

The turbulent energy for a control volume cell is given by :

$$\tau_w u_P - (\rho C_\mu^{3/4} k_P^{3/2} u^+)\Delta V / \Delta y_p \qquad (4.49)$$

where :

ΔV = volume of the cell

based on the value of the non-dimensional distance y^+, the u^+ term in the above equation is changed for the turbulent and the laminar regions. Then the source term is normalised as follows.

$$\iint_A S_\phi \, dA = (bk + c)A$$

$$b = -(\rho C_\mu^{3/4} k_P^{1/2^*} u^+) \qquad c = \tau_w u_P \qquad A = \Delta V / \Delta y_P$$

In the term b of the above equation, part of the k term is retained. This is done to conform with the linearisation of the source term. The value used for this part ($k_P^{1/2^*}$) is the value generated by the previous iteration level.

4.2.10.8 ε equation :

The desipation rate ε reaches its maximum value at the wall. For this reason a fixed value of ε is used irrespective of y^+ for the near wall cell. This constant value of ε is found using the following relation.

$$\varepsilon_P = \frac{C_\mu^{3/4} k_P^{3/2}}{\kappa \Delta y_P} \qquad (4.50)$$

The introduction of a constant value via the source term is as follows :

$b=10^{30}\varepsilon_P$ and $c=-10^{30}$

When these values are substituted into the discretised finite difference equation it has the following form for the near wall cells.

$$(a_P + 10^{30})\varepsilon_P = \sum a_{nb}\,\varepsilon_{nb} \quad + \quad 10^{30}\,\frac{C_\mu^{3/4} k_p^{3/2}}{\kappa\,\Delta y_P} \qquad (4.51)$$

Due to the very large numerical value used in the first and the third terms, in the above equation it acts as fixed value of ε for the near wall node.

4.2.10.9 species mass fraction equation :

No special modification is needed.

4.2.10.10 symmetric boundary conditions

At a symmetric boundary, conditions are as follows: 1.) no flow across the boundary 2.) no scalar flux across the boundary. In the implementation of the above, velocities normal to the symmetric axis are set to zero and the values of all other properties are equated to their values at the nearest node just inside the solution domain. (It is important to note that the symmetric axis is always outside the solution domain.)

4.2.10.11 outlet boundary condition :

It is assumed that all fluxes are zero at the outlet boundary. This implies that $\phi_{NI,J} = \phi_{NI-1,J}$.

4.3 Description of the single-phase mixing program :

4.3.1 General Overview :

The program is designed to model the mixing process involved in steady state turbulent flows inside a cylindrical combustion chamber. The partial differential equations governing the flow are descretised into finite volume form which are then solved numerically. The structure of the program is based on the TEACH-T code of Gosman *et al* [103].

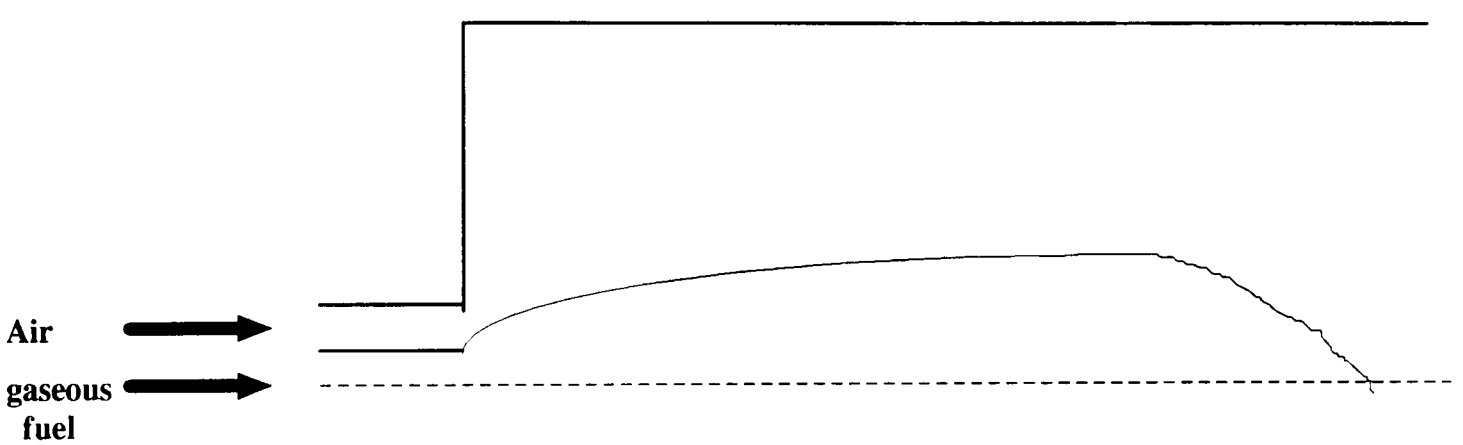

fig. 4.5 cross-sectional view of the chamber configuration

A cylindrical combustion chamber shown in figure 4.5 with fuel and air inlets placed concentrically at one end of the chamber is considered. The length and diameter of the chamber and the radius of each inlet port could be varied by the user. Fuel type can also be changed by supplying the relevant critical properties (t_c,, v_c), acentric parameter (ω), molar mass of the fuel and a temperature based function for isobaric specific heat capacity ($C_p(T)$). The program is capable of deriving all the other necessary chemical and thermodynamic data using the above information.

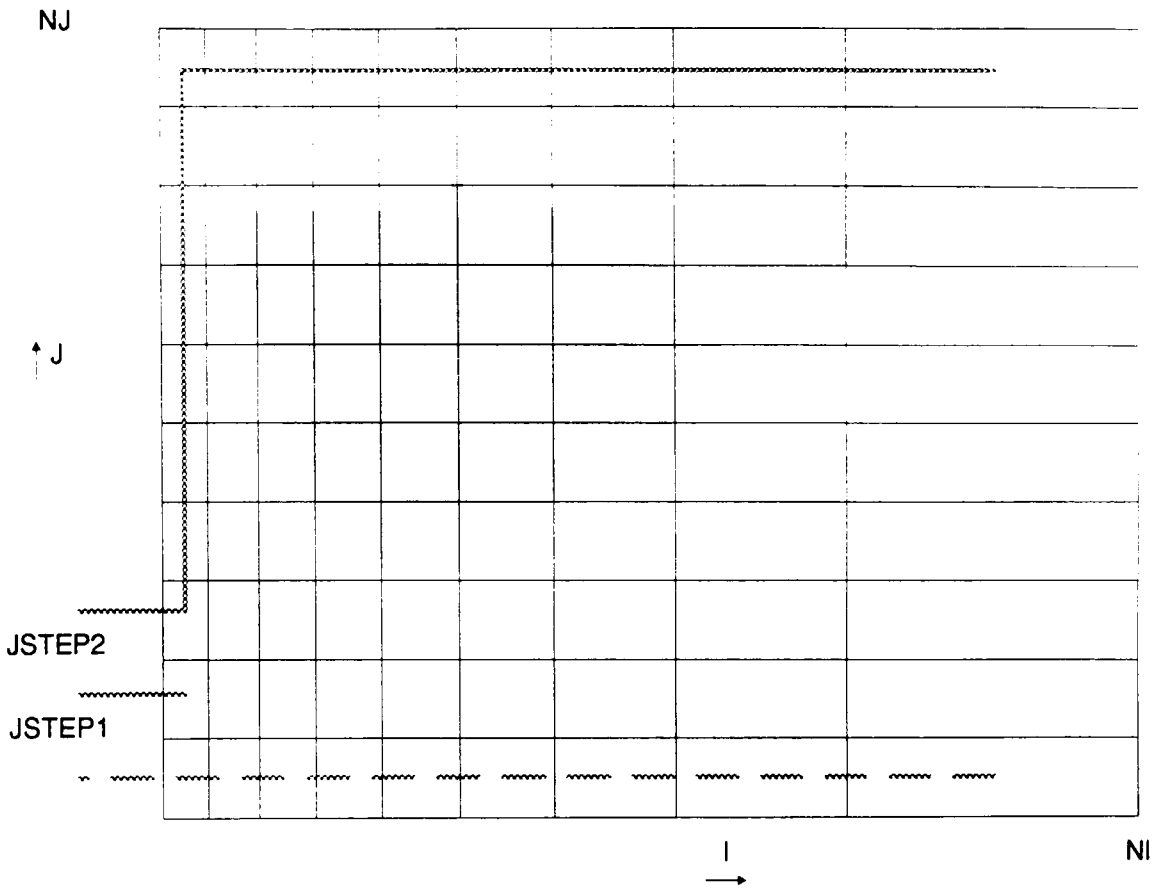

fig. 4.6 grid system

For the finite volume formulation the chamber is divided into NI grid points in the axial direction and NJ grid points in the radial direction. (fig.4.6) The terms JSTEP1 and JSTEP2 in the figure 4.6 denotes the last grid point inside each of the two inlet ports supplying air and fuel. The dark line represents the physical geometry of the cylindrical chamber and the dashed line represents the axis of symmetry. Apart from the staggered grid arrangement (section 4.2.2), the grid system used is an expanding grid in both X and Y direction. The expanding grid can be disabled at the start of the program execution if it is unnecessary.

4.3.2 Program Layout :

The program is designed to be very modular in nature. This allows for the addition of specific routines in the future. The solution procedure is based on the SIMPLE method, details of which are given in section 4.2.6.

The program operates in the following sequence. Input variables are read from the data files and the grid system is set based on user defined conditions. Initialisation of the flow and property variables are carried out next. The program then proceeds into an iteration loop, where solution of the flow variables using a TDMA algorithm, updating of property matrices and the boundary conditions are carried out. The iteration is performed until convergence is achieved or until a pre-determined maximum number of iteration steps is reached. The number of iteration steps and the convergence criteria are supplied by the user (Fig 4.7).

All flow variables have their own subroutine modules. The structure of the subroutine module is such that, for each variable the generic part of the partial differential equation and the terms other than the boundary condition source terms are evaluated in one routine (starting with letters 'CALC', i.e. CALCU, CALCV, etc.). The rest of the source terms are formulated in a separate common subroutine for all flow variables which has multiple entry and exit points for each variable (PROMOD). The reason for this arrangement is as follows. Since for the descritised equations most problem dependent modifications are done at the flow boundaries, therefore it is more practical to keep the boundary conditions separate from the rest of the equation. This allows problem dependent modifications to be carried out safely and speedily.

All gas thermodynamic and chemical properties are calculated by a separate property module which sets up the property matrices before transferring control to the main unit. When program control is transferred to this module it, in tern, calls a set of routines for the calculation of molar volume, specific heat capacities and laminar viscosity.

All output is directed to files. Output of all flow variables of the computational domain is printed at increments of a user supplied value of the iteration level. This is to facilitate for the run time check of variables. Final output is also written in a format accessible to MATLAB for processing and visualisation.

4.3.3 Definition Of Subroutines And Functions:

PRINT	routine to print all flow variables of the computational domain at user specified iteration level
PRINTVEL	routine to print data in MATLAB readable format
LISOLV	TDMA routine for line by line iteration method for the solution of the finite volume equations
CALCU	descritsed u-momentum equation
CALCV	descritised v-momentum equation
CALCT	descritised energy equation

CALCF	descritised fuel mass fraction equation
CALCED	descritsed turbulent energy dessipation rate equation
CALCEK	descritised turbulent kinetic energy equation
CALCP'	descritised pressure correction equation
PROPS	module which co-ordinates all the property subroutines, calculation of the necessary turbulent parameters and setting up of the property matrices.
PROMOD	unit which is used to calculate the boundary condition source terms of each 'CALCϕ' routine. This unit has seven entry points for each ϕ value
BWR	Benedict Web Rubin equation for molar volume calculation
CPCVIDL	ideal gas C_P(T), C_v(T) calculation routine
VISCTHRM	laminar viscosity and thermal conductivity calculation routine

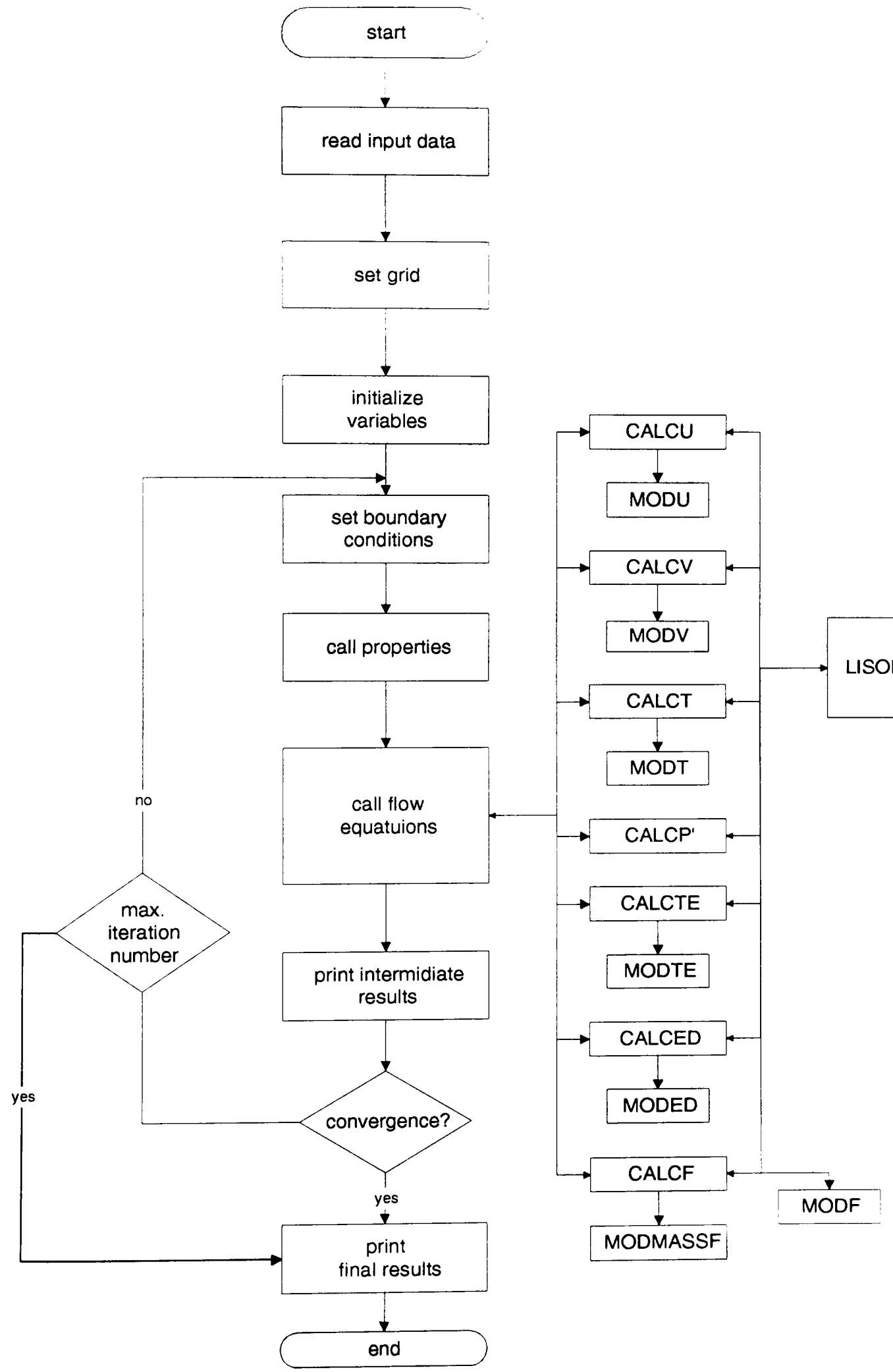

fig.4.7 flow diagram for the mixing program

4.4 Description of the two-phase evaporation program :

4.4.1 General Overview :

The two-phase evaporation model is an LHF type model formulated to simulate the droplet evaporation and the mixing process of turbulent gas-liquid flows (figs. 4.8-4.9b). In the LHF formulation, (as discussed in chapter-2) the velocity and temperature differences between the two phases are neglected in the mixing program. The presence of the disperse phase is accounted for via the mixture density, which is a linear combination of the densities of liquid fuel, vapourised fuel and air. In most LHF formulations [110, 111] the dispersed phase evaporation is calculated via a fuel saturation vapour pressure function in each control volume [110, 111]. Since the partial pressure to total pressure ratio of each component can be related to its molar fraction, this allows for the determination of the liquid fuel and fuel vapour mass fractions in a control volume, provided the total mass fraction is known. As will be explained in the discussion section, the above method of calculation of the mixture density seriously over estimate the gasification rate, therefore in this model a more realistic approach is adopted to represent the fuel evaporation. A droplet evaporation program is run parallel to the mixing program with facility for passing data between the two modules. The droplet program obtains information regarding the droplet resident time and position from the mixing program (to work out the evaporation rate). The mixing program then uses the evaporation data from the droplet module to calculate the local density for each control volume. Since the mixing part of the model is based on the previously discussed gas-phase model, a significant amount of the features are common to both programs. These include the cylindrical co-ordinate system, expanding and staggered grid arrangement,

convergence criteria for the mixing analysis, subroutine layout for flow variables u,v,T,P',k,ε , m_f, intermediate and final output control routines. Therefore these features of the program will not be discussed in this section, and the discussion will be confined to features specific to two-phase modelling, such as inclusion of the evaporation model, inlet conditions, etc.

Since the program is a steady state one it is assumed that the fuel is injected into the combustion chamber as a continuous stream through the inner tube (fig. 4.5). Due to modelling difficulties, (which are discussed in the next paragraph) at the injector exit the program starts its calculations at an empirically found distance down-stream of the injector, with a diameter much larger than the actual injector exit diameter. This is sometimes referred to by other workers as an equivalent diameter. It is also assumed that the fuel remains in liquid form throughout the time it takes to travel this distance. The above can be justified by: 1.) the fuel temperature near the inlet is relatively low causing negligible evaporation, 2.) the velocity of the flow is high in this region, leading to a smaller residence time.

Immediately outside the injector, due to high liquid mass fractions the overall density becomes very high relative to the density in a control volume of the same y-plane but outside the injector exit cross section area. This density differences cause numerical instabilities. Therefore the flow calculation needs to be started down stream of the injector where the density differences are small enough to avoid instability. In this

model the calculations are started form a radius of 4mm. Further details regarding this empirically found value are given else where [14].

Since the calculation starts from a pre-defined position down-stream of the injector, the inner tube fluid is no longer completely liquid fuel, it is a mixture of liquid fuel and air. Therefore when calculating initial density this needs to be taken into account. Also it is more appropriate to use profiles to represent the initial distribution of velocity, temperature and the mass fraction rather than use a constant set of values. This allows the inner tube fluid variables to merge with the ambient variables without sudden discontinuities. To keep the initial conditions consistent with the work of Nazha [14], the following profiles were used to generate the entry boundary conditions for the flow domain.

Inlet u-velocity profile :

$$u(j) = u_{\text{air}} + (u_{\text{c\_in}} - u_{\text{air}})\left(1 - \left(\frac{r(j)}{r_{\text{tot}}}\right)^{3/2}\right)^2 \qquad (4.52)$$

Inlet temperature profile :

$$T(j) = T_{\text{air}} + (T_{\text{c\_in}} - T_{\text{air}})\left(1 - \left(\frac{r(j)}{r_{\text{tot}}}\right)^{3/2}\right) \qquad (4.53)$$

inlet mass fraction profile :

$$f(j) = C_{\text{int}}\left(1 - \left(\frac{r(j)}{r_{\text{tot}}}\right)^{3/2}\right) \qquad (4.54)$$

Inlet density profile :

$$\rho\ (j) = \left((1 - f(j) \frac{R_{air} T_{air}}{P_{air}} + \frac{f(j)}{\rho_{lqd}} \right)^{-1} \qquad (4.55)$$

Where:

U_{air} = inlet air velocity

U_{c_in}= centre line fuel velocity

r_{tot} = radius of the fuel tube

$r(j)$ = j^{th} radial point

T_{air} = air temperature

T_{c_in} = centre line fuel temperature

C_{int} = initial concentration

P_{air} = inlet air pressure

ρ_{lqd} = liquid fuel density

It is necessary to preserve the injected mass and the injected momentum at this 'new' inlet. Therefore a separate pre-processing program is run to obtain the optimum *r*-grid for inlet mass and momentum conservation. Further details of this program are given in section 4.4.4. Once the inlet conditions are specified the program proceeds in a manner similar to the single-phase mixing program, but with a greater initial density difference. The changes that occur are the change in properties due to the evaporation of the liquid phase. These are calculated in the property module (fig. 4.9-4.9b). The property module and its features are discussed in the next sub section.

The spray evaporation is modelled as follows. A mean diameter, single droplet, evaporating along the flow axis is assumed to be representative of the spray evaporation. The start of the evaporation is at the first x-grid location inside the computational domain. The evaporation is only allowed to occur if the residence time within the control volume is greater than the droplet evaporation time step. Otherwise the evaporation rate of the upstream cell is used for the current cell. Once the evaporation rate has been derived the liquid to gas ratio of the fuel is calculated. Based on this information the density of that particular centre line cell and the specific heat capacities are derived using the following equations:

density of the mixtures in any cell on the axis :

$$\rho = \left((1 - f\frac{m_{\text{new}}}{m_{init}}) \left(\frac{(1-f)}{(1-\frac{m_{\text{new}}}{m_{\text{init}}} f)} R_{\text{air}} + \frac{f(1-\frac{m_{\text{new}}}{m_{\text{init}}})}{(1-\frac{m_{\text{new}}}{m_{\text{init}}} f)} R_{\text{fuel\_vap}} \right) \frac{T}{P} + \frac{f\frac{m_{\text{new}}}{m_{\text{init}}}}{\rho_{\text{lqd}}} \right)^{-1} \qquad (4.56)$$

Isobaric specific heat capacity of the mixture in any cell on the axis :

$$C_P = \frac{m_{\text{new}}}{m_{\text{init}}} f\, C_P(T)_{\text{lqd}} + (1-\frac{m_{\text{new}}}{m_{\text{init}}}) f\, C_P(T)_{\text{fuel\_vap}} + (1-f) C_P(T)_{\text{air}} \qquad (4.57)$$

Where :

m_{new} = current droplet mass

m_{init} = original droplet mass

$R_{\text{fuel\_vap}}$ = gas constant for fuel vapour

$C_P(T)_{\text{fuel\_vap}}$ heat capacity of fuel vapour

The droplet evaporation is activated from a single call to the droplet module (which contains all the necessary subroutines for the evaporation model to work) making the module invisible to the rest of the program. This facilitates the quick removal and addition of a different droplet module in future modifications of the program. The quasi-steady gas-phase and finite liquid-heating droplet model was used as the evaporation module in this study. This choice was purely based on computer CPU time considerations. Further information about the reasons for this selection is given in the discussion section.

4.4.2 Mathematical Features Of Importance In Relation To Combustion Flow Analysis :

There are two major sources of energy transfer between the two phases. The disperse phase absorbs energy as enthalpy of evaporation from the gas-phase. The gas-phase gains energy from the burning of the evaporated fuel mass. The above phenomena can be incorporated into the gas-phase energy equation as a sink term and a source term respectively. The above approach of accounting for the energy transfer is more suited for a separated flow (SF) type model, where the droplets are tracked individually. Since the current model is a variant of the LHF formulation, another approach could be taken, which allows a significant reduction in execution time. This is based on running the evaporation module and the mixing module at two different temperature levels, where the temperatures used are arrived at by experimental considerations. A description of this process is given in the following section.

In this model the transfer of energy between the two phases is based on the change of properties (fuel mass fraction, density, etc.) of the gas-phase due to the evaporation process. The changes that occur in the control volumes traversed by the droplet during its life time is propagated to other control volumes via the mixing process. The model therefore can be described as an 'effective property' type LHF formulation. The droplet evaporation process causes a reduction in the gas-phase cell temperatures (due to the enthalpy of evaporation). When combustion is considered there is a significant increase in the cell temperatures due to the enthalpy of combustion. Both of the above processes need to be taken into account when the initial gas temperature is specified to the program as a boundary condition. Since the combustion module is run at the end of the program as a 'mixed is burnt' type module this necessitates that the initial air temperature is reasonably high to simulate mixing with close to combustion temperature. Thus a mean value of 1500K based on known experimental findings [14] was therefore chosen as the initial inlet temperature. Based on the above temperature and the given inlet fuel mass flow rate, the inlet air velocity and density are calculated. This treatment causes the theoretical values of the velocities and densities in the second half of the chamber (fully evaporated region) to be more representative of the actual ones. Although this treatment causes the gas velocities in the near injector region to differ substantially from the actual gas velocity, since the jet velocity is more dominant in this region, which would not have decayed sufficiently by then to allow the effects of the discrepancy between the initial air velocity and the local air velocity to become significant.

The second problem that needs to be addressed is the dispersed phase evaporation. If the evaporation is simulated at the earlier discussed gas-phase temperature it can be seriously over estimated. On the other hand if the evaporation is carried out at a cell temperature based purely on the mixing process (without combustion), it can be underestimated for a combustion flow situation. Therefore the evaporation is masked from the gas-phase cell temperature. The evaporation is carried out using an empirically determined temperature function. This function provides the required ambient temperature for evaporation based on the axial distance traversed by the droplet during its life time. The form of the function used was arrived at by comparing the theoretically predicted values of temperatures with that of the experimentally observed values of Nazha [14].

As the model stands there are no source or sink terms in the bulk gas-phase energy equation to take account of energy transfer from/to the droplet phase. It was not considered necessary to use source or sink terms in the energy equation due to the following reason. Since droplet evaporation modelling is carried out only along the centre line, adding a source or a sink term to the energy equation does not give a significant increase in accuracy to the program. Because the source term will be ineffective in all the control volumes other than the centre line ones.

4.4.3 Turbulence Modelling Approximations :

It is assumed that the flow is fully turbulent. This is a reasonable assumption since the *Re* number of the flow is high. The viscosity of the flow is therefore calculated as a fully turbulent viscosity μ_t. The standard exchange coefficients (σ_x) used in gas flows

are used as exchange coefficients for the calculation of diffusion terms in the momentum, energy and mass fraction equations.

$$\mu = \mu_l + \rho k^2 C_\mu / \varepsilon \qquad (4.58)$$

4.4.4 User Supplied Data And Pre-Processing :

The initial inputs for property calculations are similar to those used in the mixing program. A major difference of this program is that the *r* co-ordinates of the grid need to be supplied to the program by the user. The need arises from to the necessity of conserving the injected mass and momentum at the end of the empirically arrived at distance from the injector tip. A separate mass and momentum conservation program (fig. 4.10) is run to obtain the optimum *r*-step expansion factor and then the *r*-grid. The *r*-grid data is written to a file accessed by the two-phase program.

The minimum number of points required in the inner tube is specified to the *r*-grid generator program. Conforming to a supplied value and based on the previously discussed inlet profiles for velocity, temperature and density, the program will generate the required grid for inlet mass and momentum conservation. The gird generation is an iterative process, based a guessed initial expansion factor. The program works in an iterative loop until percentage errors of mass and momentum are less than 0.5%.

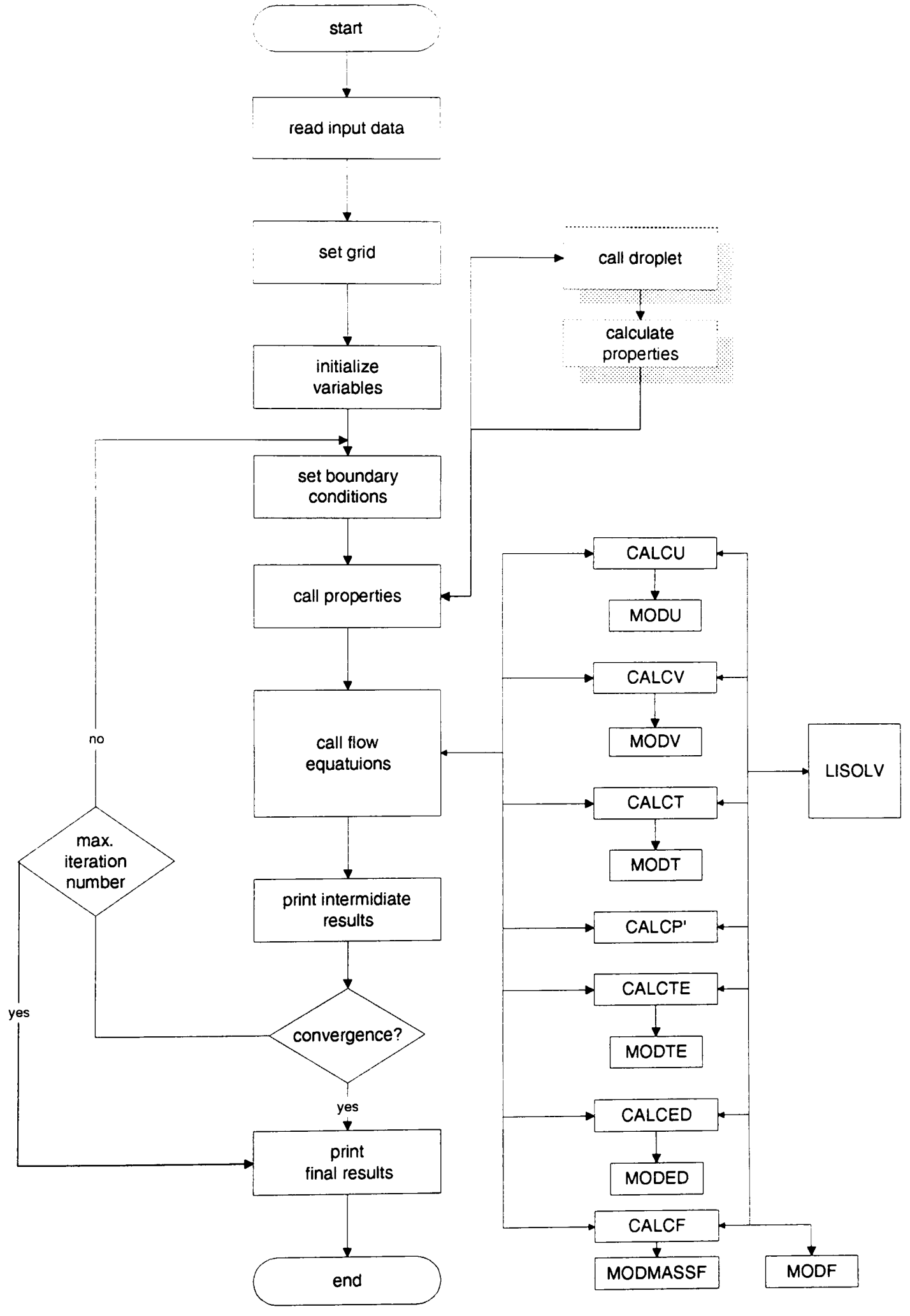

fig 4.8 droplet incoperated two phase program

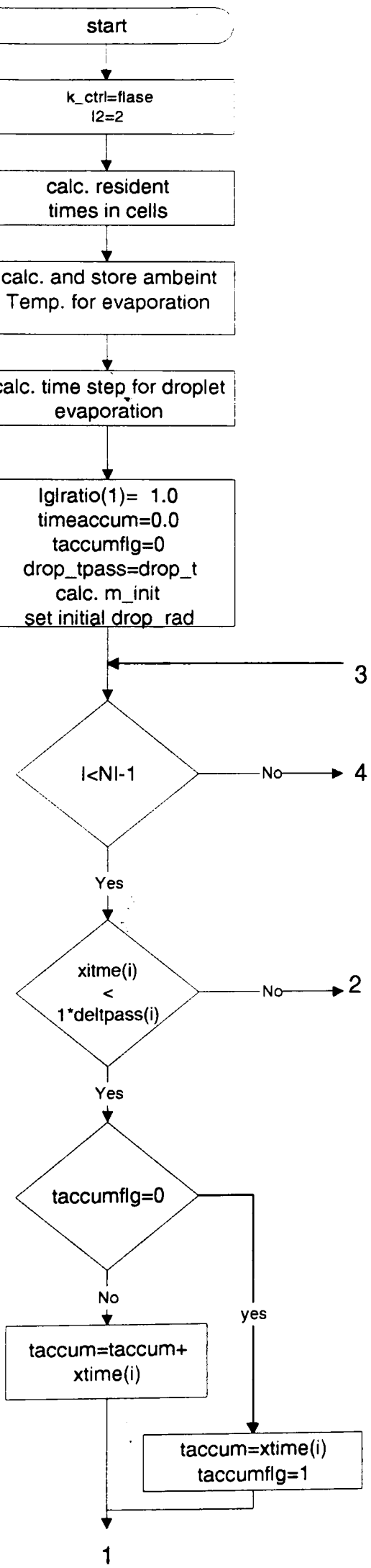

fig 4.9 part-1 of the property routine

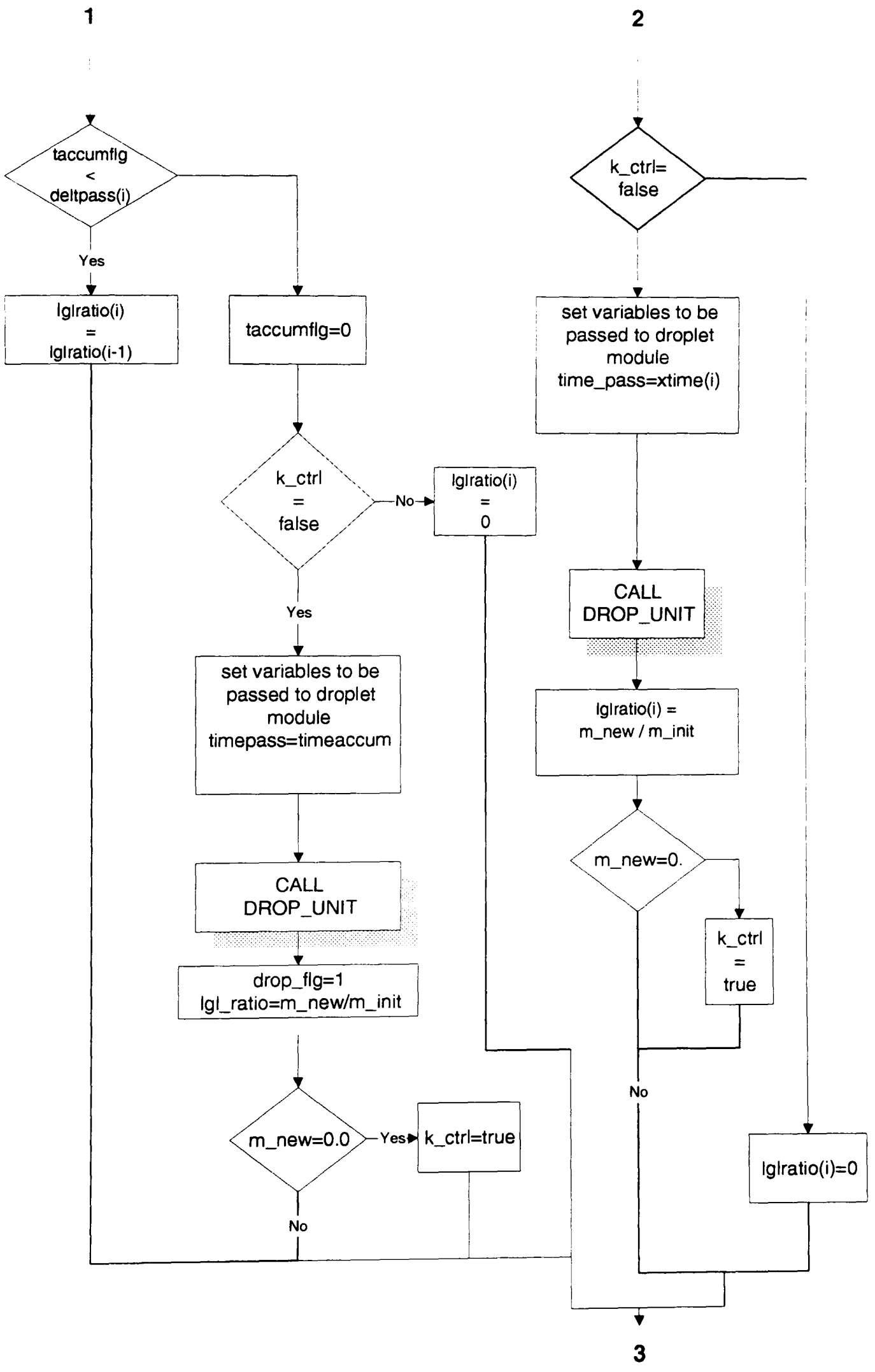

fig 4.9a part-2 of the property routine

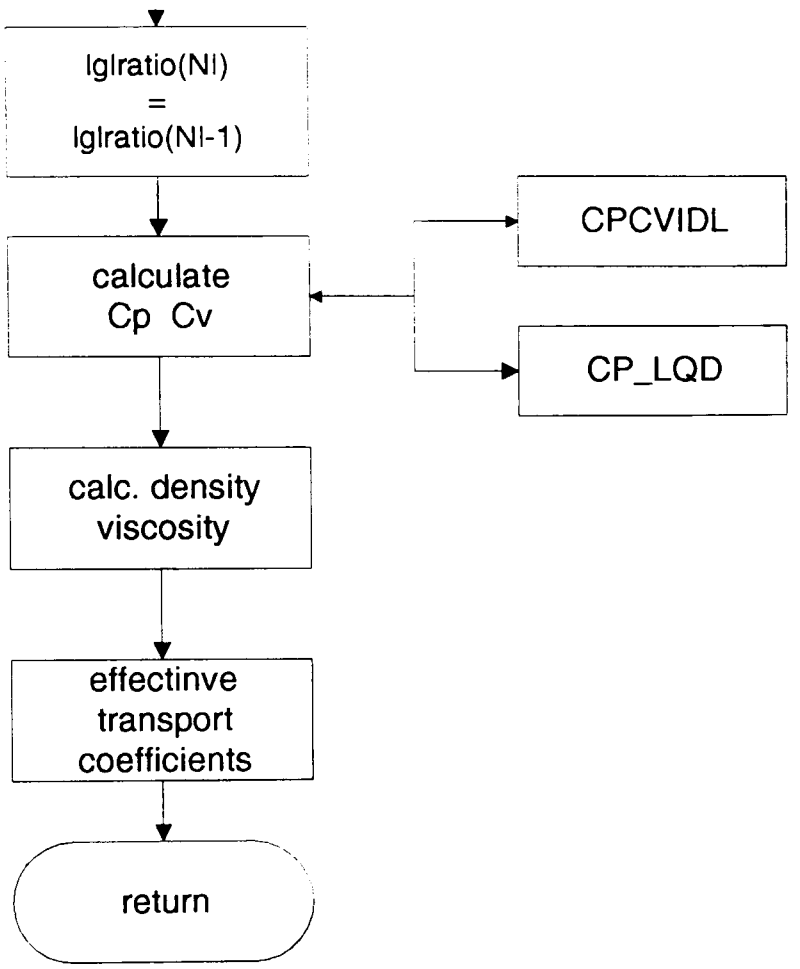

fig 4.9b part 3 of the property routine

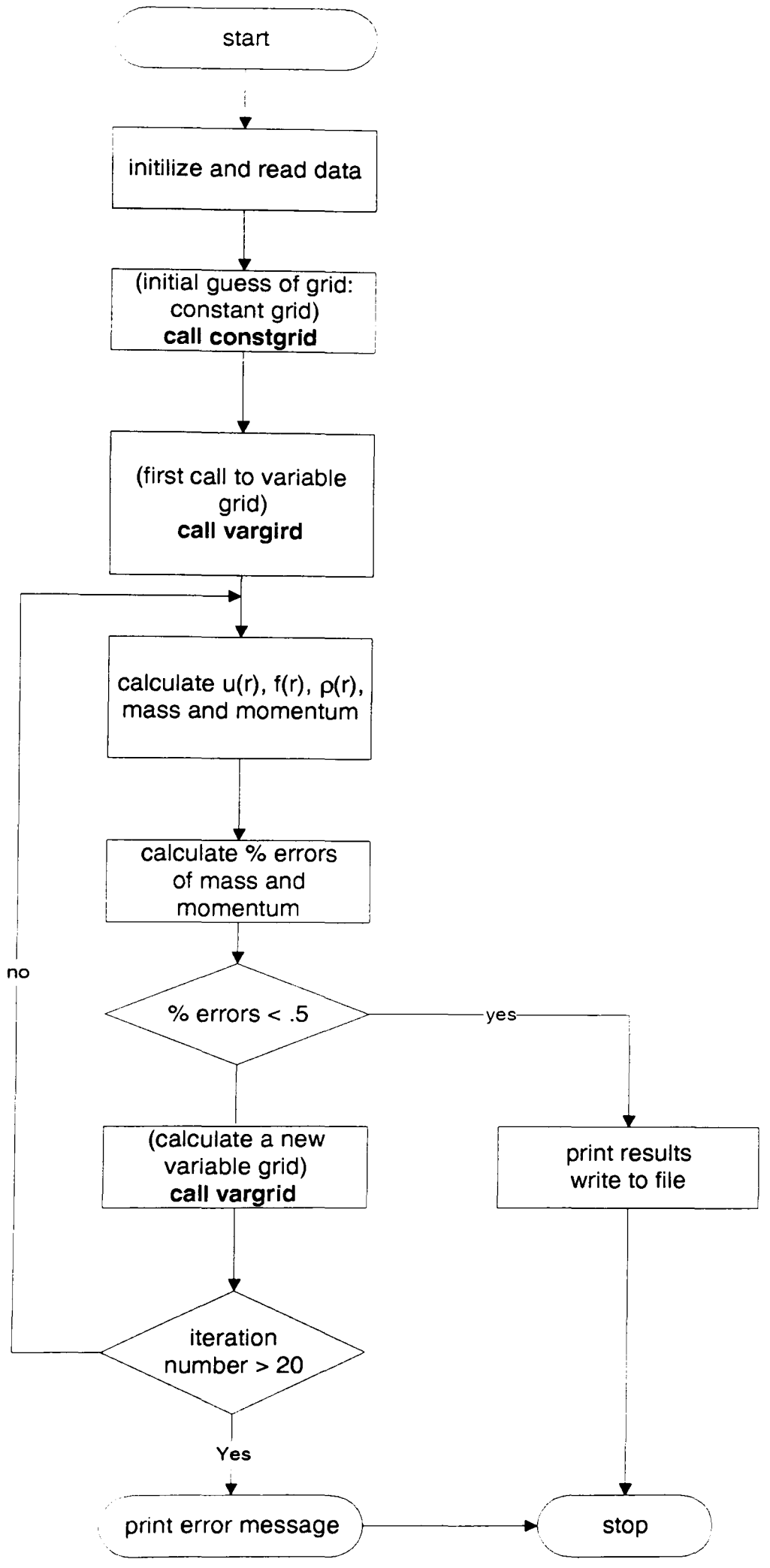

fig 4.10 *r*-grid generator

CHAPTER-5

COMBUSTION MODULE

5.1 Introduction :

Although the crux of this research is to formulate a two-phase mixing model, it became necessary to develop a combustion module to validate the results of the two-phase program. This is due to the existing experimental data [14] being only available for post-combustion analysis. Therefore a combustion module of the type, 'mixed-is-burnt' was formulated. The module is based on the minimisation of Gibbs free energy of the system. It is assumed that the combustion system is adiabatic and the combustion is governed by the steady flow energy equation. The module is based on the work of Nazha [14], therefore only the modifications that were carried out to the routines are discussed here. For the interested reader more information regarding the minimisation method can be obtained from reference [14].

5.2 Flame Temperature :

The combustion module has a driver program which passes the fuel map and the temperature map of the mixing programs in a format accessible by this module. In the module the flame temperature is initially calculated assuming stoichiometric combustion. Based on the local equivalence ratio in the control volume the local mixture could be lean, stoichiometric or rich, therefore the enthalpy balance equation needs to be modified to calculate the flame temperature depending on the strength of the mixture. The equations of interest are as follows :

stoichiometric combustion equation for initial guess :

$$C_ZH_S + b\,O_2 + f\,N_2 \rightarrow a\,H_2O + d\,CO_2 + f\,N_2 \qquad (5.1)$$

Where a, b, d and f are the number of moles of each species and z, s are the number of carbon atoms and hydrogen atoms in the fuel molecule.

flame temperature [14] :

$$T_f = \frac{\left(HC + n_p C_{Pp_{T_r}} T_r + \frac{n_{as}}{\phi_v} C_{P_a T_g} + C_{Pv T_g} T_g - \frac{n_{as}}{\phi_v} C_{PaT_r} T_r - C_{PvTr} T_r \right)}{n_p C_{PpTr}} \qquad (5.2)$$

where: HC = $(CV)_{FUEL}$ for the lean and stoichiometric mixture.

CV = lower calorific value

$HC = \frac{(CV)_{FUEL}}{\phi_v}$ for the rich mixture

$C_{P_p} = \sum_P \frac{n_i}{n_p} C_{P_i}$ mean product isobaric heat capacity

Cp_a = Cp of air

Cp_v = Cp of fuel vapour

$$\phi_v = \frac{\frac{Fuel\,mass\,fraction}{Air\,massfraction}}{(Fuel\,/\,Air)_{stoichiometric}}$$

T_r = reference temperature (298K)

T_g = initial temperature of reactant species

T_f = flame temperature (product temperature)

n_{as} = number of moles of air required for stoichiometric combustion

n_p = total number of moles of products

Since T_f and $Cp(T)$ are inter-related, the above equations need to be solved iterativly to obtain the correct value of T_f. The $Cp(T)$ values of the reactants and the products are calculated from a forth order polynomial of temperature based functions, which were generated by curve fitting the $Cp(T)$ data given in references [33, 139]. The program is designed to calculate the flame temperature with a specified convergence limit which can be changed if required. The value used in this exercise is 50K. The second step is to evaluate the flame temperature to a higher degree of accuracy, assuming the combustion proceeds according to the following equation.

$$C_ZH_S + j\,O_2 + f\,N_2 \rightarrow a\,H_2O + b\,CO_2 + d\,CO + e\,H_2 + f\,N_2 + g\,O_2 \qquad (5.3)$$

Where a, b, d, e, f and g are the number of moles of various products species found from equilibrium calculations. The new improved value of T_f can now be found from equation-5.2, bearing in mind that the heat of combustion HC is now taken as follows:

$$HC = (CV)_{FUEL} - d(CV)_{CO} - e(CV)_{H2} \qquad (5.4)$$

5.3 Prediction Of Combustion Products Via Minimisation Of Gibbs Free Energy :

The molar fractions of combustion product species are calculated assuming equilibrium concentration of product species. In the method being used, the Gibbs free energy of various combustion product species are considered and the solution is arrived at by minimising the total free energy of the system. The computer routines for minimisation are based on the routines developed by Nazha [14]. These were formulated using the theoretical analysis of White et al [149]. The Gibbs free energy calculations are further improved in this module by the use of fifth order polynomial functions to obtain the Gibbs energy for a given temperature and a given species. Twelve product species are considered (CO_2, CO, H_2O, H_2, N_2, O_2, CH_4, NO, HO, O, N, H) in this routine. The product species are supplied to the minimisation module with the relevant Gibbs functions based on the previously calculated flame temperature value. The minimisation program then works in an iterative loop to obtain the minimum total Gibbs free energy value, which it returns to the flame calculation routine with the product matrices.

The final values of the product matrices and the flame temperature matrix are passed to the driver unit, which prints the data to output files in a form accessible to the MATLAB post-processing routines for visualisation. The flow chart of the complete module is shown in figure 5.1.

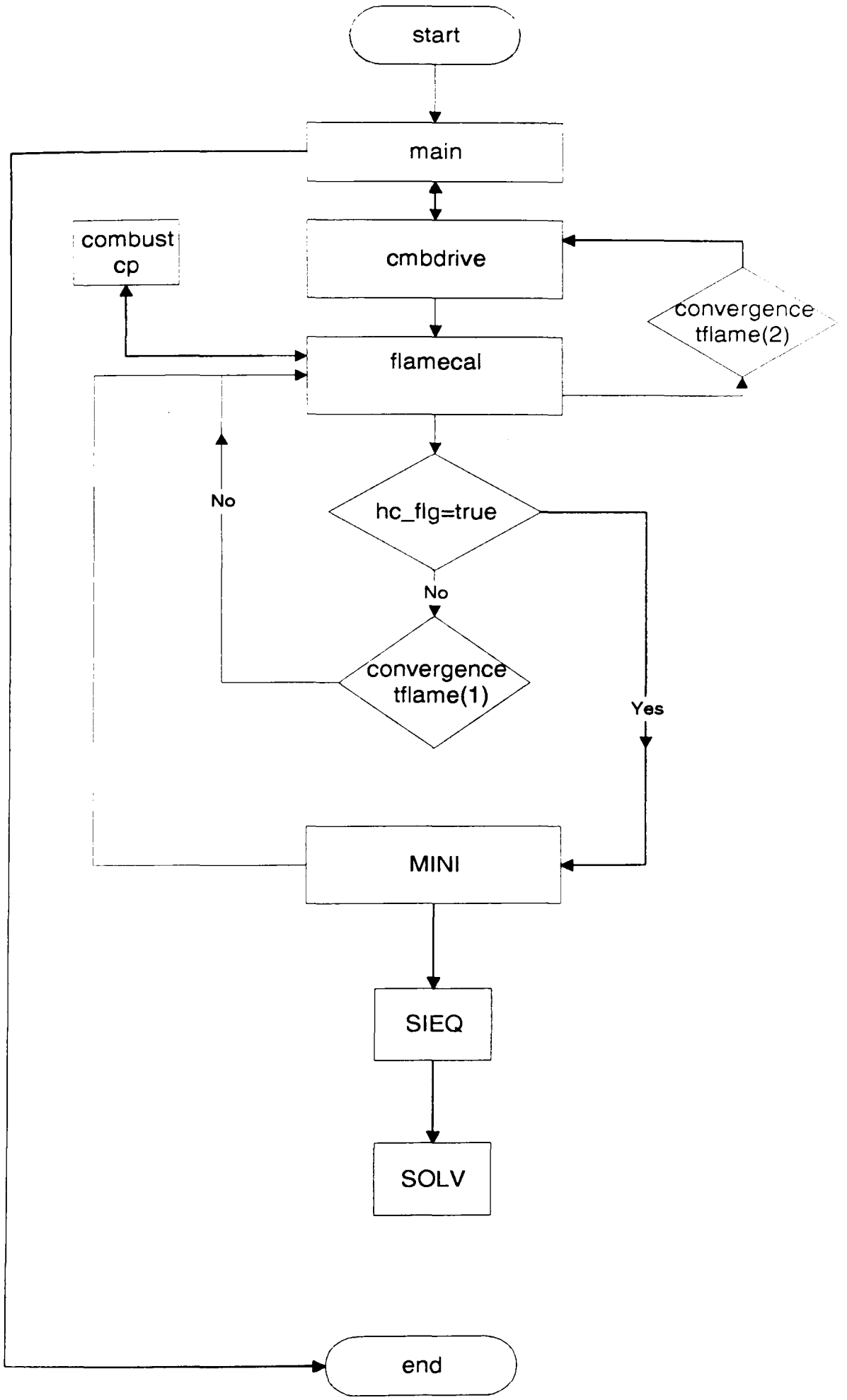

Fig. 5.1 flow chart for the combustion module

CHAPTER-6

RESULTS AND DISCUSSION

6.1 Introduction :

The chapter contains two section. In the first section results from the droplet models are discussed and compared, and the reasons for selecting the finite diffusivity model for inclusion in the two-phase spray program are explained. This is followed by section two where the results obtained from the single-phase mixing and the two-phase spray models are analysed and discussed in relation to existing experimental results and to other models of spray combustion.

6. 2 Droplet Models Analysis :

Three mathematical models describing the evaporation from a single droplet have been formulated. These are :-

1.) an infinite liquid-phase thermal conductivity with quasi-steady gas-phase model;

2.) a finite liquid heating model with quasi-steady gas-phase model, and

3.) an unsteady gas-phase with infinite liquid thermal conductivity model.

The mathematics of the models formulation and the programming techniques followed are given in chapter-3.

6.2.1 Quasi Steady Gas-Phase With Infinite Liquid Heating Model :

This is the simplest of all three models and the first one to be formulated. Due to its fast execution time, it was chosen to evaluate the effects of pressure dependent property routines and of variable liquid density on the evaporation rate. Once the significance of these variables were identified, the relevant routines were incorporated into the other models.

6.2.1.1 the effect of BWR equation of state and pressure dependent properties :

The need to use accurate variable thermodynamic and chemical properties in the air-fuel-vapour film surrounding an evaporating droplet have been highlighted by many researchers [10, 83]. Nevertheless, most existing models still rely on the use of the ideal gas equation as the equation of state, and on properties dependent on temperature only. Pressure and specific, or molar, volume have significant effects on calculated properties such as viscosity, diffusion coefficient, etc. [139]. The above model was run using two different property modules for the same droplet size and ambient conditions. The two property modules differed in that the ideal gas equation and properties dependent on temperature only were used in one, while the other contained the BWR equation as the equation of state with temperature and pressure dependent properties. It was observed that the life-time of the droplet is reduced when more accurate pressure dependent thermodynamic correlations were used. Figure-B1 shows the effect of ambient temperature on the droplet life-time at a constant pressure of 5bar, and fig.B2 shows the effect of pressure at a constant ambient temperature of 600K. These graphs show the general trends of the droplet evaporation process, which are: 1.) as the temperature is

increased there is a decrease in the life-time, 2.) As the pressure is increased there is a increase in the life-time. The above statements will be discussed in more detail in a subsequent section (6.2.2). Based on these graphs it can be stated that the relative decrease[1] in life-time when more accurate property routines are used is over 10%. The effect is more pronounced at low ambient temperatures where the droplet has a longer life-time due to the slow gasification. It is clear from these findings that the use of accurate property routines in the calculation of thermodynamic and chemical parameters in the air-fuel-vapour film have a significant effect on the evaporating droplet history and should not be neglected.

6.2.1.2 the effect of variable density in the liquid-phase :

In experimental studies of evaporating and burning droplets it has been observed that the droplet expands in the early part of its life-time [10]. This initial increase in the droplet volume has been attributed to thermal expansion. A study was therefore carried out, using the above model, to analyse the effects of variable liquid density on the overall evaporation rate. It was found that in the early part of the droplet life-time the diameter increases with time [figs B3-B4]. These graphs show the effects of ambient temperature evaluated at an ambient pressure of 5bar and the effects of pressure evaluated at a temperature of 800K respectively. This increase in droplet diameter is more evident at high pressures and low temperatures due to the longer life-time given by these ambient conditions. It was also observed that the overall effect of variable liquid density is to lower the droplet life-time slightly. Based on the graphs of figure B3 and B4 the relative

[1] relative decrease = (old-model - new-model)/old-model

decrease[2] in the life time is between 7.6% (T_{amb}=1600K and P_{amb}=5bar) and 11.2% (T_{amb}=600K and P_{amb}=30bar). This is due to the increase in droplet surface in the early portion of its life-time, leading to a higher gasification rate from the surface.

6.2.2 Liquid Heating Model :

The reasons behind the formulation of this model were:

1.) to determine the extent to which a spatially unsteady liquid-phase will affect the overall evaporation rate of the droplet.

2.) to identify the duration of the spatial unsteadiness in the liquid-phase in relation to the droplet life-time.

The model was formulated so that it could be run for a single component or for a multi-component fuel. The multi-component form of the model assumes the fuel species in the liquid to be spatially uniform at each time step, therefore this could be considered a rapid-mixing type liquid heating model. Also, the program was designed to include supercritical states; once the pressure and temperature are both above the critical condition of the specified fuel, the model assumes instantaneous evaporation for the remaining droplet mass. On a SunLX machines the model takes about 1-3 minutes to run depending on the droplet size and the ambient conditions.

---

[2] relative decrease = (constant-density value - variable-density value)/constant-density value

The main finding deduced from the results obtained with this model is that liquid heating prolongs the droplet life-time compared to the infinite conductivity type models [fig.B5]. This increase is more significant at high temperatures (when T_{amb}=600K and P_{amb}=5bar the percentage relative increase[3] is about 13.8%, but when T_{amb}=1600K and P_{amb}=5bar this difference becomes 52.5%). The increase in life-time could be explained as follows: in the infinite conductivity model the energy transferred to the liquid is evenly distributed across the liquid-phase. This causes the surface temperature to be lower in the initial portion of the droplet life-time compared to a liquid heating model. Since the rate of heat transfer is dependent on the temperature difference between the ambient and the surface, this leads to a higher amount of energy transfer in the initial part of the life-time for an infinite diffusivity model compared to the liquid heating model [fig.B6]. This results in a higher surface temperature during the latter part of the droplet life, leading to a higher gasification rate, and thus a reduced life-time of the infinite diffusivity model in comparison to the liquid heating model.

Figure-B7 (single component fuel) and fig.B8 (bi-component fuel) contain the overall effects of ambient pressure and ambient temperature on the droplet life-time for sub-critical evaporation. As shown by these graphs, an increase in ambient pressure and temperature has the following effects on the droplet life-time, respectively: 1.) an almost linear increase, 2.) a strong non linear decrease, where the rate of decrease is quite significant for lower values of the ambient temperature (below 1000K). At high temperatures the droplet reaches the wet bulb temperature very rapidly. Once the

[3] relative increase = (liquid-heating value - variable-density value)/(variable-density value)

temperature reaches this value it imposes a limiting condition on the evaporation rate. This leads to differences in life-times to become lower at high temperatures. The effect of pressure can be explained as follows: increase in the ambient pressure causes a decrease in the fuel vapour molar fraction in the air-fuel-vapour film, leading to a slower mass diffusion rate, thus causing an increase in the droplet life-time. Although the effect of pressure on an individual droplet is less significant than the temperature, it has an important consequence for evaporation as will be shown in the discussion for the two-phase spray model.

Figure-B9 and figure-B10 give the internal temperature distribution for a 20 micron *n-Decane* droplet, and the variation of the diameter, mass and temperature with time (in a single figure as subplots) respectively. In fig.B9, the x-axis represents the non-dimensional distance between the droplet centre and the surface. Where grid point 1 is the centre of the droplet and grid point 100 is the surface of the droplet. The emphasis here is on the variation of temperature with time at a particular grid point, rather than at a fixed point in space. Significant difference in the internal temperature distribution can be observed during the heating up period, apart from the very early stages of the evaporation process. Later on the temperature gets evened out leading to a constant set of temperature values. The implication of these findings is that the unsteadiness of the liquid-phase is only significant in the heating up period.

An important conclusion can be drawn from the results of the multi-component formulation of the model: for a rapid mixing type model, both species appear to remain

until the droplet mass becomes zero regardless of the differences in volatalities even though *n*-Octane is more volatile than *n*-Decane.

6.2.3 The Unsteady Gas-Phase Model :

It is reasonable to consider that the unsteadiness of the air-fuel-vapour contributes notably to the overall unsteadiness of the evaporation process. Since the liquid-phase unsteadiness has been tested already, it was decided to isolate the gas-phase effects by keeping the liquid-phase spatially uniform and the liquid density constant in this model. The model is capable of predicting the time varying spatial distribution of temperature [fig.B11] and fuel-vapour mass fraction [figs. B12-B13] within the air-fuel-vapour film. In these graphs the *x*-axis point 1 is the surface of the droplet, which is the starting point of the finite-difference grid. Since the model is a fully finite difference formulation, tests were carried out to evaluate the stability and consistency of the numerical technique. These tests are explained in the following section.

6.2.3.1 numerical stability of the model :

To evaluate the effects of the time step (delt) the program was tested with three 'delt' values, namely; 1e-4s, 1e-5s and 1e-6s. For delt=1e-4s the program becomes unstable, for delt=1e-6s the execution time becomes exceedingly long. Therefore 1e-5s was used as the optimum time step value. Similarly the grid spacing (deltr) was tested using values of: 1e-4m, 1e-5m and 1e-6m. When deltr=1e-4m the method becomes unstable, for deltr=1e-6m, more than 700 grid points were required for the method to become stable.

Therefore 1e-5m was used as the optimum 'deltr' value, which requires less amount of points. In both of the above studies a twenty micron droplet was used, since it is assumed that this diameter provides a representative mean diameter of the liquid droplets in the spray analysis. A grid dependency study was carried out using 500, 550 and 600 grid points with a grid spacing of a 1e-5m. The results obtained using these grid values were identical. Therefore 500 grid points were used for all subsequent runs.

The main drawback of the model is its long execution time. This results from the use of a large number of grid points. On a SUN LX machine the program takes between 30 - 60 minutes of run-time, depending on the droplet size, ambient pressure and temperature. Due to the fully implicit nature of the finite difference method the position of the boundary condition at infinity needs to be supplied to the program. Since this is an unknown, a large number of grid points need to be used to assure that the far-field node values are identical to the ambient ones.

6.2.3.2 extent of the gas phase unsteadiness :

As the droplet diminishes in size, the grid system moves inwards with the droplet surface this causes numerical unsteadiness which could be wrongly taken as unsteadiness of the air-fuel-vapour film. It is therefore necessary to isolate the effects of diffusion of temperature and fuel mass fraction from the moving grid system to properly access the unsteady nature of the evaporation process. This was achieved by simulating the evaporation while the droplet diameter was kept constant. It was observed that the spatial unsteady effects still persist for a significant amount of time. This unsteadiness is

more pronounced during the heat-up period and towards the end of the life-time, when the droplet diminishes in size very rapidly. The above can be clearly seen from the fuel mass fraction map, fig.B12. Figure-B14 gives the diameter and surface temperature of the droplet at the same ambient conditions of figs.B11-B13. It can be seen from fig.B14 that the heating up period occupies a major potion of the droplet life-time (85%) causing the surface to be unsteady during that period. Therefore due to the combined effects of the surface unsteadiness and the spatial unsteadiness of the fuel-vapour-air film, it can be stated that the evaporation is an unsteady process throughout the life-time of the droplet, which conforms with the findings of Dwyer [57].

6.2.4 Observations And Results In Comparison To Quasi-Steady Gas-Phase Models

As shown in the subplots of figure-B15, the characteristics of the droplet temperature, diameter and mass curves are similar to the ones obtained from the other models, but the total life-time given by this model is more than twice that of the others. This is because, in the quasi-steady gas-phase models the gas-phase temperature is taken to be constant over the film with an average value based on the surface and the ambient temperatures. This mean temperature is taken to evaluate all the properties as a mean quantities of the air-fuel-vapour film. Therefore these models have a high mass diffusion rate. In the unsteady gas-phase model the properties are calculated using the temperature at each grid point. This results in a reduced but more realistic mass diffusion rate, and hence, a longer droplet life-time. These findings have interesting implications: it can be argued that to improve droplet models to obtain a more realistic picture of the evaporation process, it is more important to accurately model the gas-phase than the liquid-phase. Figure-B16

shows the variation of d^2 with time for the four models, giving the well known linear distribution of d^2 with time conforming with the works of others [9].

Another important finding is the extent of the heating up period. All four models predicts a heating up period which amounts to at least 30% of the droplet life-time. Since the heating up period has a strong effect on the mass and the heat transfer rate from the droplet surface, therefore on the total-life time, this questions the validity of steady state models.

6.2.5 Selection Of A Droplet Evaporation Model For The Spray Program :

The quasi-steady gas-phase with finite thermal diffusivity model was chosen as the dispersed phase evaporation model in the two-phase spray program. This was primarily done due to computer execution time considerations. In each iterative step of the two-phase program the droplet evaporation module need to be run until the droplet mass is zero. This leads to a total iterative time of:

$t_{total} = (\ t_{d\text{-}total} + t_{s.})$(number of iterations gas-phase)

where :

$t_{d\text{-}total}$ = time to run the droplet model

$t_{s.}$ = time for a single iterative step of the gas-phase program

Also to achieve the specified convergence limit the program needs to be run for at least 2500 iterations. Therefore including the unsteady gas-phase evaporation model will increase the execution time tremendously.

6.3 Spray analysis :

A mathematical model describing the development of an evaporating liquid fuel spray within a co-flowing air stream has been developed. The model is of the LHF two-phase flow type and as such, it incorporates most of the single-phase Navier-Stokes solver. These 2-D, steady-state single-phase mixing model was developed to serve as the basis for the development of the two-phase model. For this reason the emphasis in this discussion is on the results of the two-phase program. Nevertheless graphs from the single-phase model are referred to when necessary to clarify certain points in the discussion.

Major problems with regard to overall numerical stability, inlet boundary condition specification etc. were encountered in moving from the single-phase model to the two-phase one. The results from the runs regarding this points are discussed first.

Validation of any model is a significant part of its development. This is best done against known experimental results. Most such studies are carried out on burning sprays and consist mainly of combustion product concentrations. For this reason an existing combustion model, developed by Nazha [14] and based on adiabatic flame temperature

calculations and the minimisation of the Gibbs function was modified slightly to make it suitable for inclusion in the model. This makes the two-phase model a 'mixed-is-burnt' type model. The results from this model are discussed in the case study presented below.

A parametric study is then followed to investigate the response of the model to changes in various parameters. Finally a general discussion of the model capabilities is presented together with comparisons with other two-phase models as well as a discussion of possible application to practical systems.

6.3.1 Numerical Stability Study :

Due to the staggered grid arrangement of the solution procedure the inlet boundary conditions of scalar variables ($I = 1$ plane) are outside the real boundary of the solution domain, which falls on the midpoint of the $I=1$ and $I=2$ planes. When the density and the temperature of the two fluids are significantly different, and there is an appreciable distance between the two planes (relatively large grid size), leads to the scalar values at $I=1$ plane differ notably from those at the $I=2$ plane. This causes the interpolated scalar variables at the inlet boundary (mid-point between $I=1$ and $I=2$ planes) to deviate significantly from the initially supplied values within a small number of iterations. This results in the converged mass balance at the end of the process to be different from that of the initial value. To overcome this problem the following techniques were used:

1.) The axial distance between the *I=1* plane and *I=2* plane was made small to ensure minimum departure of the values at *I=2* plane from that at *I*=1. This was done by setting the x-grid expansion factor to an appropriate value which gives the minimum distance between the planes whilst preserving the overall numerical stability. A value of 1.08 was used in all runs as the initial x-grid expansion factor.

2.) The *I=1* plane scalar values were updated dynamically at each iteration level such that the scalar values of the inlet plane of the computational domain (mid-point between *I=1* and *I=2* planes) remains the same as that of the initial entry conditions.

If the above value of the grid expansion factor was used all throughout the calculation domain this again leads to numerical instability. Therefore it was decided to keep the grid constant after an appropriate distance down stream of the inlet. In results discussed here the x-grid spacing becomes constant after 25mm from the inlet with a constant spacing value of 25mm. The above value is a compromise between CPU time and stability.

6.3.2 Case Study :

The experimental results against which the model was to be validated were obtained by Nazha [14] at Queen Mary College London using a high-pressure steady-state combustion facility. The facility consisted of a 800mm long cylindrical combustion chamber with an inner diameter of 150mm. The air and fuel flows inside the chamber were co-axial and the fuel was injected continuously at a pressure of 17300kPa via a nozzle of 0.2mm throat diameter giving a fuel mass flow rate of 5.4g/s. The spray was

ignited by a gas-turbine type spark igniter and the results were obtained for runs at a constant pressure of 653kPa and an input equivalence ratio[1] of 1.08. The main function of the steady state combustion system was to maintain the simplest possible configuration of a burning fuel spray in a co-axial air stream. The combustion stability of the system was achieved without any induced swirl, premixing or recirculation near the injector. Further details of the facility and the method of sample extraction and analysis are given in references [14,150,151].

The model was run for a theoretical chamber having the same dimensions as the experimental one. The runs were carried out at the same conditions of pressure and overall input equivalence ratio as those of the experimental tests. The inlet air temperature was taken as 1500K (the reasons for this are given in chapter-4) with a constant velocity of 3.7m/s and the fuel was supplied at a temperature of 300K with a nozzle exit velocity of 212m/s. The radius of the fuel/air stream at entry to the computational domain was 4mm. The properties of gas-oil with the chemical formulae and molecular mass of *n*-dodacane were used as representative of the test fuel (shell gas oil). The results from these runs are presented in figures C1-C4.

Figures-C1 shows the predicted spatial distribution of the vapour equivalence ratio, flame temperature and the concentrations of CO_2 and CO. Nazha's equivalent experimental plots interpolating the actual axial and radial results are not reproduced here but they have been published in references [14, 152]; instead the actual axial data

[1] equivalence ratio = $(\text{fuel/air})/(\text{fuel/air})_{\text{stoichiometric}}$

points and the radial data points at section D of the experimental chamber (0.393m from the injector) are superimposed on the curves predicted by this model and by Nazha's model in figures C2-C4.

Nazha analysed his experimental results and concluded the following:-

1.) the vapour equivalence ratio increases axially to a peak of 1.3 at section D followed by a gradual decrease to a value in the region of the input value somewhere between sections E (0.507m from the injector) and F (0.621m from the injector)

2.) the temperature increases very rapidly to a peak at section D, where it level off around 1750K , decreasing slightly towards the chamber exit

3.) The general trend of CO_2 concentration is to increase both axially and radially

4.) CO concentration peaks between section C (0.279m from the injector) and section D, then starts to decrease and levels off towards the chamber exit.

The spatial plots produced by the present model [fig.C1] shows similar trends. The equivalence ratio rises to a peak of 1.3 at 0.319m from the injector. This is followed by a gradual decrease to a constant value in the region of 1.1 (similar to the input value) radially and axially indicating complete evaporation and mixing. The theoretical map of temperature shows an axial trend similar to the experimental one with a maximum axial

value around 1800K in the fully mixed region. Radially the theoretical map is deviating from that of the experiment, showing a temperature increase towards the chamber wall which becomes significant half way down the chamber (between 0.3m and 0.35m). This is because in the model the combustion is carried out adiabatically neglecting the heat transfer to the walls, which in reality reduces the near wall temperature values significantly. The model predicts similar trends for CO_2 concentration both radially and axially, though the values are not of the same magnitude as the experimental ones. For CO concentration the model predicts the radial and axial trends again with the values deviating from the experimental ones. The model also predicts the occurrence of the peak between sections C and D, though the position of the predicted peak is nearer to C than the experimental one.

Figure-C2 gives the axial distributions predicted by the present model with the corresponding experimental values superimposed over them, together with the distributions predicted by Nazha's model. Nazha developed a model to describe an axi-symetrical steady state spray combustion. His model makes use of the universal similarity profiles of velocity temperature and concentration as suggested by Abromovich [153]. The mixing is accounted for by Prandtl's mixing length theory. This makes his turbulence model of the zero equation type.

The graphs in fig.C2 show that the results predicted by the present model agree reasonably well with the experimental values. This agreement is closer than that exhibited by Nazha's model, particularly in the case of CO_2 and CO concentrations. The

model, however appears to underestimate the vapour equivalence ratio and the temperature in the early stages and to exhibit the peak values closer to the injector. This is probably, due to basing the evaporation from the spray on that of a mean droplet on the axis and neglecting the droplet dynamics. Smaller droplets will tend to evaporate earlier giving rise to a higher vapour equivalence ratio in the early stages while larger droplets will penetrate further shifting the peak vapour equivalence ratio downstream from the injector.

Figure-C3 gives the radial distributions at section D. This is where the experimental vapour equivalence ratio exhibits its peak. The present model, however predicts the corresponding peak a little earlier at 0.319m from the injector. Subsequently, fig.C4 was produced to compare the radial distribution at the cross-section of the predicted axial peak position with the experimental data at section D (the experimental peak position).

At section D the experimental vapour equivalence ratio starts from a value of 1.3 then decline rapidly to a value about 0.85 which is followed by a gradual decrease to a value of 0.58. The curve predicted by the present model start from a value of 1.18 then decreases gradually to a value around 1.05, showing a similar trend to that of the experimental data but exhibiting greater uniformity indicating more complete mixing. This uniformity is clearly not present at the section of maximum value of the axial vapour equivalence ratio [fig.C4] where the predicted curve starts at a value of 1.3 and decline steadily to a value of 0.98. The curve predicted by Nazha's model dips towards the wall to coincide with the experimental value. This results from a variation in the

radial evaporation function introduced by Nazha and not incorporated in the present model which assumes a constant radial profile of the evaporation.

The experimental temperature decreases gradually at first, then dips sharply towards the wall. The present model initially under estimates the temperature by about 170K which then gradually rises to attain a steady value around 1830K. Nazha's model follows a similar trend but dips towards the wall, consistent with the vapour equivalence ratio dip. The departure of the predicted temperature from the experimental one as one moves away from the axis and towards the chamber wall can be explained by the near stoichiometric predicted vapour equivalence ratio and by the fact that the predicted temperature is based on an adiabatic flame temperature calculation.

The predicted radial distribution for CO_2 and CO concentrations show close agreement with experimental data in the case of CO_2 and the right trend in the case of CO. The agreements are arguably better than those exhibited by Nazha's model. The departure from the corresponding experimental values can be explained as follows: the higher predicted vapour equivalence ratio tends to result in over-prediction of both CO_2 and CO concentrations while the over predicted temperature may result in reducing CO_2 and increasing CO concentrations due to disassociation.

When a liquid is injected into a confining chamber, the resulting spray entrains the surrounding air as it grows and spreads. The air available for entrainment is limited by the flow rate at the inlet conditions. When this limit is reached recirculating eddies are

set in. In a burning spray the recirculating flow will have an effect on the product concentration. The experimental results of Nazha [14] show this, particularly in CO_2 iso-contour maps. This is more evident in earlier results [154] obtained on the same facility but with a higher input equivalence ratio of 1.2. Nazha's model is not able to predict the existence of recirculation due to its similarity profile approach and the use of a first order turbulence model. In contrast the CO_2 iso-contour map predicted by the present model shows the occurrence of these regions [fig.C1]. This can be seen more clearly in the velocity map given in figure-C5. The top subplot of figure-C5 shows the velocity distribution upto 0.65m from entry, and the bottom subplot shows a magnified view of the recirculation region. The centre of the recirculation region is about 0.27m and 0.063m axially and radially respectively.

6.3.3 Parametric Study :

A parametric study was carried out to investigate the response of the model to changes in system pressure and vapour equivalence ratio. These two parameters provide important information regarding the combustion characteristics in practical systems. Also they provide information regarding the numerical stability of the model.

6.3.3.1 effect of system pressure :

The two-phase program was run with an inlet equivalence ratio of 1.1 for 4 different pressures (1, 2, 3 and 10MPa). The 1MPa is sub-critical, the 2MPa is close to the critical point of the fuel and the 3MPa and 10MPa are super-critical. The fuel was assumed to have the properties of gas-oil/*n*-dodacane and the air temperature for all runs was set to

1500K. The combustion program was run on the converged fuel vapour map returned by the mixing program taking the initial temperature of the system to be 300K for all control volumes. The iso-contour map of vapour equivalence ratio for this study is presented in Figure-C6.

It can be seen that with the increase of pressure the beginning of meaningful evaporation is shifted downstream from the injector. The reason for this is as follows: as the pressure increases the droplet evaporation slows down (as was noted in the droplet studies). This results in less fuel vapour being available for mixing in the early stages. As the droplet temperature rises, the evaporation rate increases (temperature effects are more significant than pressure effects as was argued in the droplet section). This is evident from the tightly packed contours of the higher pressure subplots. When the droplet temperature reaches the critical value (in the super-critical plots) the fuel evaporate instantaneously. The effect of pressure on evaporation is even more significant if it is measured against residence time (the residence time at 0.4m downstream of the injector is 1.731e-2s for 1MPa, and 1.775e-2s for 10MPa).

It is not clear from the above argument whether there is a pressure effect on mixing irrespective of the evaporation rate. To determine this, results were obtained from runs carried out using the single-phase mixing program, and these are presented in figure-C7. The fuel used was methane, the other relevant parameters are given in the figure itself. It can be seen that the system pressure has only a minute effect on the mixing. Therefore

it can be concluded that the main effect of pressure on the spray combustion is purely due to its effects on the spray evaporation.

6.3.3.2 effects of inlet equivalence ratio :

The program was run for four inlet equivalence ratio values (E=1.08, E=1.0 E=0.9 E=0.8). The system pressure for all these runs was 0.65MPa. The inlet air temperature and the conditions for fuel were the same as for the previous study. The iso-contour maps of this study are presented in figs. C8-C10. It can be seen that with a decrease in the inlet equivalence ratio complete mixing occurs further downstream of the injector [fig.C8]. This is a direct result of the increase in air momentum accompanying the decrease in the equivalence ratio. This high surrounding momentum impedes the radial mixing by keeping the fuel vapour rich region constrained towards the central axis of the tube for a longer distance. The recirculation region is also more pronounced and occurs earlier for the higher equivalence ratios as evident from the CO_2 iso-contour maps [fig.C9]. The Higher the value of the input equivalence ratio, the less air is available for entrainment. This leads to the formation of recirculation eddies earlier than with the lower equivalence ratios.

Figure-C10 shows the post-combustion maps for the four equivalence ratios. The post-combustion temperature is higher for E=1 and E=0.9 studies. This is due to the presence of more near stoichiometric regions in these two runs. The relatively high CO_2 percentages [fig.C9] (E=1 E=0.9 study) also reiterates this fact.

6.3.3.3 temperature effects:

The two-phase program was run with two different air inlet temperature settings of 800K and 1500K. Both runs were carried out at a pressure of 0.65MPa and at an input equivalence ratio of 1.08. The fuel used was gasoil/*n*-dodacane. Figures C1 and C11 show the relevant iso-contour maps of the two runs, only minute differences can be detected in these plots. Nevertheless there is a slight radial spread with the lower temperature [fig.C11], indicating a slightly better mixing.

In general a decrease in air temperature causes the air density to rise, therefore to keep the mass flow constant the air velocity needs to be reduced. This results in a reduction in the air momentum which should result in better mixing due to the decrease in the constraining effect caused by the air stream. However in these runs, the air velocity was more or less kept constant, the change in air momentum was caused by the change in density. Also for both runs, the air momentum was accompanied by an equivalent change in the fuel jet momentum (to keep the input air/fuel ratio constant), this eliminated the effect on mixing due to momentum changes. Since the initial velocities (both fuel and air) are constants in these runs, the residence times were almost the same. Also the same temperature function for droplet evaporation was used in both cases, which leads to the dispersed phase evaporation to be the same for both studies. Based on the above, it can be argued that these minute effects are not due to changes of evaporation, residence time or momentum. Therefore they must be due to the effect of temperature on the properties.

To highlight the effect of momentum the single-phase program was run for the same pressure (1MPa), input equivalence ratio (1.1) and fuel (methane). Two runs were carried out; one with an air temperature of 500K and the other with a temperature of 1000K. The initial fuel temperature in both runs were kept at 300K and the inlet air velocity was kept constant (20m/s) for both runs. Only the fuel velocity was varied to keep the equivalence ratio the same for both studies (62m/s for 500K and 125.6m/s for 1000K). Figure-C12 shows the equivalence ratio iso-contour maps. For an air temperature of 500K the momentum of the air stream was 45.36kgm/s^2 and that of the fuel stream was 17.58 kgm/s^2. For the 1000K the corresponding values were 22.70 kgm/s^2 and 4.54 kgm/s^2 respectively. It can be seen that the fuel momentum has quadrupled whilst the air momentum has doubled for the lower temperature run, leading to a higher ratio of fuel momentum to air momentum. This is because the decrease in temperature had caused an increase in the density of the air stream. In order to keep the equivalence ratio constant the mass flow rate had to be changed accordingly. This was achieved by increasing the fuel inlet velocity. The relatively high momentum of the fuel stream causes the jet to spread more in the radial direction overcoming the confining effect of the air stream. This caused the gases to mix earlier than in the high temperature run.

The change in density due to temperature effects is similar to the change resulting from pressure changes. Therefore it is possible to compare figure-C12 with figure-C7 to establish the momentum effects regardless of whether they have been caused by pressure or temperature changes. The conditions for figure-C7 are as follows: the ambient

temperature is 1000K, the system pressure is 1MPa and 2MPa, the fuel velocity is 63m/s and 62m/s respectively. The air velocity and the input equivalence ratio are the same as those of figure-C12. Based on these runs the following can be stated : both the air and the fuel momentums have doubled when moving from 1MPa to 2MPa (for 1MPa the air and fuel momentums were 22.70kgm/s^2 and 4.54kgm/s^2 and for 2MPa 45.42kgm/s^2 and 9.04kgm/s^2 respectively). Unlike the temperature the change in pressure acts on the density of both species causing a magnitude increase or decrease in momentum. Since both momentums have doubled (for 2MPa run) the mixing is almost the same for the two runs. If the 500K and 1MPa run was compared with the 1000K and 2MPa run, whilst the air momentum is the same for the two conditions, the fuel momentum has doubled for the lower temperature run, resulting in an iso-contour map similar to the 1MPa and 1000K run.

6.3.4 General Discussion :

The model developed is of the LHF type. The capabilities of the model are that it can predict the mixing and combustion of gas-gas flows or gas-liquid flows with reasonable accuracy. Since it is designed in a modular form, routines such as the combustion module, turbulence module etc. can be replaced or new ones developed and added without causing drastic changes to the program.

Another important feature of the model is its ability to incorporate extra terms such as buoyancy affects via the modification of the source term of each flow equation. Since source terms of all partial differential equations are calculated in a separate subroutine,

extra terms can be added by modifying this particular routine, as long as the 2-D formulation of the overall program is conserved. The main drawbacks are that the model cannot account for the individual droplet characteristics due to the LHF formulation.

Compared to other LHF models the present model has a significant new feature: a droplet model that takes heating up period into account. As explained in chapter-2 the LHF formulation of Faeth and co-workers [110, 111] takes account of the dispersed phase evaporation via a saturation vapour pressure function. Simulating the flow by this method has the following drawbacks:

1.) It is assumed that the liquid phase temperature is equal to the cell temperature at any given iteration level, this amounts to neglecting the droplet heating up period, which leads to a serious over estimation of the gasification rate in the near injector region.

2.) The fuel vapour mass fraction is calculated for each control volume (based on the saturation vapour pressure function), irrespective of the presence of a droplet in the control volume, this also leads to an over estimation of the fuel vapour diffusion rate from the liquid phase.

As shown in a preceding section the effect of pressure on the overall spray development is primarily due to its effect on the droplet evaporation. Therefore the effect of pressure on the mixing process cannot be properly accounted for by the kind of analysis carried out by Faeth and co-workers. The overestimation of the rate of spray development of

LHF models, observed by Faeth and co-workers [110, 111] has been attributed by them to the neglect of slip, in these type of models. It can be argued that over estimation of the gasification rates of the dispersed phase in their method is also a major source of overestimation of the rate of spray development. Therefore the use of a suitable droplet evaporation model with an appropriate temperature function correlated to the experimental temperature data does increase the accuracy of LHF models.

6.3.5 Applications To Practical Systems :

Qualitative information regarding the spray development and combustion in practical combustion systems such as diesel engines, gas-turbines etc. can be obtained by running the program with appropriate input parameters. Two such studies have been considered and they are discussed briefly below.

6.3.5.1 application to diesel engine combustion :

The nature of the diesel engine combustion is that; the flow is intermittent, 3-dimensional, and there is a substantial change of pressure and volume. Although the model describes a 2-dimensional, steady-state, continuous combustion system, it could be run for conditions representative of certain instances of the engine cycle. Such studies may prove helpful in providing valuable information with regard to how the spray develops and burns inside the engine.

To simulate a possible diesel engine environment just at the moment of injection, the program was run for an input equivalence ratios of 0.8 at a pressure of 3MPa and an inlet air temperature of 793K. The air temperature was arrived at by considering an adiabatic temperature rise for an increase of pressure from 0.1MPa to 3MPa. The fuel inlet temperature was set to 300K and the evaporation of the liquid phase was carried out using the gas phase control volume temperature as the ambient temperature. The combustion module was run taking the temperature of each control volume as the corresponding pre-combustion temperature. The fuel used was gas-oil with the chemical formulae and molecular mass of *n*-dodacane. Figures C13-C16 show the iso-contour maps of vapour equivalence ratio, flame temperature CO_2 and CO concentrations respectively. These maps give some information about the spray development at the condition during the start of injection. By themselves they will not be of great value. However as stated above, the program could be run for subsequent different conditions of pressure, temperature, volume etc. covering the combustion period. The accumulated information may provide a better insight into the mixing and combustion processes inside the engine.

Also it is possible to take account of swirl by giving a known set of radial velocity values at entry as a boundary condition to the air tube. This will cause the flow to deviate from the symmetric axis, allowing the curvature of the spray to be calculated.

6.3.5.2 application to gas turbine combustion :

The model has certain similarities to gas turbine combustion. Theses include the steady state and continuous nature of the combustion process. The program was run using kerosene/*n*-decane as the fuel to simulate a gas turbine combustion situation. Two runs were carried out at an input equivalence ratio of 1.1 for a pressure of 1MPa with an inlet air temperature of 652K and for a pressure of 2MPa with an inlet air temperature of 706K. Again the air temperature was arrived at by considering an adiabatic temperature rise due to compression. The initial fuel temperature was set to 300K and the evaporation was performed at the gas phase pressure and temperature within the control volume. The combustion module was run taking the temperature of each control volume as the pre-combustion temperature. Figures C17-C24 show the iso-contour maps of vapour equivalence ratio, flame temperature, CO_2 and CO concentrations for 1MPa and 2MPa studies respectively.

The figures show that with the increase of the system pressure there is an increase in the residence time, a trend similar to that of the system pressure parametric study. It can be seen that the dispersed phase evaporation occurs much earlier in these runs due to the relatively fast evaporation rate of Kerosene [figures C17 and C21], which leads to a better distribution of the fuel vapour. This result is more evident in the 2MPa run due to the higher initial gas-phase temperature. The initially high gas-phase temperature of the 2MPa study also increases the post-combustion temperature of this run [figure C22] which leads to an increase in CO mass fraction due to disassociation of CO_2 into CO [figures C20 (1MPa) and C24 (2MPa)].

These findings can be compared with the experimental results of Moss *et al* [155]. Though the conditions of operation of the experimental burner are not the same as those used for these runs (pressure, input equivalence ratio etc.), it can be seen from the predicted results that the equivalence ratio increases axially to a peak then decreases gradually to the input value of 1.1 [figs. C17-C21]. This trend is similar to that of Moss *et al* if the results are interpreted as mixture fraction values (i.e. total fuel fraction); this would then show as an initially high values of mixture fraction and then as a gradual decrease. Radially the figures show that the mixture fraction is decreasing, again similar to that of Moss *et al* mixture fraction results. A similar trend is observed from the temperature maps; the model predicts a sharp increase in temperature along the axis then a levelling off around 2000K (1MPa Study) and 2100K (2MPa study) [figs. C18-22]. This is similar in trend, if not in magnitude to Moss *et al* results. The differences in magnitude are due to the different chamber configuration, dimensions and to the use of pre-vaporised Kerosene in Moss *et al* study.

CHAPTER -7

CONCLUSIONS AND RECOMMENDATIONS

7.1 Conclusions :

The following points can be concluded from the study:

1.) Three droplet evaporation models have been formulated and compared. These are:

- An infinite liquid phase thermal conductivity with quasi-steady gas phase
- A finite liquid heating model with quasi-steady gas-phase, and
- An unsteady gas-phase with infinite liquid thermal conductivity

2.) The importance of using pressure and temperature dependent variable properties in the air-fuel-vapour film surrounding the droplet, (which was highlighted by other researchers) has been confirmed in this study.

3.) A relative decrease in the life-time of the droplet of over 10% has been observed when more accurate pressure dependent property routines were used.

4.) The use of variable liquid density increases the droplet diameter in the early stages and lowers the total life-time of the droplet slightly.

5.) The heating up-period of an evaporating droplet in a hot environment amounts to at least 30% of the droplet's total life-time.

6.) Liquid heating prolongs the life-time of an evaporating droplet compared to the infinite conductivity type models.

7.) The effect of liquid heating is only significant in the heating up period of the droplet.

8.) Ambient pressure and temperature have the following effects on the droplet life-time: an increase in ambient pressure causes an almost linear increase in the life-time, while an increase in temperature causes a strong non linear decrease.

9.) The droplet evaporation is an unsteady process throughout the droplet life-time.

10.) The unsteady gas-phase droplet evaporation model predicts a droplet life-time more than twice that of the quasi-steady gas-phase models. This implies that the unsteady gas-phase effects are significant and need to be taken into account.

11.) An LHF type, two-phase mathematical model, applicable to high pressure combustion flows has been formulated. The model has the advantage over most existing LHF type formulations in that it accounts for the disperse phase evaporation via a simultaneous solution of a droplet module with the gas-phase equations.

12.) A case study using the two-phase model has demonstrated its suitability for predicting axial and radial distributions of combustion products, temperature and vapour equivalence ratio in a burning liquid fuel spray with reasonable accuracy.

13.) The ability of the model to capture recirculation regions has been demonstrated.

14.) The applicability of the model over a wide range of pressure, temperature and input equivalence ratios has been investigated in a parametric study.

15.) The effect of pressure and input equivalence ratio on the overall process of evaporation, mixing and combustion has been demonstrated.

16.) The response of the model to changes in ambient temperature has been investigated

17.) Possible applications of the model to practical combustion systems, with some modifications, have been suggested.

7.2 Recommendations for future work :

- The unsteady gas-phase droplet evaporation model is the most advanced model developed in this study. Nevertheless it was not incorporated into the spray model due to its longer run time. However it is recommended that the use of a factor correlating the results from the unsteady gas-phase droplet model with those from the liquid heating model in the spray model should be explored.

- The evaporation from the spray is based on that of a mean droplet on the centre line. This can be improved by considering packets of droplets of different sizes and corresponding droplet dynamics for a better representation of the dispersed phase. This was not considered in the current study due to the substantial increase in computational time that would result from running the droplet evaporation model for different sizes.

- Partial equilibrium consideration of products species should be tried in future development of the model. Such a treatment may provide better predictions of the concentrations than the present method, but this would involve more computational time.

- A major disadvantage of separated flow (SF) type two-phase models to date is their limited applicability to dense sprays. Since LHF models are better suited for the dense spray regions, a combined approach could be used in the future for spray modelling. A locally homogeneous approach for the dense region, a separated flow approach for the dilute region and a fully evaporated flow approach for the remainder of the spray. The three models could then be linked together in a single model with appropriate switches to select the correct approach for the right zone within the spray. This use of the right aspects of single-phase and two-phase modelling could also ensure that the code is optimised minimising the computational requirement.

APPENDIX-A

PROPERTY CALCULATIONS

A.1 Introduction :

To solve the equations in sections 3 and 4 a gas equation and correlations for thermodynamic properties are necessary. In this appendix summary of these properties is given.

A.2 Equation of state :

In most droplet and spray models researchers tend to obtain the specific volume of the fuel-vapour and air mixture by using the Ideal gas equation as the equation of state. This can only approximate a real gas at low pressures and high temperatures. Since the environment in most practical combustion chambers is at a high pressure a modified Benedict Webb Rubin (BWR) equation [139-140] is used in all the droplet programs and in the mixing of two gaseous species program developed in this study. It was not possible to use the BWR equation for the liquid-gas mixing program due the two-phase nature of the flow. Therefore a modified form of the Ideal gas equation is used in this program, further details of this is given in chapter-4. The BWR equation is only valid for a specified reduced pressure and temperature range. Therefore during the calculation process, if the temperature or pressure is outside its respective range the program switches to the Ideal gas equation for the calculation of the specific volume.

The Benedict Webb Rubin equation used in the calculation is given below. The solution is by Newton-Raphson method, with first approximation for specific volume taken from the Ideal gas equation. The combined flow chart for the solution of the BWR equation and heat capacity calculations (section A.3) is given in figure A.1.

The necessary equations set can be summarised as follows:

$$Pv=zRT \tag{A.1}$$

$$z = z^0 + \frac{\omega}{0.3978}\left(z^r - z^0\right) \tag{A.2}$$

$$z^* = \left(\frac{P_r V_r}{T_r}\right) = 1 + \frac{B}{V_r} + \frac{C}{V_r^2} + \frac{D}{V_r^5} + \frac{c_4}{T_r^3 V_r^2}\left(\beta + \frac{\chi}{V_r^2}\right)\exp\left(-\frac{\chi}{V^2_r}\right) \tag{A.3}$$

where :

P = pressure in N/m^2

T = temperate in K

z = compressibility factor

R= universal gas constant in J/(molK)

v = specific volume in m^3/mol

T_r= reduced temperature (T/T_C)

V_r= reduced volume (V/ V_C)

P_r = reduced pressure (P/P_C)

The equation for z^* is used for the calculation of both compressibility factors z^0 and z^r given in equation (A.2). The parameters B, C, D which are functions of the reduced temperature and β, c_4,χ which are known constants, are different for the two equations of z^* [140].

The above equation can be used for a gas mixture if suitable mixing rules are used. In this program the mixing rules formulated by Lee *et al* [140] based on the corresponding states theory of thermodynamic properties[139-140] is used.

Mixing rules :

- mixture eccentric factor :

$$\omega = \sum_j x_j \omega_j \qquad \text{(A.4)}$$

- critical compressibility factor of the i^{th} component :

$$z_{ci} = 0.2905 - 0.085\omega_i \qquad \text{(A.5)}$$

- mixture critical volume :

$$V_c = \frac{1}{8}\sum_j \sum_k x_j\, x_k \left(V_{c\,j}^{\ 1/3} + V_{c\,k}^{\ 1/3}\right)^3 \qquad \text{(A.6)}$$

- mixture critical temperature :

$$T_c = \frac{1}{8V_c}\sum_j \sum_k x_j\, x_k \left(V_{c\,j}^{\ 1/3} + V_{c\,k}^{\ 1/3}\right)^3 \sqrt{T_{cj}\, T_{ck}} \qquad \text{(A.7)}$$

• mixture critical pressure :

$$P_c = \frac{z_c RT_c}{V_c} = (0.2905 - 0.085\omega)\frac{RT_c}{V_c} \qquad \text{(A.8)}$$

In the above mixing rules x_i denotes the molar fraction of species i in the mixture.

A.3 Specific heat of a gaseous mixture :

The heat capacity of a real gas mixture is the sum of the ideal gas heat capacities and the residual heat capacity known as the heat capacity departure function.

$$C_{pm} = \sum_i x_i C_{pi} + \Delta C_p \qquad \text{(A.9)}$$

Where:

x_i is the molar fraction of the i^{th} species

If the ideal gas heat capacities are known then the departure from the ideal can be calculated using Lee Kesler [140] method. In all these programs the ideal gas isobaric heat capacities of pure gases are calculated from a third order polynomial function of temperature as shown below. The relevant coefficients A, B, C and D are calculated based on the data given in references [139, 33].

$$C_p = A + BT + CT^2 + DT^3 \qquad \text{(A.10)}$$

When C_p for a particular gas is known then the isochoric heat capacity C_v for the gas can an be calculated from the following relationship.

$$R = C_p - C_v \qquad \text{(A.11)}$$

Again the departure function is calculated using the Lee Kesler method [140].

A.4 Gas phase mixture viscosity and thermal conductivity:

To calculate thermal conductivity and viscosity, correlations developed by Chung *et al* [139, 156] have been used. The set of equations developed by Chung *et al* are valid for both low and high pressure gas mixtures.

The equation for low pressure gas viscosity is given as :

$$\eta_0 = (4.0785\times10^{-5})\frac{(MT)^{1/2}}{V_c^{2/3}\Omega^*}F_c \qquad \text{[in P]} \qquad \text{(A.12)}$$

where;

$$\Omega^* = (\frac{A}{T^{*B}}) + \frac{C}{\exp(DT^*)} + \frac{E}{\exp(FT^*)} + GT^{*B}\sin(ST^{*W} - H)$$

(A.13)

The constants *A-H, S* and *W* are given in reference [156]

$$\left.\begin{aligned} T^* &= kT/\varepsilon \\ \sigma &= 0.809 V_c^{1/3} \\ \frac{\varepsilon}{k} &= T_c / 1.2593 \end{aligned}\right\} \qquad \text{(A.14)}$$

$$F_c = 1 - 0.2756\omega + 0.059035\mu_r^4 + \kappa \qquad \text{(A.15)}$$

In the above equations μ_r and κ are taken as zero in these models. This is due to:

1.) the dipole moment is zero for all the fuels considered

2.) the correction factor is only necessary for hydrogen-bonding effects.

The correlation for low pressure thermal conductivity is given as :

$$\lambda_0 = 7.452\left(\frac{\eta_0}{M}\right)\Psi \qquad \text{[in cal/(cm.s.K)]} \qquad \text{(A.16)}$$

where :

$$\Psi = 1 + \alpha \frac{[0.215 + 0.28288\alpha - 1.061\beta + 0.26665z]}{[0.6366 + \beta z + 1.061\alpha\beta]} \qquad \text{(A.17)}$$

$$\left.\begin{aligned} \alpha &= \frac{C_v}{R} - \frac{3}{2} \\ \beta &= 0.7862 - 0.7109\omega + 1.3168\omega^2 \\ z &= 2 + 10.5T_r^2 \end{aligned}\right\} \qquad \text{(A.18)}$$

where :

η_0 = low-pressure gas viscosity in P

M = molar mass of fuel mixture in g/mol

T = temperature in K

T_C = critical temperature in K

V_C = critical volume in cm^3/mol

μ_r = dimensional dipole moment

κ = correction factor for hydrogen-bonding effects

ω = acentric factor

λ_0 = low pressure thermal conductivity in cal/(cm.s.K)

C_V = heat capacity at constant volume in cal/(mol.K) [for equation A-18 only]

R = universal gas constant cal/(cm.s.K) [for equation A-18 only]

k = Boltzmans constant

ρ = density mol/cm^3 [for equation A-23]

For gases at high pressures extending the above equations, viscosity [in P] and thermal conductivity [in cal/(cm.s.K)] are given as follows :

$$\eta = \eta_k + \eta_p \qquad \text{(A.19)}$$

$$\lambda = \lambda_k + \lambda_p \qquad \text{(A.20)}$$

Where the terms with suffix 'p' denote the high pressure effects. For a low pressure gas calculation these terms will be negligible.

Formulation of η

$$\eta_k = \eta_0\left(1/G_2 + A_6 Y\right) \tag{A.21}$$

$$\eta_p = \left(36.344\times10^{-6}(MT_c)^{1/2} / V_c^{2/3}\right)A_7 Y^2 G_2 \exp\left(A_8 + A_9/T^* + A_{10}/T^{*2}\right) \tag{A.22}$$

$$Y = \rho V_c / 6 \tag{A.23}$$

$$G_1 = (1.0 - 0.5Y)/(1-Y)^3 \tag{A.24}$$

$$G_2 = \{A_1[1-\exp(-A_4 Y)]/Y + A_2 G_1 \exp(A_5 Y) + A_3 G_1\}/(A_1 A_4 + A_2 + A_3) \tag{A.25}$$

$$Ai = a_0(i) + a_1(i)\omega + a_2(i)\mu r^4 + a_3(i)\kappa \tag{A.26}$$

Formulation of λ :

$$\lambda_k = \lambda_0\left(\frac{1}{H_2} + B_6 Y\right) \tag{A.27}$$

$$\lambda_p = (3.039\times10^{-4}(Tc/M)^{1/2} / V_c^{2/3})B_7 Y^2 H_2 T_r^{1/2} \tag{A.28}$$

$$H_2 = \{B_1[1-\exp(-B_4 Y)]/Y + B_2 G_1 \exp(B_5 Y) + B_3 G_1\}/(B_1 B_4 + B_2 + B_3) \quad \text{(A.29)}$$

$$Bi = b_0(i) + b_1(i)\omega + b_2(i)\mu r^4 + b_3(i)\kappa \quad \text{(A.30)}$$

The parameters $a_j(i)$ and $b_j(i)$ are given in reference [156].

Again the mixing rules[156] are based on the Corresponding States theory. They are as follows :

$$\sigma_m^3 = \sum_i \sum_j x_i x_j \sigma_{ij}^3 \quad \text{(A.31)}$$

$$\frac{\varepsilon_m}{k} = \frac{[\sum_i \sum_j x_i x_j \left(\frac{\varepsilon_{ij}}{k}\right)\sigma_{ij}^3]}{\sigma_m^3} \quad \text{(A.32)}$$

$$V_{cm} = \left(\frac{\sigma_m}{0.809}\right)^3 \quad \text{(A.33)}$$

$$T_{cm} = 1.2593\frac{\varepsilon_m}{k} \quad \text{(A.34)}$$

$$\omega_m = [\sum_i \sum_j x_i x_j \omega_{ij} \sigma_{ij}^3]/\sigma_m^3 \quad \text{(A.35)}$$

$$M_m = \{[\sum_i \sum_j x_i x_j (\frac{\varepsilon_{ij}}{k})\sigma_{ij}^2 M_{ij}^{1/2}]/[(\varepsilon_m/k)\sigma_m^2]\}^2 \quad \text{(A.36)}$$

The binary interaction parameters in the above equations are given as follows :

$$\sigma ij = (\sigma i\, \sigma j)^{1/2} \quad \text{(A.37)}$$

$$\frac{\varepsilon_{ij}}{k} = [(\varepsilon_i / k)(\varepsilon_j / k)]^{1/2} \qquad \text{(A.38)}$$

$$\omega_{ij} = \frac{1}{2}(\omega_i + \omega_j) \qquad \text{(A.39)}$$

$$M_{ij} = 2M_iM_j / (M_i + M_j) \qquad \text{(A.40)}$$

where :

x_i = molar fraction of the i^{th} species

A.5 Diffusion coefficient of a binary gas :

To calculate the diffusion coefficient several methods were considered, from these methods the one that gives the least relative errors for a hydro-carbon fuel, air binary mixture (taking air as a single component gas) was used in the computer programs. The equation used is based on the Fuller *et al* method [139, 157-158] (modified by Reid *et al* [139]). Which has the form shown bellow:

$$D_{AB} = \frac{0.00143T^{1.75}}{PM_{AB}^{1/2}\ [(\sum_v)_A^{1/3} + (\sum_v)_B^{1/3}]^2} \qquad \text{(A.41)}$$

$$M_{AB} = 2[(1/M_A) + (1/M_B)]^{-1} \qquad \text{(A.42)}$$

where :

D_{AB} = binary diffusion coefficient in cm^2/s

M_A M_B = molecular weights of A and B in g/mol

P = pressure in bar

T = temperature in K

The unitless parameter $\sum_v$ is found for each component by summing atomic diffusion volumes [139]. The value for air is 19.7. For any hydro-carbon the value can be calculated from the following formula.

15.9x(number of Carbon atoms) + 2.31x(number of Hydrogen atoms) (A.43)

This method is only accurate for a low pressure system (less than 10 bar). As far as the author is aware, there is no other method which will significantly improve the calculated values at high pressure, therefore Fuller *et al* method is used in the subroutine where the diffusion coefficient is calculated.

A.6 Saturation vapour pressure calculation :

Saturation vapour pressure of hydro-carbon fuels are calculated using the graph given in Technical Data on Fuel [33]. For an arbitrary number of points (approximately 25) the temperature and corresponding saturation vapour pressure were read from the graph.

These values were then used in a least squared curve fit program to calculate the coefficients of the equation of best fit. Once the polynomial function was known, it was incorporated into the droplet program as a separate subroutine, where the input is droplet surface temperature in Kelvin and the output is the corresponding saturation vapour pressure value of that particular fuel in N/m^2. In all the fuels considered in these programs the relative error between the value given by the graph and the value calculated by the subroutine is less than 1%.

A.7 Specific enthalpy of vaporisation :

The method of calculation is based on the correlation given in Technical Data on Fuel [33]. This correlation is valid only for single component hydro-carbon fuels.

$$L = (251.3 - 0.377T) / d \qquad \text{(A.44)}$$

Where:

L = specific latent heat of gasification in kJ/kg

T = Temperature in ^0C

d = fuel density at 15.6 ^0C in g/cm^3

A.8 Isobaric heat capacity of a single hydro-carbon fuel :

The method of calculation is based on the correlations given in reference [33].

for liquid hydro-carbon fuel :

$$C_{pl} = (1.6848+0.00339T)/\sqrt{d} \qquad \text{(A.45)}$$

and for the fuel vapour :

$$C_{pg} = C_{pl} - 0.377/d \qquad \text{(A.46)}$$

where :

C_{pl} = specific isobaric heat capacity of liquid fuel in kJ/kgK

C_{pg} = specific isobaric heat capacity of fuel vapour in kJ/kgK

T = Temperature in ^{0}C

d = fuel density at 15.6 ^{0}C in g/cm^3

A.9 Liquid thermal conductivity :

The method of calculation is based on the correlation given in reference [33].

$$k = 0.1172(1-0.00054T)/d \qquad \text{(A.47)}$$

where :

k = thermal conductivity in W/mK

d = density at 15.6 ^{0}C in g/cm^3

T = temperature in ^{0}C

A.10 Thermal diffusivity of a liquid fuel :

Since thermal diffusivity is a parameter in the heat transfer equation in the liquid heating model it is calculated as a spatially uniform but temporally varying function of pressure and temperature. The definition of thermal diffusivity is as follows :

$$\alpha = \frac{k_l}{\rho_l C_{pl}} \tag{A.48}$$

Where :

k_l = liquid thermal conductivity [W/(mK)]

ρ_l = liquid density [kg/m3]

C_{pl} = liquid isobaric heat capacity [J/(kg.K))

A.11 Liquid density :

Liquid density is calculated using a modified Hankinson-Brobst-Thomson technique (HBT) [159]. This method calculates liquid density as a function of pressure and temperature. The only draw back of this routine is that, it is only valid for reduced temperature range of $0.25 < T_r < 0.95$. If for some reason T_r is outside this range the subroutine will pass the previously calculated value until Tr is within the range. Further details about the method of calculation is given in references [139, 159].

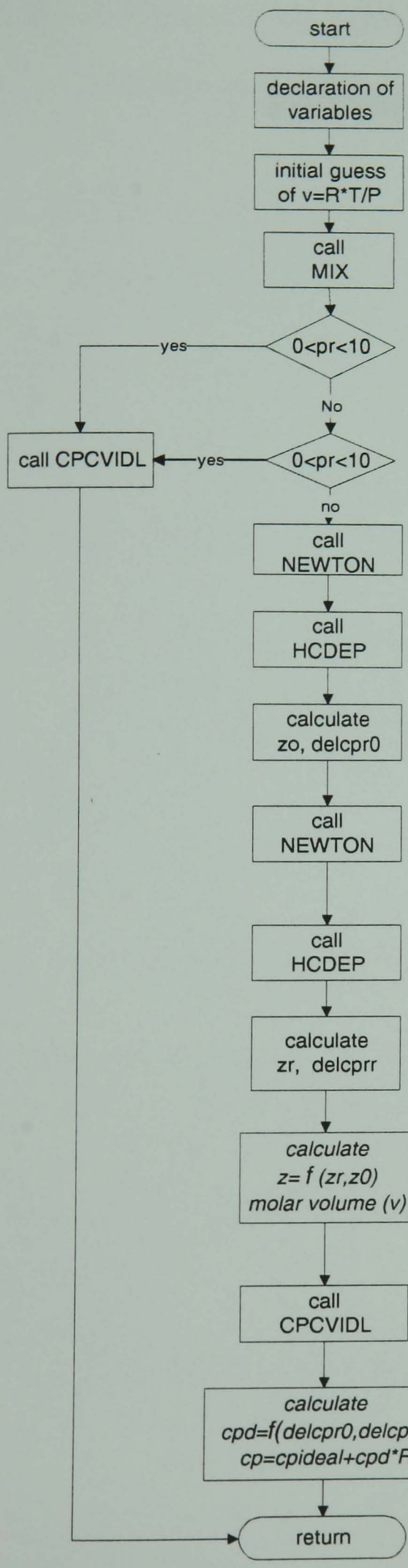

Subroutines called by BWREOS :

MIX : calculates mixture properties

NEWTON : Newton-rhapson iterative method

CPCVIDL : Ideal gas Isobaric heat capacity

HCDEP : Heat capacity departure function

fig.A.1 flow chart of BWREOS routine

APPENDIX-B

FIGURES: DROPLET RESULTS

Fig. B1 Effect of BWR-equation of state and pressure dependent property routines

variation of droplet diameter, mass, and surface temperature with time
effect of ambient temperature

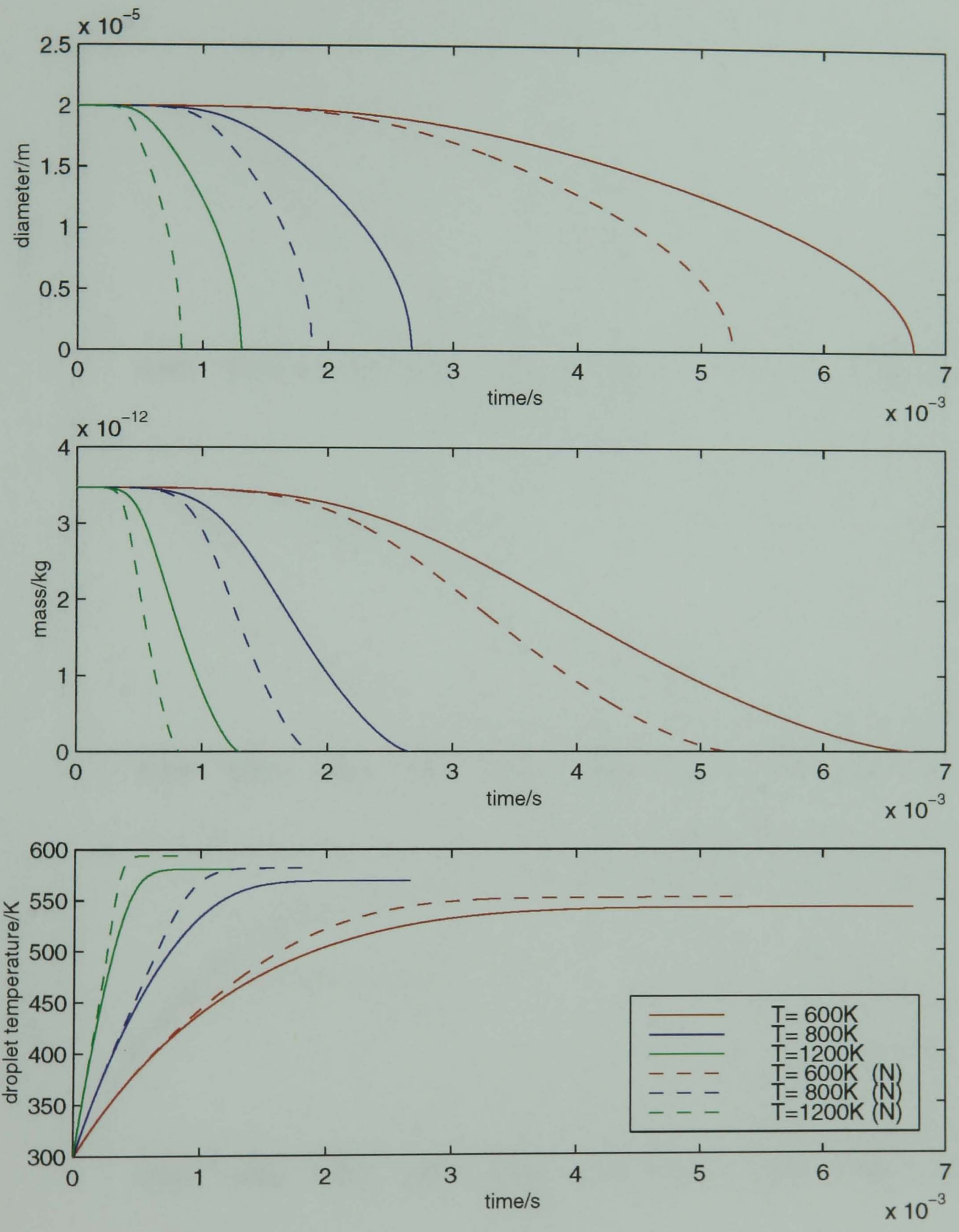

ambient pressure =5bar
fuel=gasoil/*n*-dodacane
initial diameter=20μm

Fig. B2 Effect of BWR-equation of state and pressure dependent property routines

variation of droplet diameter, mass, and surface temperature with time
effect of ambient pressure

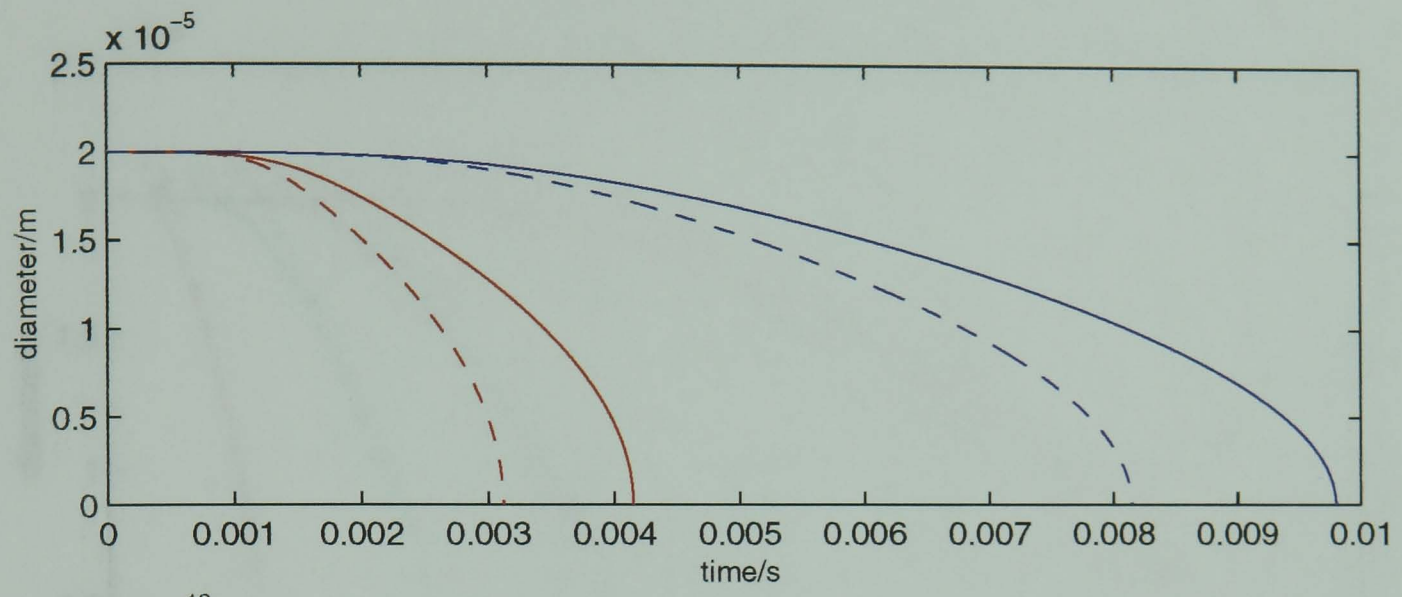

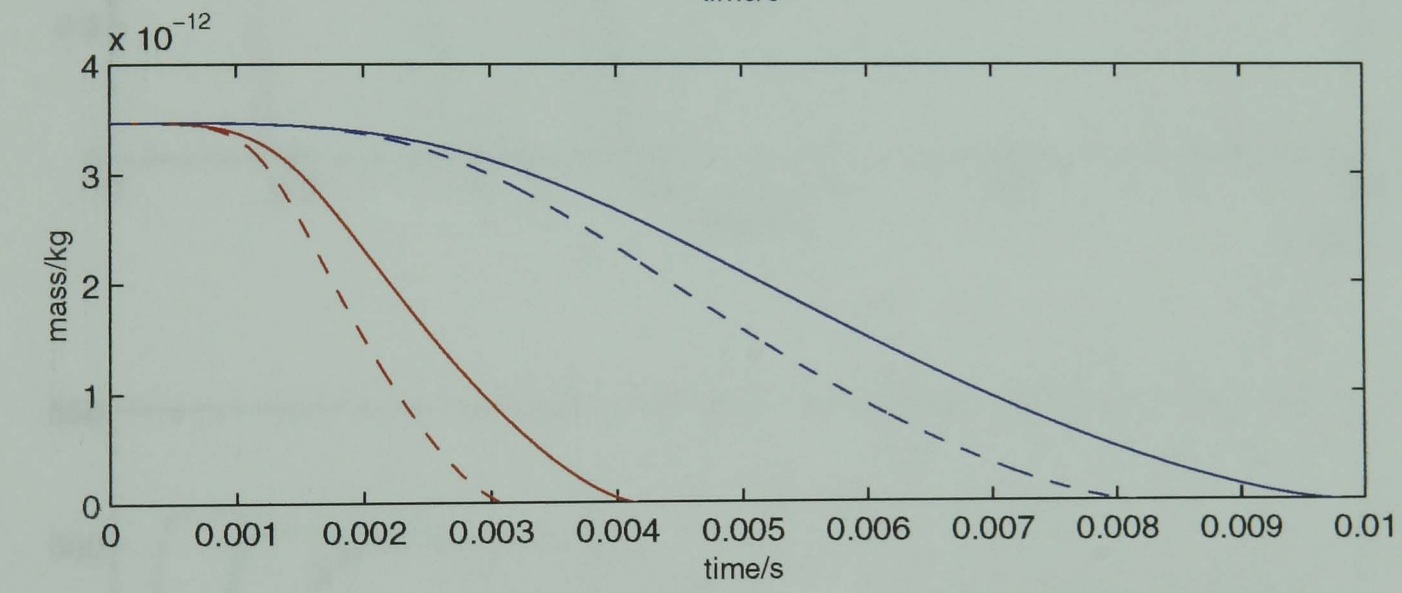

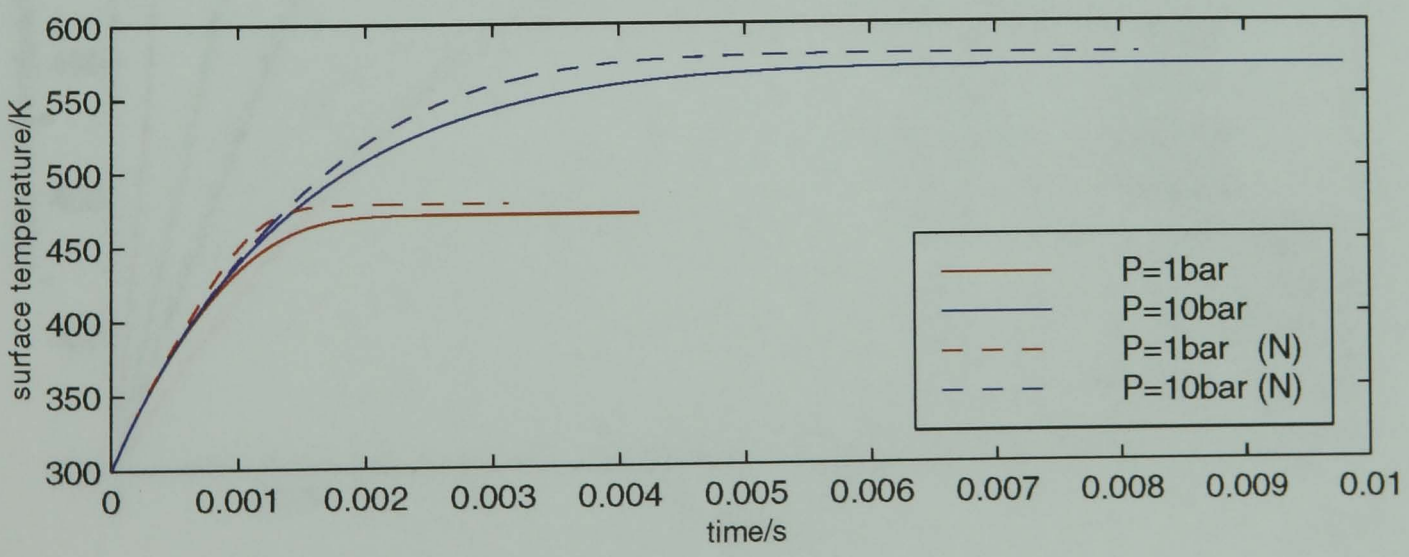

ambient temperature =600K
fuel=gasoil/*n*-dodacane
initial diameter=20μm

Fig. B3 Effect of variable density

variation of droplet diameter, and surface temperature with time
effect of ambient temperature

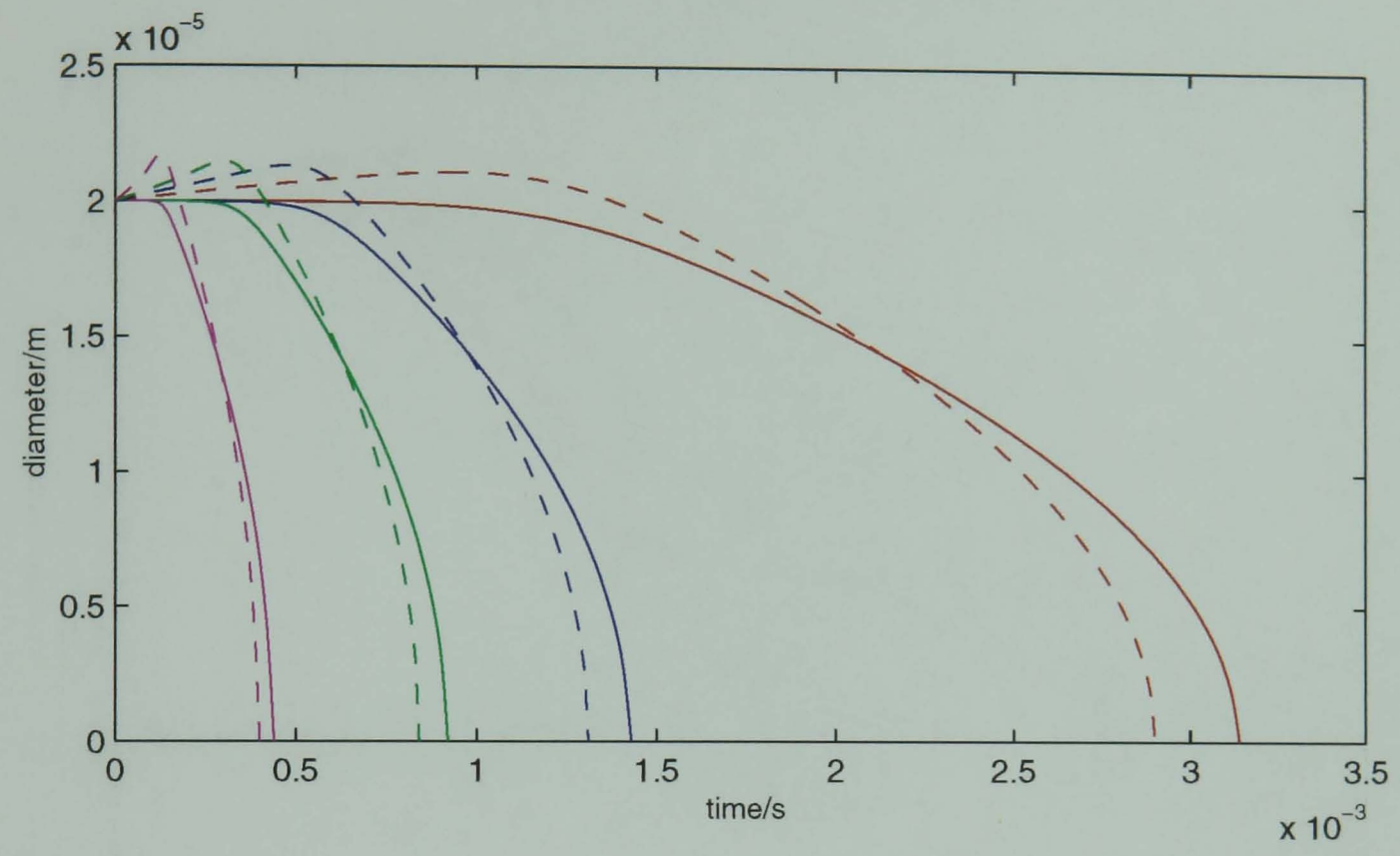

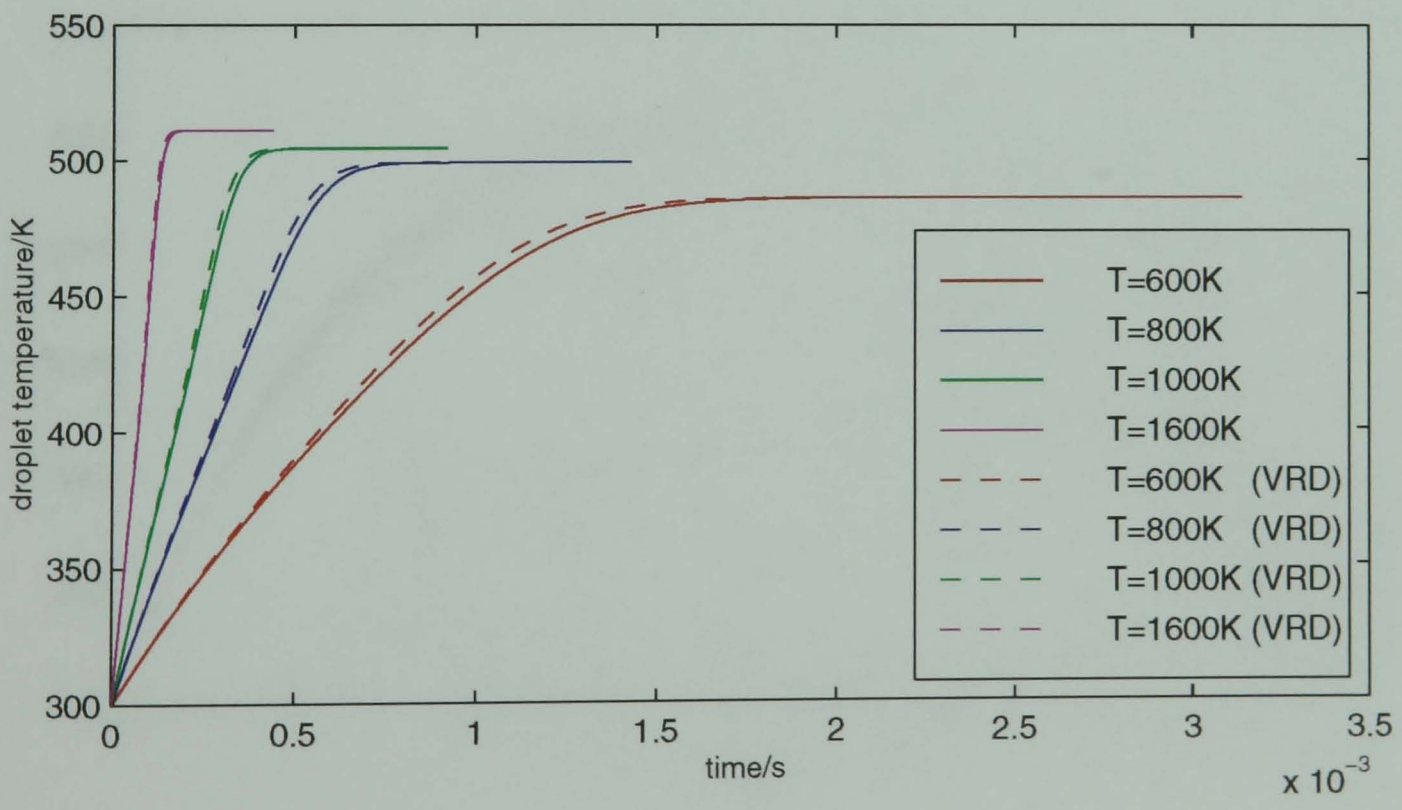

ambient pressure =5bar
fuel=*n*-decane
initial diameter=20μm

Fig. B4 Effect of variable density

variation of droplet diameter, and surface temperature with time
effect of ambient pressure

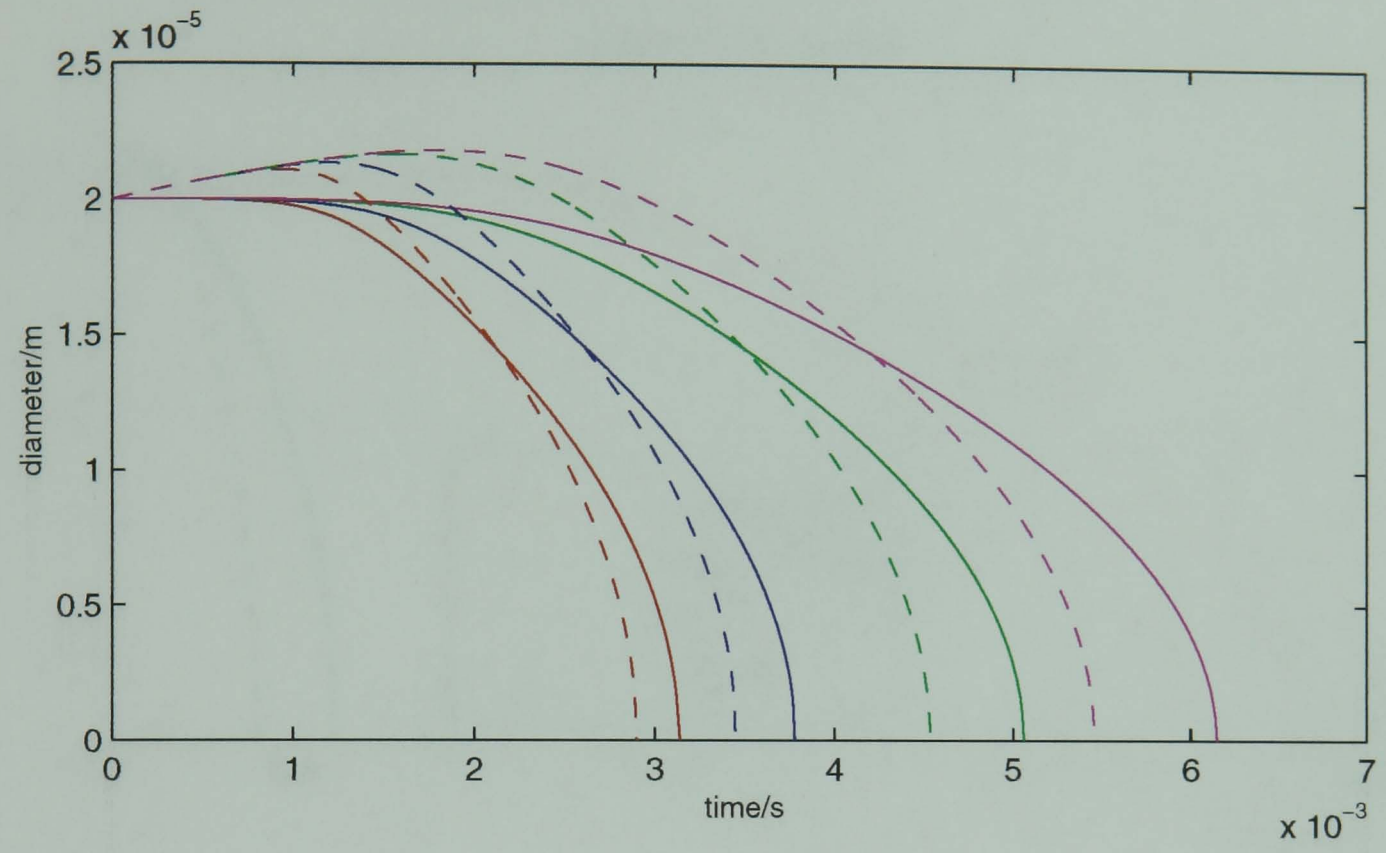

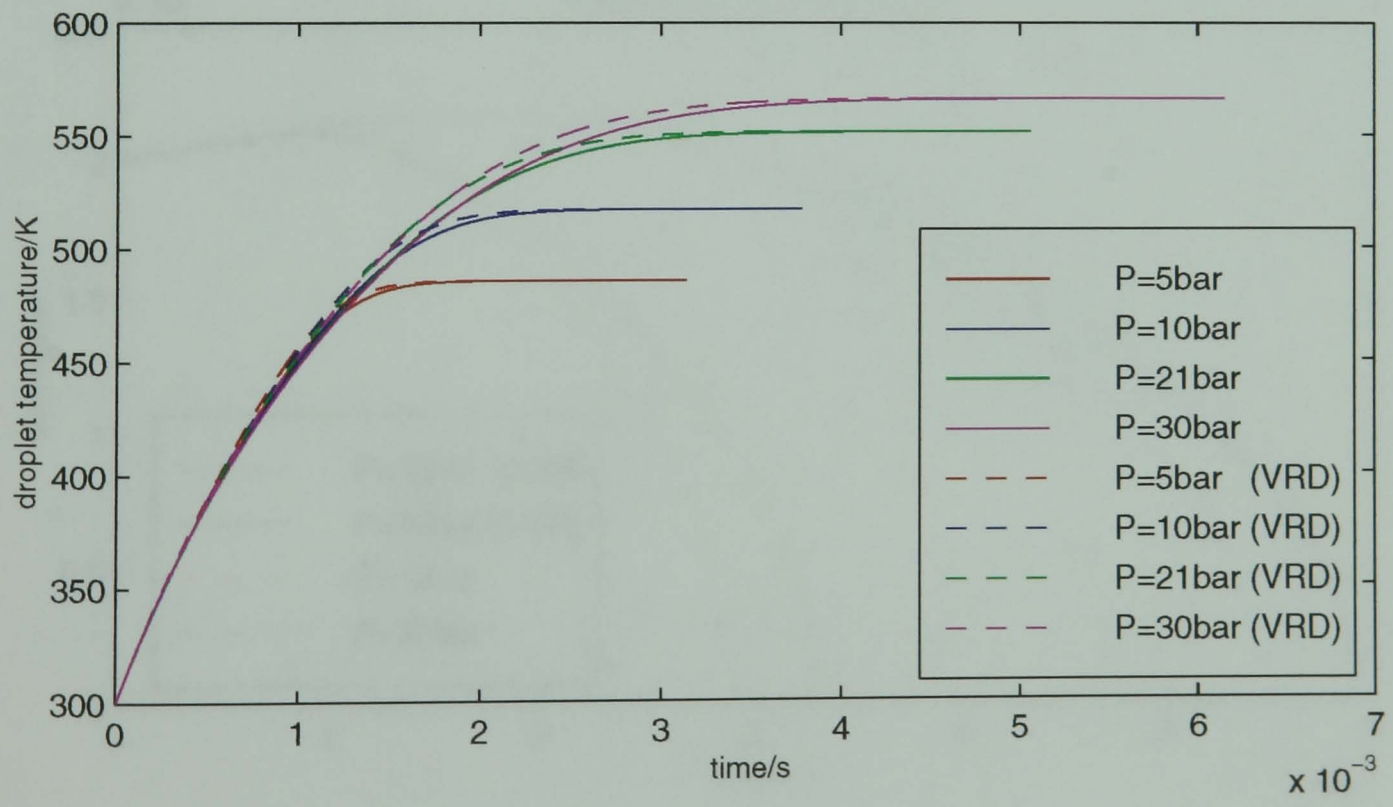

ambient temperature =600K
fuel=*n*-decane
initial diameter=20μm

Fig. B5 Effect of liquid heating

variation of droplet diameter with time

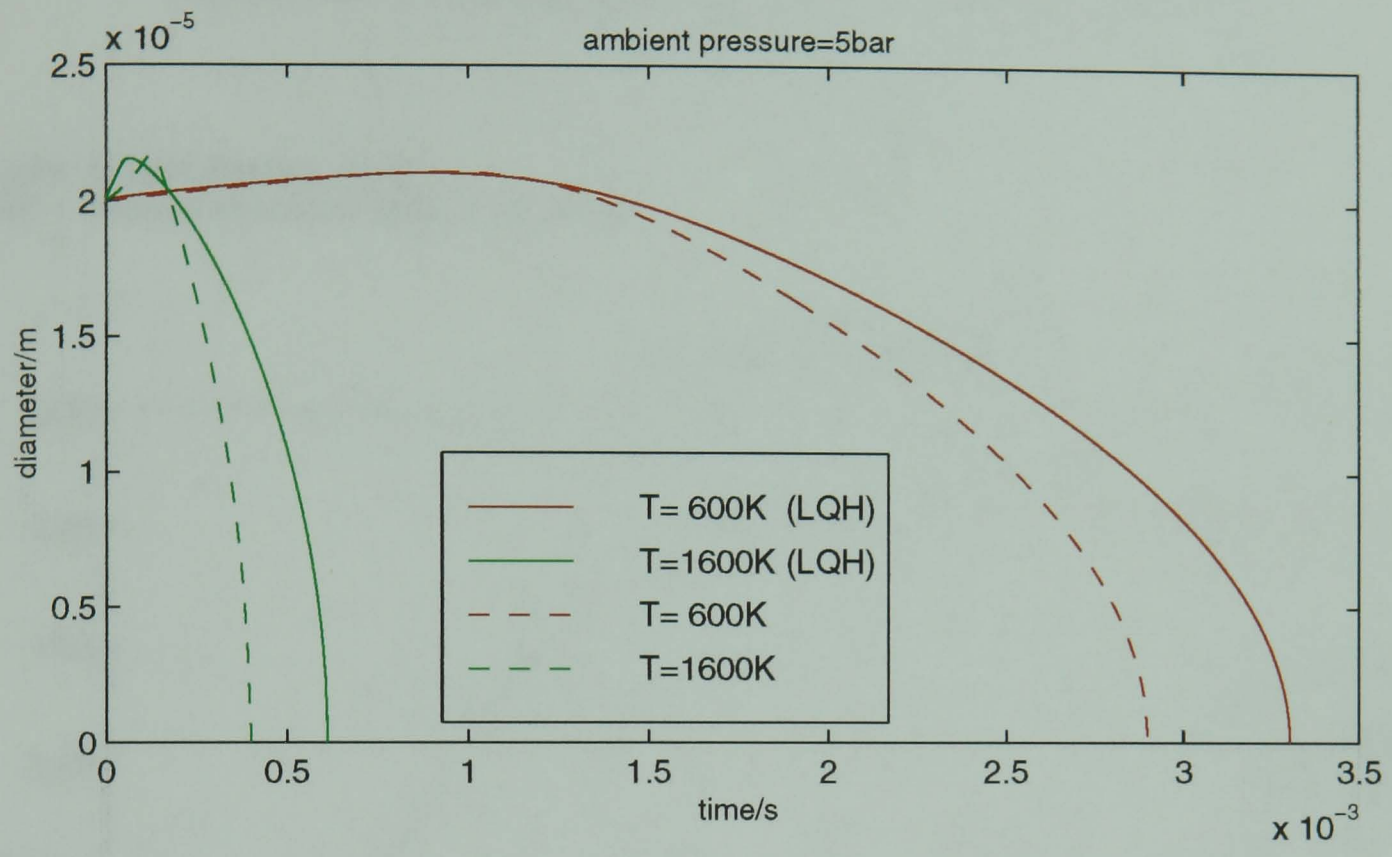

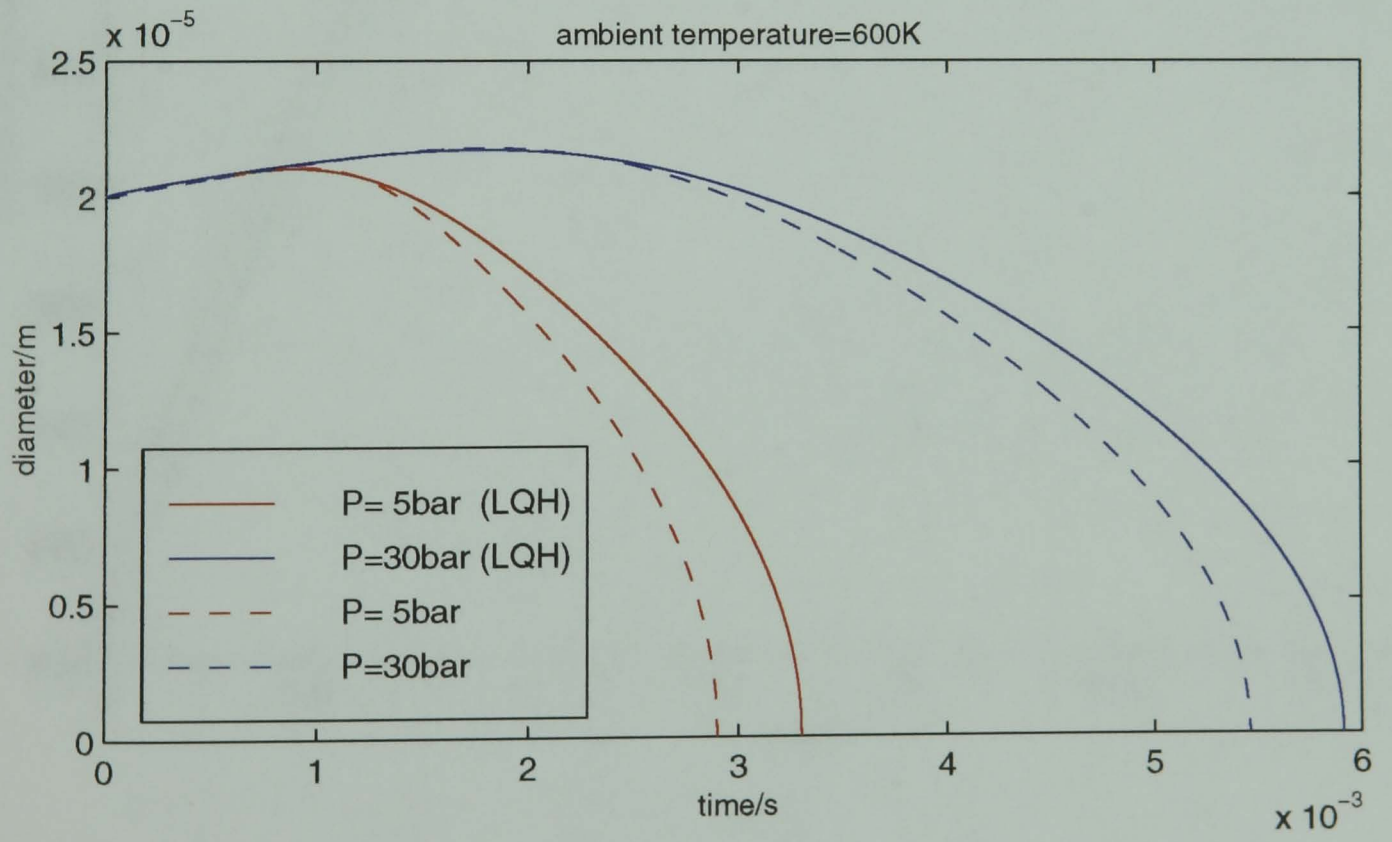

fuel=*n*-decane
initial diameter=20μm

Fig. B6 Effect of liquid heating on droplet surface temperature

LQH: LiQuid Heating model
ITC : Infinite Thermal Conductivity model

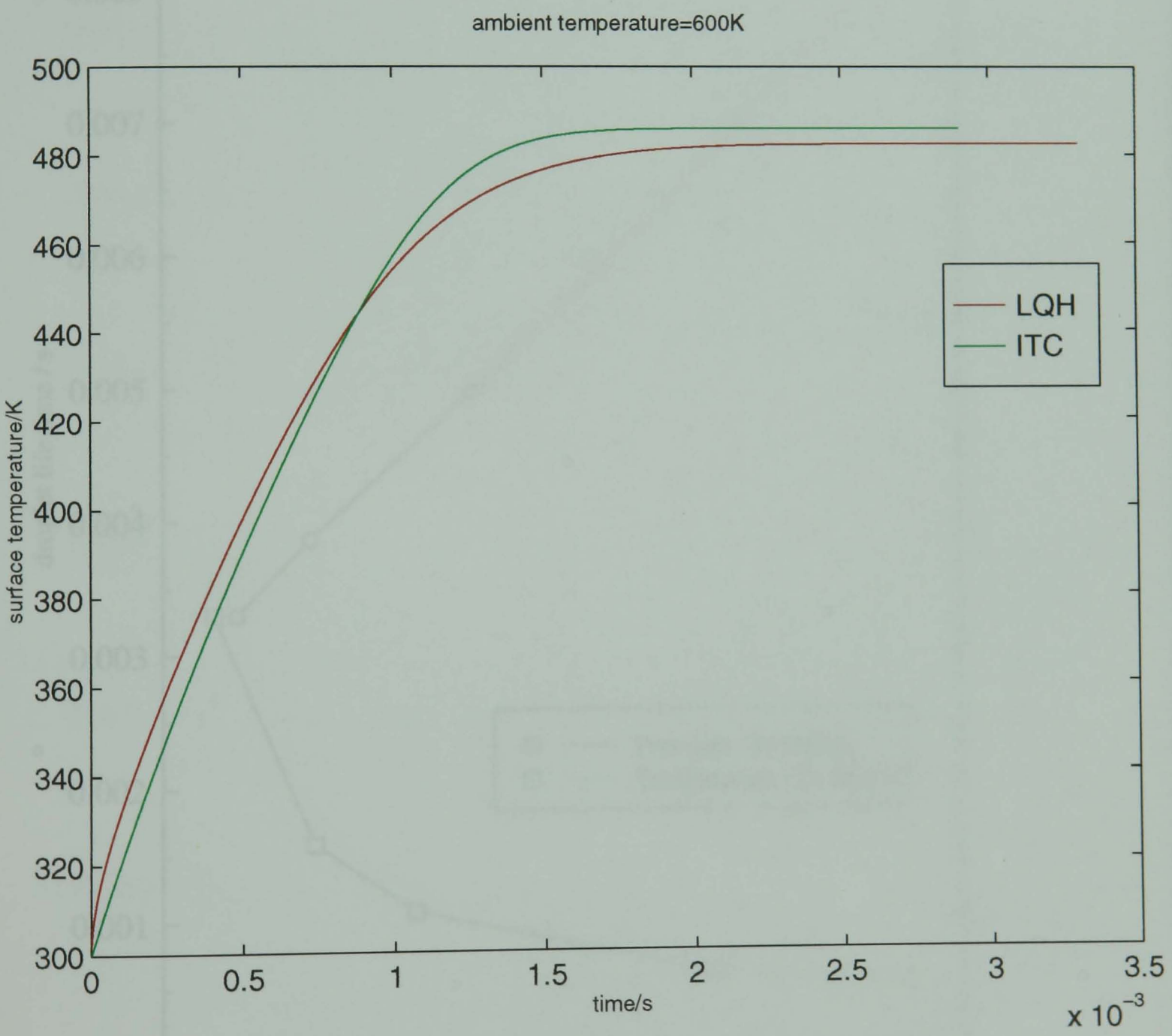

ambient pressure 5bar
fuel=*n*-decane
initial diameter=20μm

Fig. B7 Overall effect of ambient temperature and pressure on droplet life time
single-component fuel

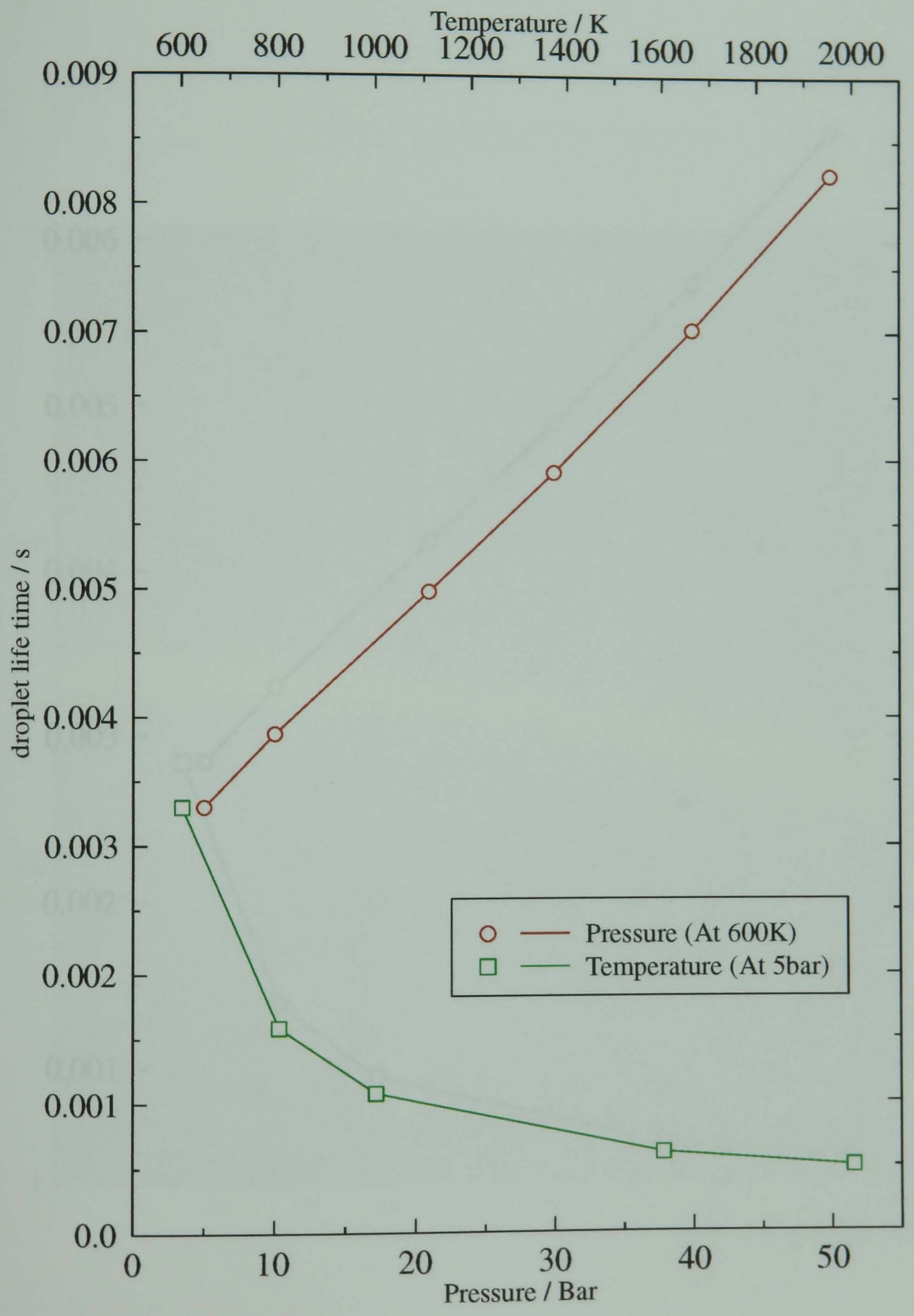

fuel : n-Decane
droplet size 20microns

Fig. B8 Overall effect of ambient temperature and pressure on droplet life time
bi-component fuel

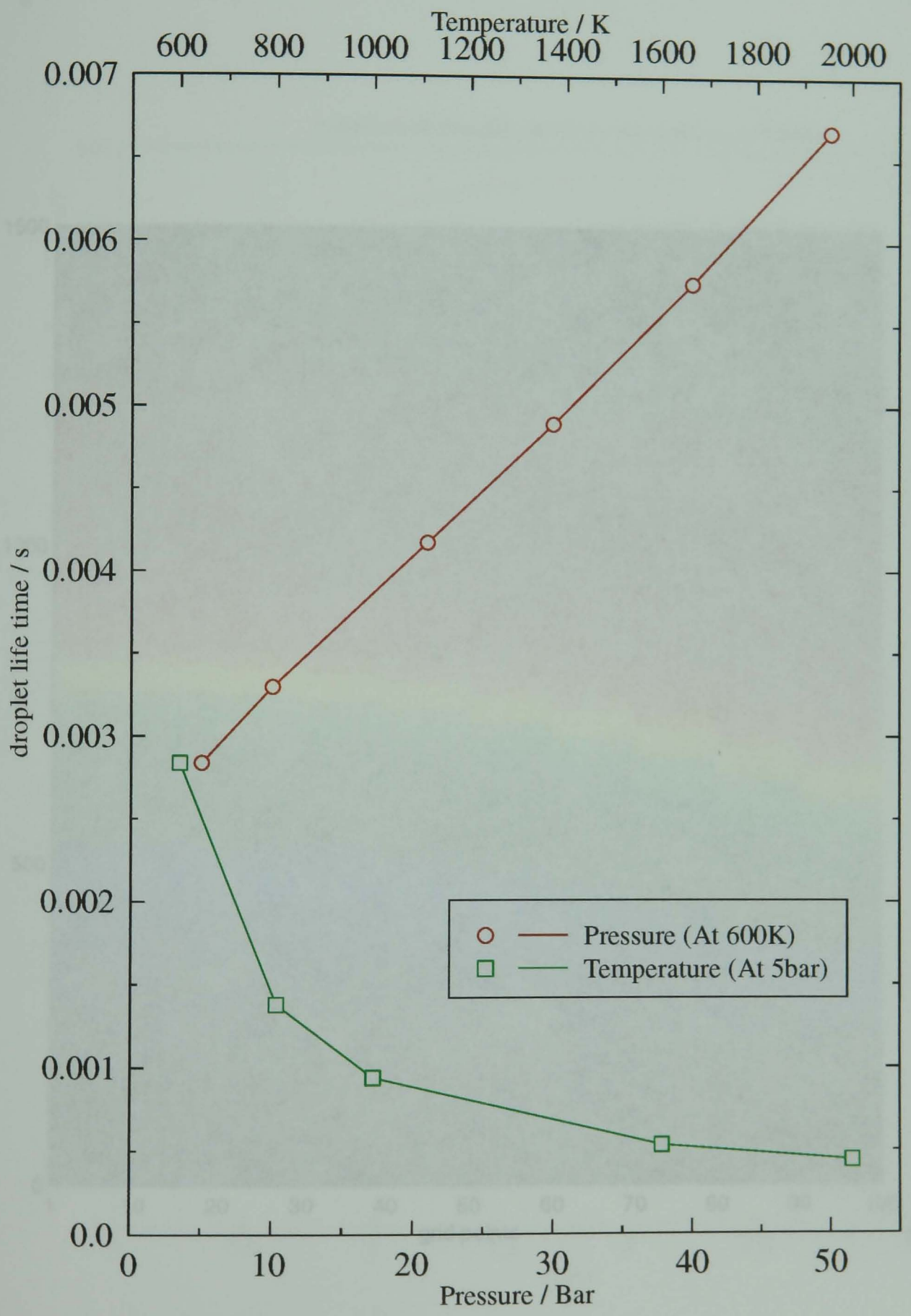

initial fuel mass fractions: 50% Octane and 50% Decane

droplet size 20microns

Fig. B9 Liquid-phase internal temperature distribution of a *n*-decane droplet

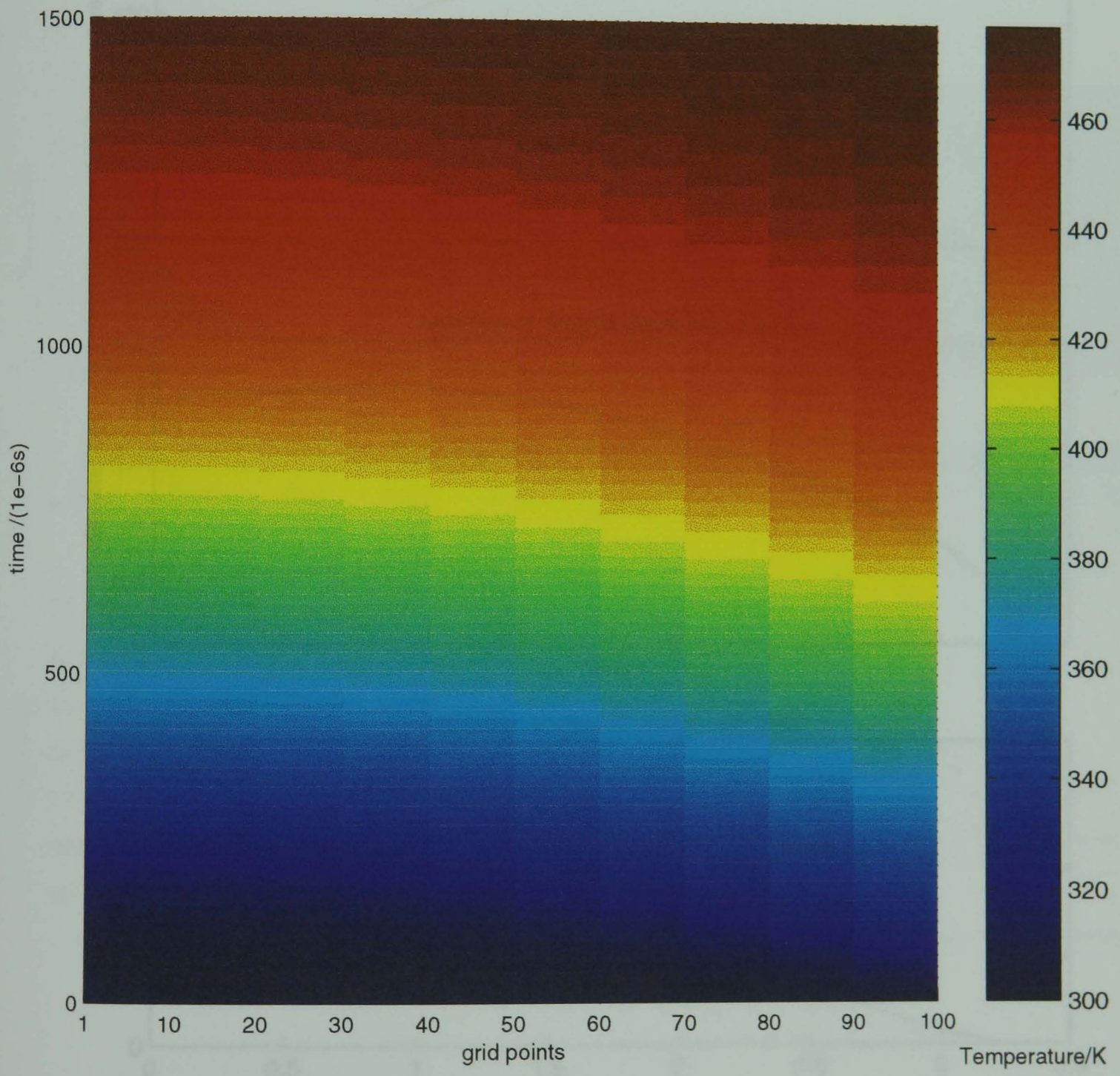

ambient temperature =800K
ambient pressure = 5bar
fuel = *n*-decane

Fig. B10 Variation of temperature, diameter and mass with time for a *n*-Decane droplet

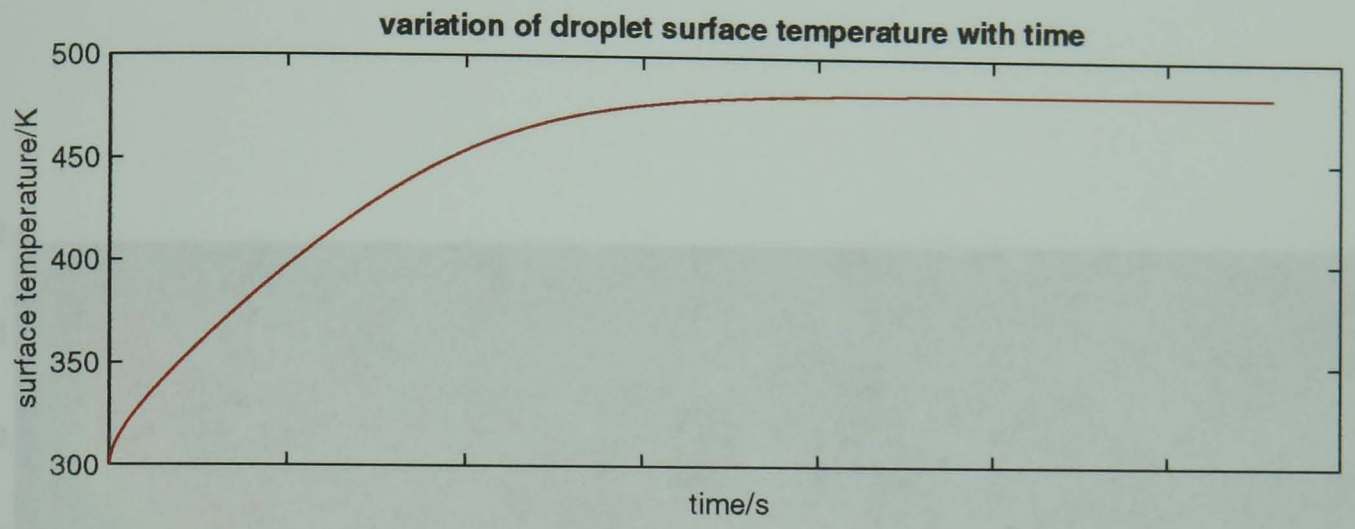

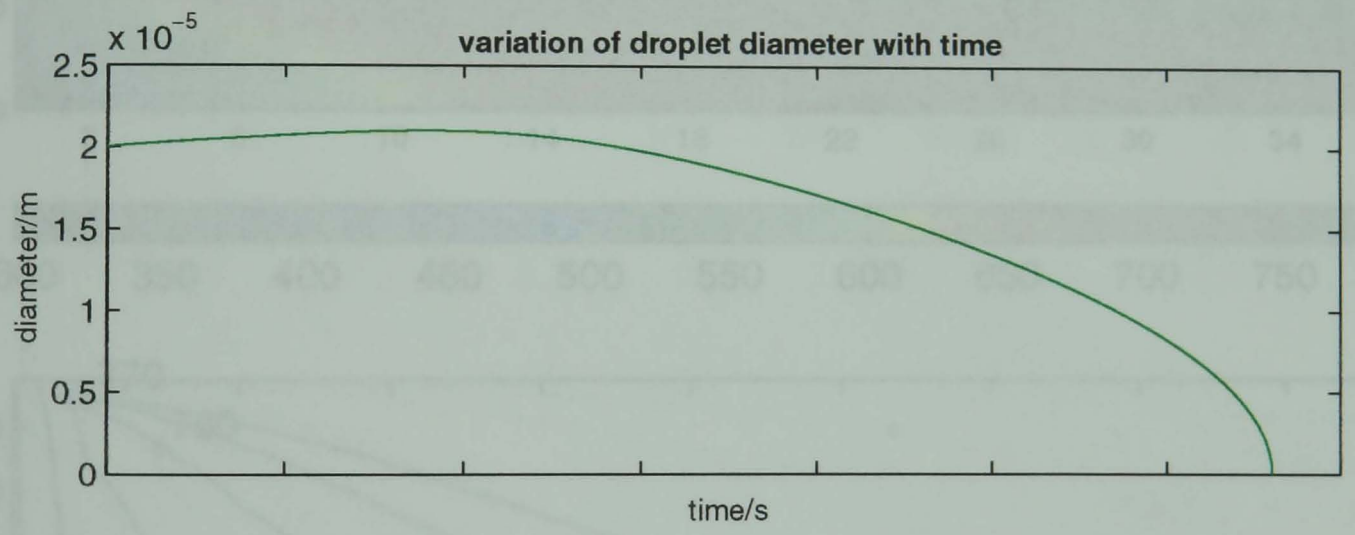

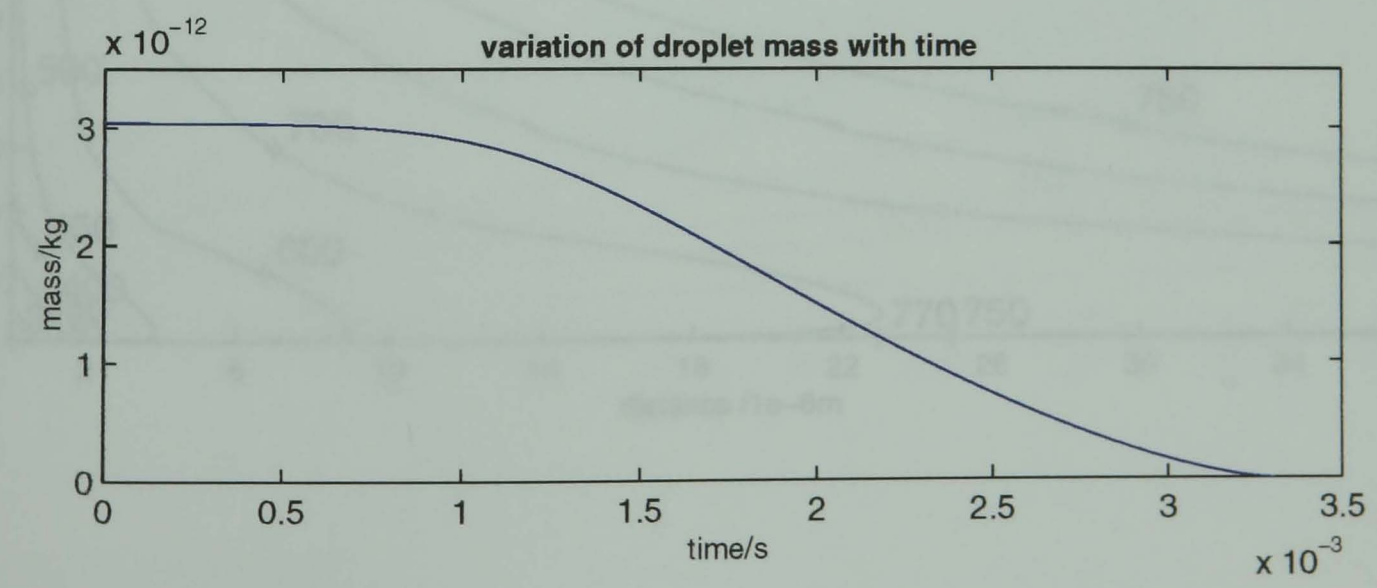

ambient temperature =800K
ambient pressure = 5bar
initial diameter =20μm

Fig. B11 Temperature iso-contours in the air-fuel-vapour film surrounding an evaporating fuel droplet

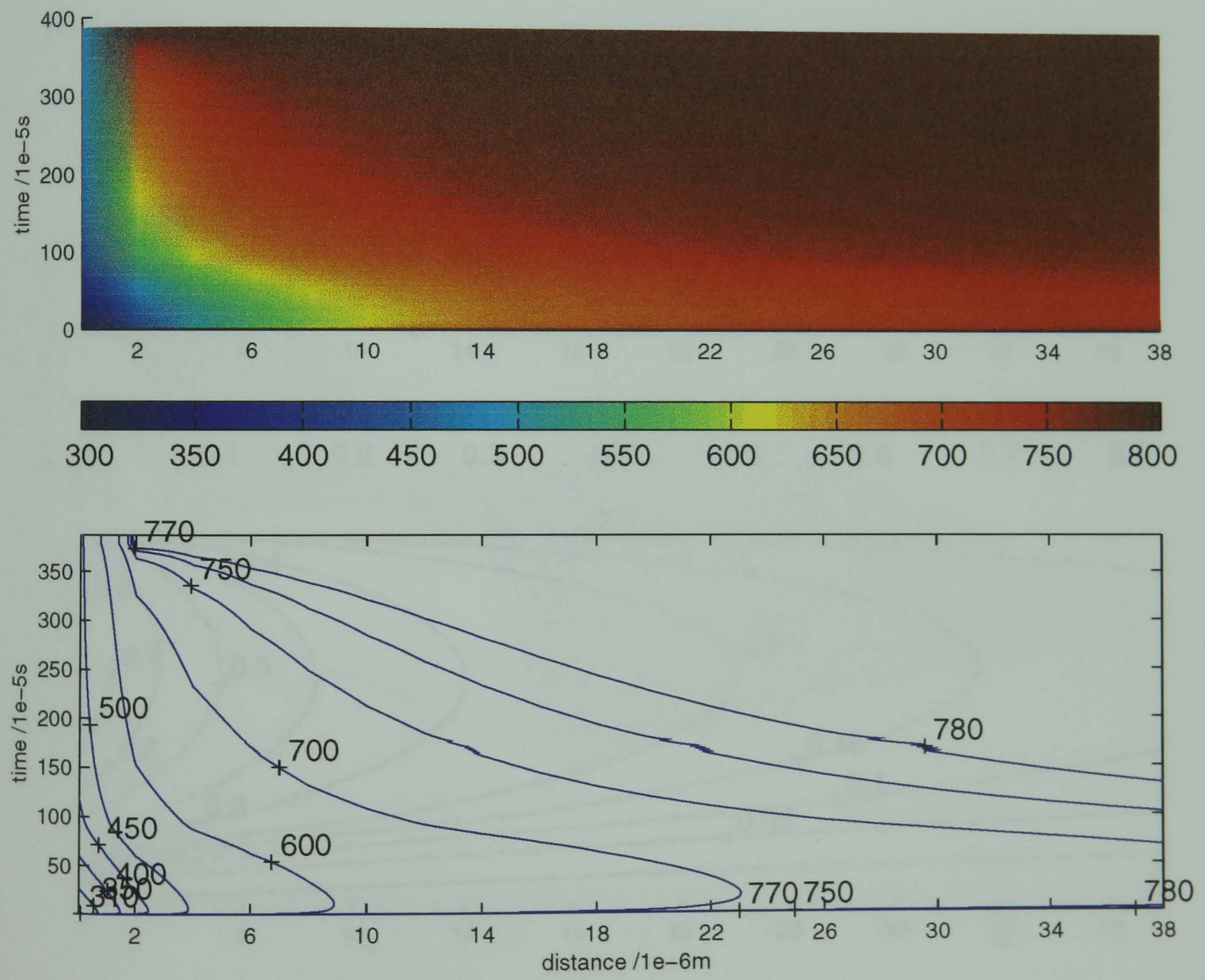

ambient temperature =800K
ambient pressure =5bar
fuel = *n*-decane
initial diameter =20μm

Fig. B12 Fuel vapour iso-concentration in the air-fuel-vapour film surrounding an evaporating fuel droplet

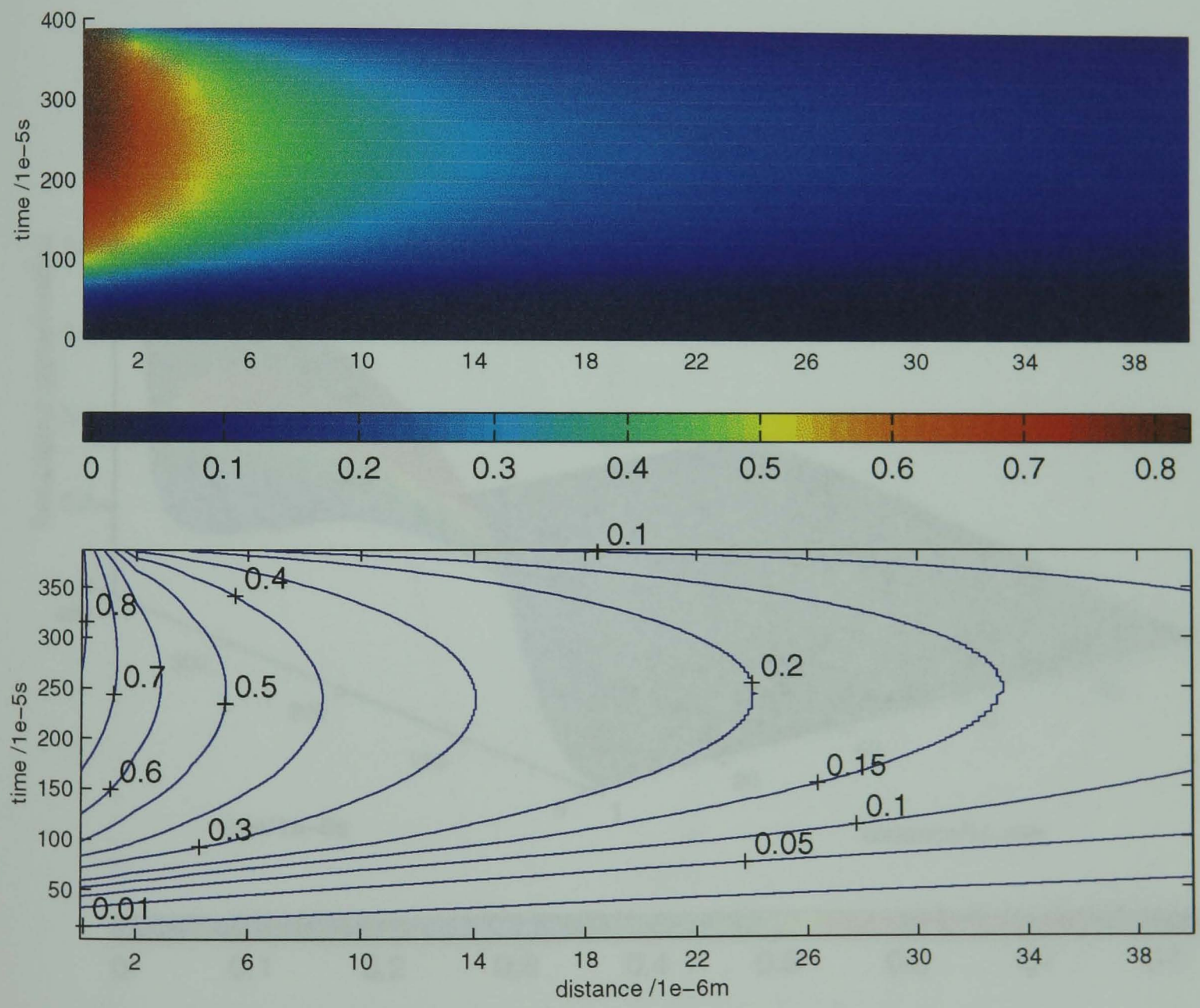

ambient pressure =5bar
ambient temperature =800K
fuel = *n*-decane
initial diameter =20μm

Fig. B13 3-D fuel vapour concentration in the air-fuel-vapour film surrounding an evaporation droplet

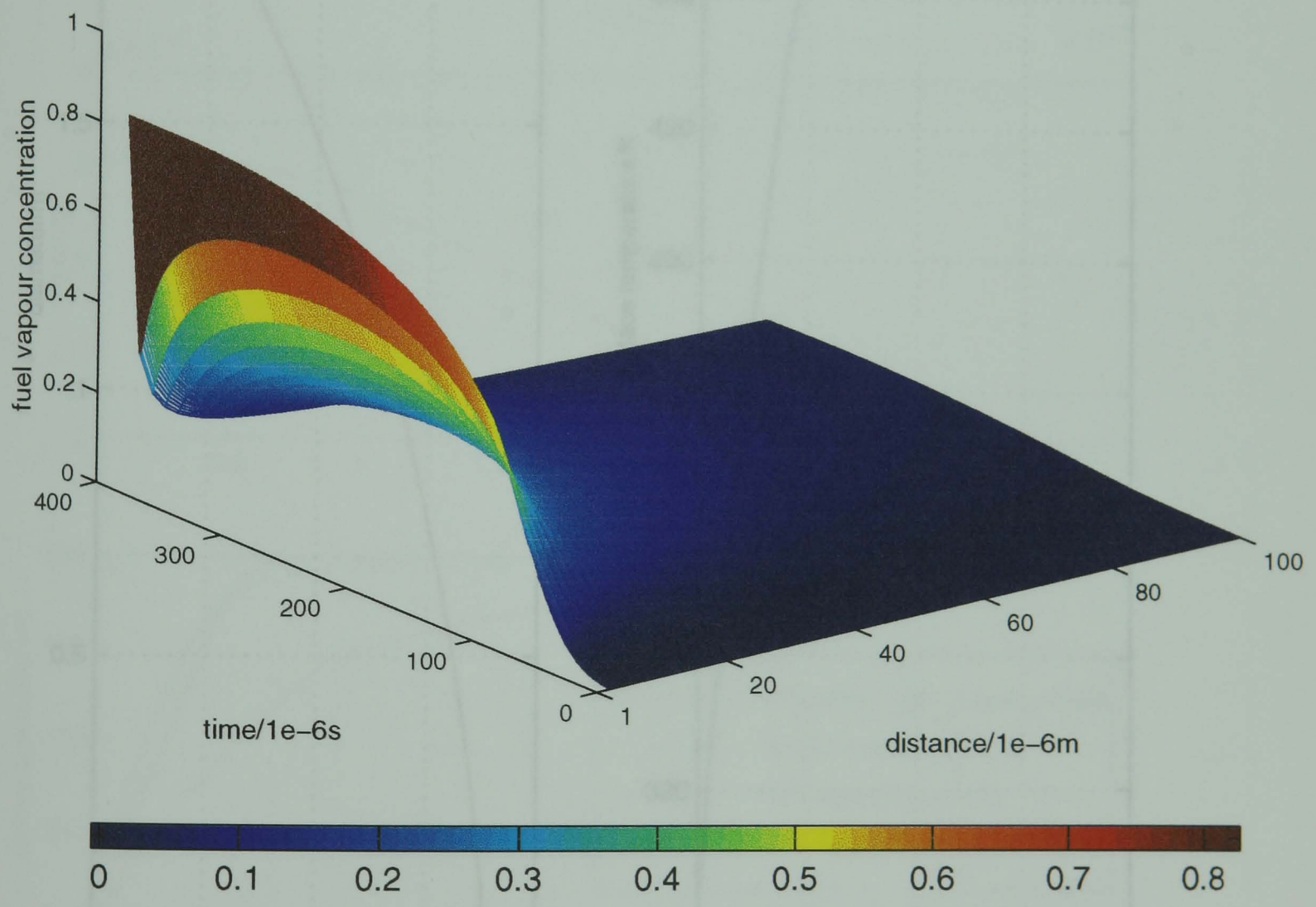

ambient temperature =800K
ambient pressure =5bar
fuel = *n*-decane
initial diameter =20μm

Fig. B14 Variation of droplet diameter and surface temperature with time for an unsteady formulation

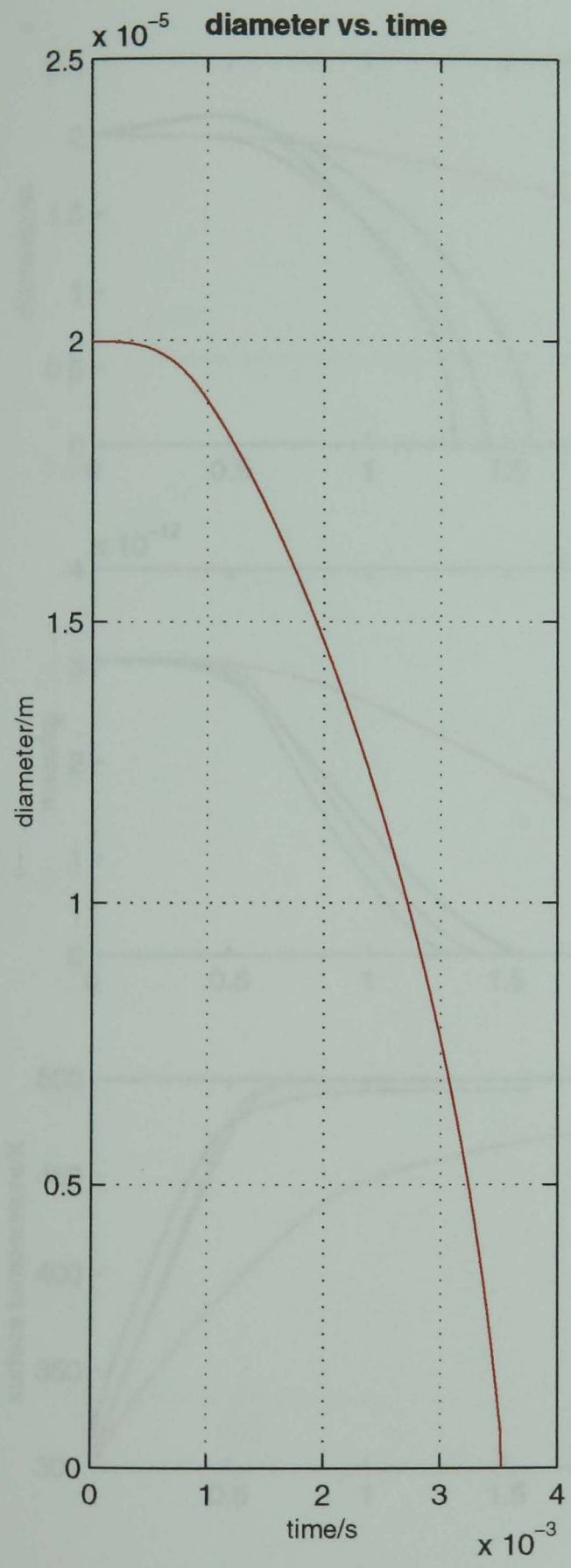

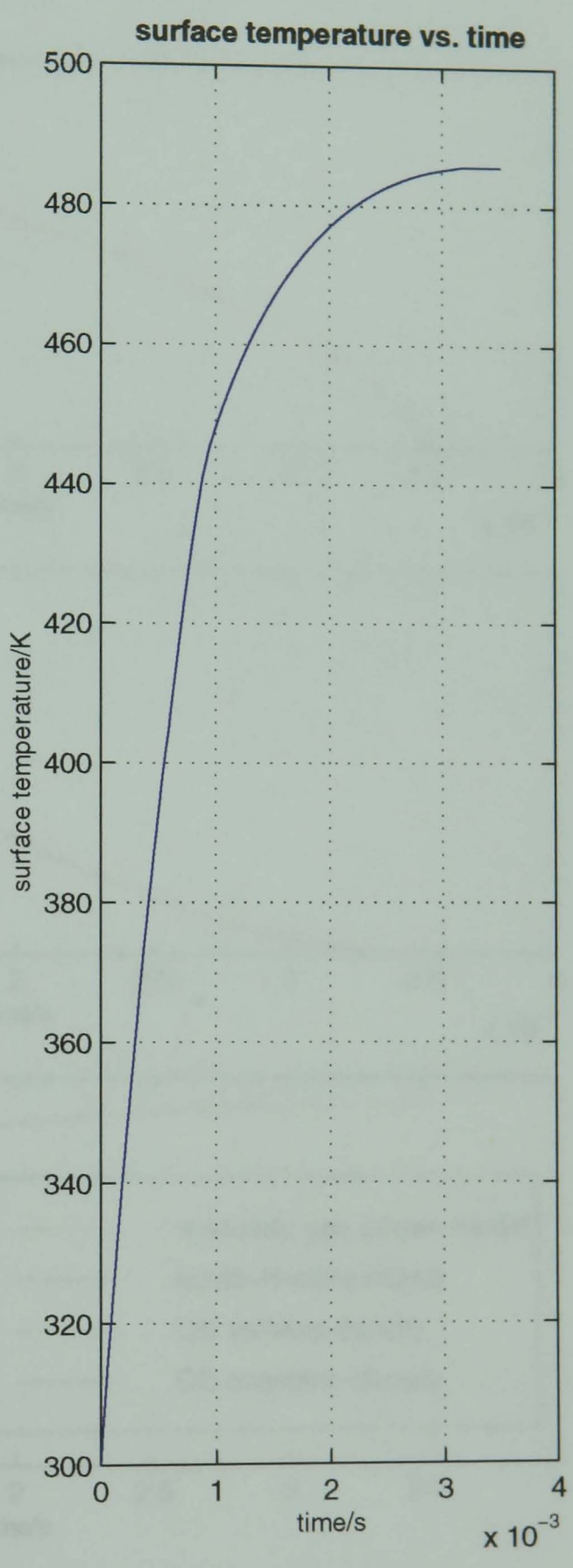

ambient pressure =5bar
ambient temperature =800K
fuel = *n*-decane
initial diameter =20μm

Fig. B15 Comparative results of the four models
variation of diameter, mass and surface temperature with time

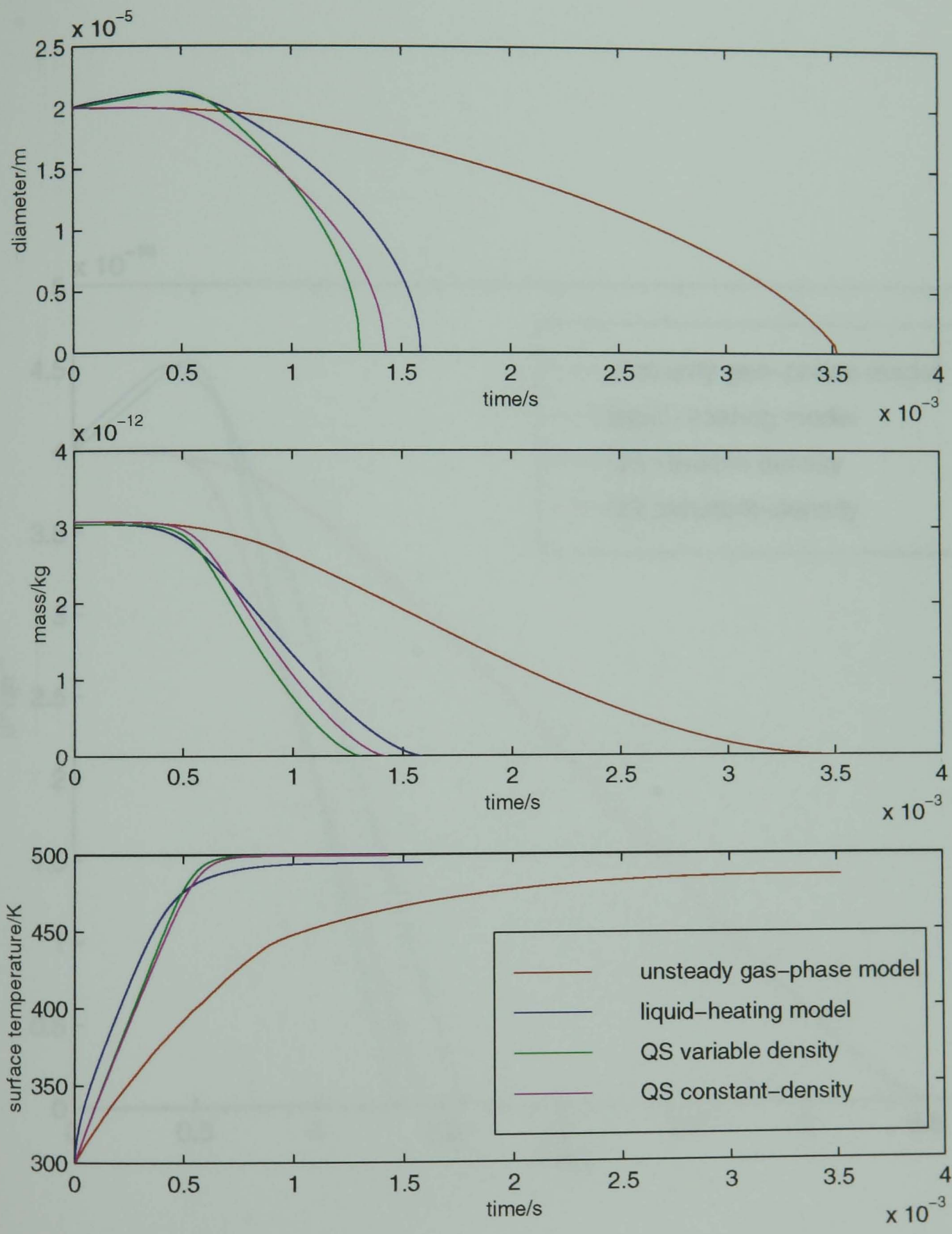

ambient temprature= 800K ambient pressure= 5bar fuel= n–Decane

Fig. B16 Variation of d^2 with time

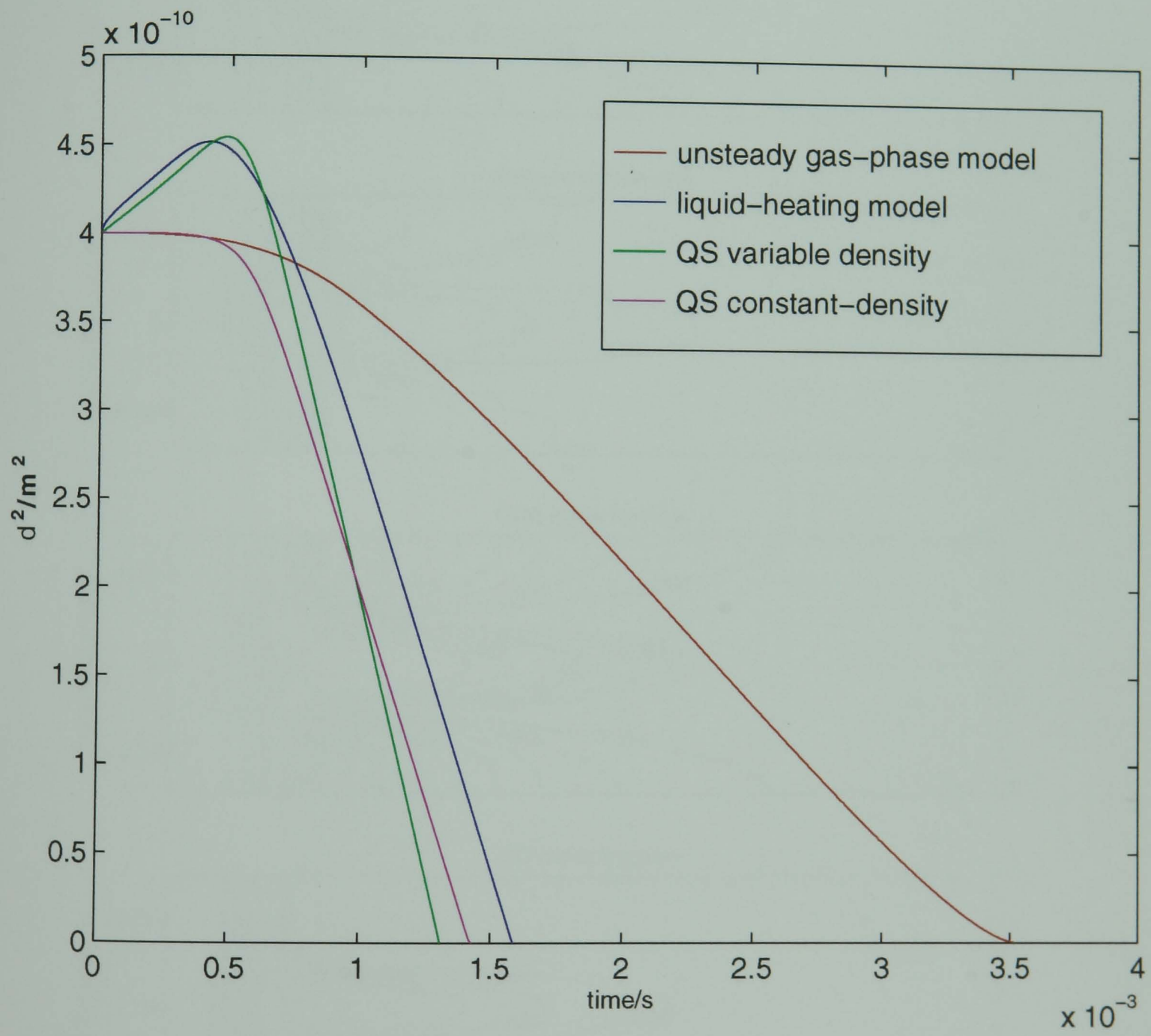

ambient temperature =800K
ambient pressure =5bar
fuel = *n*-Decane
initial diameter =20μm

APPENDIX-C

FIGURES: SPRAY RESULTS

Fig. C1 Predicted iso-contour maps at experimental conditions
(input equivalence ratio=1.08 pressure=0.65MPa)

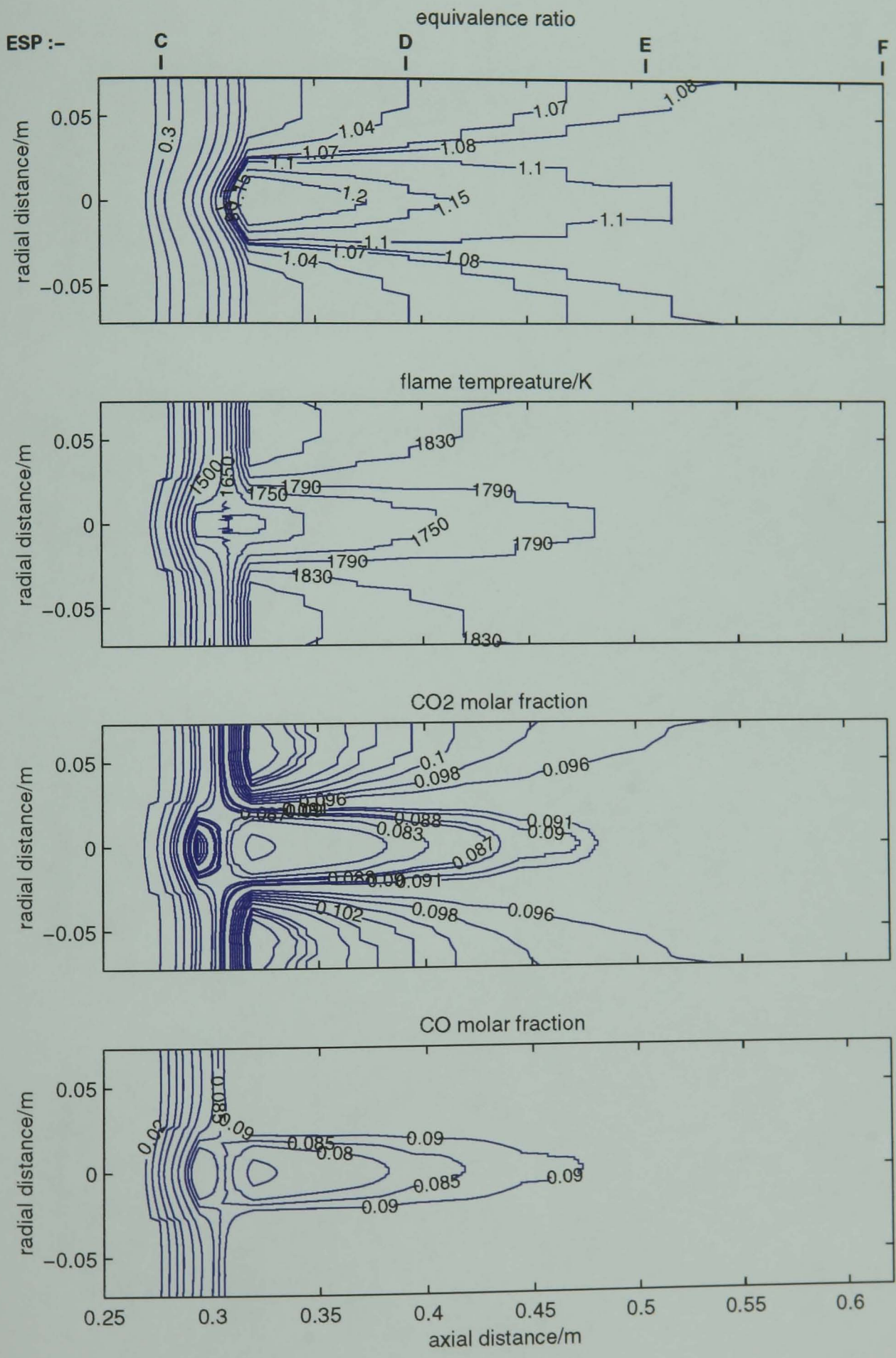

ESP : Equivalent Sample Position

Fig. C2 Comparative axial distributions

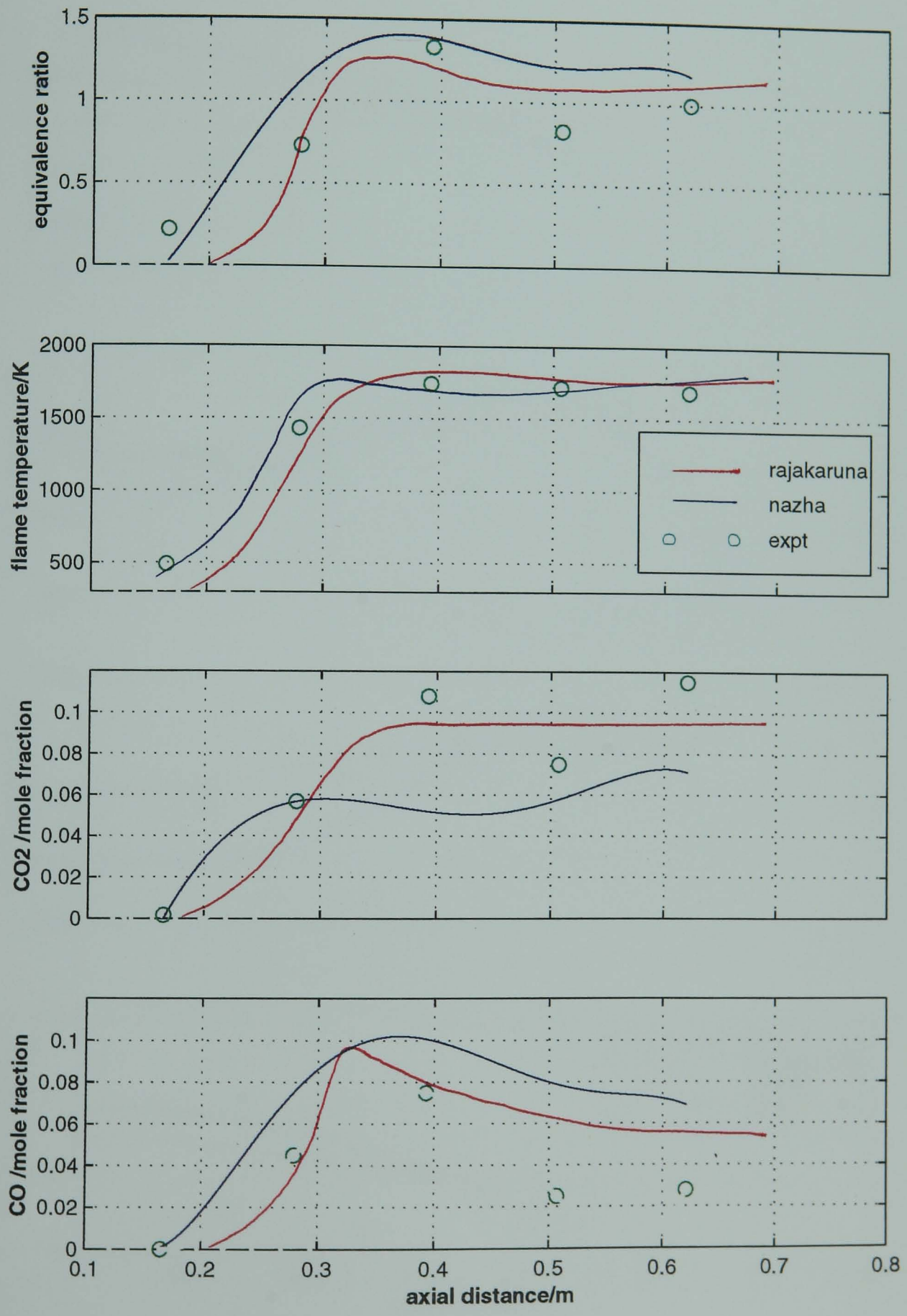

Fig. C3 Comparative radial distributions at section D [0.393m from the injector]

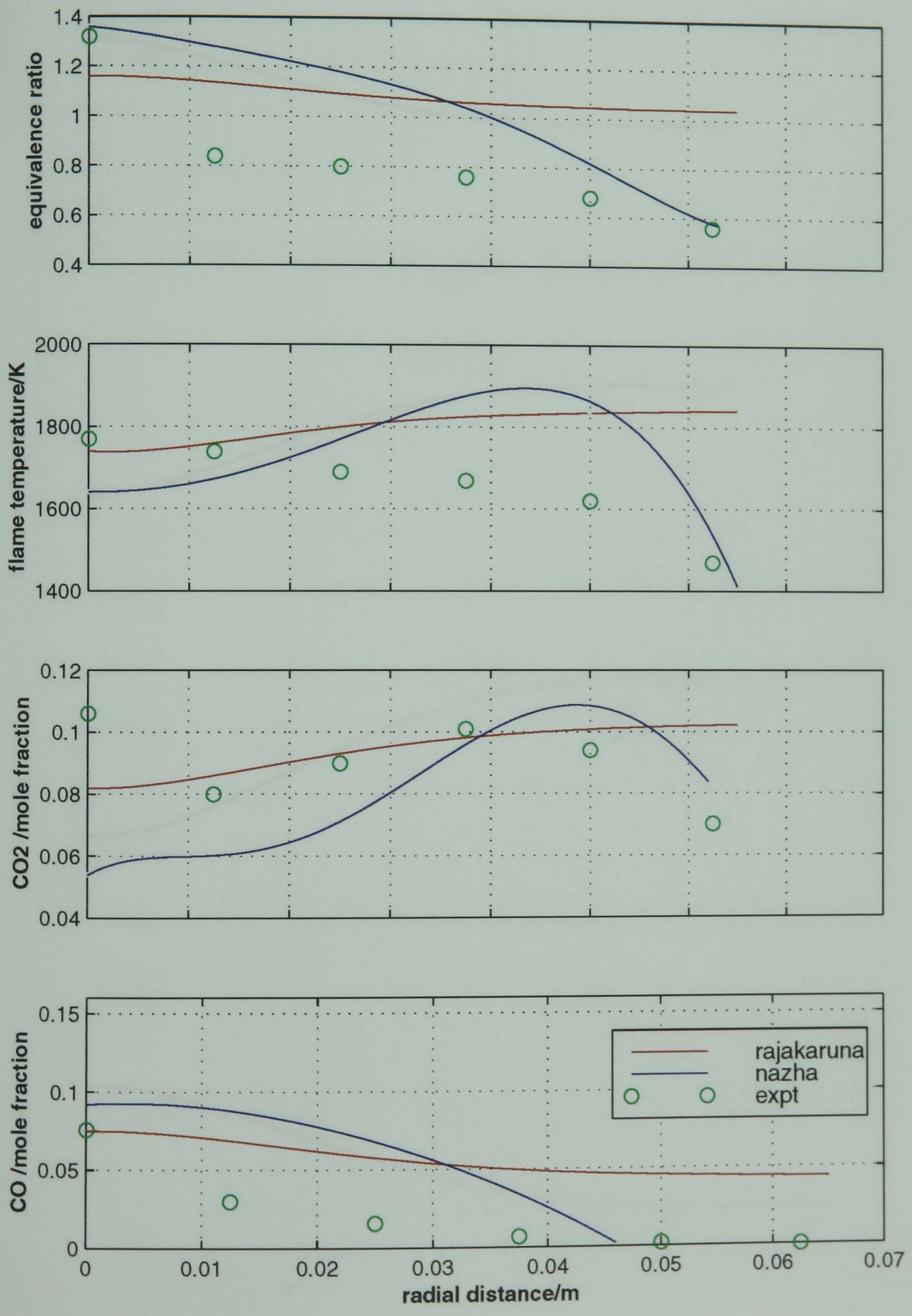

Fig. C4 Comparative radial distributions at predicted maximum axial equivalence ratio position

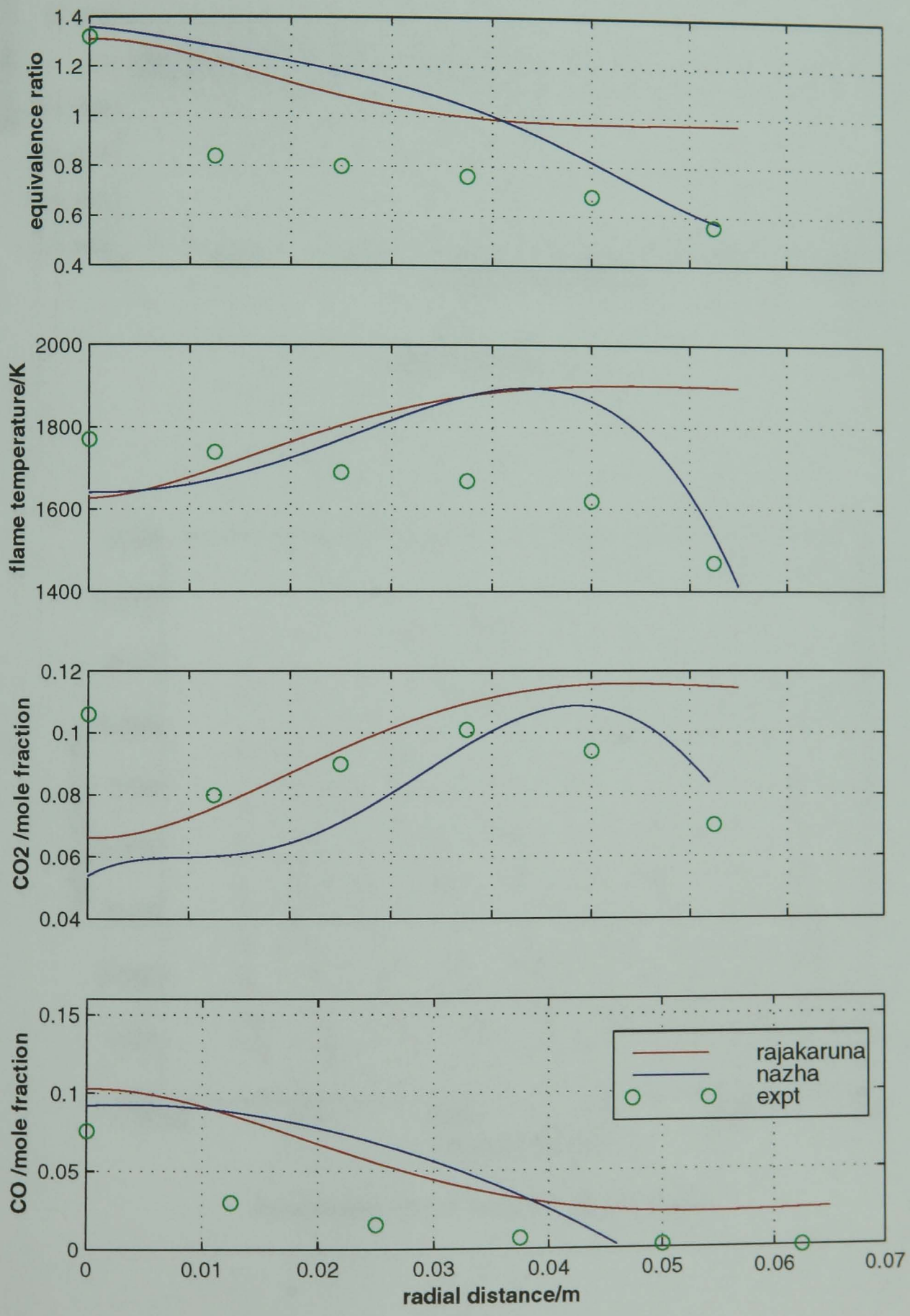

Fig-C5 Predicted velocity distribution and recirculation inside the chamber

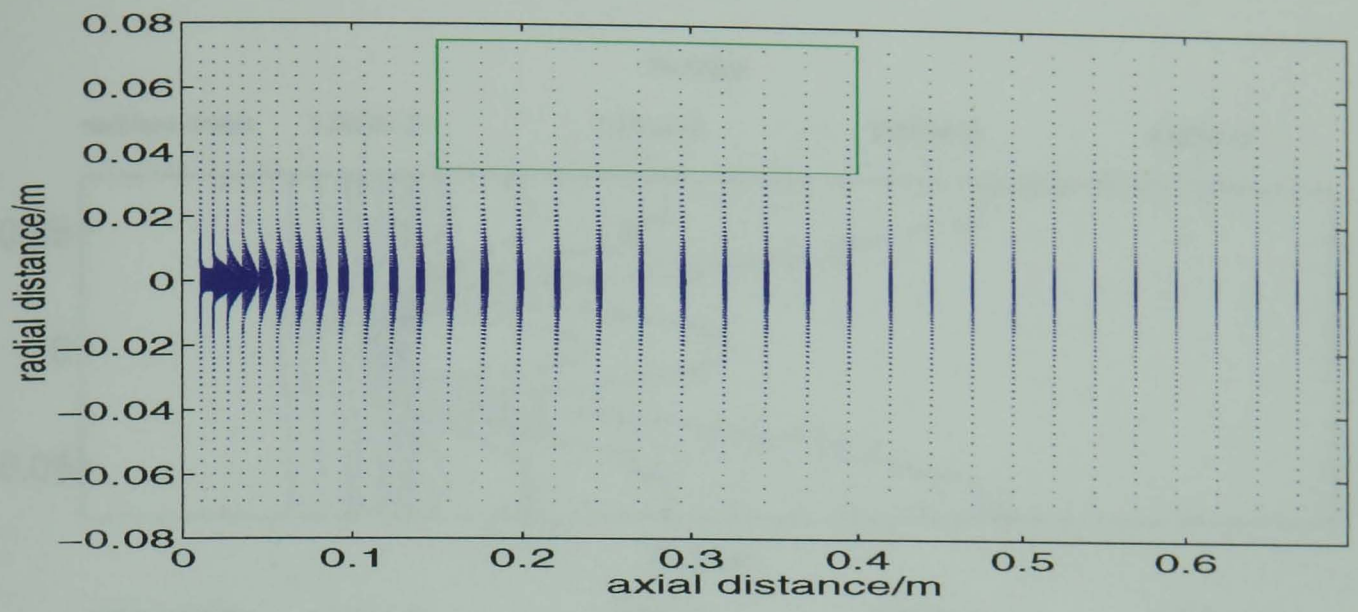

velocity distribution

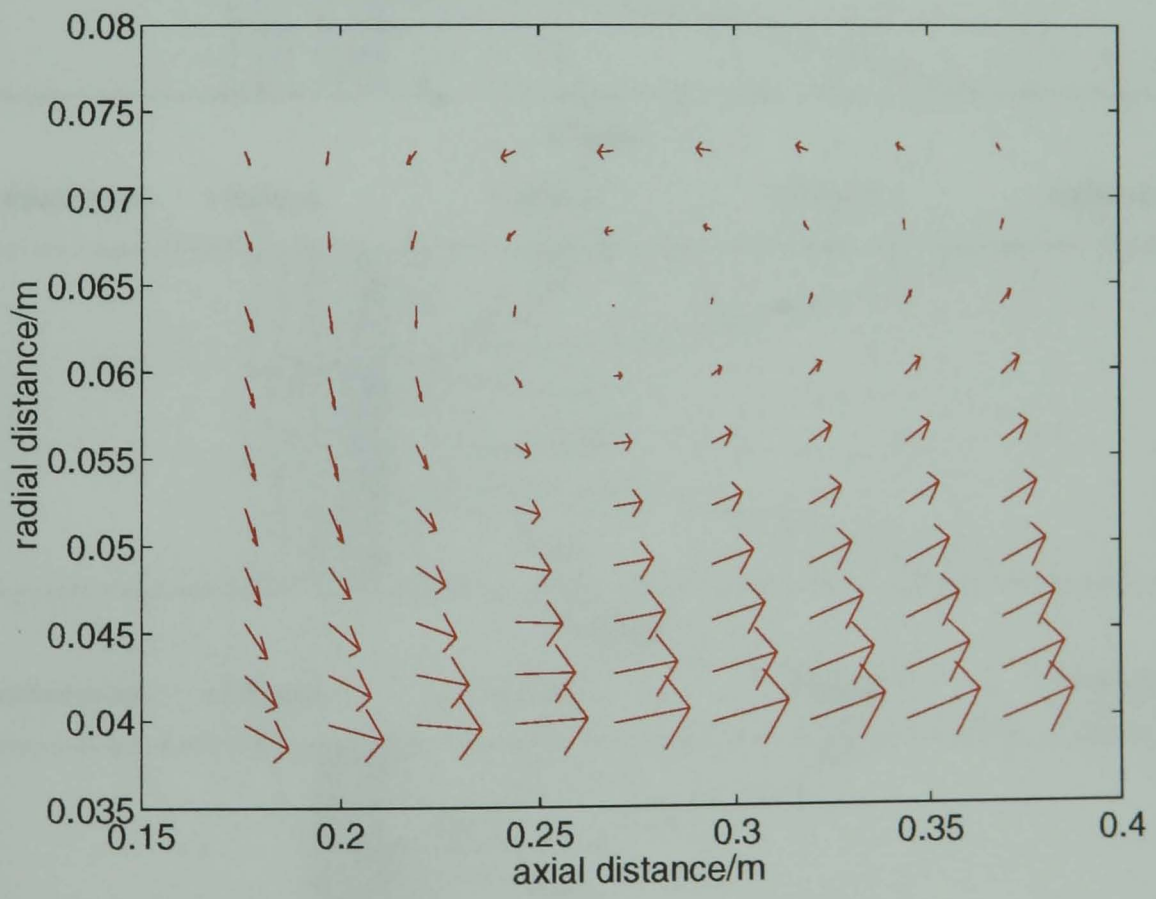

An enlarged view of the recirculation region

Fig. C6 Predicted vapour equivalence ratio spatial distribution for four ambient pressure conditions

(input equivalence ratio=1.1)

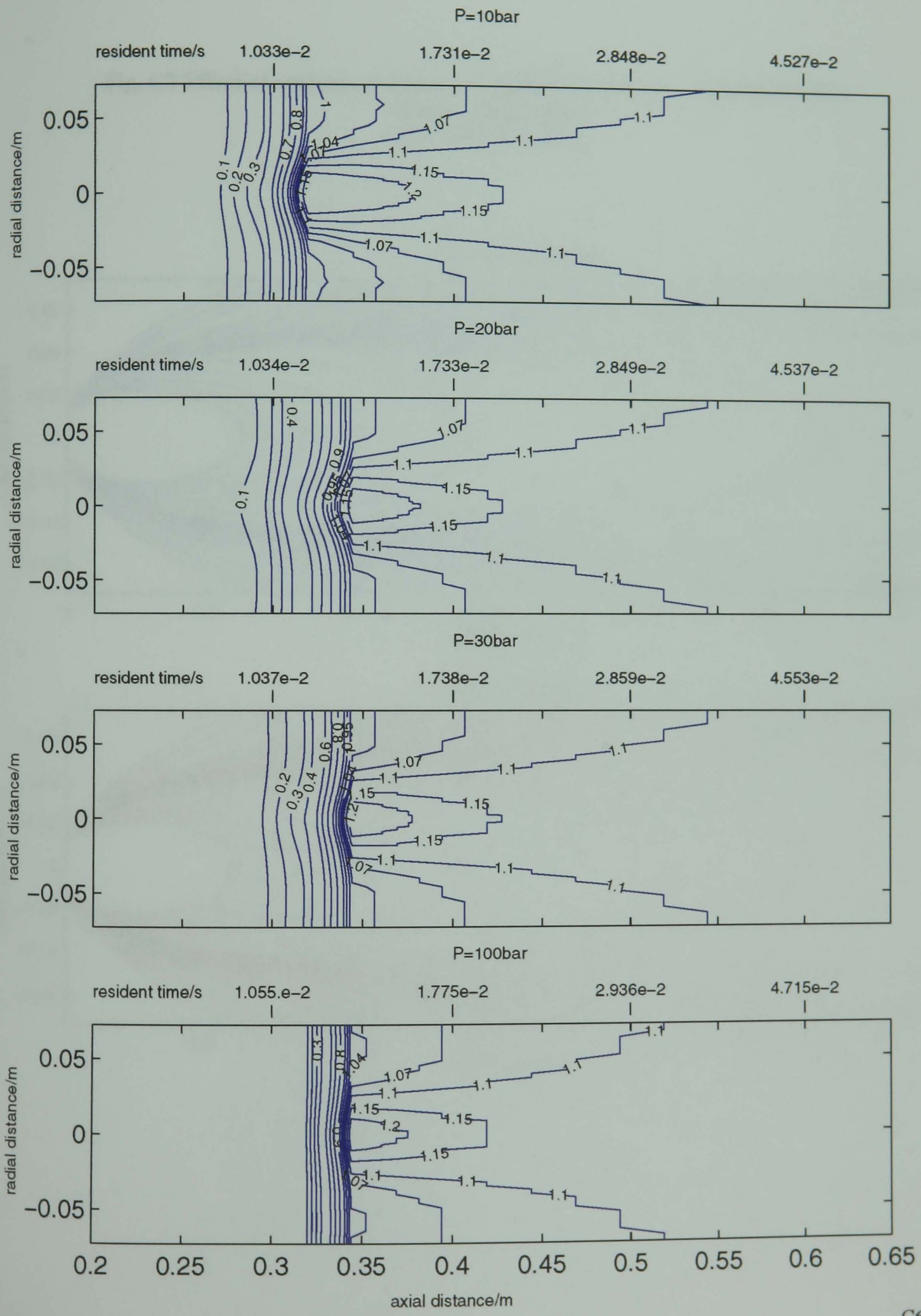

Fig. C7 Effect of ambient pressure on vapour equivalence ratio distribution - single-phase model
(T_{air}=1000K fuel=CH_4)

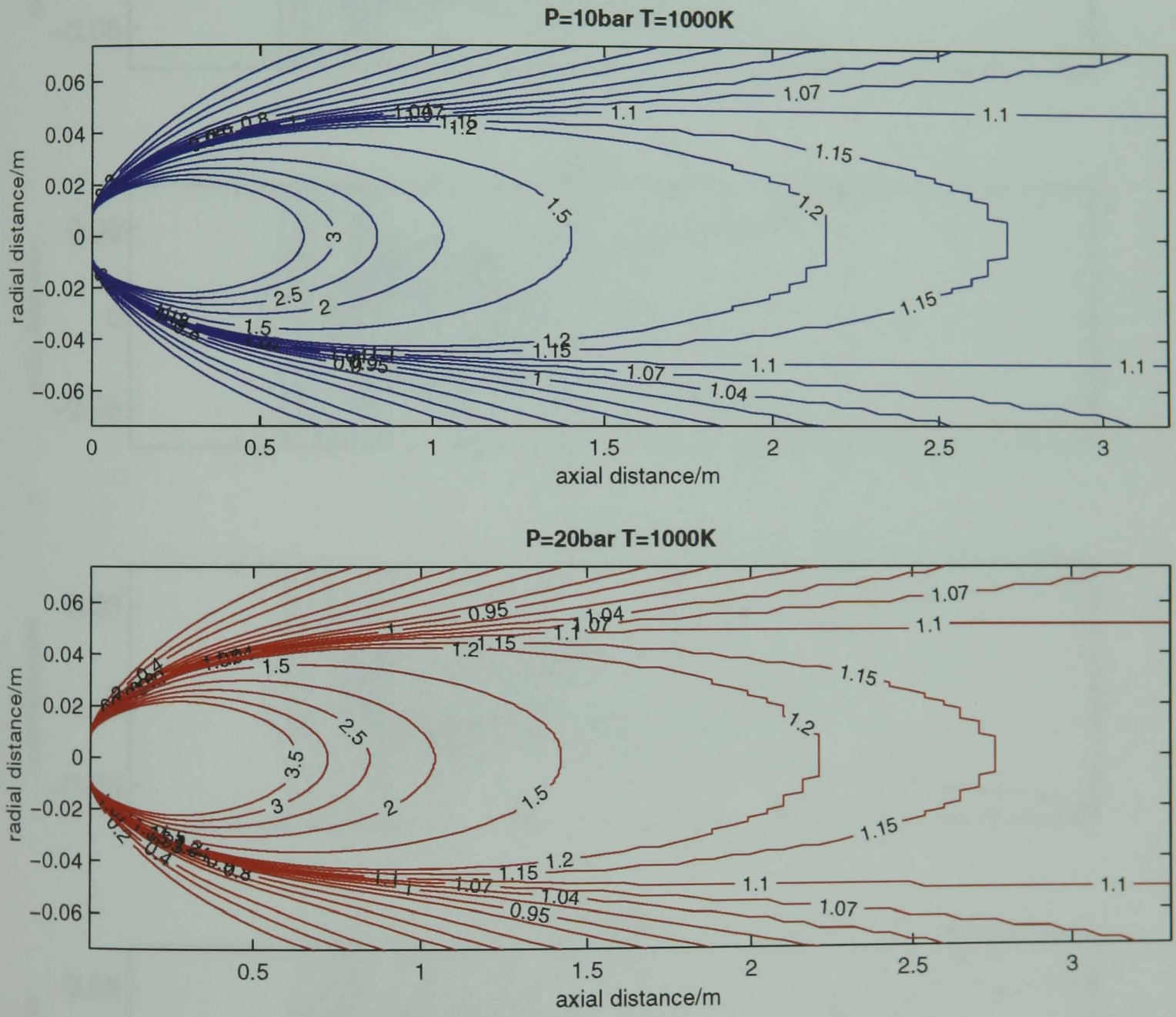

Fig. C8 Effect of input equivalence ratio on local vapour equivalence ratio distribution

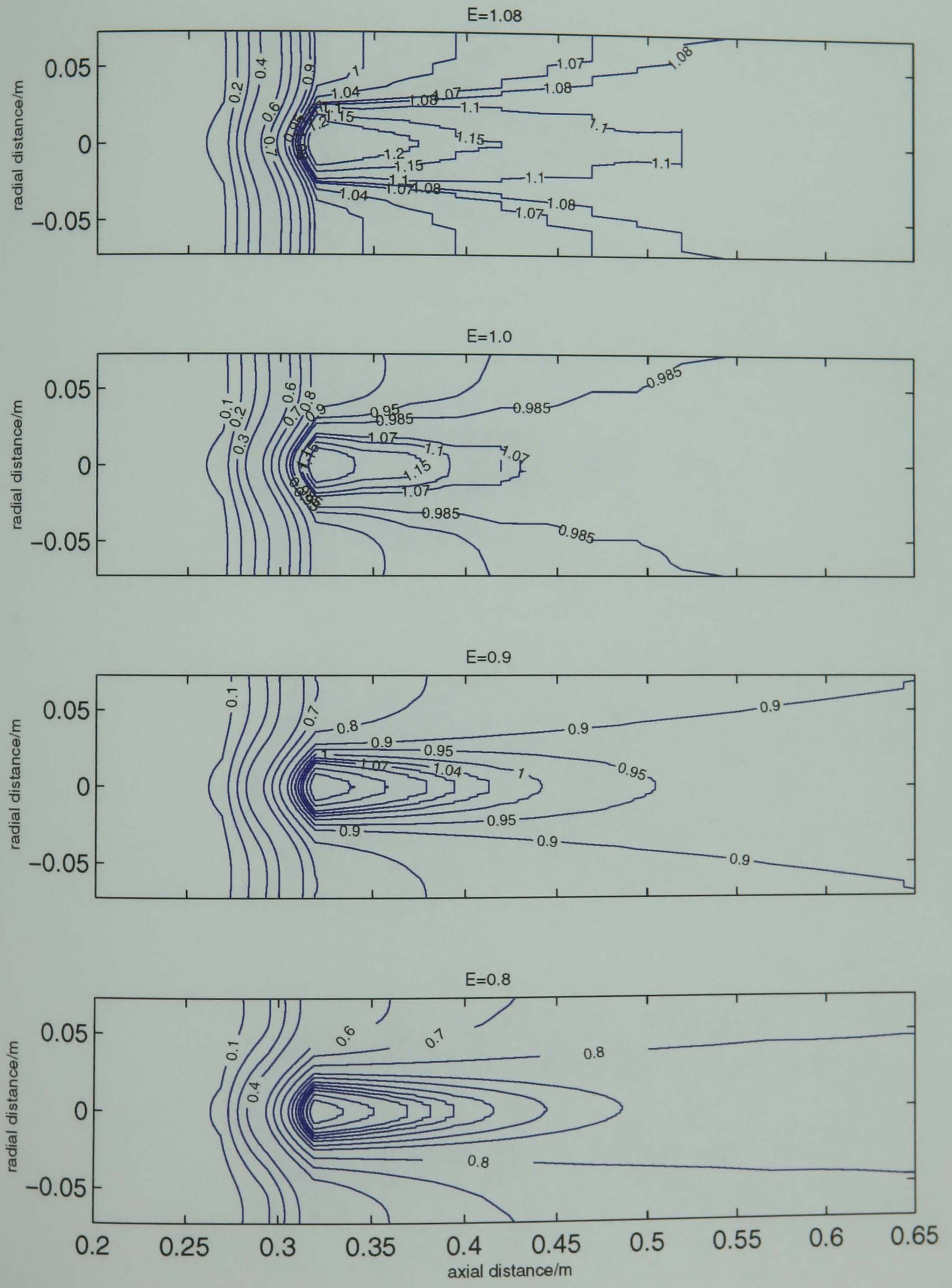

Fig. C9 Effect of input equivalence ratio on CO_2 mole fraction distribution

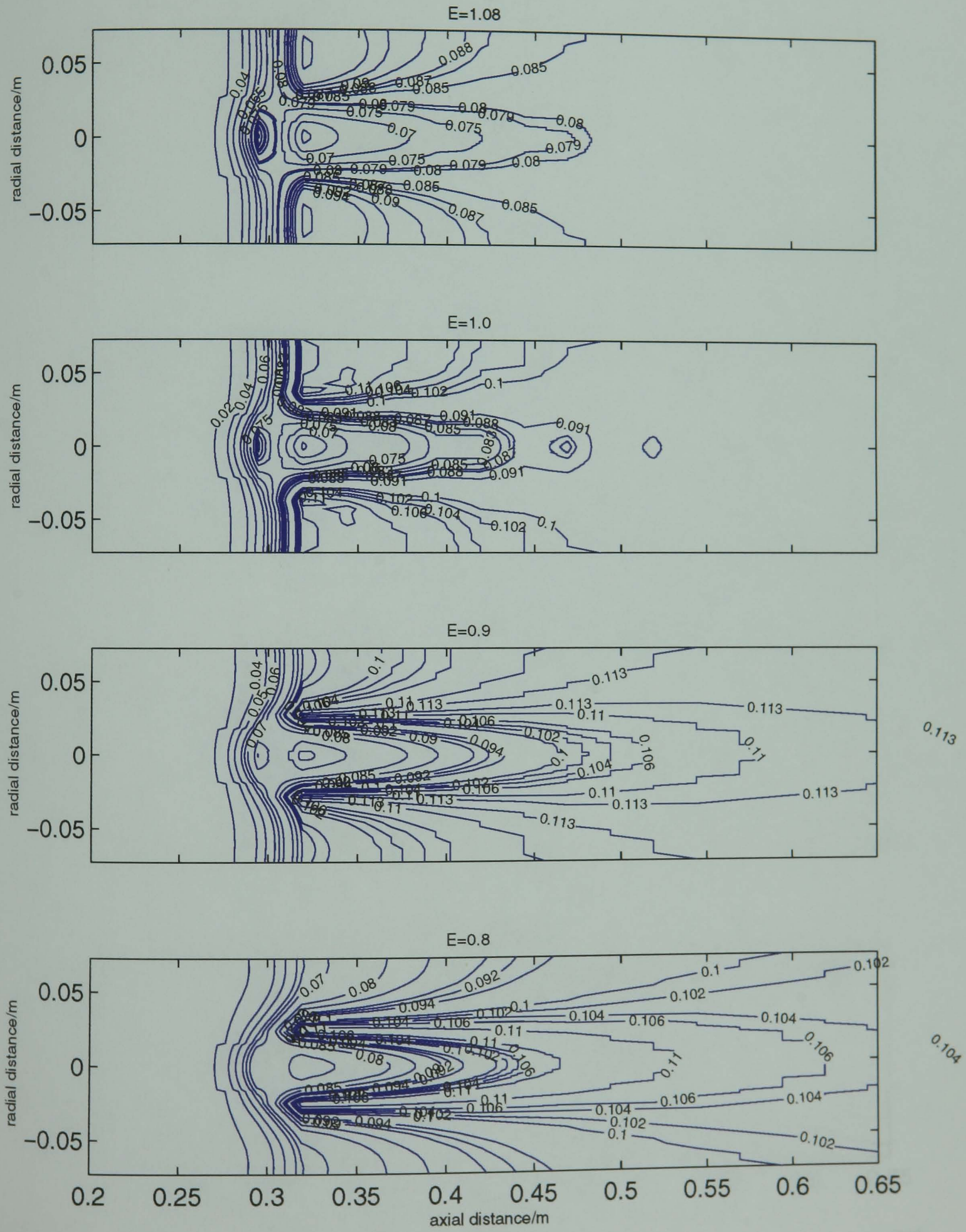

Fig. C10 Effect of input equivalence ratio on flame temperature distribution

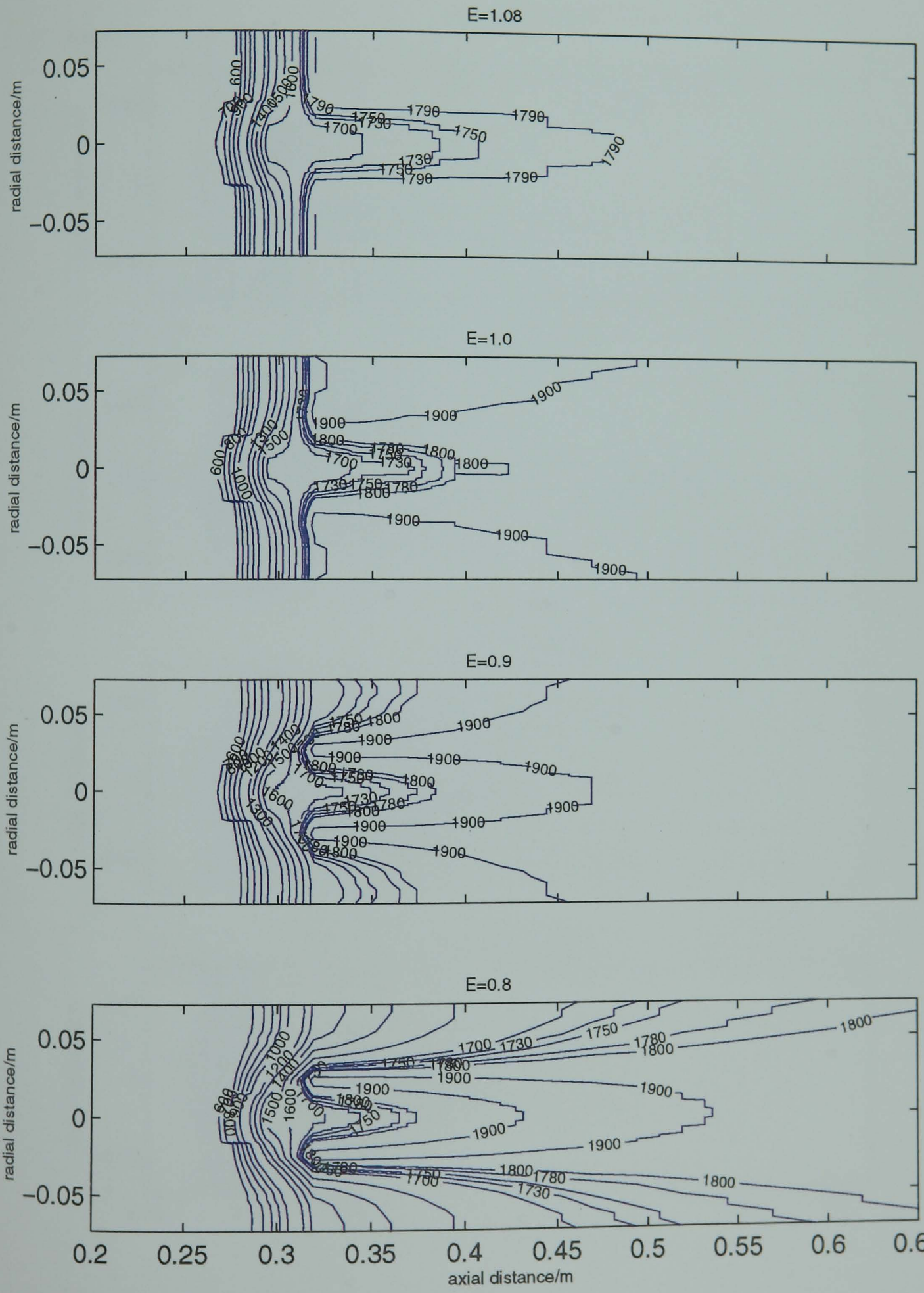

Fig. C11 predicted iso-contour maps for an inlet air temperature of 800K
(input equivalence ratio 1.08 P_{amb}=6.5bar)

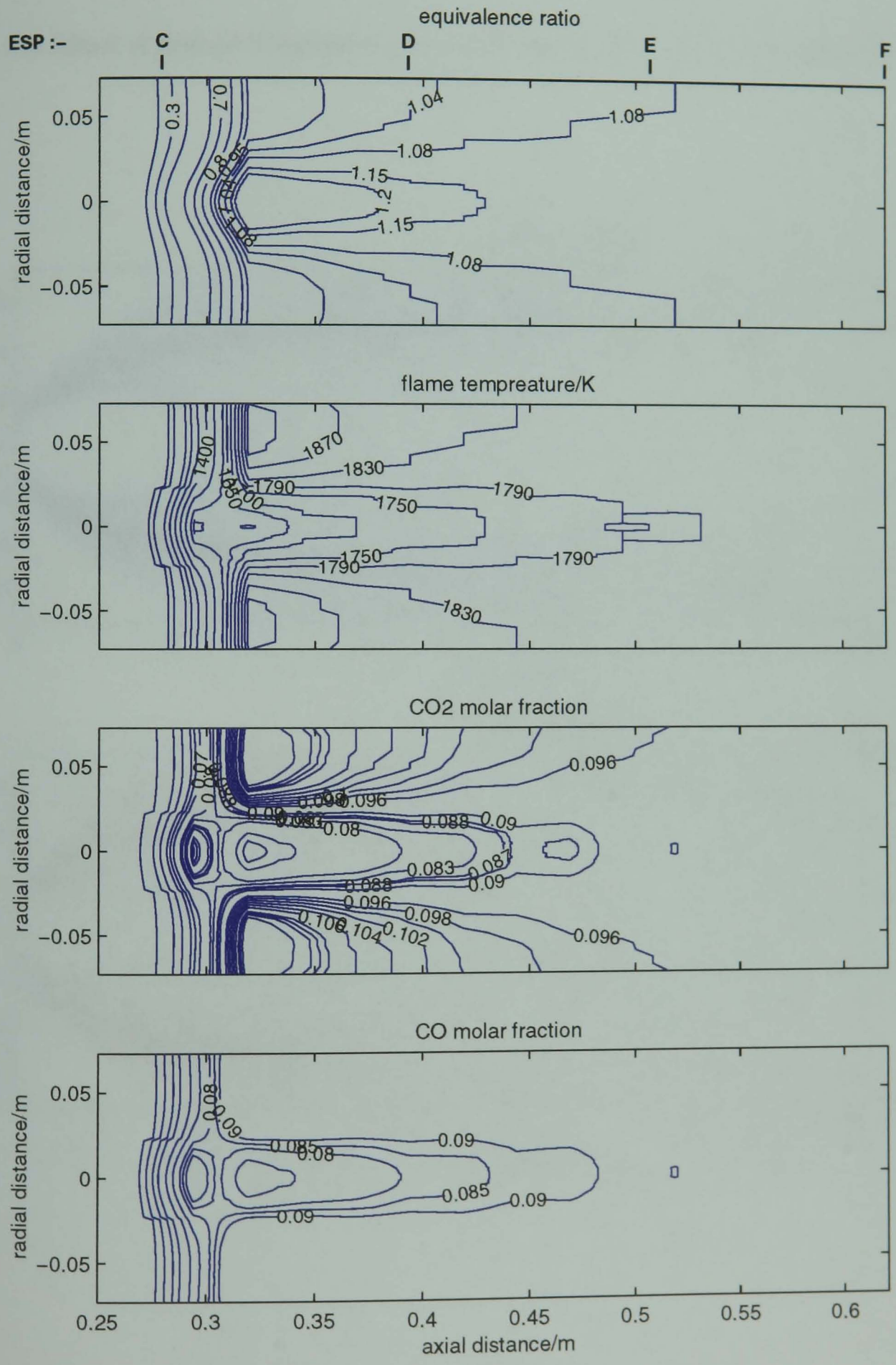

Fig. C12 Effect of inlet air temperature on vapour equivalence ratio -single phase model

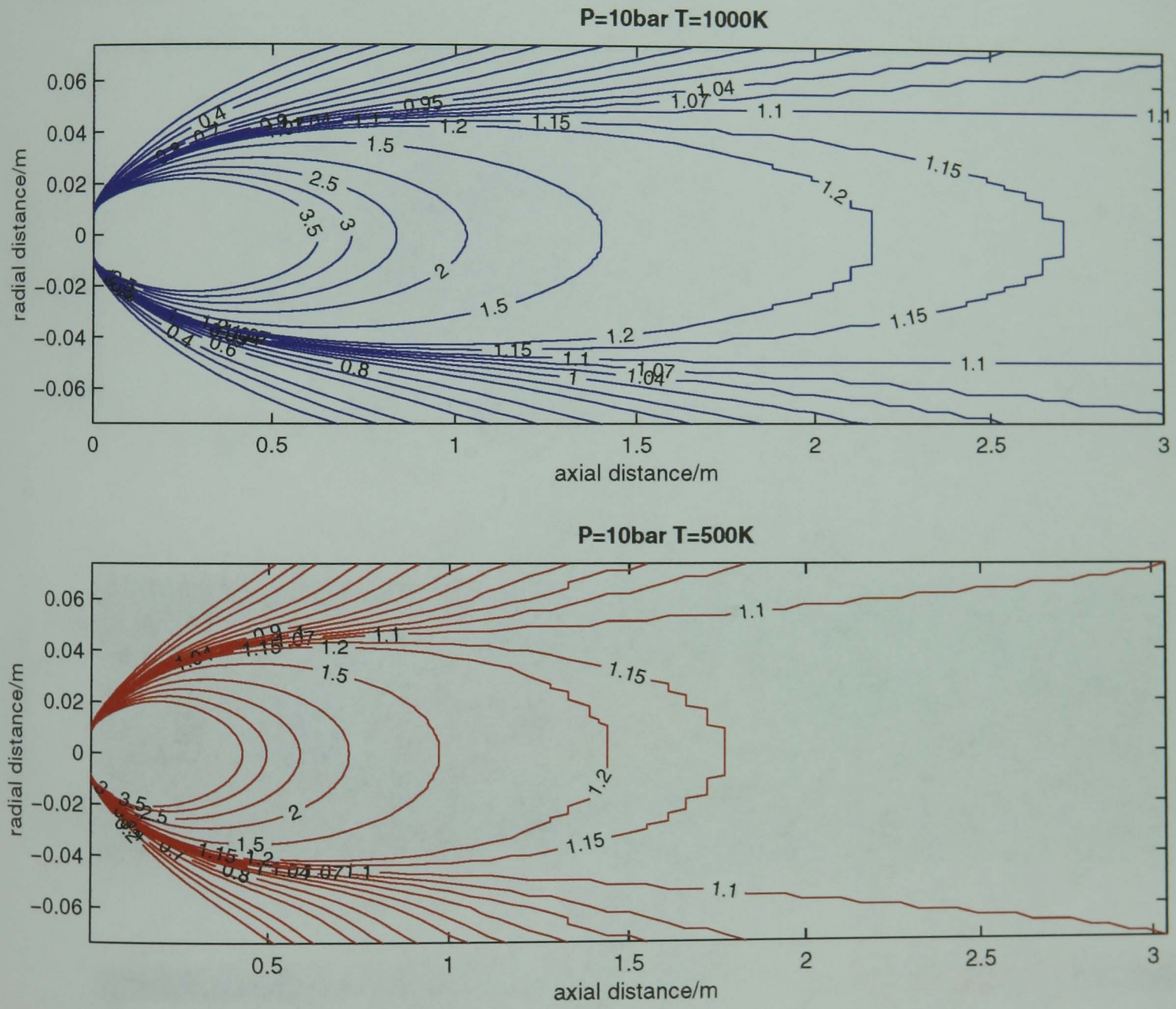

Fig. C13 Application to diesel engine combustion: -equivalence ratio iso-contours

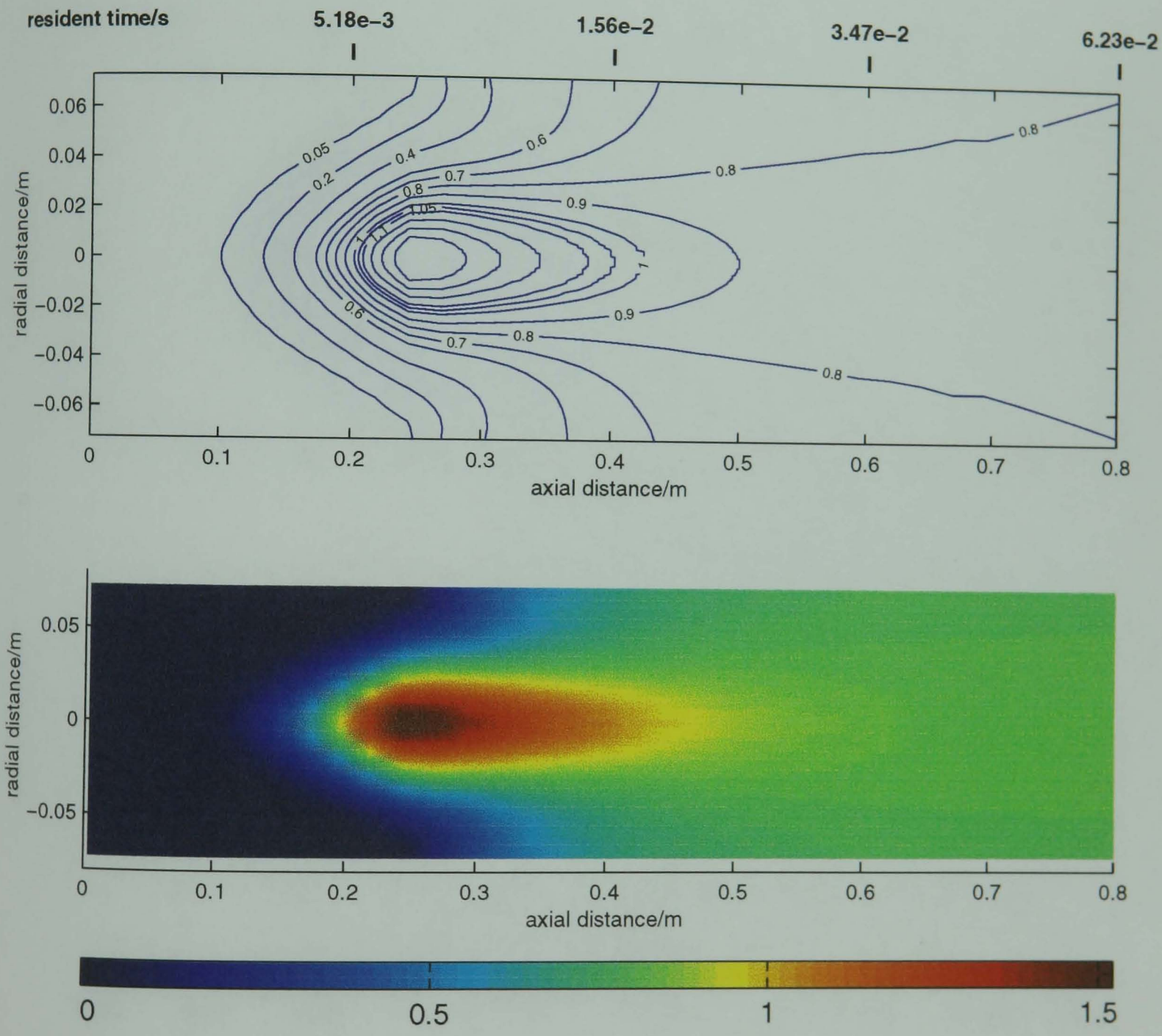

Fig. C14 Application to diesel engine combustion: -Flame temperature/K iso-contours

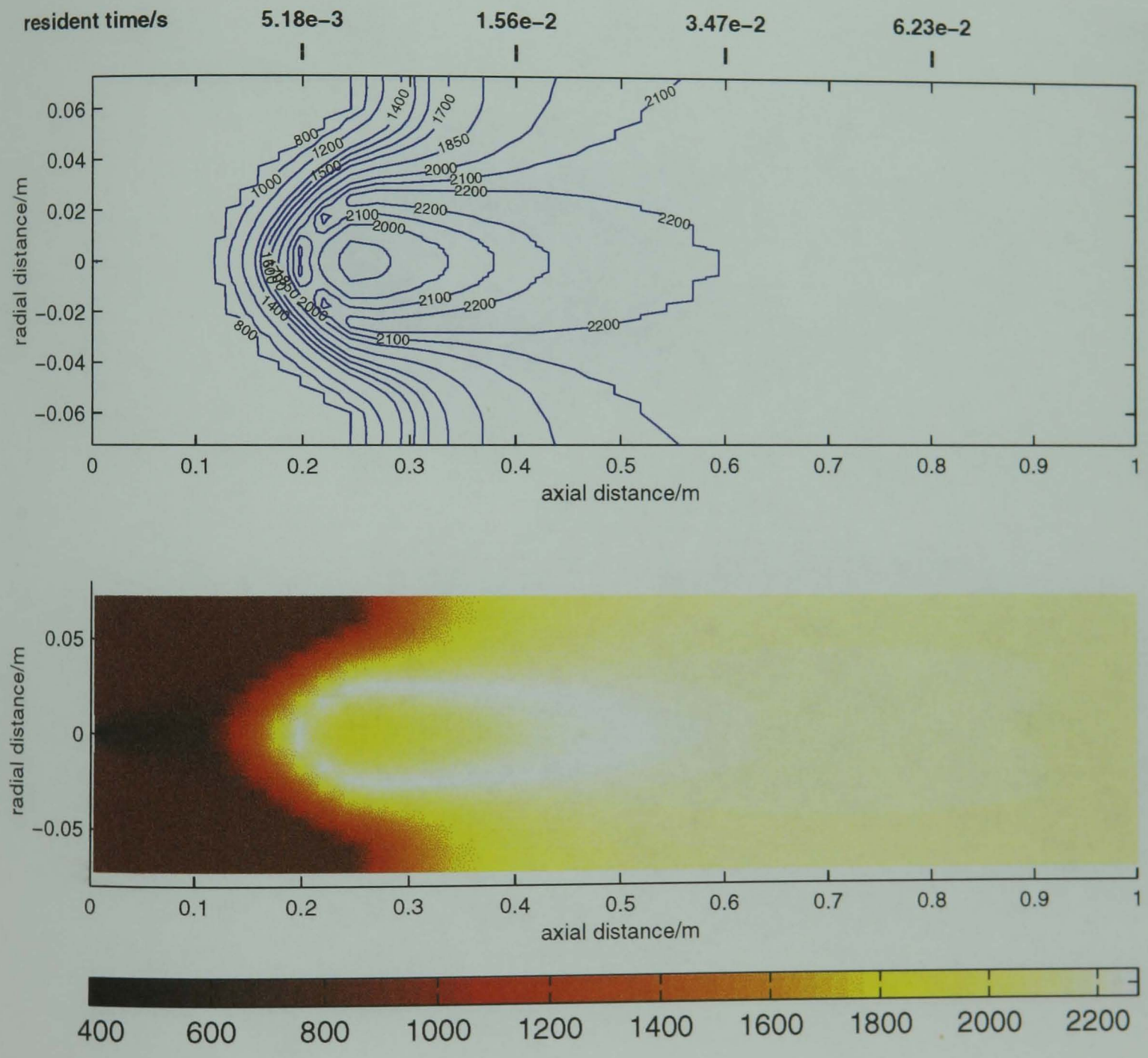

Fig. C15 Application to diesel engine combustion: CO_2 mole fraction iso-contours

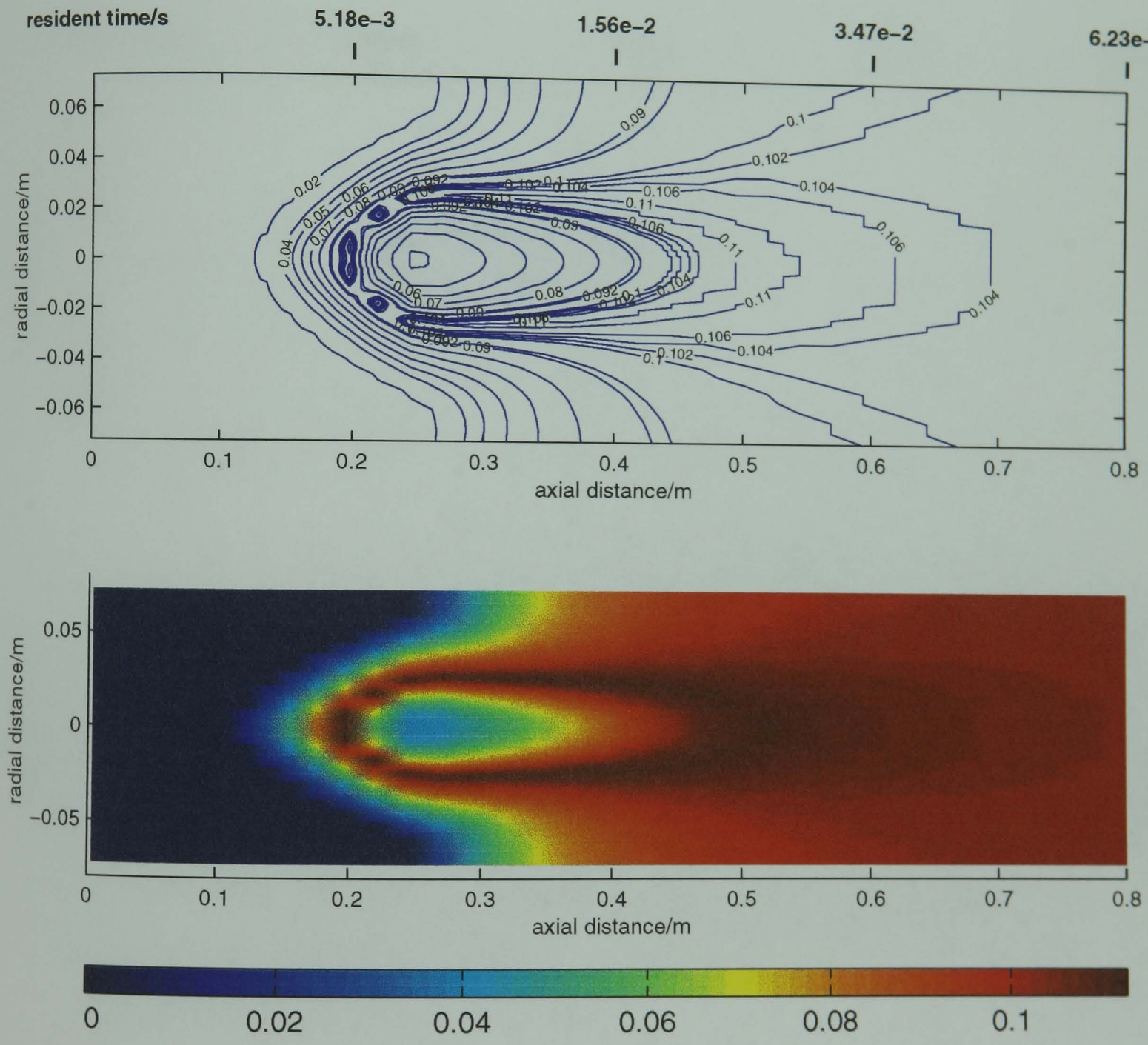

Fig. C16 Application to diesel engines: CO mole fraction iso-contours

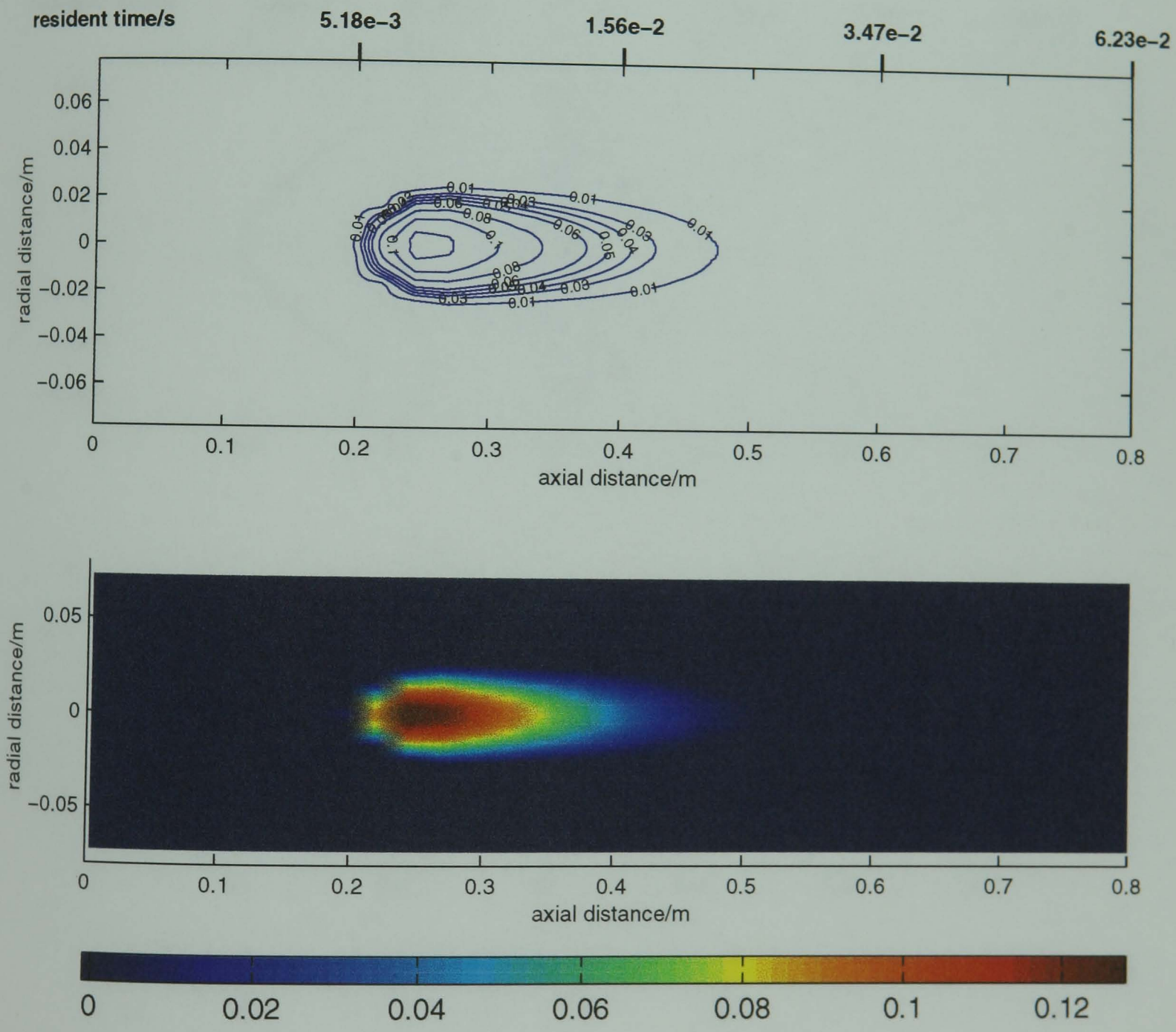

Fig. C17 Application to gas turbine combustion: -equivalence ratio iso-contours
(ambient pressure 1MPa)

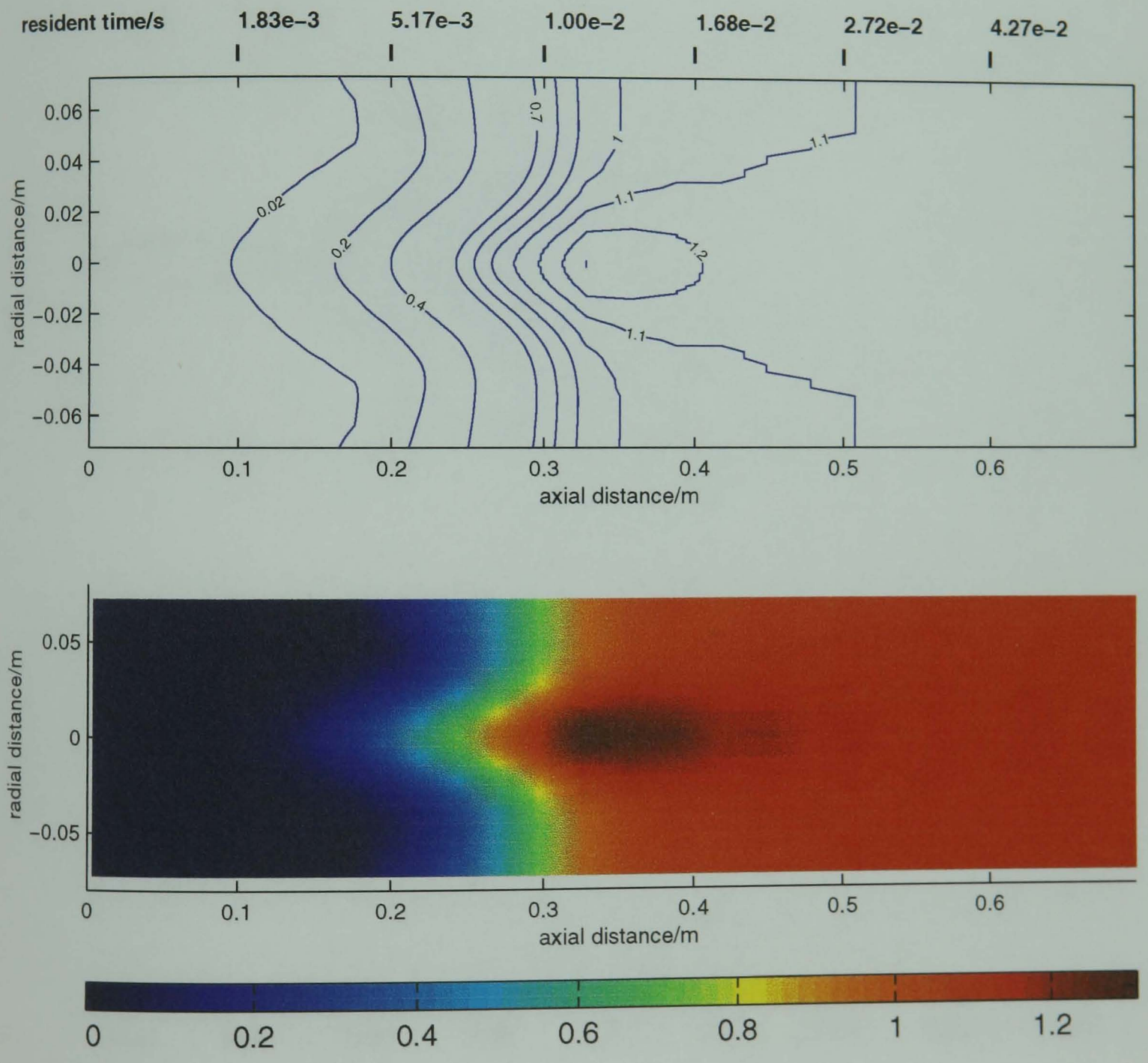

Fig. C18 Application to gas turbine combustion: -Flame temperature/K iso-contours
(ambient pressure 1MPa)

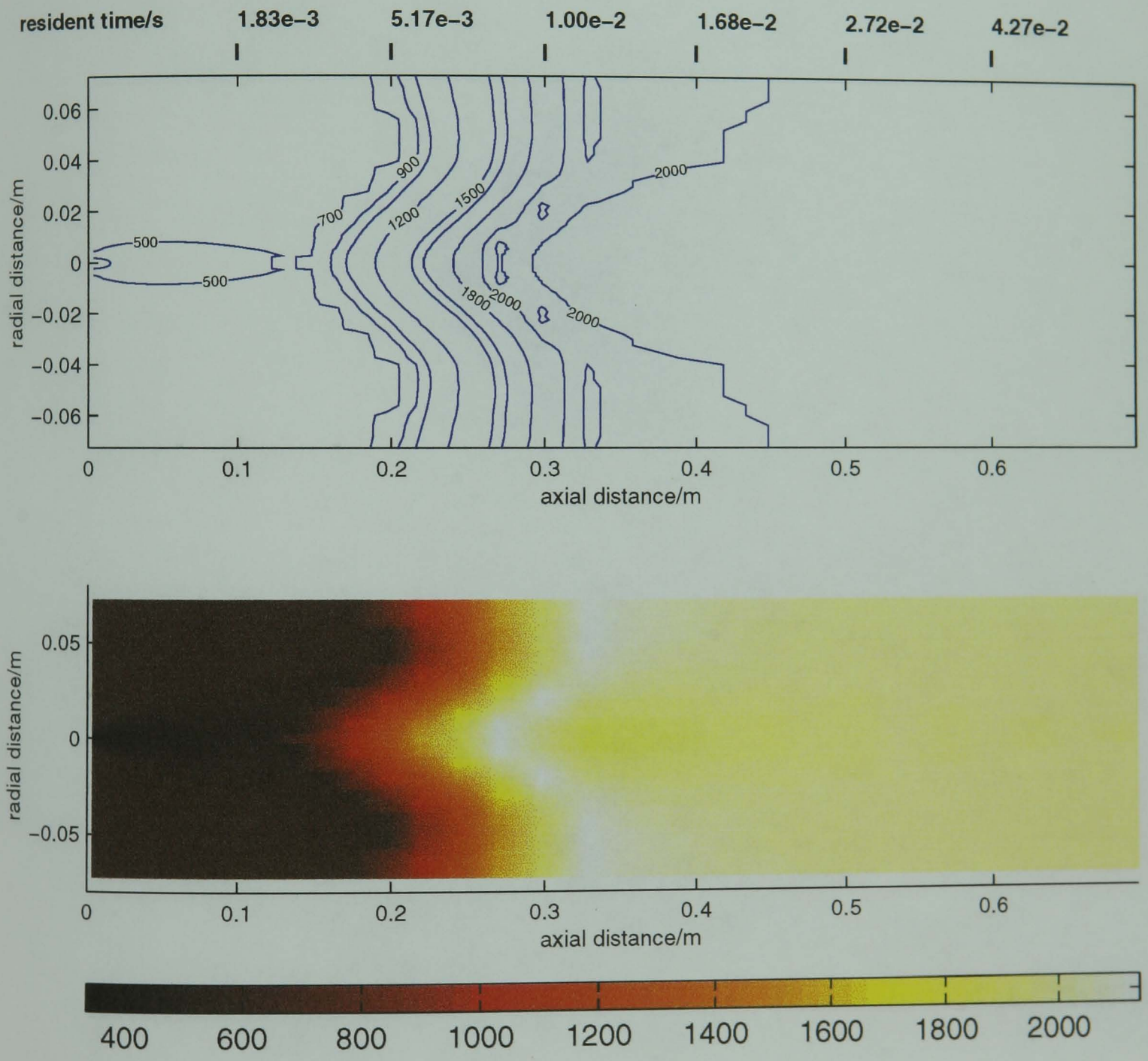

Fig. C19 Application to gas turbine combustion: -CO_2 mole fraction iso-contours
(ambient pressure 1MPa)

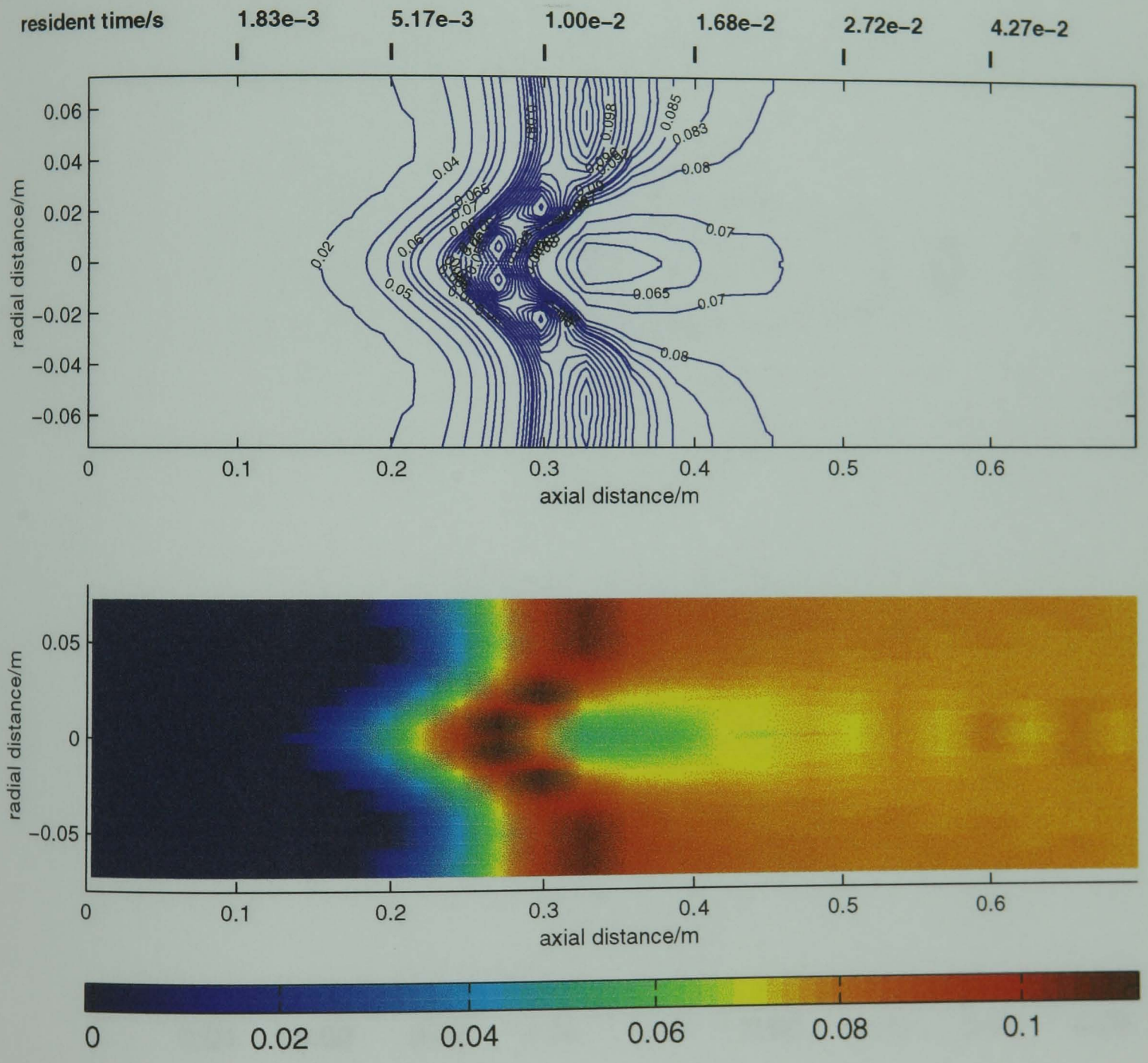

Fig. C20 Application gas turbine combustion: -CO mole fraction iso-contours
(ambient pressure 1MPa)

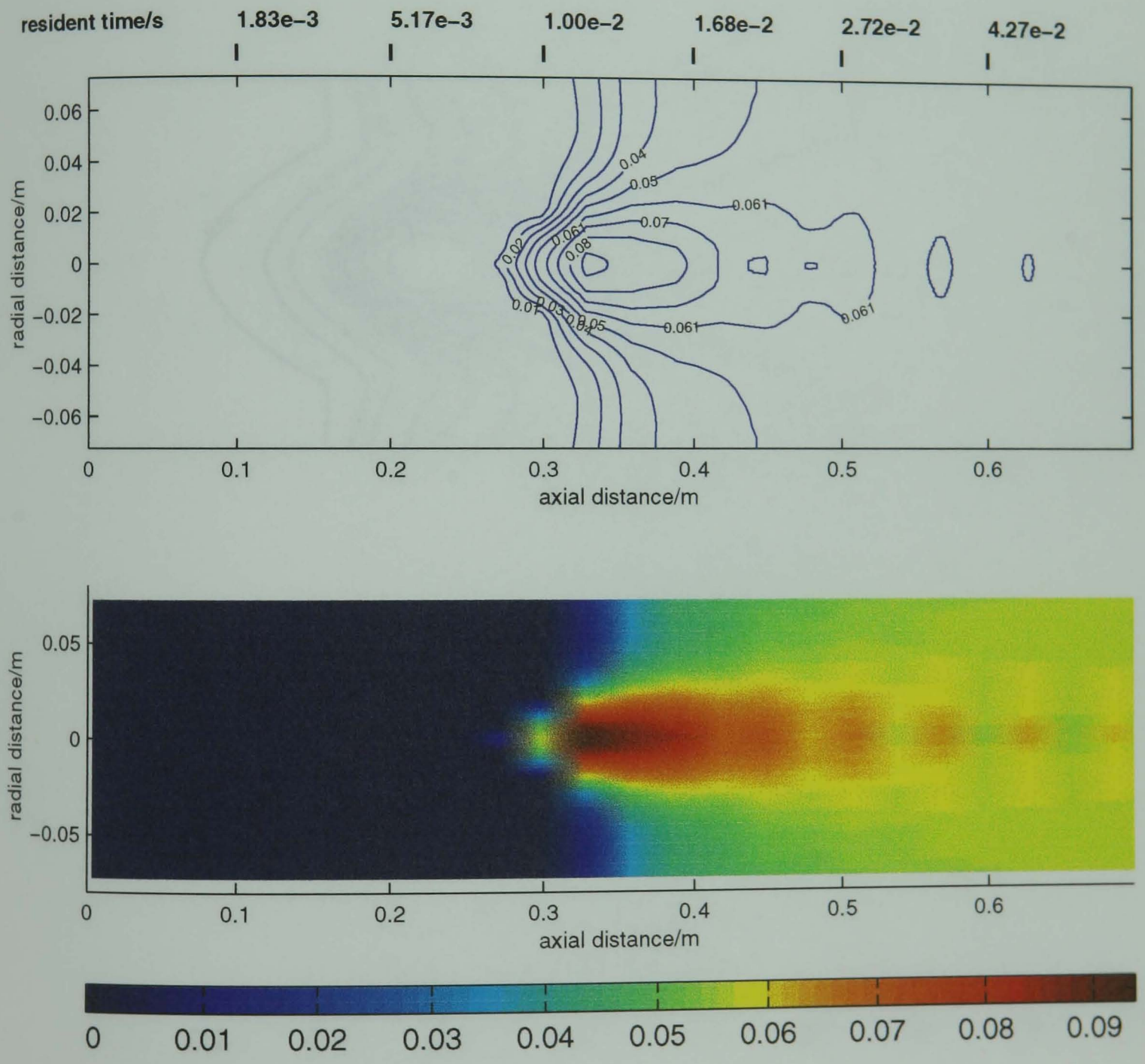

Fig. C21 Application to gas turbine combustion: -equivalence ratio iso-contours
(ambient pressure 2MPa)

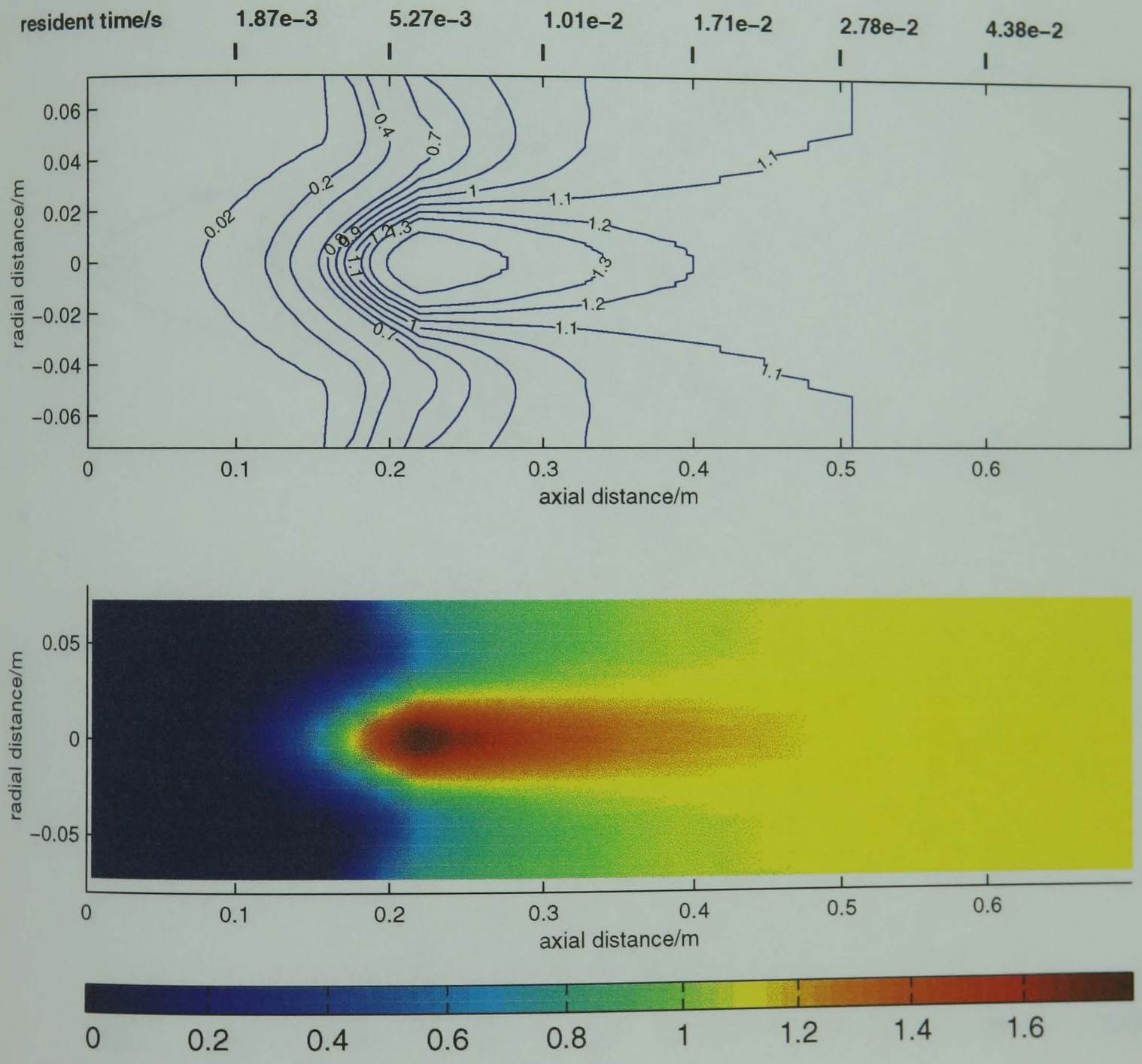

Fig. C22 Application to gas turbine combustion: -Flame temperature/K iso-contours
(ambient pressure 2MPa)

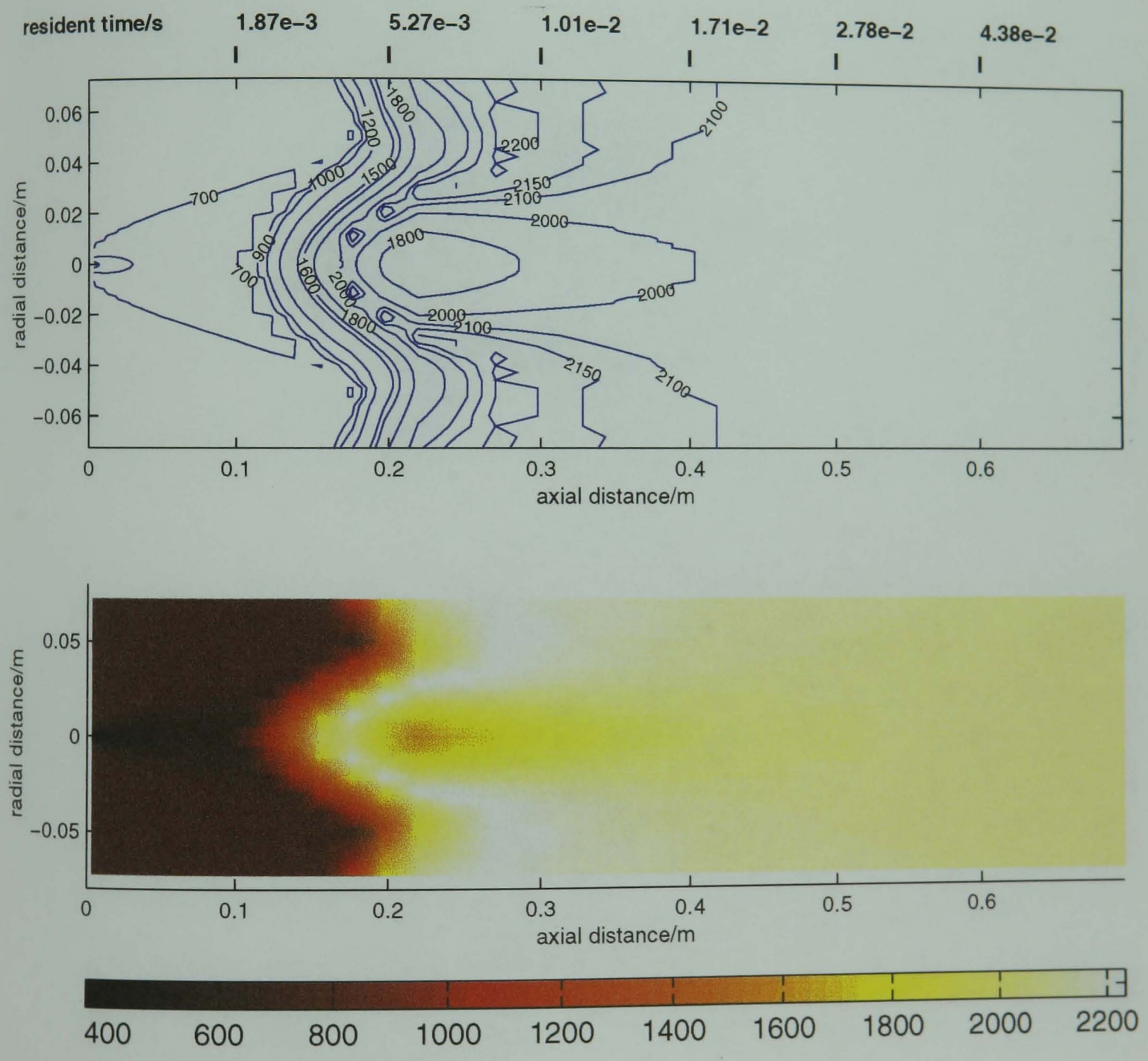

Fig. C23 Application to gas turbine combustion: -CO_2 mole fraction iso-contours
(ambient pressure 2MPa)

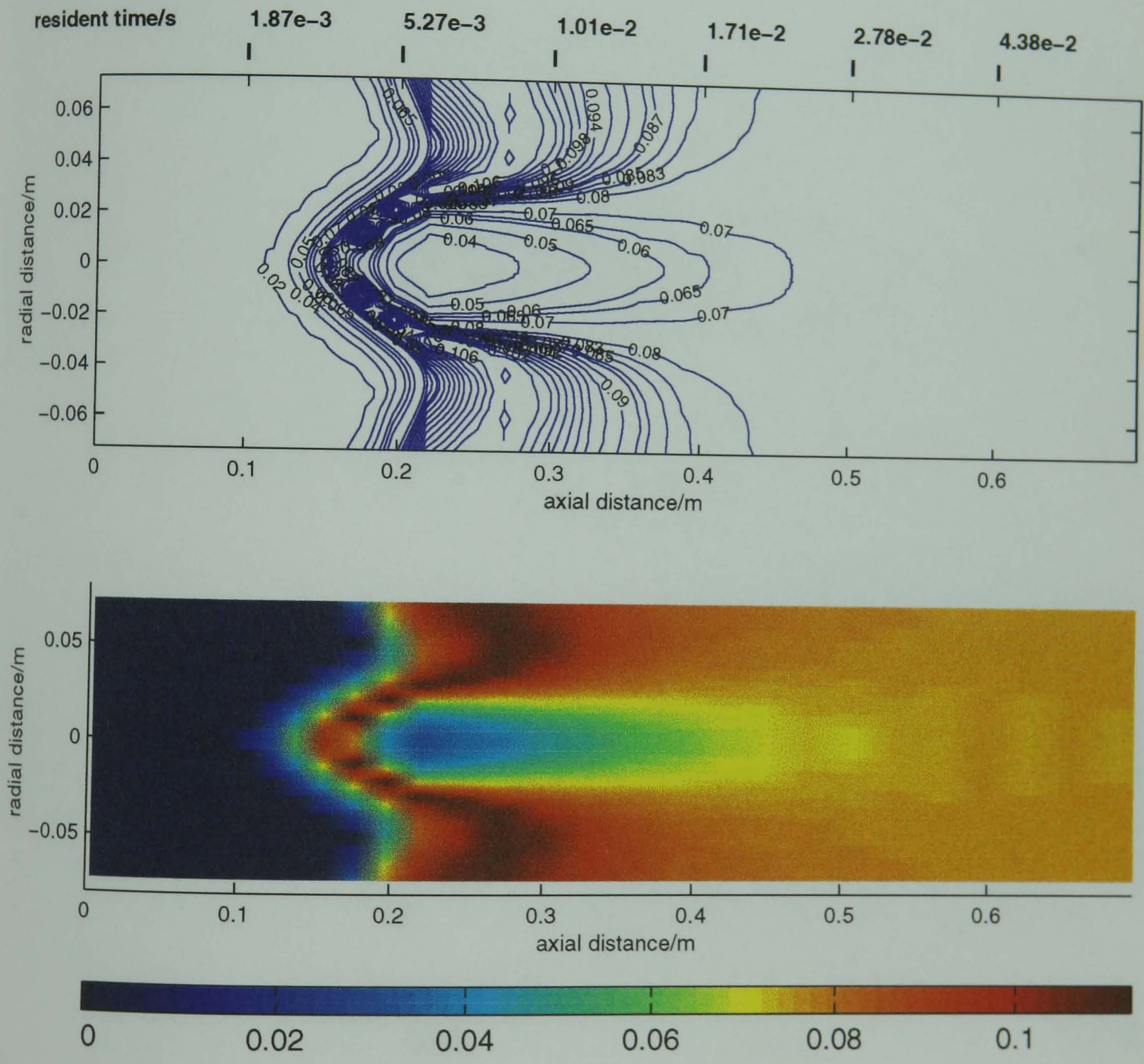

Fig. C24 Application gas turbine combustion: -CO mole fraction iso-contours
(ambient pressure 2MPa)

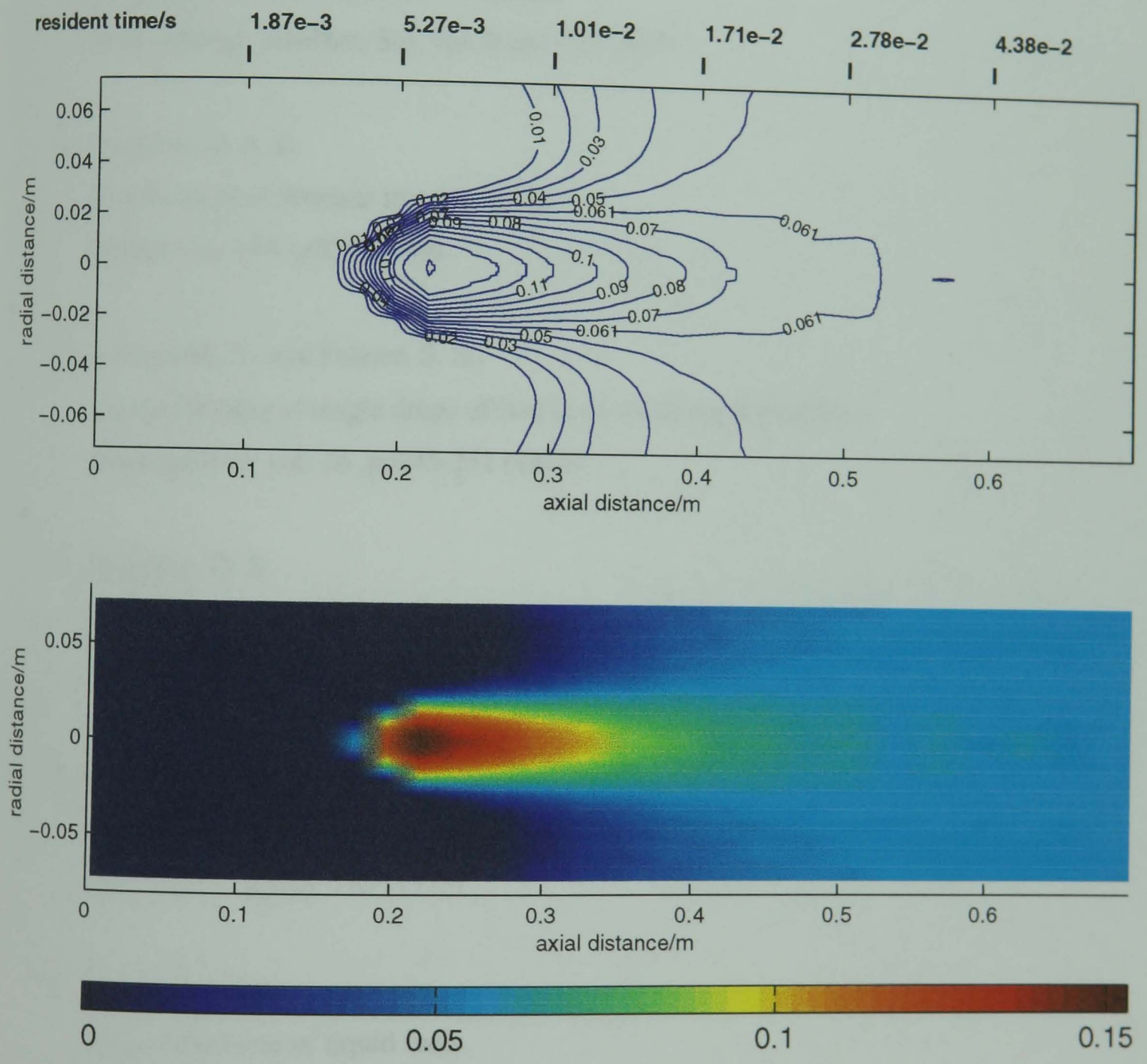

APPENDIX-D

REFERENCES

1. Faeth, G. M.
   Evaporation and combustion of sprays
   Prog. Energy combust. Sci. vol. 9 pp1-76 (1983)

2. Godsave, G.A. E.
   Combustion of droplets in a fuel spray
   Nature vol. 164 p708 (1949)

3. Goldsmith, N. and Penner, S. S.
   On the burning of single drops of fuel in an oxidizing atmosphere
   Jet propulsion vol. 24 pp245-251 (1954)

4. Spalding, D. B.
   Combustion of liquid fuel in a gas stream II
   Fuel vol. 29 pp25-32 (1950)

5. Spalding, D. B.
   Experiments on burning and extinction of liquid fuel spheres
   Fuel vol. 32 pp169-185 (1953)

6. Spalding, D. B.
   The combustion of liquid fuels
   4th symposium (*Int.*) on combustion Baltimore pp847-864 (1953)

7. Agafanova, F.A. ; Gurevich, M.A. and Paleev, I.T.
Theory of burning of a liquid fuel drop
Sov. Phys. Tech. Phys. vol. 2 pp1689-1695 (1958)

8. Williams, F. A.
Combustion theory, Addison-Wesley, Reading Mass. (1965)

9. Williams, A.
Combustion of droplets of liquid fuel : A review
Combust. Flame vol. 21 pp1-31 (1973)

10. Law, C. K.
Recent advances in droplet vaporisation and combustion
Prog. Energy Combust. Sci. vol. 8 pp171-201 (1982)

11. Wise, H. ; Lorell J. and Wood, B.J.
The effects of chemical and physical parameters on the burning rate of a liquid droplet.
5th symposium (*Int.*) on combustion. The combustion institute. pp132-141 (1955)

12. Kassoy, D.R. and Williams, F. A.
Variable property effects in liquid droplet combustion
AIAA J. vol. 6 pp1961-1965 (1968)

13. Law, C. K. and Law, H. K.
Quasi-steady one dimensional diffusional combustion
with variable properties including distinct binary diffusion coefficients.
Combust. and Flame vol. 29 pp269-275 (1977)

14. Nazha, M. A. A.
Burning Sprays of water-diesel fuel emulsions
PhD thesis Queen Mary College, University of London (1983)

15. Law, C. K.
Unsteady droplet combustion with droplet heating
Combust. and Flame vol. 26 pp17-22 (1976)

16. Hubbard, G. L, Denny, V.E. and Mills, A. F. , Droplet evaporation : Effect of transient variable properties
Int. J. Heat and Mass Transfer vol. 18 pp1003-1008 (1975)

17. El-Wakil, M. M. ; Priem, R. J. ; Brikowski, H. J. ; Mayer, P. S. ; Uyehara, O. A.
Experimental and calculated temperature and mass histories of vaporisation fuel drops.
NACA TN 3490 (1956)

18. Prakash, S. and Sirignano, W. A.
Liquid fuel droplet heating with internal circulation.
Int. J. Heat and Mass and Transfer vol. 21 pp885-895 (1978)

19. Prakash, S. and Sirignano, W. A.
Theory of convective droplet vaporisation with unsteady heat transfer in the circulating liquid phase.
Int. J. Heat and Mass Transfer vol. 23 pp253-268 (1980)

20. Chung, T. J.
Numerical modelling in combustion. pp471- 498 (1993)
Taylor and Francis

21. Law, C. K. ; Chung, S. H. and Sirinivasan, N.
Gas phase quasi-steadiness and fuel vapour accumulation effects in droplet burning
Combust. Flame vol. 38 pp173-198 (1980)

22. Landis, R. B. and Mills, A. F.
Effects of internal diffusional resistance on the vaporisation of binary droplets.
paper B7.9, 5th international heat transfer conference, Tokyo Japan

23. Law, C. K. and Sirignano, W. A.
Unsteady droplet combustion with droplet heating II - conduction limit.
Combust. Flame vol. 28 pp175-186 (1977)

24. Law, C. K. ; Prakash , S. and Sirignano, W. A.
Theory of convective transient multi-component droplet vaporisation.
16th symposium (*Int.*) on combustion .The combustion institute Pittsburgh Pa.,
pp605-617 (1977)

25. Ivanov, V. M. and Nefedov, P. I.
Experimental investigation of the combustion process of natural and emulsified
liquid fuels
NASA TT F-258 (1965)

26. Lasheras, J. C. ; Fernandez-Pello, A. C. and Dryer F. L.
Experimental observations on the disruptive combustion of free droplets of
multi-component fuels
Combust. Sci. Tech. vol. 22 pp195-209 (1980)

27. Law, C. K.
Internal boiling and superheating in vaporising multi-component droplets.
AIChE J. vol. 24 no. 4 pp626-632 (1978)

28. Law, C. K. ; Lee, C. H. and Sirinivasan, N.
Combustion characteristics of water in oil emulsion droplets.
Combust. flame vol. 37 pp125-143 (1980)

29. Wang, C. H. and Law, C. K.
Microexplotion of fuel droplets under high pressure
Combust. and Flame vol. 59 pp53-62 (1985)

30. Nazha, M. A. A. and Crookes, R. J.
Effects of water content on pollutant formation in a burning spray of water-in-diesel fuel emulsion
20th Symp. (*Int.*) on combustion p2001 (1984)

31. Nazha, M. A. A. and Crookes, R. J.
Combustion characteristics at elevated pressures of plant derived oils
Inst. Energy Applied Energy Research Conference Session II, P. 91 (1989)

32. Rose, J. W. and Cooper, J. R.
Technical Data on Fuels (1977)
The British national committee
The world energy conference
34 St. James St. London

33. Ranz, W. E. and Marshall, W. R.
Evaporation from drops part I
Chem. engr. Prog. vol. 48 no.3 pp141-146 (1952)

34. Ranz, W. E. and Marshall, W. R.
Evaporation from drops part II
Chem. engr. Prog. vol. 48 no.4 pp173-180 (1952)

35. Milne-Thompson, L. M.
Theoretical Hydrodynamics
Macmillan, New York (1975)

36. Lara-Urbaneja, P. and Sirignano, W. A.
Theory of transient multicomponent droplet vaporisation in a convective field.
18th symposium (*Int.*) on combustion. The combustion institute Pittsburgh Pa..
pp1365-1374 (1981)

37. Tong, A. Y. and Sirignano, W. A.
Analysis of vaporising droplet with ,slip internal circulation ,unsteady liquid phase and quasi-steady gas phase heat transfer .
ASME-JSME Thermal joint Eng. Conference Honolulu, Hawaii (1983)

38. Tong, A. Y. and Sirignano, W. A.
Multi-component droplet vaporisation in a high temperature gas.
Combust. Flame vol.66 pp221-235 (1986)

39. Tong, A. Y. and Sirignano, W. A.
Multi-component transient droplet vaporisation with internal circulation :
Integral equation formulation and approximate solution.
Numerical Heat Transfer vol. 10 pp253-278 (1986)

40. Prakesh, Satya
Unsteady theory of droplet vaporisation with large gas and liquid Reynolds numbers.
PhD Thesis October 1978
Princeton University USA

41. Aggrawal, S. K. ; Tong, A. Y. and Sirignano, W. A.
A comparison of vaporisation models in spray combustion
AIAA J. vol.22 pp1448-1457 (1984)

42. Tong, A. Y.
Final report, AFOSR/SCEEE 84-RCP-35 March 1986

43. Abramzon, B. and Sirignano, W. A.
Droplet vaporisation for spray combustion calculations
Int. J. Heat and Mass Transfer vol.32 pp1605-1618 (1989)

44. Johns, L. E. and Beckman, R. B.
Mechanisms of dispersed-phase mass transfer in viscous single drop extraction system.
AIChE J. vol.12 pp10-16 (1966)

45. Yuen, M. C. and Chen, L. W.
On drag of evaporating droplets
Combust. Sci. Tech. vol. 14 pp147-154 (1976)

46. Continillo, G. and Sirignano, W. A.
Numerical study of multi-component fuel spray flame propagation inn spherical Closed volume.
22nd symposium (*Int.*) on combustion. The institute of combustion ,Pittsburgh Pa. pp1941-1949 (1988)

47. Delpalanque, J.-P. , Rangel, A. and Sirignano, W. A.
Liquid waste incineration in a parallel-stream configuration : Effect of auxiliary fuel.
Progress in Astro. and Aero.,
Dynamics of Deflagrations and reactive systems vol. 132 pp164-186 (1991)

48. Renksizbulut, M. and Yuen, M. C.
Numerical study of droplet evaporation in a high temperature stream
J. of heat transfer vol. 105 pp389-397 (1983)

49. Heywood, R. J.
variable property, blowing and transient effects in convective droplet evaporation with internal circulation
MS Thesis University of Waterloo (1986)

50. Dwyer, H. A. and Sanders, R. B.
Ignition and Flame propagation studies with adaptive numerical grids
Combust. and Flame vol. 52 pp11-23 (1983)

51. Dwyer, H. A. ; Kee, R. J. ; Barr, P. K. and Sanders, B. R.
Transient droplet heating at a high Peclet number
J. of fluids engineering vol. 105 pp83-88 (1983)

52. Dwyer, H. A. and Sanders, B. R.
Comparative study of droplet heating and vaporisation at high
Reynolds and Peclet numbers
Presented at 9th ICDERS (International Colloquium on Dynamics and Reactive Systems) Poitiers, France, July 3-8, 1983

53. Dwyer, H. A. ; Sanders, B. R. and Raiszadek, F.
Detailed computation of unsteady droplet dynamics
20th Symposium (*Int.*) on combustion. The combustion institute pp1743-1749 (1984)

54. Patnaik, G. ; Sirignano, W. A. ; Dwyer, H. A. ; Sanders, B. R.
A numerical technique for the solution of vaporising fuel droplet
10th ICDERS (International Colloquium on Dynamics and Reactive Systems) Berkeley, California, August 4-9 1985

55. Dwyer, H. A. and Sanders, B. R.
A detailed study of burning fuel droplets
21st Symposium (*Int.*) on combustion. The combustion institute pp633-639 (1986)

56. Dwyer, H. A. and Sanders, B. R.
Unsteady influences in droplet dynamics and combustion
Comb. Sci. and Tech. vol. 58 pp253-265 (1988)

57. Dwyer, H. A.
Calculations of droplet dynamics in high temperature environments
Prog. Energy Combust. Sci. vol. 15 pp131-158 (1989)

58. Chiang, C. H,. Raju M. S. and Sirignano, W. A.
Numerical analysis of convecting vaporising fuel droplet with variable properties
Int. J. Heat Mass Transfer vol. 35 pp1307-1324 (1992)

59. Patnaik, Gopal
A numerical solution of droplet vaporisation with convection.
PhD Thesis April 1986
Carneige-Mellon University, Pittsburgh, Pennsylvania USA

60. Dash, S. K. and Som, S. K.
Ignition and combustion of liquid fuel droplet in a convective medium
Journal of energy resources technology vol. 113 pp165-170 (1991)

61. Renksizbulut, M. and Yuen, M. C.
experimental study of droplet evaporation in a high temperature air stream
J. of heat transfer vol. 105 pp384-388 (1983)

62. Westbrook, C. and Dryer, F. L.
Simplified reaction mechanisms for the oxidation of hydrocarbon fuels in flames
Combust. Sci Tech. vol. **27** pp31-43 (1981)

63. Godsave, G. A. E.
Rates of combustion of solid fuel particles
Nature vol. 171 p86 (1953)

64. Monaghan, M. T. , Siddal, R. G. and Thring, M.
The influence of initial diameter on the combustion of single drops of liquid fuel
Combustion and Flame vol. 12 pp45-53 (1968)

65. Wise, H. and Agoston, G. A.
Literature of the combustion of Petroleum
American Chemical Society Washington DC p125 (1958)

66. Williams, A.
The mechanism of combustion of droplets and sprays of liquid fuels
Oxidation and combustion Reviews vol.3 pp1-45 (1968)

67. Rex, J. F. ; Fuhas, A. E. and Penner, S. S.
Interference effects during burning in air for stationary n-heptane ethyl alcohol and methyl alcohol droplets
Jet propulsion vol. 26 p179 (1956)

68. Kanevsy, J.
Jet propulsion vol. 26 p778 (1956)

69. Okijama, S. and Kumagai, S.

Further investigations of combustion of free droplets in a freely falling chamber including moving droplets.

15 th symposium (*Int.*) on combustion. The combustion institute. Pittsburgh, Pa., pp401-417 (1975)

70. Miyasaka, K. and Law, C. K.

Combustion of strongly interacting linear droplet arrays

18th Symposium (*Int.*) on combustion. The combustion institute Pittsburgh Pa., pp283-292 (1981)

71. Kudyakov, J. N.

Izu. Akad. Nauk. SSR Otd Nauk. vol. 4 p508 (1949)

72. Abdel-Khalik, S. I. ; Tamaru, T. and El-Wakil, M. M.

A chromatographic and interferometric study of the diffusion flame around a simulated fuel drop.

15th symposium (*Int.*) on combustion. The combustion institute. Pittsburgh, Pa., pp389-399 (1975)

73. Ross, P. A. and El-Wakil, M. M.

Liquid rockets and propellants

Academic press New York p265 (1960)

74. Aldred, J. W. and Williams, A.

The burning rates of drops of n-Alkanes

Combustion and Flame vol. 10 pp396-397 (1966)

75. Aldred, J. W. , Patel, J. C. and Williams, A.
The mechanismof combustion of droplets and spheres of liquid n-heptane
Combustion and Flame vol. 17 pp139-148 (1971)

76. Rosser, W.
The shape and size of a droplet diffusion flames
Combustion and Flame vol.11 pp442-444 (1967)

77. Stupar, J. and Dawson, J. B.
Theoretical and experimental aspects of the production of aerosols for use in atomic absorption spectroscopy
Appl. Opt. vol. **7** p1351 (1968)

78. Hottel, H. C. ; Williams, G. C. and Simpson, H. C.
Combustion of droplets of heavy liquid fuels
5th (*Int.*) Symposium on combustion. Reinhold New York pp101-109 (1966)

79. Mizutani, Y. and Ogasawara, M.
Laminar flame propagation in droplet suspension of liquid fuel
Int. J. Heat and Mass Transfer vol. 8 p921 (1965)

80. Eisenklam, P ; Arunachalm, S. A. and Weston J. A.
Evaporation rates and drag resistance of burning drops
11th Symposium (*Int.*) on combustion. p715 (1967)

81. Sangiovani, J. J. and Labowsky, M.
Burning times of linear fuel droplet arrays : A comparison of experimental fuel droplet arrays.
Combust. and Flame vol. 41 no. 1 pp15-30 (1982)

82. Kumagi, S. and Isoda, H.
Combustion of fuel droplets in a falling chamber
6th symposium (*int.*) on combustion, Reinhold N. Y. pp726-731 (1957)

83. Sirignano, W. A.
Fuel droplet vaporisation and spray combustion theory
Prog. Energy Combust. Sci. vol. 9 pp291-322

84. Kee, R. J. ; Miller, J. A. and Jefferson, T. H.
CHEMKIN: A general purpose, problem independent, transportable, FORTRAN chemical kinetics code package.
Sandia Rep. SAND80-8003 (1980)

85. Kee, R. J. ; Dixon-Lewis, G. ; Warnatz, C. and Miller, J. A.
A FORTRAN computer code package for evaluation of gas phase multi component transport properties.
Sandia Rep. SAND86-8246 (1986)

86. Manrique, J. A. and Borman, G. L.
Calculation of steady state droplet vaporisation at high ambient pressure
Int. J. Heat and Mass transfer vol.12 pp1081-1095 (1969)

87. Matlosz, R. L. , Leipziger, S. and Torda, T. P.
Int. J. Heat and Mass Transfer vol. 15 pp831-852 (1972)

88. Shuen, J. S. ; Vigor, Y. and Hasio, C. C.
Combustion of liquid-fuel droplets in supercritical conditions
Combustion and Flame vol. 89 pp299-319 (1992)

89. Lixing Zhou

Theory and numerical modelling of turbulent gas-particle flows and combustion

Science Press (1993)

90. Launder, R. E. and Spalding, D. B.

Mathematical models of turbulence

Academic Press 1972

91. Prandtl, L.

Beritch Ü ber Untersuchungen zer ausgebildeten Tutbulenz

ZAMM vol.5 p136 (1925)

92. Kolmogorov, A. N.

Equation of turbulent motion of an incompressible turbulent fluid

Izv. Akad. Nauk SSSR Ser. Phys. vol. VI no. 1-2 p473 (1942)

93. Prandtl, L.

Ü ber ein Untersuchungen zur ausgebildeten Turbulenz Nachrichten von der

Akad. der

Wissenschaft in Gottingen (1945)

94. Rodi, W. Spalding, D. B.

A two parameter model of turbulence and its application to free jets

W ärme und Stoffü bertragung vol. 3 p85 (1970)

95. Spalding , D. B.

Concentration fluctuations in a around jet

J. of Chemical Engineering Science vol. 26 p95 (1971)

96. Spalding, D. B.
k-W model of turbulence,
Imperial College Mechanical Engineering Report TM/TN/A/16 (1972)

97. Harlow, F. H. and Nakayama, P.
Transport of turbulence energy decay rate
Los Alamos Science Lab., University of California Report LA-3854 (1968)

98. Jones, W. P. and Launder, B. E.
The prediction of laminarization with a 2-equation model of turbulence
Int. J. of Heat and Mass Transfer vol. 15 p301 (1972)

99. Jones, W. P. and Launder, B. E.
Prediction of low Reynolds number phenomena with a 2-equation model of turbulence
Int. J. of Heat and Mass Transfer vol.16 p1119 (1973)

100. Launder, B. E. and Spalding, D. B.
The numerical computation of turbulent flows
Computational methods in applied mechanics and engineering vol. 3 p269 (1974)

101. Daly B. J. and Harlow, F. H.
Transport equations in turbulence
The Physics of Fluids vol.13 p2634 (1970)

102. Patel, V. C. ; Rodi, W. and Scheurerer, G.
Turbulence models for near walls and low Reynolds number flows : a review
AIAA J. vol. 23 pp1308-1319 (1985)

103. Gosman, A. D. and Pun, W. M.
'The TEACH program', HTS Course Notes
Mech. Eng. Dept, Imperial College (1974)

104. Turbulence
Hinze, J. O.
McGraw-Hill Series in Mathematical Engineering (1959)

105. Jayathilaka, C. L. V.
The Influence of Prandtl Number and Surface roughness on the Resistance of the Laminar Sublayer to Momentum and Heat transfer
Imperial College, Mech. Eng. Dept. Report TWF/R/2 (1966)

106. Jones, W. P. and Whitelaw, J. H.
Calculation Methods for Reacting Turbulent Flows: A Review
Combustion and Flame vol. 48 pp1-26 (1982)

107. Malalasekara, W. M. G. ; James E. H. ; Tayali N. E. And Lee N. E. K.
Flow and heat transfer in a secondary heat exchanger of a condensing boiler
29th US national heat transfer conference,
Atlanta GA HTD Vol. 237 pp83-92 (1993)

108. Patankar S. V.; Basu, D. K. And Alpay S. A.
prediction of a three dimensional velocity field of a deflected turbulent jet
J. Fluids Eng. vol.99 p758 (1977)

109. Ramsey, J. W. and Goldstein, R. J.
Interaction of heated jet with deflection stream
NASA CR-72613 (1970)

110. Shearer, A. J. and Feath, G. M.
Evaluation of locally homogeneous model for spray evaporation
NASA Contractor Report 3198 (1979)

111. Mao, C. P. ; Wakamatsu, Y. and Faeth, G. M.
A simplified model for high pressure spray combustion
18th symposium (*Int.*) on combustion. The combustion institute (1981)

112. Feath, G. M.
Evaporation and combustion of sprays
Prog. Energy Combust. Sci. vol. 9 pp1-76 1983

113. Faeth, G. M.
Mixing and transport and combustion in sprays
Prog. Energy and Combust. Science (1987) vol. 13 pp293-345 (1987)

114. Crowe, C. T. , Sharma, M. P. and Stock D. E.
The Particle-Source-In Cell (PSI-Cell) Model for Gas Droplet Flows
J. of Fluids Engineering (Transactions of the ASME) pp325-332 June 1977

115. Crowe, C. T.
A numerical model for the gas-droplet flow field near an atomiser
Proceedings of the 1st international conference on liquid atomisation and spray systems. Tokyo August 27-31 1978

116. Gosman A. D. and Ioannides, E.
Aspects of computer simulation of liquid fueled combustors
J. of Energy vol.7 no.6 482-490 (1983)

117. Hutchinson, P ; Khalil, E. E. and Whitelaw, J. H.
Measurement and calculation of furnace flow properties
J. of Energy vol.1 no.4 212 (1977)

118. Haselman, L. C. and Westbrook, C. K.
A theoretical model for two-phase fuel injection in stratified charge engines.
SAE 780318 (1978)

119. Huang, X. and Z. Lixing
Simulation of three dimensional turbulent recirculating gas particle flows
By an energy equation model of particle turbulence
FED-V v.121 Gas-Solid Flows ASME pp261-265 (1991)

120. Bray, K. N. C.
The interaction between turbulence and combustion
17th symposium (*Int.*) on combustion. The combustion institute pp223-232

121. Spalding, D. B.
Concentration fluctuations in a round turbulent free jet
Chemical engineering science vol. 26 p95 (1971)

122. Malalasekara, W. M. G.
Mathematical modelling of fires and related processes
PhD thesis Imperial College London (1988)

123. Lookwood, F. C.
The modelling of turbulent premixed and diffusion combustion in the
computation of engineering flows
Combustion and Flame vol. 29 pp111-122 (1977)

124. Lookwood, F. C. and Naguib, A. S.
The prediction of the fluctuations in the properties of free round jet, turbulent diffusion flames
Combustion and Flame vol. 24 p109 (1975)

125. Richardson, J. N. ; Harward, Jr. H. C. and Smith Jr. R. W.
The relation between sampling and concentration fluctuations in a turbulent gas jet
4th symposium (*Int.*) on combustion. The combustion institute p814 (1953)

126. Jones, W. P. and Whitelaw, J. H.
Coupling of turbulence and chemical reaction. Fluid section report FS/78/13
Department of mechanical engineering Imperial college, London (1978)

127. Smith, P. J. and Smoot, D.
The gaseous combustion part II : Theory and evaluation of local properties
Combustion and Flame Vol.42 pp277-285 (1981)

128. Jones, W. P.
PACE : A computer program for solving three dimensional flow problems
Rolls Royce limited Report (1975)

129. Owen, K.
Measurements and observations in turbulent recirculating jetflows
AIAA Journal vol. 14 pp1556-1562 (1976)

130. Pope, S. B.
The probability approach to the modelling of the turbulent reacting flows.
Combustion and Flame vol. 27 pp299-312 (1976)

131. Pope, S. B.
Implication of probability equations for turbulent combustion models
Combustion and Flame vol. 29 pp235-246 (1977)

132. Pope, S. B.
A Monte Carlo Method for the PDF equations of turbulent flows
MIT-EL 80-012 (1980)

133. Pope, S. B.
A Monte Carlo method for the PDF equations of turbulent reactive flows
Combustion Science and Technology vol. 25 pp159-174 (1981)

134. Pope, S. B.
PDF methods for turbulent reactive flows
Prog. Eng. Comb. Sci. vol. 11 pp119-192 (1985)

135. Taylor, A. M. P. K.
Instrumentation for flows with combustion
Academic press (1993)

136. O'Rourke, P. J. and Amsden, A. A.
The TAB Method for numerical calculation of spray droplet break-up
SAE 872089

137. O'Rourke, P. J. and Bracco F. V.
Modelling of drop interactions in thick sprays and comparison with experiments
Stratified Charge automotive engine conference IMechE (1980)

138. Wu, K. J. ; Su C. C. ; Steinberger, R. L. Santavicca, D. A. Bracco, F. V.
Measurements of spray angle of atomisation jets
J. of Fluids Engineering vol. 105 pp406-413 (1983)

139. Reid, R. C. ; Prausnitz, J. M. and Poling, B. E.
The Properties of Gases and Liquids, fourth edition (1987)
McGraw-Hill Book Company

140. Lee, B. I. and Kesler, M. G.
A Generalised Thermodynamic correlation based on three-parameter corresponding states
AIChE Journal vol. 21 pp510-527 (1975)

141. Patankar, S. V.
Numerical heat and mass transfer
Taylor and Francis (1980)

142. H. K. Versteeg and W. Malalasekera
An introduction to computational fluid dynamics
Longman Scientific and Technical (1995)

143. Patankar, S. V. and Spalding, B. D
A calculation procedure for Heat, Mass and Momentum transfer in three dimensional parabolic flows
Int. J. of Heat and Mass transfer vol. 15 p1787 (1972)

144. Patankar, S. V. and Spalding, B. D
A computational model for three dimensional flow in furnaces
14th Symp. (*Int.*) on combustion. The combustion Inst. p605 (1972)

145. Harlow, F. H. and Welch, J. E.
Numerical Calculation of time-dependent viscous incompressible flow of fluid with free surface
phys. Fluids, vol. 8 pp2182-2189 (1965)

146. Caretto, L. S. ; Curr, R. M. And Spalding, D. B.
Two numerical methods for three dimensional boundary layers
Comp. Methods Appl. Mech. Eng. vol. 1 p39 (1972)

147. Novel finite-difference formulation for differential expressions involving both first and second derivatives
Int. J. Num. Methods Eng., vol. 4, pp551-559 (1972)

148. Patankar, S. V. and Spalding, B. D.
Heat and mass transfer in boundary layers, 2d ed.
Intertext London (1970)

149. White, W. B. ; Johnson, S. M. Dantzig, G. B.
Chemical equilibrium in complex mixtures
The journal of chemical physics vol. 28 no. 5 (1958)

150. Crookes, R. J. ; Janota M. S. and Tan, K. J.
A study of soot and gaseous pollutant formation in a diesel type burning fuel spray
Proceedings of the combustion institute European symposium Sheffield
Academic Press (1974)

151. Crookes R. J. ; Daie, S. J. ; Janota, M. S ; Nazha, M. A. A. and Sodha, M. N.
Soot and gaseous pollutant formation in a burning fuel spray in relation to pressure and air/fuel ratio
Archiwum Procesow Splania vol. 7 p323 (1976)

152. Nazha, M. A. A. and Crookes, R. J.
Measurement and prediction of soot and gaseous species in a burning fuel spray at elevated pressure
Archivum Combustionis Vol. 10 pp49-69 (1990)

153. Abramovich, G. N.
The theory of turbulent jets
MIT Press (1963)

154. Janota M. S. ; Crookes R. J. Daie S. J. ; Nazha, M. A. A. and Sodha, M.
Soot and gaseous pollutant formation in a burning fuel spray in relation to pressure and air/fuel ratio
Journal of the institute of fuel pp10-13 (1977) March

155. Moss, J. B.
Modelling of soot formation for turbulent flame prediction
Soot formation in combustion by H. Bockhorn
Springer Series pp551-565 (1994)

156. Chung, T. ; Ajlan, M. ; Lee, L. L. and Starling, K. E.
Generalized multi-parameter correlation for nonpolar and polar fluid transport properties
Ind. Eng. Chem. Res. vol.27 pp671-679 (1988)

157. Fuller, E. N. ; Ensley, K. and Giddings, J. C.
Diffusion of halogenated hydrocarbons in Helium
The effect of structure on collision cross sections
J. Phys. Chem. vol. 73 pp3679-3685 (1969)

158. Fuller, E. N. ; Schettler, P. D. and Giddings, J. C.
A new method for prediction of burning gas-phase diffusion coefficients
Ind. Eng. and Chem. vol. 58 no. 5 pp19-27 (1966)

159. Thompson, G. H.; Brobst, K. R. and Hankinson, R. W.
An improved correlation for densities of compressed liquids and liquid mixtures
AIChE J. vol. 28 pp671-676 (1982)

APPENDIX-E

NOMENCLATURE

All variables and constants not listed here are listed in the relevant chapter.

Chapter-1

None used

Chapter-2

[Droplet Section]

B	Spalding mass transfer number
C_p	isobaric specific heat capacity
D	mass diffusivity
f	Blasius function in Sirignano and Prakesh models
H	effective energy of gasification: Enthalpy of evaporation + Heat needed for the droplet heating per unit mass
h	surface heat transfer coefficient
k	burning rate coefficient
K	chemical reaction rate
L	enthalpy of evaporation
Le	Lewis number
$\dot{m}$	mass gasification rate
Pr	Prandtl number
Q	heat of combustion per unit mass of fuel
R	radial distance to droplet surface
Re	Reynolds number
r	radial distance
r_{fs}	flame front stand of ratio
r_s	droplet radius
Sc	Schemidt number
Sh	Sherwood number
T	temperature
t	time
u	velocity
Y	mass fraction

Greek Symbols

α	thermal diffusivity
ϕ	normalised stream function
λ	thermal conductivity
ρ	density
δ	diffusion coefficient
σ	stoichiometric oxidiser to fuel ratio

Subscript

F	fuel
f	flame
g	gas phase
i	i^{th} species
L	liquid phase
o	oxidiser
ov	overall
s	surface
0	initial state
*	modified values
∞	ambient condition
-	mean value

[Spray Section]

f	mixture fraction
g	variance of the mixture fraction

Greek symbols

μ	viscosity

Subscript

w	wall
l	laminar
T	turbulent
t	turbulent

Superscript

-	mean component
~	mean component
`	fluctuating component
^	instantaneous value

Chapter-3

C_p	isobaric specific heat capacity
D	binary diffusion coefficient
h	enthalpy
h_c	surface heat transfer coefficient in
k	thermal conductivity
K_c	mass transfer coefficient
L	latent heat of gasification
m	mass
$\dot{m}$	mass transfer rate
p_{fl}	saturation vapour pressure
R	droplet radius
r	radial co-ordinate
T	temperature
t	time
w	creation of species
z	a unitless parameter

Greek Symbols

α	correction factor for mass transfer
ρ	density
ω	mass fraction

Subscripts

d	droplet
f	fuel vapour
g	fuel-vapour-air
i	i^{th} species
L	liquid
s	surface
T	total

Chapter-4 [spray]

r	radial co-ordinate
T	temperature
P	pressure
P'	pressure correction term
k	turbulent kinetic energy
u	axial velocity
v	radial velocity
x	axial co-ordinate
Y	mass fraction

Greek Symbols

ε	turbulent dessipation rate
μ	viscosity
σ	exchange coefficient
τ	shear stress

Subscripts

w	wall

Chapter-5

All variables and constants are declared in the chapter itself.

Chapter-6

None used

Chapter-7

None used

APPENDIX-F

ABBREVIATIONS

BWR	Benedict Web Rubine equation of state
CARS	Coherent Anti-stokes Raman Spectroscopy
CDM	Continuous Droplet Model
CFD	Computational Fluid Dynamics
CFM	Continuum Formulation Model
DDM	Discrete Droplet Model
DNS	Direct Numerical Simulation
DSF	Deterministic Separated Flow
FEM	Finite Element Method
FVM	Finite Volume Method
LDV	Laser Doppler Velcoimetry
LHF	Locally Homogeneous Flow
PDE	Partial Differential equation
PDF	Probability Density Function
PSIC	Particle Source In Cell
RK	Runge-Kutta model
SF	Separated Flow
SIMPLE	Semi-Implicit Method for Pressure Linked Equations
SSF	Stochastic Separated Flow
TDMA	Tri-Diagonal Matrix Alimentation